IMPACT OF VAGINAL SYNTHETIC PROLAPSE MESHES ON THE MECHANICS OF THE HOST TISSUE RESPONSE

by

Andrew Jordan Feola

BS, University of Pittsburgh, 2006

Submitted to the Graduate Faculty of

Swanson School of Engineering in partial fulfillment

of the requirements for the degree of

Doctor of Philosophy

University of Pittsburgh

2011

UNIVERSITY OF PITTSBURGH

SWANSON SCHOOL OF ENGINEERING

This dissertation was presented

by

Andrew Jordan Feola

It was defended on

July 14th, 2011

and approved by

Pamela Moalli M.D., Ph.D., Associate Professor, Obstetrics, Gynecology and Reproductive Sciences

Richard Debski Ph.D., Associate Professor, Department of Bioengineering

Naoki Yoshimura M.D., Ph.D., Associate Professor, Department of Urology

Michael S. Sacks Ph.D., Professor, Department of Bioengineering

Maiti Spandan Ph.D., Assistant Professor, Department of Bioengineering

Dissertation Director: Steven D. Abramowitch, Assistant Professor, Department of Bioengineering

IMPACT OF VAGINAL SYNTHETIC PROLAPSE MESHES ON THE MECHANICS OF THE HOST TISSUE RESPONSE

Andrew Jordan Feola, PhD

University of Pittsburgh, 2011

The vagina helps support the bladder, urethra, uterus, and rectum. A lack of support leads to pelvic organ prolapse, and vaginal delivery is a prevalent risk factor; however, there is little research on vaginal biomechanical properties. Despite numerous complications, clinical practice involves surgical repair with synthetic meshes. Complications can be partially attributed to our lack of knowledge regarding the mesh-tissue complex (MTC) after implantation. However, it is difficult to perform rigorous studies without utilizing animal models. Therefore, we evaluated how parity affected the mechanical properties of vaginal tissue in three animal models: rodent, sheep, and non-human primate (NHP) to compare their mechanically properties to parous women who typically undergo prolapse surgery. Parity negatively impacted the mechanical properties of the vagina in NHP, which were biomechanically similar to parous women, making it a suitable model for studying the effects of mesh implantation. Second, we examined the textile and structural properties of commonly used meshes (Gynemesh, UltraPro, SmartMesh, Novasilk, and Polyform) utilizing uniaxial and ball-burst tests. These meshes had significantly different porosity and structural properties. To investigate the host response, three meshes were implanted into the abdominal wall of the rodent and NHP, and on the vagina in the NHP. The MTC was removed, and the tissue contribution was calculated. We did not observe notable changes in the tissue properties following mesh implantation in the rodent; however, implantation of the stiffest mesh (Gynemesh) in the NHP resulted in an exhibition of a stress-

shielding response manifested by inferior biomechanical properties of the abdominal and vaginal tissues. Less stiff meshes (UltraPro and SmartMesh) resulted in preservation of tissue properties. To gain insight into how mesh properties affect the tissue contribution, we began developing a finite element model. Utilizing the co-rotational theory with a fiber-recruitment stress-strain relationship, we could describe the behavior of SmartMesh and UltraPro. While an in-depth characterization of these meshes revealed multiple fiber populations, further development of modeling may be instrumental in closing the current knowledge gap. Ultimately, understanding the mesh-tissue interaction will improve clinical outcomes by identifying mesh properties that are essential for providing structural support while maintaining tissue integrity.

TABLE OF CONTENTS

LIST OF TABLES

LIST OF FIGURES

PREFACE

I would like to thank and acknowledge my mentor and friend Dr. Steven Abramowitch. I do not believe I can portray in words all of the lessons or guidance I have gained from being in your laboratory. The mentoring began prior to me even being a graduate student. I recall just over five years ago when I was faced with a difficult decision on where to attend graduate school or the research I wanted to focus on. To help talk about my options and figure things out I met with Steve, a newer faculty member at the University of Pittsburgh. I am still not quite sure what he was thinking but somehow he wanted me to work in his new laboratory. I remember saying I would be afraid that I would not have enough to do, but he assured me I would have more than enough to work on; and he was right. Steve, I could not have asked for a better mentor during the last five years, I believe you will continue to conduct outstanding research and continue to educate and inspire future undergraduate and graduate students. The research presented in this dissertation is only a fraction of what I have learned and been a part of during my doctorate studies. I will try to continue teaching and conducting research as I was taught.

I would also like to extend a special thanks to Dr. Pamela Moalli; who served more as a co-advisor throughout my entire graduate career than a committee member to me. You have been an unbelievable mentor and inspiration to me. If I could have but a small portion of your talents as a researcher, physician or parent than I would truly have a successfully career and a

wonderful family. I hope to make both you and Steve proud one day, as I hope my actions will one day speak louder than words.

I am sincerely appreciative to the remaining members of my thesis committee including Drs. Sack, Debski, Spandan, and Yoshimura. Dr. Sacks I would like to specially thank for teaching me the framework and theories behind biomechanical testing and constitutive modeling, and the supplementary meetings about biaxial testing and modeling have taught me a great deal about biomechanics. Dr. Debski, thank you for always making me think more critically about my presentations by asking the difficult questions, which pushed me to better understand my projects and an improved researcher. Dr. Spandan, I appreciate the time you took in helping me understand the background to finite element modeling. Lastly, I would like to thank Dr. Yoshimura for his knowledge on smooth muscle tissues and their contractile properties.

Aside from my committee members I would like to say a special thank you to Dr. Savio L-Y. Woo. You have provided me with much advice and philosophy over the years, which I will carry with me where ever I go. You were a part of my first journal publication and it was an honor to work at the MSRC. I am grateful for the opportunities on an academic and personal level that you have provided for me.

I would also like to take a moment and thank Dr. Harvey Borovetz for his support throughout my undergraduate and graduate careers, and his continued support throughout my future career. I would also like to acknowledge Lynette Spataro, Diann DeCenzo and the rest of the Bioengineering staff for their help and support over the last five years. Aside from my mentors and Bioengineering staff I would like to thank my co-workers, collaborators and fellows at Magee Hospital for aiding me in work conducted within this dissertation. I would also like to thank my fellow graduate students Zegbeh, Bill, and Katrina. It has been wonderful getting to

know you, and I am sure each of you will have successful careers it was a pleasure working with each of you. To the undergraduates that I have worked with over the years at the Musculoskeletal Research Center, I thank you sincerely for the opportunity to work with you. Although I only named a few individuals from Magee and the MSRC, please know that everyone I have worked with on a personal and professional level, have each contributed to the work presented here and without you I would not have been able to complete all of this work.

These years have been challenging and engaging to the point of being hectic at times, and I have enjoyed every minute of it; no matter how much I complained. I would like to tell Carrie that even though I am slightly upset she finished before me I couldn't have imaged a better friend over the last few years to go through raduate school with. I wish you nothing but the best in the future. To Suzan: we have each been here almost from the beginning and I am so lucky to have had you as a co-worker and friend all of these years. To Megan: I would like to thank her for her patience and help proof-reading my thesis I know it was not easy but I appreciate all the time you have spent. In addition, I would like to thank my friends who have continuously gone above and beyond with their support and belief for me over my time in Pittsburgh.

Lastly, I would like to express my gratitude and appreciation to my family. Their continuous support over my life has had a significant impact on who I am today and where I go tomorrow. Janis, thank you for always being there to listen and offer advice. To her husband Dave for his support and my nieces for their love. To David, for believing I could finish my Ph.D. and always being a better brother than I could have ever asked for. To my parents, Mom and Dad, it is hard to imagine that I would be where I am today without your love, support and of course making sure I kept my options open. For you, and everyone else, I am eternally indebted; therefore, I dedicate this dissertation and the last five years of my life to each of you.

1.0 INTRODUCTION

1.1 PELVIC ORGAN PROLAPSE

Pelvic floor disorders comprise a wide spectrum of interrelated clinical conditions including pelvic organ prolapse, urinary incontinence, fecal incontinence, voiding dysfunction, defecatory dysfunction, and sexual dysfunction [1]. In addition to the physical symptoms that accompany these disorders, they also have a substantial emotional impact resulting in psychosocial distress that includes social isolation, anxiety, and depression [2-4]. Pelvic floor disorders affect nearly one-third of premenopausal women and nearly half of postmenopausal women [5, 6].

Pelvic organ prolapse, or simply prolapse, is a major pelvic floor disorder that is estimated to affect half of the women over the age of fifty [7] and is often defined as the descent of the pelvic organs into the vagina. Each year, an estimated 225,000-280,000 women undergo surgery for pelvic floor disorders in the United States [8, 9]. The cumulative incidence of a primary operation for pelvic organ prolapse or related condition by age 80 is 11.1%, with a direct cost of over $1 billion dollars annually in the United States [5, 8-10]. Since support to the pelvic organs (urethra, bladder, uterus and rectum) is provided directly by the vagina and indirectly by the muscles and connective structures involved in vaginal support [11-13], it is generally thought that damage to any component of this complex support mechanism can result in loss of vaginal support and prolapse of the pelvic organs. This concept is largely based on epidemiological data

that suggests that vaginal delivery is the greatest independent risk factor for the development of pelvic floor disorders [14-18]. Transient and long term injury to the vagina and its supportive tissues has also been documented following vaginal delivery, and most parous women have some anatomical evidence of disrupted support [19-21]. However, the majority of parous women never progress to symptomatic prolapse and those that do progress, often do not develop symptoms until years or decades later. These observations have led to the speculation that factors, in addition to vaginal birth, negatively impact the vagina and its supportive tissues, resulting in further deterioration and prolapse progression. Other known/suggested risk factors include menopause, obesity, age, prior surgery, and a genetic predisposition [15, 17, 18, 22].

The field of urogynecology is relatively young compared to disciplines such as orthopaedics and cardiovascular surgery. The latter disciplines have had the unique opportunity to mature alongside the growing field of biomechanics, which began to gain significant clinical recognition in the 1960's [23]. Since that time, biomechanical research has helped to provide a more thorough understanding of normal tissue function, the effect of pathology, and the impact of treatment in a variety of systems in the human body. Thus, the clinical disciplines that have embraced biomechanics have undergone significant changes in the clinical management of patients over the last few decades. As urogynecology begins to mature, it is clear the potential rigorous biomechanics research has to improve the care of women. It is now well accepted that biomechanics can assess the functional properties of the vagina and pelvic supportive structures by studying common risk factors including childbirth and menopause. Due to the relative infancy of this field it is obvious that much can be learned by simply translating and adapting concepts, techniques, and approaches that have already been established in other fields to the study of pelvic floor disorders. Certainly, the details may be different due to the relative

complexity of the pelvic floor and the enormous changes it must undergo throughout the reproductive cycle; yet, many of the same concepts can still be applied, as the pelvic floor is inherently a load bearing structure that must respond to physiologic forces and undergo significant deformation similar to many other tissues. In this way, a biomechanical perspective can help us to more clearly define what constitutes normal function of the pelvic floor, the changes related to pathology, and the impact of treatment. By doing so, the application of biomechanics will undoubtedly lead to changes in the management of urogynecological disorders in the same way it has done for vascular and orthopedic problems [24, 25].

1.2 ANIMAL MODELS OF THE PELVIC FLOOR

1.2.1 Background

While there is clearly much to learn regarding the biomechanics of the pelvic floor, a lack of significant progress thus far can at least be partially attributed to the difficultly of performing controlled, longitudinal studies in human patients along with the ethical issues surrounding the procurement of human tissue. This can be especially problematic in biomechanics research for which larger tissue samples are frequently required to perform experiments appropriately. Animal models, on the other hand, afford the opportunity to test hypotheses more rigorously in a controlled environment. In addition, by using an appropriate model, it is possible to examine healthy subjects in an attempt to distinguish the impact of a specific variable. Moreover, animals provide significantly improved access to tissue such that more detailed biomechanical

experiments can be performed. The following sections elaborate on the gross anatomical similarities and differences between these animals relative to humans including relevant information on the histomorphology of the vagina which follows a general overview of vaginal tissue and pelvic floor support.

1.2.1.1 Vagina and Connective Tissue Anatomy

The vagina is supported by a highly interdependent system comprised of striated muscle, smooth muscle, and connective tissue, which in turn provides additional support to the pelvic organs [10, 26]. This complex is often referred to as the pelvic floor. The striated muscle component, referred to as the levator ani muscle complex comprises the inferior most portion of the system and consists of the pubococcygeous, ileococcygeous and coccygeous muscles. Tonic contraction of the levator ani provides support to pelvic organs by acting as a shelf upon which the organs rest with anatomical interruptions to afford passage of the urethra, vagina and rectum. For conceptual purposes, the connective tissue support of the vagina in the female pelvis has been artificially divided into three levels of support. Level I provides support to the upper one-third of the vagina and is comprised of the uterosacral and cardinal ligaments. Level II supports the midvagina, and consists of lateral attachments of the vagina to the arcus tendineous fasciae pelvis (ATFP). Level III describes the support to the distal vagina consisting of the perineal body and perineal membrane. A detailed description of these levels of support has been previously described by DeLancey *et al.* [11, 12]. Current dogma generally assumes that both the levator ani and connective tissues are necessary for normal vaginal support of the pelvic floor in women [27]. However, one of the main differences between humans and every other animal is that humans are bipedal. In addition, humans have lost the need for a tail. Thus, as a

consequence of walking upright, the human anatomy appears to have adapted by recruiting the striated muscle, which is important for tail function in so many other species, to assist in resisting the downward forces on the vagina and its supportive connective tissues resulting from a combination of abdominal pressure and gravity [28, 29]. Thus, a load sharing relationship has developed between the connective tissue and striated muscle making both critical to the maintenance of normal vaginal support in humans.

As we will observe, many mammals appear to have analogous connective tissue support to the human (Levels I-III). However, the major anatomical difference between humans and other species appears to be the degree to which the levator ani muscles contribute to vaginal support. In animals with more bipedal behavior (e.g. Rhesus Macaques), the levator ani muscles appear to have a more important role in vaginal support than in quadrupeds (e.g. rat), for which the primary function of the levator muscles is movement of the tail [30]. Thus, when designing studies, it is important to recognize these anatomical differences and subsequently, whether the primary support to the pelvic organs is provided primarily by connective tissue or a combination of both muscle and connective tissue. Depending on the research question under investigation, the rat, despite its anatomical differences, may indeed be a better choice because it offers two opportunities: first to isolate the contribution of the connective tissue component and second to examine different risk factors (e.g. maternal injury or menopause). This emphasizes the importance of clearly defining the research question of a study, establishing objective criteria that an animal model must possess, and validating that the model satisfies those criteria in terms of its pelvic anatomy, histological appearance, biochemical constituents, and mechanics.

The supporting structures of the pelvic floor mentioned above are composed mainly of connective tissue containing fibrous elements (collagen and elastic fibers), proteoglycans (PGs),

and extracellular matrix (ECM) [31]. In addition, the supportive connective tissues contain a significant amount of smooth muscle. An understanding of connective tissue remodeling is of interest because it directly affects the mechanical integrity of the vagina and its supportive tissues [32].

The last supporting structure in the pelvic floor and the location of most surgical focus is the vaginal tissue. The vagina directly supports the urethra and bladder by maintaining their proper anatomical location and providing a backstop to help urethra function during voiding of the bladder. Patients suffering from prolapse often have displacement or descent of the vagina. This lack of vaginal support to the urethra and/or bladder can lead to the development of urinary incontinence [16]. Aside from the urethra, the vagina provides support posteriorly to the rectum and medially to the uterus. A deficiency in posterior support may lead to prolapse of the rectum into the vagina resulting in fecal incontinence [33]. To adequately perform its multiple functions the vaginal wall consists of four layers, which include the epithelium, subepithelium, muscularis and adventitia (Figure 1).

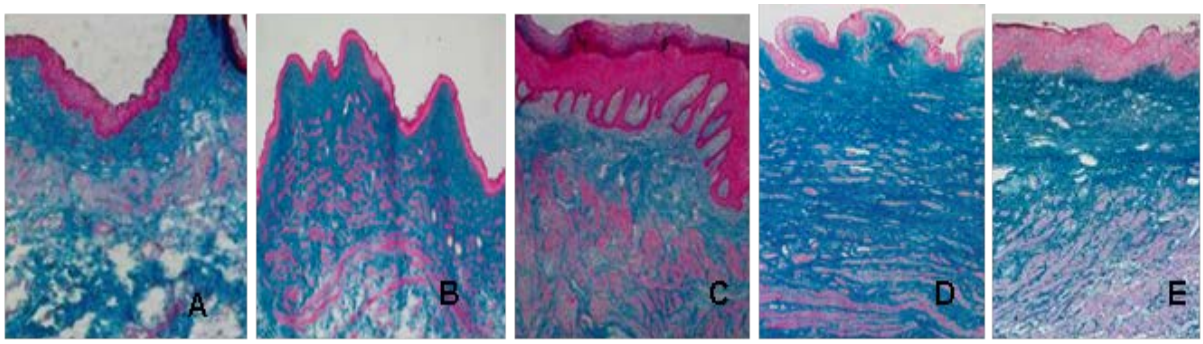

Figure 1 Histological trichrome images indicating the difference in morphology of the animal model, rat (A), rabbit (B), primate (C), sheep (D), with respect to humans (E). The thickness of the epithelium varies among the animal models and with respect to human, however, it is evident that the vaginal wall of the sheep (D), holds a high degree of similarity to the human vaginal wall (E) [34].

The epithelium is the first line of defense against infection. It is composed predominantly of squamous cells in various stages of maturation, which are constantly being replenished due to hormonal changes. The subepithelium lies beneath the epithelium and is a thin, dense collagen layer that provides a large degree of the passive mechanical integrity to the vagina. These passive mechanical properties play an important role in maintaining the integrity of vaginal support to the pelvic organs. The vaginal muscularis, a fibromuscular layer, lies directly beneath the vaginal subepithelium and provides active support to the vagina along its longitudinal and circumferential axes [11]. The muscularis is often plicated via gynecologic surgery to repair prolapse of the bladder or rectum into the vaginal canal. Finally, the adventitia is a loose connective tissue layer shared with the bladder anteriorly and the rectum posteriorly.

1.2.2 Rodent

Currently, rodents are the most widely used animal model for prolapse and incontinence research. While both rats and mice are small, they are inexpensive and easy to work with in large numbers. In addition, mice have the clear advantage of affording the option of working with transgenic knockout animals. Rats have oestrus cycles that last for four days, and undergo gestation for 21-23 days before delivering litter sizes that can range from 4-25 fetuses [35]. Mice have shorter oestrus cycles with a duration of 2-5 days depending on environmental factors [36]. In this way, both rats and mice allow for evaluation of processes that would normally take a longer time in more evolved species. Additionally, aged rodents undergo a decrease in the release of sex hormones similar to menopausal women. This has proved advantageous for

questions concerning how menopause and the sex hormones may affect the properties of the pelvic floor [37].

Anatomically, the gross connective tissue anatomy of the rodent pelvis is similar to that of humans [30]. The rodent pelvis has uterosacral ligaments that also attach the upper vagina to the lower spine. Paravaginal attachments from the distal to the proximal vagina insert on a dense band of connective tissue extending from the pubic symphysis to the lateral bony pelvis that serves a role similar to that of the ATFP in humans. The similarity between the structure and function of the vaginal connective tissues in rodents and humans makes the rodent a preferred model when evaluating connective tissue support. However, as mentioned, the anatomy of the vaginal muscles is quite different in the rat. Although the levator ani (pubocaudalis and iliocaudalis muscles in the rat) are present in rodents and humans (Figure 2), the primary function of these muscles in the rodent seem to be to support the tail, while the connective tissue attachments serve as the vaginal support in humans [30].

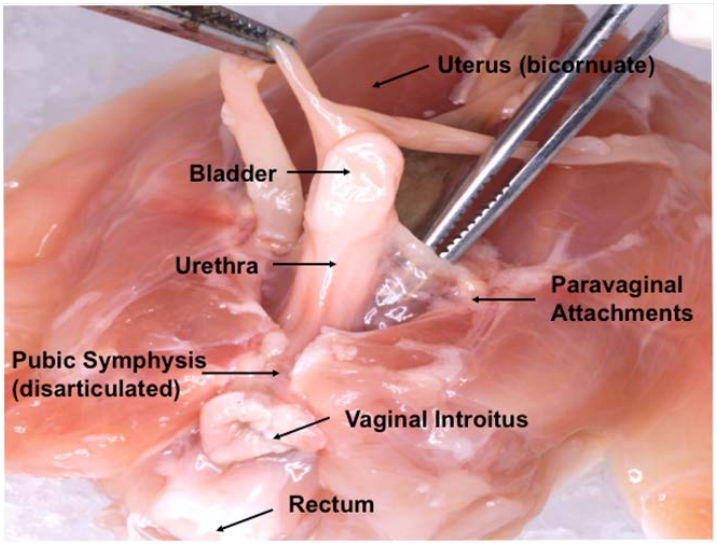

Figure 2 An anterior view of the pelvic anatomy of the rat. The pubic symphysis has been split open to provide a better view of the vagina. As indicated in the figure, the rat's vagina contains paravaginal attachments to the ATFP, uterosacral ligaments and distal attachments to the pubic symphysis all of which provide support to the vagina. The location of the other pelvic organs have also been identified with arrows [30]

Conversely, the small size of rodents, the difference in posture, and the small size of the fetus, collectively make prolapse unlikely and renders the rodent model undesirable for studying the direct development of prolapse. However, recent developments of several transgenetic mouse models have shown that these mice can develop prolapse spontaneously [38, 39]. Although the mechanism may not be the same as the natural progression and development of prolapse, it is a way to utilize a smaller animal model to begin to understand changes that occur during prolapse, which are described more elaborately in later sections.

1.2.3 Rabbit

The rabbit model has many of the same advantages of the rodent, with the added benefit of being a larger model, which allows for larger tissue acquisition and improved access to the vagina transperineally. Rabbits, however, do not have an oestrus cycle in which ovulation occurs spontaneously, but require induction of ovulation via vaginal stimulation (i.e. coitus). Their gestation period is approximately 31-35 days.

In addition, the vaginal anatomy of the rabbit is exceedingly different. The vagina of the rabbit consists of two parts, an intra-adominal cephalad portion and a caudal/retroperitoneal external portion. The cephalad portion is roughly twice as long as the external portion; it directly communicates with the uterus, has no adjacent supportive connective tissues and is histologically more similar to the small bowel in humans than it is to the vagina. The caudal/external portion of the vagina is easily accessible; however, the entire length of the anterior external vagina contains the body of the clitoris making it difficult to access tissue for analysis.

Like the rodent, the rabbit does not incur significant maternal injury during vaginal birth and does not develop spontaneous prolapse. The differences in anatomy make it difficult to study the effects of various risk factors of prolapse on the remodeling of the connective tissues, and subsequently the vaginal wall. The rabbit has been used, however, in studies aimed to evaluate prolapse meshes applied to the external posterior vagina using anatomical, histological, biochemical and biomechanical outcomes discussed later [40].

1.2.4 Sheep

Interestingly, the sheep has been evolving as a model for evaluating prolapse, however, more research on this model is needed. Similar to the rabbit, this animal model allows for easier access to the vaginal tissue with increased tissue quantity relative to the rodent models. The sheep oestrus cycle is 17 days long, which is more similar to that of humans than rabbits, and the average gestation is 147 days. Advantages of the sheep model are that they are inexpensive, available in large numbers, are an established reproductive model for humans, have prolonged labors with relatively large fetuses in which dystocias are common, and they spontaneously develop pelvic organ prolapse related to pregnancy and vaginal birth [41-47]. Indeed, similar to women, uterovaginal prolapse occurs commonly in sheep (8 -12%; [42]). Predisposing factors are also similar to those affecting humans including increased intra-abdominal pressure, intra-abdominal fat, advancing age, multi-fetal gestation, and history of uterovaginal prolapse [42].

The pelvic connective tissue anatomy of the sheep is similar to that of the macaque and human with three primary levels of support and it is amenable to prolapse repairs (abdominal and

vaginal) and mesh implantation. In these ways the sheep model is surprisingly similar to humans and may be an appropriate alternative to the more expensive and less accessible primate model.

1.2.5 Nonhuman Primate

Nonhuman primates (NHPs) are considered to be the experimental model for pelvic organ prolapse that is most similar to humans [29, 48, 49]. Indeed, the rhesus macaque is an old world primate that shares similar gross and microanatomy, as well as reproductive physiology with humans. They have similar reproductive cycles and parturition practices, similar estrogen and progesterone responsive supportive tissues, and similar tendencies to spontaneously develop pelvic organ prolapse related to vaginal delivery (Figure 3) [29, 48].

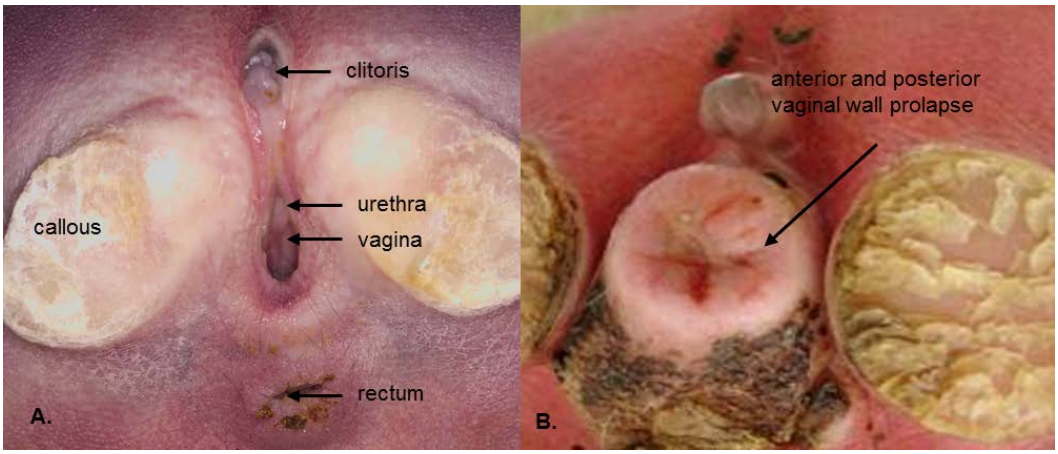

Figure 3 (A) Perineal view of normal rhesus macaque anatomy. Callouses appear secondary to prolonged sitting. (B) Anatomy of animal with prolapse demonstrating descent of the anterior vaginal wall with prolapse of the bladder, the posterior wall with prolapse of the rectum and apical descent of the uterus (not shown) [34].

The rhesus gives birth after roughly 164 days of gestation to infants with relatively large heads requiring a roughly 5-fold increase in vaginal diameter with considerable straining for

expulsion of the fetus. Thus, they generally incur significant maternal injury during the birthing process which is similar to humans [50]. Anatomically, they have a marked connective tissue condensation that serves as a lateral vaginal attachment and apical attachment of the vagina. Similar to humans, the dense condensation of connective tissue is also seen paravaginally, attaching the vagina to the levator ani complex, via the ATFP (Figure 4). As in humans [11, 51, 52], accelerated remodeling of the ATFP has been shown to be associated with prolapse of the anterior and posterior vaginal wall of primates [48]. NHP levator ani muscles consist of the iliocaudalis (IC), pubocaudalis, and puborectalis muscles, which have analogous function to the iliococcygeus, puboccygeus, and puborectalis muscles in humans.

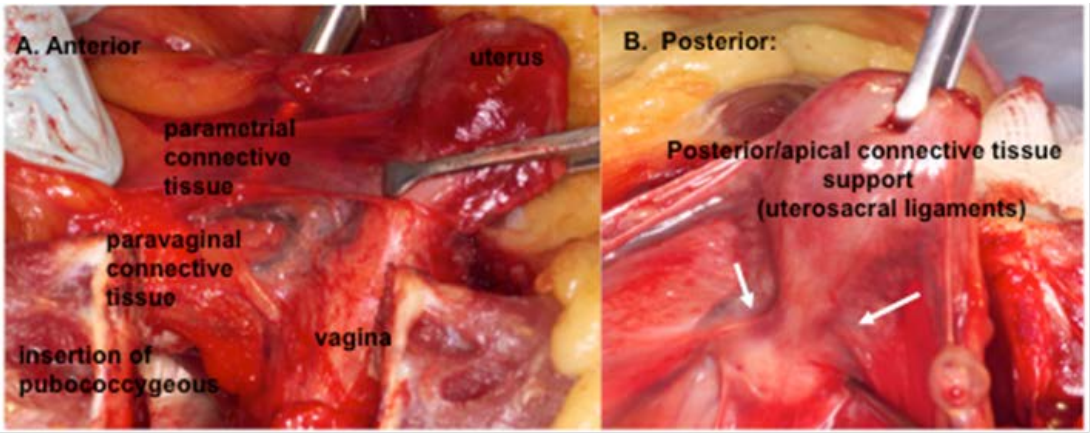

Figure 4 Anterior and posterior views of the non-human primate pelvic anatomy. The anatomy is similar to humans with uterosacral ligaments, paravaginal attachments to the pelvic sidewall and insertion of the pubococcygeous into the distal vagina [34].

The longer gestation periods of the nonhuman primate and large fetal size enable studies on the effect of pregnancy and delivery, on the development of prolapse. The effect of gravity can also be evaluated in rhesus macaques since they have a more upright posture. We have observed that, similar to humans, following recovery from vaginal delivery, there is a distinct increase in vaginal and supportive tissue laxity that appears to persist long-term.

Squirrel monkeys have also gained widespread use since they have a pelvic anatomy that is quite similar to humans. Squirrel monkeys are new world monkeys with a large term fetus, but they do not have similar reproductive cycles (no menstruation), and their posture is quite different. Their pelvis is usually suspended above the ground when sitting, thus increasing the strain on it [49]. The frequent stress applied to the pelvic floor may put them at higher risk for developing prolapse, than humans. Nonetheless, these animals have been useful in answering some important research questions. For example, DeLancey *et al.* compared levator ani defects in magnetic resonance imaging (MRI) images from women with and without prolapse and found that 55% of women with prolapse had measurable defects [21]. Pierce *et al.* challenged the levator injury model in a well-controlled animal study in which the levator ani nerve of nulliparous squirrel monkeys was ablated via an excisional biopsy [53]. Interestingly, although all of the monkeys with ablated nerves had evidence of marked levator atrophy by MRI, none developed pelvic organ descent; thus, challenging the central role of levator injury in the pathogenesis of prolapse.

1.2.6 Knowledge Gap

There are several similarities and differences between commonly used animal models in urogynecology including the rodent, rabbit, sheep, and nonhuman primate. It is important to comprehend the differences between these animal models, specifically those directly related to prolapse development: menstrual patterns (hormonal), gestation periods, and the ratio of fetal head to vaginal diameter.

Vaginal delivery, or parity, is cited as a major risk factor for the development of prolapse. Earlier work has shown that after one or two vaginal deliveries a woman increases her risk for prolapse by 4 and 8 times respectively [54]. Research on ligaments, tendons, and other biological soft tissues has shown that injury to these tissues often results in a decrease in the collagen I/III or collagen I/(III+V) ratios and biomechanical properties of the tissue [55-57]. Consequently, women who have developed prolapse display similar symptoms to those of a degradation or injury response including a decrease in the collagen I/III ratio, altered biomechanical properties, and modified matrix metalloproteinase (MMP) activity [51, 58-61]. It is important to note that although parity is often regarded as the largest risk factor for the development of prolapse, it often does not become symptomatic for another 20-30 years after the time of delivery. Parity may be an initial incident that leads to a decrease in the collagen I/III ratio and altered activity of the degradation enzymes that predispose the vaginal tissue to prolapse. Therefore, many clinicians advocate the need for a permanent surgical option to help provided continued support because the vagina and other supportive structures no longer can support the pelvic organs.

Studying the vaginal mechanical properties of commonly used animal models prior to and after vaginal delivery can provide insight into the native function of the vagina. However, minimal research has been done on vaginal biochemical and biomechanical properties. Furthermore, examining these animal models can help us assess the effect of parity on the biomechanical properties of the vaginal wall. Further, we can assess how the vaginal biomechanical properties of these animal models compare to those of parous women who typically undergo prolapse repair. Therefore, we need to improve our understanding of the

maternal adaptations required for delivery of these animal models and determine how vaginal delivery may set the stage for the development of prolapse later in life.

1.3 PROLAPSE REPAIR

1.3.1 Surgical treatment

Roughly 225,000-280,000 women undergo corrective surgery for pelvic floor disorders [8, 9]. A woman has about an 11% chance of requiring at least a single surgery for prolapse or incontinence treatment and is often performed with a graft augmentation [62]. Synthetic meshes are commonly used in most urogynecologic procedures including sacrocolpopexy, sub-urethral slings, colposuspension, and anterior and posterior repairs. A recent web-based survey of the surgeons of the American Urogynecological Society revealed that 93% of respondents use some form of synthetic mesh when performing a sacrocolpopexy and 58% when performing vaginal reconstructive surgery [63]. There is consistent and robust evidence supporting the use of synthetic mesh in an abdominal approach with sacrocolpopexy [64]; however, data supporting the use of synthetic material in vaginal reconstructive surgery is limited to case series and observational studies [65, 66]. Biochemical data and clinical experience suggests that the endogenous tissues of women with prolapse are weaker [67, 68] and therefore, prone to failure. Thus, clinicians who advocate the use of mesh aim to improve the permanency and success of reconstructive procedures that currently have a failure rate in excess of 30% [5].

A wide range of biomaterials are available to clinicians for incontinence and prolapse procedures with little quantitative data on which to base the selection of a particular material. Although limited data suggests that in terms of anatomical [69] and biomechanical [70] outcomes, synthetic polypropylene (PP) meshes are superior to biologic meshes, there is significant evidence that the complications associated

with synthetic meshes can cause serious morbidity including infection, erosion, exposure, and pain [69, 71]. In addition, the vaginal tissue to be augmented is often structurally compromised, atrophic and devascularized. Such poor tissue quality increases the risk of poor tissue incorporation into the mesh potentially resulting in suboptimal healing and mesh exposure or erosion into an adjacent tissue. Erosion can be defined as the mesh wearing, or slowly grinding through the vaginal wall. This is a serious complication and moreover, there is evidence that meshes shrink *in vivo* leading to increased stiffness, pain and poor restoration of the normal properties of the vagina [70]. These complications commonly lead to a sizeable decrease in the quality of life for patients and are thought to be related to a mismatch between the vagina and meshes biomechanical properties. For example, a discrepancy in stiffness of the vaginal wall and mesh properties are believed to be the root cause of the morbidities observed from these surgical repairs. In this way, the choice of the appropriate mesh for surgical augmentation is exceedingly important.

1.3.2 Synthetic Biomaterial Considerations

These synthetic meshes are currently intended as permanent implants to help alleviate prolapse symptoms, however with the large number of complications and failures it is clear that the ideal graft has yet to be discovered. The complications associated with these grafts can largely be attributed to the lack of knowledge about the host tissues at the implantation site along with the response of the host to the graft material. When introducing a graft material into a patient there is a response paradigm to the foreign material. The body must react simultaneously to an injury due to the surgical dissection and to the graft material. Briefly, the host reaction includes inflammation, granulation formation, foreign body reaction, encapsulation, and possibly an immunologic response [72]. Inflammation is a nonspecific response to the surgical injury and

graft material. The main purpose of inflammation is to begin the healing process by neutralizing and isolating the injured areas or foreign materials. Generally, there is acute and chronic inflammation response to implanted materials. Each stage of inflammation has a specific duration and is associated with certain cell types (i.e. neutrophils and macrophages) and is important for sending signals to the body for forming granulation tissue and the eventual encapsulation of the graft material [72]. After inflammation the body begins to form granulation tissue, which is loose connective tissue at the site of an injury. Lastly, the foreign body reaction begins to encapsulate the graft materials via macrophages and foreign body giant cells [72]. This fibrous encapsulation is designed to isolate the host from the graft materials for the duration of the implant.

Each stage of the host response (e.g. acute or chronic inflammation, granulation formation etc.) can vary in length and intensity depending on the extent of the injury sustained during implantation, the local loading and chemical environment, and the graft material. The graft's physical properties (structural or mechanical properties), chemical interaction, and material properties can also affect inflammation [72]. Here, we will focus on the characteristics of the meshes and how they influence the host response. To date, graft materials used in prolapse repair are largely based on those successfully used for abdominal hernia repairs. As previously mentioned most synthetic prolapse meshes are made with polypropylene which has been shown to be mainly chemically inert within the body; however, these synthetic graft materials may differ by composition (monofilament vs. multifilament), pore size, surface properties (coated vs. non-coated), and architecture (knit vs. woven). Meshes are often classified based on several of these characteristics to provide an idea of how they will perform after implantation. A recent classification system is shown in Table 1.

Table 1. Classification of synthetic meshes

Type	Properties	Pore Size
I	Macoporous	>75 µm
Ia	Lightweight	< 50 g/m^2
Ib	Heavyweight	>50 g/m^2
II	Microporous	< 10 µm
III	Macroporous and Multifilament	>75 µm
IV	Composite Mesh (Absorbable and Non-absorbable components)	>75 µm
V	Bonded Mesh	< 10 µm
VI	Submicronic	N/A

In short, previous clinical and experimental research has shown that macroporous, lightweight, monofilament and knitted fibers (Type Ia) materials have a better host response and fewer complications. The overall inflammation and foreign body response has been shown to be different between monofilament and multifilament materials [73]. Monofilaments often create less of a foreign body reaction and have lower rates of infection both of which are desired to reduce complication rates post-operatively. Due to the small gaps between the fibers in a multifilament mesh host cells often times cannot penetrate the mesh and removal of the entire graft is required [74]. This complication can also be influenced by the pore size of the mesh, and the classification of the pore size of meshes is dichotomized as >75 µm (macroporous) or < 10 µm (microporous). Microporous materials can, similar to multifilament fibers, harbor infections because of the inability of the native cells to access these areas [72]. Pore size, along with specific weight, also plays an important role with mesh incorporation within the tissue. It has been shown that larger pore sizes facilitate tissue ingrowth and tissue incorporation [74-76]. However, it should be noted that if the mesh has pores that are too large (> 5 mm), the tissue may not incorporate as quickly or as well [72]. Specific weight, or density, has been shown to affect

the inflammatory response [74-78]. However, recently there has been a further sub-division based on the specific weight of these meshes. Heavyweight is comprised of 70-100 g/m^2, mid-weight is between 40-60 g/m^2, and lightweight meshes are defined from 20-30 g/m^2. The last addition to the defined weight spectrum, which applies to several new generation meshes, is the category of ultra-lightweight meshes (<20 g/m^2). Lastly, the stiffness of the material has been linked to clinical complications with stiffer materials correlating to a higher complication rate [79, 80]. The current trend is for lightweight meshes (<50 g/m^2) and less stiff meshes to be used during prolapse repair to induce a lower inflammatory response relative to heavier meshes.

In summary, a Type Ia, large pore, monofilament mesh is the preferable synthetic material [69, 71, 81-83]. The goal of a synthetic mesh is to improve the durability of a prolapse repair by increasing tissue strength with the least amount of burden on the host tissue. In general, it is thought that knit, monofilament, lighter specific weight, larger pore size, decreased stiffness, and overall increased porosity are associated with improved host tolerability and consequently lower rates of exposure, erosion and infection.

1.3.3 Previous Research

Interestingly, several of these hernia meshes have been adapted for use during pelvic floor reconstruction. A separate study examined six synthetic meshes used during hernia repair, of which Infinit, UltraPro, and Prolite are all additionally used in urogynecological procedures. This study illustrated that each of these meshes, excluding one (Dualmesh), displayed some degree of anisotropic behavior, or these meshes were found to not be isotropic. Each mesh had significantly different structural properties dependent on the loading axis [84]. This data from

this study suggested that the anisotropic nature of these meshes may affect the clinical success rate of implantation; therefore it should be characterized to better understand the functional properties of commonly used meshes.

While, the main focus of evaluation of synthetic materials used in urogynecological procedures has been the pore size and specific weight, recent studies have indicated the importance of mesh structural properties (e.g. stiffness) on the clinical outcome [77, 79, 80, 83]. One study examined the biomechanical properties of 4 commonly used full length prolapse meshes: [Gynecare PS^{TM} (Ethicon), Pelvitex ^{TM} (Bard), Popmesh^{TM} (Mpathy), Timesh ^{TM} (Caldera), and Polyform ^{TM} (Boston Scientific)] [80]. With the exception of Popmesh which displayed a uniform stiffness throughout the test, meshes were characterized by bilinear behavior with a very low initial stiffness that increased by an order of magnitude after transitioning into a region of higher stiffness. Relative to Gynecare PS^{TM}, these prolapse meshes were significantly less stiff than the Gynecare PS^{TM}, with irreversible deformation at significantly lower loads [80]. This biomechanical behavior may be an important factor to consider when balancing the opposing effects of increased mesh stiffness to resist excess loading in the early postoperative period versus a low stiffness to afford increased compatibility with tissue properties following tissue incorporation.

This wide range of structural properties of polypropylene materials has also been observed in urinary incontinence slings. Two studies examined different slings under uniaxial tension and again found a bilinear response to the deformation [83, 85]. Additionally, Afonso *et al.* examined the flexural stiffness under a tae ring test [85]. Both of these studies further indicate that these frequently used polypropylene materials often display significantly different structural properties under variable loading conditions.

Developing a good constitutive model of polypropylene is important for actuate simulation and predictions of the FEM [86-88]. Early work on polypropylene has been to develop constitutive models of single polymer fibers [89, 90]. Most of these models have to assume a semi-crystalline form and similar to biological tissue follow the general hyperelastic form. Several studies have modeled the tissue under uniaxial tensile loading, which is suitable given homogeneous and isotropic assumptions of propylene [90, 91]. However, many of these studies are interested in repeated loading and the effect of temperature on the polymer. Assuming a constant temperature and pseudoelasticity and given the assumptions of polypropylene in all of these studies a simple isotropic constitutive model may be utilized.

Previous work has been invested to develop FE models of synthetic meshes used in hernia repair [92]. For specific formation of a constitutive model three approaches were taken, validated, and evaluated on their ability to predict the meshes response from one loading condition to another. Two continuous and one discrete model were utilized to evaluate different constitutive models: 3rd order reduced polynomial, Rubin-Bodner, and discrete mesh geometry model. Due to the assumptions required for the 3rd order reduced polynomial of homogeneity, isotropic, fiber alignment, and no interaction between the fibers the Rubin- Bodner and discrete model produced the best fits. Previously, the Rubin-Bodner model allowed for the incorporation of different families of fibers. Two perpendicular fiber families have been used to describe the mesh and could fit the data from a uniaxial test; however, was not able to be validated against uniaxial tests in the transverse direction of a stamp test. Discrete modeling of the synthetic meshes has, at least thus far, been shown to be the most reliable means to model mesh behavior [92]. This model design allows for accurate representation of the mesh geometry and can

describe the general anisotropic behavior due to the mesh interactions using the simple 3rd order reduced polynomial constitutive law.

1.3.4 Gap in knowledge

In light of the previous studies, there is a clear need to collect scientific data on newly developed synthetic meshes used for urogynecological procedures. Characterization of the *ex vivo* structural properties and other textile properties (e.g. pore size, multi- vs. monofilament) of these meshes has already significantly improved our understanding of how meshes relate to clinical complications after implantation [74, 76, 77, 80, 81, 93, 94]. However, with the designing and manufacturing of a newer generation of synthetic meshes for urogynecological procedures there is an increased demand for researchers to better characterize the structural properties prior to patient implantation. The textile and structural properties of these synthetic grafts can have a significant impact on the host response. Based on the current classification system, the majority of widely used urogynecological meshes (e.g. Gynemesh, UltraPro, SmartMesh, Novasilk, and Polyform) are considered Type Ia. Again, this simply means that each mesh is macroporous (>75 μm) and lightweight (<40 g/m^2); however, previous research has shown us that the anisotropic behavior and structural properties can be significantly different between these Type Ia materials. Therefore, a more mature characterization beyond Type Ia is required to increase the knowledge of how these materials behave *in vivo*.

Although characterization of these meshes can improve our understanding of why particular meshes succeed and others fail after manufacturing, it is important to consider and understand how changes in the textile and structural properties may improve clinical outcomes

and be used to guide the production process. It is then possible to see how the development of constitutive and finite element (FE) models of these meshes would be greatly beneficial as shown in other biomechanical areas [86-88, 95-101]. Accurate modeling of the mesh material *ex vivo* may be able to better guide production and lead to a better clinical outcome for women. Although previous work has been done on the modeling of polypropylene meshes, these models are often complex and offer limited insight into what dictates the structural properties of these meshes. Therefore, a more detailed characterization, specifically of polypropylene meshes used in prolapse repair, accompanied by constitutive modeling is required. In general, the degree of connectivity, or overlapping fibers, the location of local stress and strain increases, and the overall mesh fiber orientation can be examined through modeling. An accurate modeling program would be advantageous in addressing complicated questions including how fiber interaction affects the stiffness of the material.

1.4 ANIMAL MODELS OF MESH IMPLANTATION

1.4.1 Background

Ex vivo testing of these meshes is valuable, but clearly it is not enough to understand the complex behavior after implantation. To adequately test these grafts, both *ex vivo* and *in vivo* studies are necessary. For studying *the in vivo* properties of these synthetic materials, it is extremely important to examine animal models that are most beneficial for evaluating the current problem. For example, the animal model should behave similarly to humans either anatomically

or biochemically [72]. Anatomical parallels expose the graft material to a similar loading environment and surrounding tissues and can make the results easier to interpret and more clinically translatable. However, it is often difficult to mimic all human physiological locations in an animal model. Therefore, it is advantageous to examine animal models that parallel the human host response through biochemical reactions to the synthetic graft. This can provide valuable information on how the graft is incorporated into the native tissue.

Several things to consider when utilizing an animal model are the vascularity, macrophages and fibrous encapsulation potential, and mechanical stresses or strains of the implantation site [72]. If an implanted graft is continuously loaded and deformed during the encapsulation process, it may lead to a different healing response. Examining how the tissue incorporates into the mesh and forms a mesh-tissue complex can be evaluated through a number of methods. First, the overall relative incorporation can be examined through histology or histochemistry. To quantify tissue ingrowth, biochemistry of total collagen or collagen sub-types may be performed; and to examine function of the mesh-tissue complex, mechanical testing is often utilized. This dissertation is primarily focused on examining the mechanical properties of the mesh-tissue complex; however, it is important to highlight other areas of research that warrant investigation.

1.4.2 Previous Research on of the Tissue-Mesh Complex

Currently used animal models used for synthetic prolapse mesh implantations include the rodent, sheep, and rabbit [34, 44, 46, 70, 78, 102-106]. A study examined the use of the sheep and rabbit for vaginal mesh models, and found that both were of suitable size for surgical implantation of

graft materials. Interestingly, in their small sample size they observed erosion of the mesh though the epithelium [105]. However, this is not always true with future studies. Using the rabbit model a polypropylene mesh and cross-linked porcine dermis were shown to behave similarly in the short-term stiffness values; however, the porcine dermis degraded over time and cannot offer long-term support to the vagina or surrounding structures [107, 108]. These results have suggested that for tissue that may already be mechanically inferior, the use of synthetic meshes is most likely required. Following studies in rodents and rabbits examined the effect of several synthetic meshes and concluded that monofilament and macroporous characteristics were required for adequate host integration [40, 74, 78, 104].

A large degree of research has examined the effect of heavy-weight, mid-weight, and light-weight polypropylene meshes with large and small pore sizes for abdominal hernia repair [74-78, 107]. Utilizing the rodent model, investigators found that both heavy weight and light weight mesh implantation resulted in a chronic inflammation with a lower fibrotic response, but the light weight mesh had a higher degree of tissue integration relative to the heavy weight mesh [74, 76]. Klinge *et al* went on to illustrate that the mobility of the light weight mesh was greater as compared with the heavy-weight mesh. A separate analysis of hernia repaired abdominal walls of New Zealand white rabbits found similar trends with several different meshes. Most notably the UltraPro mesh, also commonly used in urogynecological procedures, was found to have a larger amount of tissue incorporation and increased levels of mRNA for collagen I and collagen III compared to heavy-weight or smaller pore size mesh materials [75]. A functional study was performed by Cobb *et al.* to examine the *ex vivo* ball-burst properties of Marlex, Prolene Soft (Gynemesh), and UltraPro in the porcine abdomen [77]. Marlex is a heavy weight mesh while Gynmesh and UltraPro are both considered light weight meshes based on the earlier

described classification system. Of these three meshes, Gynemesh and UltraPro are meshes that are often used during urogynecological procedures. This study found that after implantation the light weight polypropylene mesh may best resemble the compliance of the abdominal wall and lead to lower complication rates [77].

Studies interested in prolapse, due to vaginal size, have continued to implant these meshes via the abdominal model. Skin tends to be thicker and keratinized compared to vaginal tissue, and in the rabbit model, a group found that the vagina had a higher rate of inflammation and neovascularization but lower fibroblast proliferation when compared to abdominally placed meshes. Although differences were found between vaginally and abdominally placed meshes, valuable information (i.e. rejection, incorporation) can be obtained from abdominal studies. A study showed that after 90 days mature connective tissue was present with little bacterial formation. Another study showed no significant increases in the number of macrophages, polymorphonuclear cells, and blood vessels after infection as it was observed that short term results invoked the body's response to the foreign substance but the response decreases overtime [109].

To study the biomechanical properties of synthetic meshes that have been implanted *in vivo,* a number of different approaches have been taken [60, 77, 104, 110, 111]. Several studies examined how the tissue-mesh complex behave under uniaxial tension and have shown that after abdominal placement of several urogynecological meshes, these meshes maintained their stiffness overtime. A study on abdominally placed meshes in the rodent model utilized a scaled down version of an American Society for Testing and Materials (ASTM) standard ball-burst test [111]. Similarly to previous studies, the limitation of the rodent model is the amount of material able to be implanted; therefore, Horan *et al.* developed a modified ball-burst test which has

shown reliable and repeatable results within their study [111]. They showed that stiffness and load of the mesh was maintained from 1 to 3 months after implantation. Although this is early work, the development of a modified ball-burst test allowed for experimental testing under more realistic physiological loading of the tissue-mesh complex, and could be utilized to understand how these materials behave together.

1.4.3 Gap in Knowledge

These studies have greatly contributed to the knowledge in the urogynecological field; however, it is important to consider many different factors when utilizing animal models. Additional research is necessary to understand how the *ex vivo* textile and structural properties connect to the tissue in-growth and the overall host response. Animal models have proven invaluable in performing these rigorous mesh implantation studies. As illustrated in the previous section, a unique host response can be observed based on the location of implantation (vagina vs. abdomen). Even though these studies have provided a general insight into the host response of synthetic grafts histologically and biomechanically, a more in-depth understanding is required.

The current lack in understanding of how prolapse meshes affect the biomechanical properties of the grafted tissue has led to the high rate of complications and the recent Public Health Notification from the FDA. Utilizing a similar abdominal model it is possible to evaluate new generational meshes in comparison to previously published literature and the abdominal approach permits the use of multiple animal models for larger scale studies. Aside from locational differences on the host response, a second important consideration is the potential differences in biomechanical properties between the different species. Lastly, for

urogynecological studies examining vaginal implantation it is important to consider how parity, or vaginal delivery, impacts the biomechanical properties of vaginal tissue. Although studying the effects of meshes implanted in the abdominal wall, is useful it is ideal to employ the use of an anatomically and physiologically similar animal model. These similarities allow us to perform clinically relevant surgical procedures on animal models to improve our understanding of how these graft implantations affect the function of vaginal tissue. These studies have the potential to greatly impact the field and clinical practice.

1.5 MOTIVATION AND SPECIFIC AIMS

As previously described, the vagina, when properly supported, helps support the bladder, urethra, uterus, and rectum. However, when changes to the vagina occur or its support breaks down the organs begin to protrude into the lumen of the vagina towards the hymen. In the worst instances, the vagina will invert and begin to protrude beyond the hymen outside of the body. Vaginal wall laxity has been associated with the development of urinary and fecal incontinence due to a lack of structural support. Prolapse is also associated with pain, dyspareunia, social isolation, and an overall reduction in their quality of life. Parity, or vaginal delivery, is a considerable risk factor in the development of prolapse. Parous women often present with a greater degree of vaginal wall laxity compared to nulliparous women though the cause and mechanism are unknown [7]. Knowledge on principle vaginal properties and parity's effect on vaginal tissue is fundamental in understanding how vaginal delivery can set the stage for pelvic floor disorders later in life.

Therefore, to gain insight into the effects of parity on vaginal tissue each commonly used animal model needs to be examined.

Based on previous studies and clinical experience, women with prolapse are believed to have weaker and/or more distensible pelvic supportive tissues, which are therefore prone to failure. This concept has led to the use of synthetic meshes for the surgical repair of prolapse to replace the loss of structural integrity that is no longer present [65]. Indeed, there is consistent and robust evidence supporting the widespread use of synthetic meshes for prolapse repair [64]. However, there are also a number of common complications due to mesh implantation. Briefly, these complications are similar to those associated with prolapse (pain, dyspareunia, and decreased quality of life), but also include erosion of the mesh through the vagina, infection, and recurrence of prolapse. These frequent complications have led to a Public Health Notification issued by the Food and Drug Administration (FDA) in 2008 about the use of synthetic meshes for prolapse surgery. Under the current material classification system, most widely synthetic meshes are lightweight, macroporous polypropylene material even though they differ greatly in pore size, knit pattern, and surface characteristics. In-depth characterization of mesh textile properties (i.e. porosity, and anisotropy) and structural properties would improve our knowledge of these meshes *ex vivo* properties prior to implantation.

Additionally, models of these meshes may be used to distinguish how the textile and structural properties affect the load-elongation behavior prior to implantation. Validation of these models may be useful in guiding the design of future meshes by improving our understanding of what predicts the structural response. Future models would also provide insight into the mesh-tissue complex through finite element analysis. These types of models will eventually be ideal for understanding the properties and interaction of the mesh-tissue complex

leading to an increased understanding of how *ex vivo* properties can impact *in vivo* properties. A major problem with the current prolapse meshes is that they are based on devices used for hernia repair of the abdomen, which were developed prior to the 1976 Medical Devices Amendment Act. This states that all medical devices established prior to the afore-mentioned act can avoid undergoing strict pre-clinical testing. Therefore, little work has been done to determine how the different *ex vivo* characteristics of these meshes (e.g. stiffness or porosity) affect the functional properties of the grafted tissue after implantation. In this dissertation, I hope to address some of these issues by examining the effect of parity on the mechanical properties of commonly used urogynecological animal models to identify a suitable model for mesh studies. Also, I intend to examine several different material characteristics (e.g. uniaxial stiffness, relative elongation, burst-load, and burst stiffness) between commonly used prolapse meshes *ex vivo*, and how these different material characteristics affect the incorporation of these meshes into a native tissue. Lastly, this dissertation will develop a finite element model that will characterize the uniaxial tensile properties of these synthetic meshes.

Specific Aim 1) To characterize the mechanical properties of vaginal tissue from nulliparous and parous animals utilizing the rodent, non-human primate, and sheep

1. To assess the effect of parity on the vaginal wall by examining the differences between the collagen I/III ratio and uniaxial biomechanical properties between nulliparous and parous rodents, sheep, and nonhuman primates.

Specific Aim 2) To characterize the *ex vivo* textile and structural properties of five commonly used synthetic prolapse meshes

2.a. To compare several textile properties including pore size, specific weight, porosity and degree of anisotropy between Gynemesh, SmartMesh, UltraPro, Novasilk, and Polyform

2.b. To characterize the uniaxial tensile (e.g. ultimate load, relative elongation, uniaxial stiffness, permanent deformation) and ball-burst (e.g. burst load, stiffness) properties of commonly used synthetic meshes. Furthermore to determine how these structural properties correlate to the textile properties from Aim 2.a.

Specific Aim 3) To examine meshes with varying uniaxial stiffness values (Gynemesh, SmartMesh, and UltraPro) and evaluate the functional biomechanical properties of the grafted mesh-tissue complex relative to native tissue

3.a. To examine and compare the commonly used abdominal model for mesh incorporation by assessing the tissue contribution to the mesh-tissue complex via a modified ball-burst protocol (e.g. estimated tissue stiffness and burst load) in the rodent and non-human primate.

3.b. To characterize the tissue contribution to the mesh-tissue complex of three synthetic meshes after vaginal implantation via an abdominal sacrocolpopexy procedure utilizing the nonhuman primate model.

Specific Aim 4) To develop and fully characterize a constitutive model of commonly used synthetic mesh material

4.a. To develop and validate a constitutive model to describe the structural properties of a synthetic mesh undergoing a simple uniaxial tensile test by predicting the load response to a specific level of displacement.

4.b. To perform an in-depth analysis of each mesh's fiber architecture through characterization of the fiber diameter distribution and pore size aspect ratio.

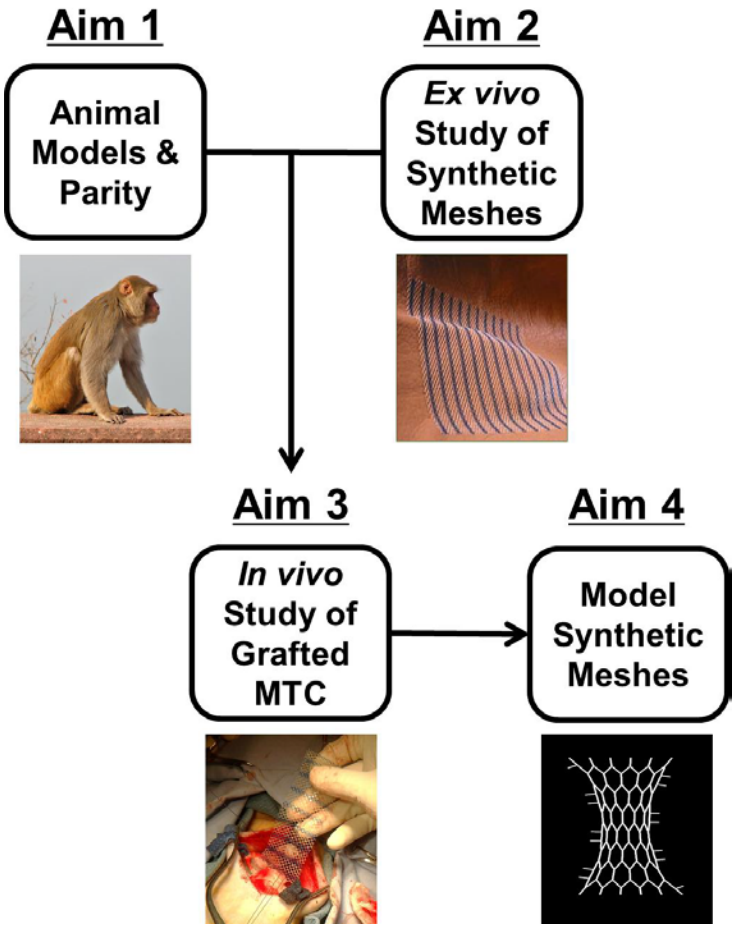

Figure 5 Overview of the dissertation aims and designs.

2.0 EVALUATING ANIMAL MODELS FOR PARITY

2.1 OVERVIEW

Treatment of symptomatic prolapse often requires surgical repair. Prolapsed vaginal tissue is considered prone to failure and therefore clinical practice advocates the need to augment prolapsed tissue with a permanent synthetic mesh to restore lost support. Epidemiological evidence suggests that injury to the vagina and it supportive tissues at the time of vaginal birth is probably the largest risk factor for developing prolapse [19-21], since most parous women have mild asymptomatic prolapse and vaginal delivery. Quantifying vaginal support has shown a detectable deterioration of support in parous women by the Pelvic Organ Prolapse Quantification Exam (POP-Q; [62]).

Mechanically, it is well known that all supportive tissues require a minimum stiffness and strength in order to meet the demands of physiological loading. However, surprisingly little is known of the mechanism by which vaginal birth alters the supportive function of the vagina and affects biochemical and biomechanical properties. Collagen is the major load bearing protein throughout the body, and changes in ratios and architecture of these collagens architecture likely contribute to altered vaginal tissue behavior [51]. Collagen fibrils I, III, and V are common within tissues that are required to provide mechanical strength. Collagen I forms the largest fibril diameter and is associated with increased tensile strength for a tissue. Compared to

collagen type I, collagens III and V which are increased in tissues following trauma and associated with inferior mechanical properties: increased distensibility and lower tensile strength, compare to tissues with high concentration of collagen type I [112-115]. The ratio of collagen subtypes within a fibril, specifically collagen I/(III+V), has been established as an indirect measure of the biomechanical properties of a tissue. Along with collagen composition, collagen alignment has been shown to be related to the mechanical integrity of soft tissues. For example, a higher collagen I/(III+V) ratio and/or increased alignment of collagen in the direction of applied forces is associated with superior mechanical properties. Tissues that have to withstand high level of forces (e.g. ligaments and tendons) typically have a large amount of collagen I. Elevated collagen III to type I is associated with smaller fibrils and a larger degree of distensibility (e.g. skin and blood vessel). It has been found to be elevated immediately after injury only to return to normal levels in the long-term [34, 55]. Collagen types III and V play a role in regulating collagen fibril diameter during fibrillogenesis [112-115].

Previous research utilizing animal models on the medial collateral ligament, skin, and vaginal tissue have shown that injury to these soft tissues correlated with a decrease in the collagen I/III ratio and inferior biomechanical properties [55-57, 116]. A similar decrease in the collagen I/III ratio was found in pelvic floor connective tissues of women with prolapse relative to controls [51, 52]. Other studies have illustrated that prolapsed patients also have altered activity of extracellular matrix degradation enzymes compared to non-prolapsed vaginal tissue: specifically examining matrix metalloproteinase (MMP)-2 and MMP-9 [117]. This evidence suggests that women suffering from prolapse have undergone a remodeling process impacting the biochemical properties of their pelvic floor tissues; however, little is understood about how these biochemical alterations are manifested in functional, or biomechanical, properties of

vaginal tissue that make them susceptible to prolapse. There is a growing concern that the mismatch between synthetic mesh and vaginal biomechanical properties has led to the current high complication rate [80]. The growing number of reported complication rates has prompted many companies to develop a new generation of meshes which are less stiff; however, to design an appropriate synthetic graft characterizing the native properties of the vaginal wall is critical.

One of the primary limitations in establishing the required properties of these synthetic grafts are the access to study the biomechanical properties of compromised, or prolapsed, vaginal tissues. Indeed, the small quantity of tissues obtained from biopsies of women precludes conventional mechanical testing. Thus, studies investigating how changes in the structural proteins such as collagen and their impact on the mechanical properties of the vagina and supportive tissues subsequent to vaginal delivery, relate to the pathogenesis of pelvic organ prolapse have been limited. To overcome these issues, we have turned to animal models; however, choosing the appropriate model for the research question at hand is an important factor to consider. Animal models must meet specific criteria to successfully address specific a research question. The overall goal of this thesis is to perform thorough studies examining the effects of prolapse mesh on the biomechanical properties of grafted tissues. To adequately assess this question, the appropriate animal model would contain similar pelvic floor support, hormonal response, and mechanical properties as the patients clinically implanted. Although no animal model is a perfect surrogate for the human pelvic floor, understanding these similarities and differences can help us better assess

Reviewing the literature, there are several animals that are commonly used in urogynecology research: rodent, rabbit, sheep, and non-human primate (NHP). Animal models provide us with several distinct advantages. First, utilizing animal models, we can control for

age, weight, body mass index, hormonal status, and parity which are all confounding risk factors for the development of prolapse. Examining several animal models allows us to understand the changes that not only occur throughout pregnancy, but also the impact of pregnancy in terms of postpartum remodeling that make the vaginal tissue prone to prolapse. Second, they allow for rigorous *in vivo* characterization of the mesh-tissue complex (MTC) after implantation. Last, unlike small biopsies that are often collected from clinical patients, animal models allow for adequate tissue collection which can undergo mechanical testing and biochemistry. A preliminary study of these nulliparous animal models revealed that the rabbit had significantly different biochemical and biomechanical properties compared to the other animal models (Appendix A). From this information, combined with previously depicted differences in the anatomy and physiology of the rabbit (Section 1.2.3), it was concluded that the rabbit was an inappropriate animal model to examine how biomechanical properties of the vaginal tissue change after implantation. Therefore, we specifically examined three commonly used animal models the rodent, sheep, and NHP. To examine the vaginal tissue of these animal models, we aimed to assess the effect of parity on the collagen I/III ratio and uniaxial mechanical properties.

2.1.1 Quantifying Pelvic Floor Support

One of the most common ways a clinician can measure pelvic floor descent in patients is through the pelvic organ prolapse quantification scale, or POP-Q exam [62]. During this exam six points are commonly recorded. Two of these points are exterior measurements. First the gential hiatus (gh) which is a measurement from the urethra to the posterior opening of the hymen. The second exterior measurement is of the perianal body (pb). This is the distance between the posterior

periphery of the hymen at roughly midline to the middle of the rectal opening. The total vaginal length (TVL) is recorded from the hymen to the most proximal point in the vagina. TVL measurements are not taken while abdominal pressure is applied through either valsalva or a crede maneuver. However, C, which is the distance from the hymen to the cervix, and D, which measures to the posterior fornix, are measured while the patient is performing valsalva or a clinician is applying abdominal pressure via the crede maneuver.

The anterior and posterior walls of the vagina are estimated between a range of -3 cm to 3 cm. Negative values suggest supported tissues above the hymen and positive values indicate a laxity of the vaginal walls past the vaginal introitus. The anterior wall measurements are examined in the distal (Aa) and proximal (Ba) vagina. These measurements are reflected to the posterior wall as Ap and Bp. Together these six measurements are utilized to stage the degree of prolapse a patient may have. Currently, widely used POP-Q scale ranges from stage 0 to stage IV. Stage 0 indicates a fully support pelvic with the anterior and posterior wall points consistently at -3 cm. In contrast, Stage IV describes a severe case of prolapse with the boundary of the vagina measuring +3 in an anterior or posterior measurement. Stages I through III illustrate worsening degree of pelvic floor support between Stage 0 and Stage IV. POP-Q is an early means to better diagnose patients suffering from prolapse and may be adapted to help describe the degree of pelvic floor support in animal models.

2.1.2 Passive Mechanical Properties of Soft Tissues

2.1.2.1 Uniaxial Mechanical Properties

Mechanical properties of a material provides specific information about the relationship between the amount of stress (force divided by cross-sectional area) applied to a tissue versus the amount of strain (change in elongation relative to the initial length) that the tissue undergoes. In this way, mechanical properties describe a material independent of its size and geometry. Thus, they are a direct reflection of the composition and microstructural arrangement of a tissue, i.e., they provide quantitative results about the tissue quality. Just as there are many different approaches to determine the structural properties of a complex of tissues, there are also many testing methodologies that can be used to determine the mechanical properties of a specific tissue [25]. For simplicity, we will focus on those that can be determined from a uniaxial tensile test to failure. An example of a stress-strain graph obtained from uniaxial tensile testing is shown in Figure 6. This curve is also nonlinear, displaying distinct toe, linear, and failure regions. The parameters that describe the mechanical properties that can be obtained from this curve and include the tensile strength (maximal stress), ultimate strain (strain corresponding to the tensile strength), tangent modulus (slope of the stress-strain curve in the linear region), and the strain-energy density (area underneath the stress-strain curve).

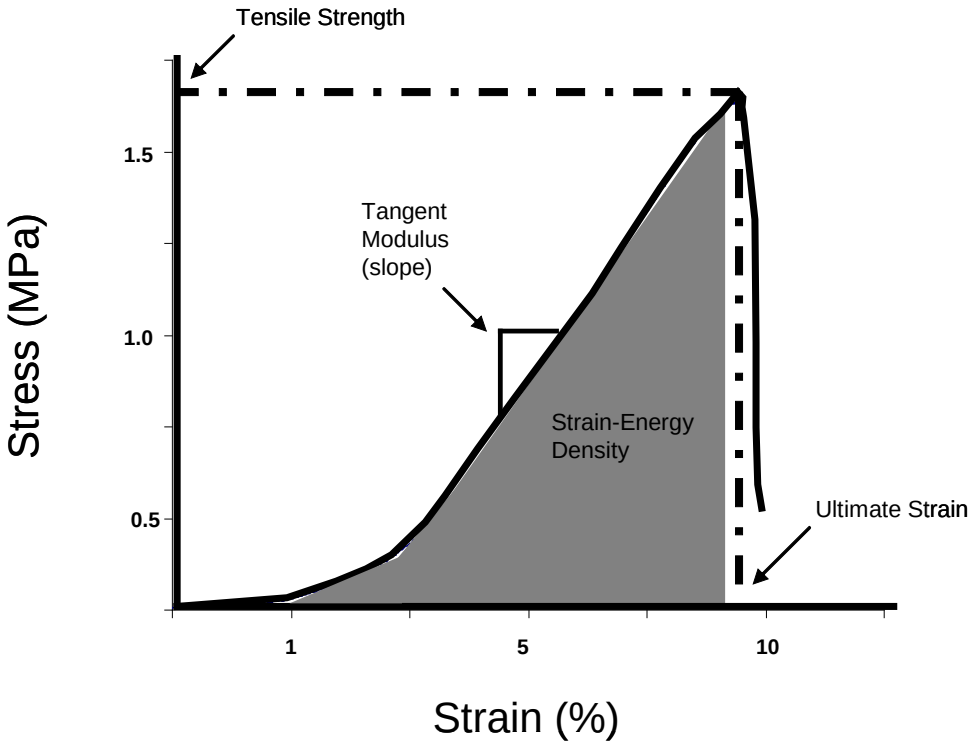

Figure 6 A representative stress-strain curve from a uniaxial tensile test to failure. The parameters describing the mechanical properties are highlighted and include the tensile strength, ultimate strain, tangent modulus, and strain-energy density.

It is important to note, however, that the accurate determination of the mechanical properties of a tissue is dependent on accurate cross-sectional area and strain measurements. As a brief review, cross-sectional area measurements for soft-tissues can be divided into two groups: contact and noncontact methods [118, 119]. Previously studies have shown that contact methods for soft tissues may result in errors due to the need to apply external pressure to the sample, which in turn causes a change in shape. Moreover, these approaches commonly rely on the assumption that the area of the tissue can be described by common geometrical shape (e.g. rectangle, circle, elliptical, etc.). Since tissues are often irregularly shaped, these assumptions can also lead to errors.

To reduce these errors, noncontact methods have been developed. Several of the most often used methods include the shadow amplitude method, the profile method, and the use of laser technology [118, 119]. Within our research center, a laser micrometer system has been developed to accurately and reliably determine the cross-section area and geometry of soft convex biological tissues in a non-contact manner (Figure 7) [118]. More recently, a new laser reflectance system has been developed that can measure the cross-sectional area and shape of concave surfaces [119]. These non-contact approaches have been shown to be accurate to 0.2%, thus allowing for an accurate determination of tissue stress.

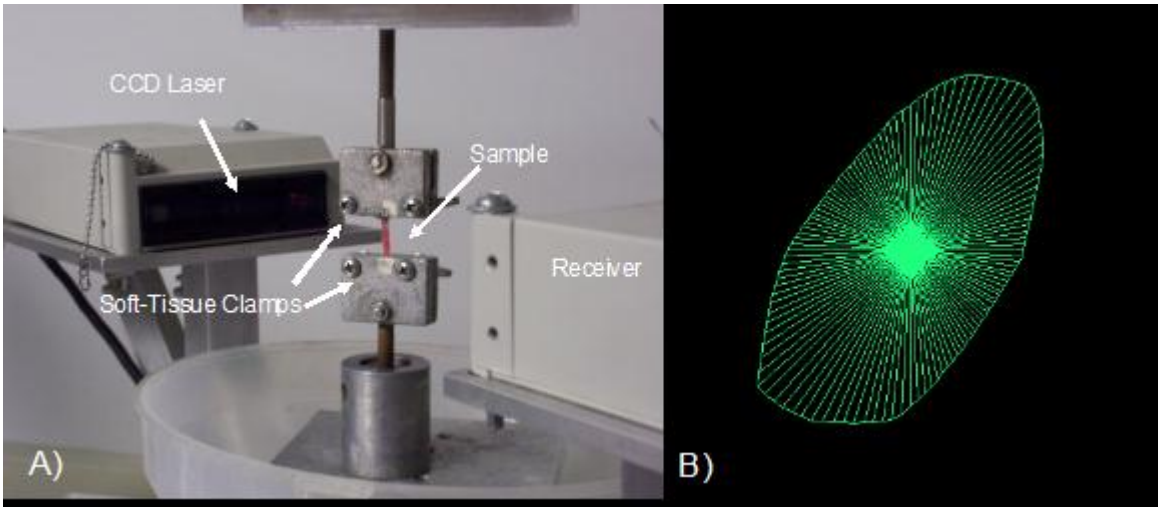

Figure 7 Laser micrometer system with a tissue sample. A) The tissue is placed in custom designed soft-tissue clamps where the tissue blocks part of the laser from hitting the receiver on the opposite side. After the laser rotates 180 degrees the cross-section area and geometry (B) can be calculated.

The second obstacle to overcome when determining the mechanical properties of soft tissue is accurate measurements of tissue strain during experimental protocols. For *ex vivo* testing, it is important to isolate the tissue and clamp it on two or more sides. While many laboratories will simply utilize the clamp-to-clamp distance to determine the initial length of the specimen for calculations of stretch or strain, this approach can lead to significant errors in strain

measurement. This is because the clamp imposes an artificial boundary condition on the tissue, as well as local damage. Thus, it has been measured that strains near the clamp can be many times greater than those measured away from the clamp [98]. To avoid these errors optical techniques utilizing markers and video tracking have been developed. Optical techniques are advantageous because these systems require only the placement of small optical markers on the tissue surface in a region sufficiently far from the clamp. The marker can be reflective tape, ink, or contrast beads. Briefly, a camera records the original marker position (gauge length) and movement based on a pixel coordinate output. Previous literature has presented this approach in further detail [120-122]. The change from the gauge length to its current position can be output in terms of percent strain and used in calculating the mechanical properties of biological tissues [121, 123, 124]. Using this approach, issues with clamp slippage are also minimized.

2.1.2.2 Experimental and Environmental Conditions

While accurate cross-sectional area and strain measurements are important for determining reliable stress and strain values, there are also several experimental factors that could influence the stress-strain relationship. Previous, studies have examined the effects of orientation, strain rate, storage, or experimental conditions on many biological tissues [106, 124-131].

In terms of strain rate, studies in ligaments and tendons have noted that, for mature animals, these tissues are generally insensitive to changes in strain rate [126, 127, 131]. Studies of vaginal tissue from sheep, on the other hand, found that there was a slight decrease (30%) in the tangent modulus of the vaginal wall with a 100-fold increase in strain rate [106]. This result is interesting in that most tissues, and viscoelastic materials in general, demonstrate an increase in tangent modulus with increasing strain rate. Thus, additional work needs to be done to

confirm this finding and determine the mechanism behind this result. The aforementioned study also found that data obtained at higher and higher strain rates remained relatively consistent to each other. Thus, according to these findings, it appears that vaginal tissue from sheep may be minimally sensitive to strain rate.

Several environmental factors are often considered to ensure a repeatable and reliable protocol, including storage, hydration, and temperature. Rubod *et al.* also examined these conditions for the vaginal wall of sheep and found that a decrease in the tangent modulus of vaginal tissue was associated with increased exposure to ambient air [106]. This study also noted minimal effects due to temperature (levels ranging from 18 – 37 °C) and storage in saline for up to 24 hours [106]. Similar results have been reported on previous work examining the patella tendon (PT) [125, 130]. A decrease in the tangent modulus was indeed reported for specimens tested in ambient air dripped with saline. However, inconsistent with the findings form Rubod *et al.*, these studies noted an increase in the tangent modulus due to a decrease in temperature [125, 128, 130]. Thus, further work needs to be performed to confirm the findings for vaginal tissue. Until these findings can be confirmed, however, it is recommended that all specimens be tested in a chamber that maintains a physiologic environment and temperature.

Due to the lengthy and complex testing protocols, samples are often frozen for storage and then thawed prior to testing, which may alter the mechanical properties of biological tissues [106, 124, 132]. Rubod *et al.* also explored the differences between fresh and frozen samples in terms of the mechanical properties of vaginal tissue [106], and found that the effect of frozen storage was negligible in terms of the mechanical properties of the vagina. This is consistent with previous studies done on the medial collateral ligament (MCL). A study in our research center showed that freezing and re-freezing cycles had a minimal effect on the tangent modulus

of the MCL [124, 132]. However, we have noticed that the viscoelastic behavior (to be discussed later) may be impacted by freezing. Thus, if viscoelastic tests of vaginal tissue are being considered, the effect of storage needs to be investigated more rigorously.

Finally, it should be emphasized that the experimental factors outlined in this section, while they can have profound effects on the measured mechanical properties of tissue, the effects do vary from tissue type to tissue type and possibly from species to species. Thus, we must take caution when trying to extrapolate the results of the vagina to the other tissues of the pelvic floor and from animal models to humans. Clearly, much more testing needs to be done in order to standardize testing protocols such that meaningful data can be collected that can be directly compared between laboratories.

2.1.3 Active Mechanical Properties

Characterizing the passive mechanical properties of the vagina is important but, as described above, the vagina is comprised of both a passive (e.g. collagen, elastin, basement membrane) and active (e.g. smooth muscle) components. Smooth muscle is often a minor contributor in resisting passive mechanical loading; however, it is extremely important in maintaining vaginal tone and actively resisting the forces of the surrounding connective tissues.

2.1.3.1 Drug Response

To understand the function of smooth muscle, tissues are often subjected to a contractility assay. For example, a tissue may be subjected to increasing concentrations of a contractile drug or agent, such as potassium (K^+). K^+ plays a major role in maintaining intracellular membrane

potential and is important in the electrical stimulation of nerves and muscles cells. Since K^+ is a native ion in these contractile cells, it is often applied to achieve the maximum contraction because it forces all smooth muscle cells within a tissue to depolarize their cellular membranes and contract. Typically this type of protocol results in a force-dose curve that peaks when the tissue has reached its maximum contractile potential. After applying the various doses of an agent, a relationship between the concentration of K^+, or drug, and the resulting effect, or concentration-effect curve, is often generated. Here, we reference this response as a force-dose curve for simplicity. This force-dose curve can have different magnitudes and shape. This is often due to the nature of the contractile agent, or drug, and the mechanism of response the sample has to said drug. This can result in quite complex force-dose relationships that are concave, convex, linear or more often sigmoidal. In this dissertation we will discuss examining the sigmoidal response to increasing concentrations of a contractile agent as they are the most often seen as shown in Figure 8. These curves often have four examined characteristics which include potency, maximal efficacy, slope, and biological variability. An in-depth discussion about these characteristics has been explained in 1990 by Goodman [133]. However, the biological variability of contractile data can be significantly different not only within a single population, but also within a single individual. In order to report consistently not only between groups but between samples, it is important to consider these force values relative to some type of mass or volume measurement. The entire force response is often normalized to volume (mm^3) or mass [dry weight (g) or wet weight (g)], and this peak force value is then reported as a function of mm^3 or g. This method is applied to account for different amounts of smooth muscle per sample and decrease the variability of the contractile data. Variability can also be attributed to other confounding factors including age, sex, weight, height, etc. [133]. Therefore, it is

important when designing studies to control for these factors or account for them during interpretation and statistical comparisons.

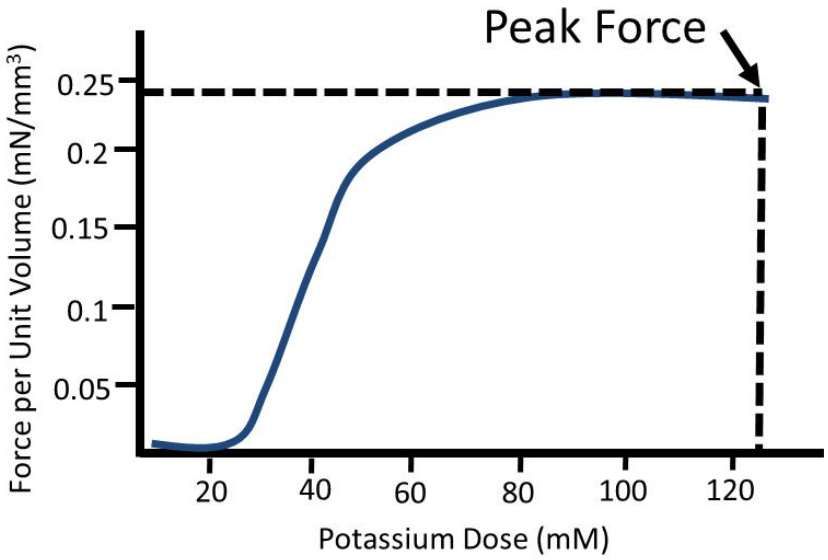

Figure 8 Representative force per volume - dose curve highlighting the peak force parameter

The contractile agent or drug is typically given at higher doses until the tissue can no longer increase its contraction and has reached a peak force (Figure 8 Peak Force). Often separate groups of specimens respond differently to the application of a drug even if they have the same peak force value. Therefore, to further characterize a sample's force-dose curve the effective concentration to achieve 50% of the maximum response (EC_{50}) and the effective contraction to achieve 100% (EC_{100}) are also calculated (Figure 9).

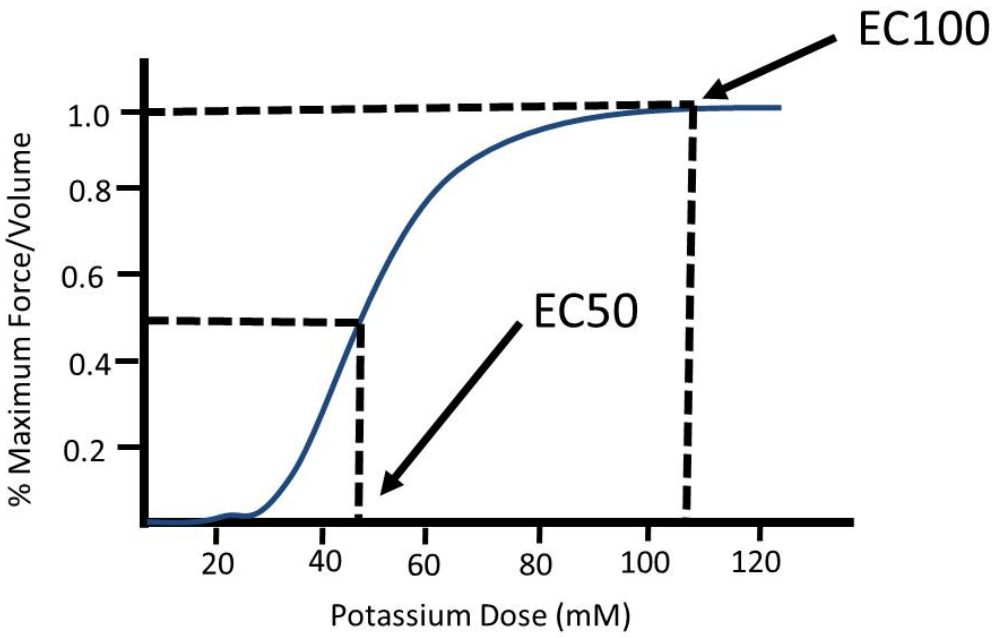

Figure 9 Normalized force per dose curve and the calculations of EC_{50} and EC_{100}

This is done by normalizing the entire force-dose curve to the peak maximum contractile force (peak force). The EC_{50} and EC_{100} help characterize the tissue's response to a specific drug or contractile agent. While the peak load can identify the maximum ability of a tissue to generate force the EC_{50} and EC_{100} define the tissue's sensitivity and plateau dose, respectively. This is just a simple overview of a vast field and a further detailed methodology for inducing and interrupting the contractile behavior of biological tissues has been previously described [133].

2.2 RODENT

2.2.1 Introduction

The rodent model has several advantageous as a model for the pelvic floor. It has similar connective tissue support, including the level I, III, and III connective tissues. The composition of the vaginal cross-section is comparable between rodents and women. The rodent is also small, easy to work with, and inexpensive. Based on these characteristics the rodent is an excellent animal model for studying the biomechanical properties of the vagina. The major limitation of the rodent model is the small vaginal canal. Due to its relatively small size it would be difficult to implant a synthetic graft on the vagina and perform traditional mechanical analysis on the explanted tissue.

However, due to this animal models superior advantage in terms of expense, we can utilize the rodent to examine not only the effect that parity may have on permanently weakening the vaginal tissue, but also assess how changes throughout pregnancy can led into this permanent effect on the mechanical properties of the vaginal tissue.

In mechanical terms, vaginal remodeling during pregnancy likely impacts 1) the passive mechanics of the vagina by altering the composition and organization of the fibrillar extracellular matrix [31] and, 2) the active mechanics by altering the amount, organization, and contractile ability (reactivity) of the smooth muscle. As collagen is the primary component of the fibrillar matrix contributing to the vagina's physical stability and smooth muscle is primarily responsible for short-term changes in geometry through contraction and relaxation, it is likely that

remodeling of both vaginal collagen and smooth muscle play a critical role in mediating maternal adaptations in preparation for vaginal delivery.

In this study, we aim to focus on the changes specific to the vagina by examining both passive (collagen) and active (smooth muscle) mechanical properties. We define vaginal remodeling in terms of its mechanical function by investigating how the passive mechanical and active contractile properties adapt throughout pregnancy and recover postpartum using the rat model. The findings of our previous work suggest that the rat may be capable of successfully adapting to meet the mechanical demand of labor and delivery resulting in minimal tissue injury to both its passive and active components. Thus, based on our previous studies of the VSTC [30, 134], we hypothesize that the passive properties will adapt during pregnancy to increase the ability of vaginal tissue to distend at the time of delivery and that the active properties will display a concomitant decrease in the contractile force generated by the tissue in response to K^+ stimulation. We further hypothesize that the tissue will rapidly remodel to pre-pregnancy levels of mechanical function (passive and active properties) by 4 weeks postpartum. Data obtained from our study are important to establish a baseline understanding of the normal delivery process such that future studies can aim to infer the impact of injury when the mechanical demand exceeds these adaptations.

2.2.2 Animals

A total of 71 3-month old female Long Evans rats (Harlan Laboratories, Indianapolis, IN) were utilized in this study, which was approved by the Institutional Animal Care and Use Committee at the University of Pittsburgh (IACUC #0905469). Animals were housed with a 12 hour

alternating light-dark cycle and provided free access to food and water ad libitum. Rats were divided into five separate groups: virgin (n=17), mid-pregnant (Day 14-16, n=12), late-pregnant (Day 20-22, n=14), immediate postpartum (0-2 hours after delivery, n=14), and 4 weeks postpartum (n=15). Pregnancy status of the animals was checked daily and confirmed by the presence of a seminal plug. The first appearance of the plug was considered day 1 of gestation. To obtain the immediate postpartum group, rats were examined every 2 hours over a 48 hour period during late gestation and euthanized immediately after delivery. The number of fetuses, when applicable, was recorded for each rat along with the maternal length and weight. Total vaginal length (TVL) and genitial hiatus (GH) measurements were taken using a measuring device marked in millimeters and used to note changes throughout pregnancy and after delivery.

2.2.3 Passive Mechanical Methods

For evaluation of the passive mechanical properties, virgin (n=8), mid-pregnant (n=7), late-pregnant (n=7), immediate postpartum (n=8), and 4 week postpartum (n=6) rats were dissected to expose the pelvic anatomy immediately after they were euthanized. The vagina, cervix, and uterine horns were isolated from the surrounding tissue and placed in saline soaked gauze and frozen at -20^{o}C, which has been previously shown to have minimal effects on the passive biomechanical properties of the vagina and other tissues [106, 124]. Prior to testing, each specimen was allowed to thaw at room temperature and then was further dissected to prepare for mechanical testing. The uterine horns and cervix were removed and the vagina was cut along its length at the urethra. Periurethral tissue was removed and not included in any of the samples

tested. The specimen was placed in custom designed soft tissue clamps to form a clamp-vagina-clamp complex and was cut to form a dog-boned shape (Figure 10).

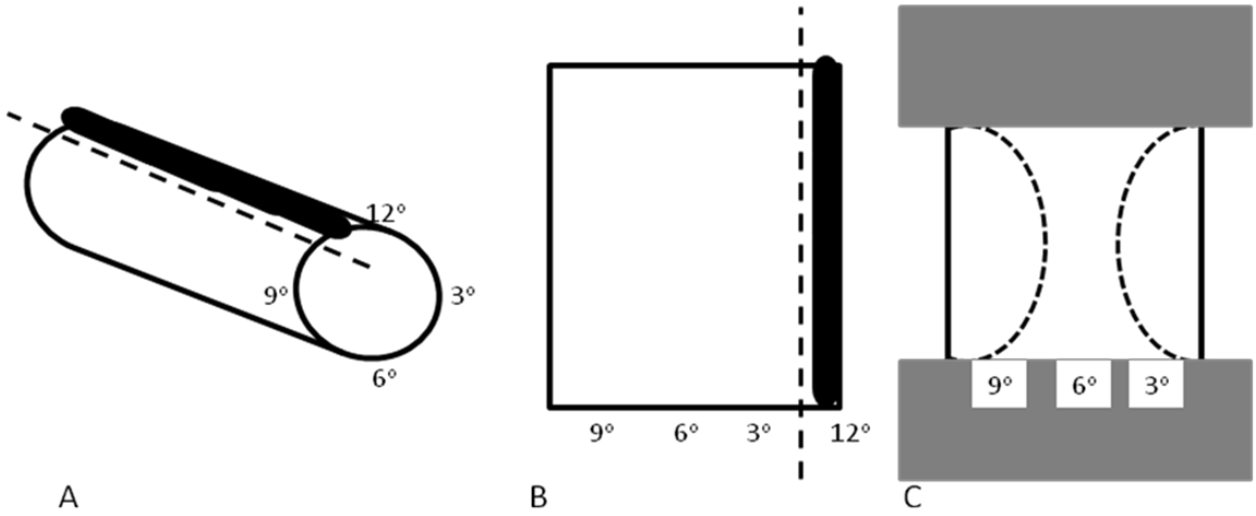

Figure 10 Illustrating the method for dividing the tissue for the uniaxial tensile test. A) Represents the vagina as a tube (not drawn to scale) with the urethra at the 12 o'clock position. The dashed line indicates were the vagina was cut so the vagina would create a square piece of tissue (B) The urethra was removed (dashed line) and the sample was placed into custom design soft tissue clamps (C). The tissue was cut into a dog-boned (dashed lines) shape to create an adequate aspect ratio (not drawn to scale) [135].

This was done to achieve a minimal aspect ratio of 5 (length to width ratio) that would ensure a uniform stress and strain distribution along the mid-substance of the tissue. This is essential to obtain reliable and repeatable results that are representative of the tensile behavior of the tissue when performing a uniaxial tensile testing protocol [123, 136].

The cross-sectional geometry and area measurements were made using the non-contact laser micrometer with an accuracy of 0.1 mm^2 [136, 137]. Measurements were taken at three locations along the length of the sample (distal, mid, proximal) and averaged together. This average cross-sectional area value was used to calculate the Lagrangian stress, which is defined as the force divided by the initial, unloaded cross-sectional area. Subsequently, two contrast markers were placed on the luminal surface of the vagina near the mid-line, roughly 5 mm apart.

A camera system (Keyence CV-2600) and motion analysis software (Spicatek, Inc. Maui, HI) were used to track these markers and calculate strain. Strain was defined as the change in distance between the two markers divided by the original marker distance measured immediately after the application of a preload. Throughout tissue preparation the samples were kept moist with 0.9% saline.

For testing, the clamp-tissue-clamp construct was submerged in a 37^{o}C physiological saline bath with the distal clamp (introitus) attached to the base of a Instron^{TM} testing machine (Instron^{TM5565}) and the proximal clamp (proximal vagina) attached to a load cell (Honeywell Model 31; 50 lbs), which was rigidly fixed to the cross-head of the machine. The tissue was subjected to a small 0.1 N preload and aligned to the loading axis of the testing system. The initial clamp-to-clamp distance was measured and the specimen was then allowed to equilibrate in the bath for 30 minutes in a slacked position. For the load to failure test, the preload (0.1 N) was once again applied followed by 10 cycles of preconditioning to 7% of the previously measured clamp-to-clamp distance (7% clamp-to-clamp strain was previously determined to be approximately 4% tissue strain and within the toe-region of the stress-strain curve) at an elongation rate of 10 mm/min. The tissue was then loaded to failure and a load-elongation curve was obtained. The corresponding stress-strain curve was then computed utilizing the cross-sectional area and tissue strain measurements made via our optical system. The parameters describing the mechanical properties of the tissue were then obtained from this curve. The tangent modulus, an indicator of tissue stiffness on a per unit basis, was the maximum slope of the stress-strain curve recorded over a 1% interval of strain. The tensile strength was defined as the maximum stress achieved at failure and the ultimate strain was the strain corresponding to

the tensile strength. The strain energy density, or tissue toughness on a per unit basis, was calculated from the area underneath the stress-strain curve until failure.

2.2.4 Active Methods

To characterize the active properties of the vagina, virgin (n=9), pregnant (mid- n=5 and late- n=7), and postpartum (immediate - n=6 and 4 week- n=8) animals were dissected to isolate the vagina immediately following euthanasia. Vaginas were cut longitudinally along the urethra, which was removed as described for the passive properties. During dissection, tissues were continuously moistened with 0.9% saline. The vagina was oriented along its longitudinal axis and the entire sample, from the distal vagina at the edge of the intriotus to the distal edge of the cervix, was immediately placed in a 20 mL organ bath and secured to a force transducer (20 grams) bubbled by 95% air balanced with 5% CO_2 in PSS HEPES (37^{o}C, pH 7.4). Contractile responses were monitored with a pressure transducer (Transbridge 4M, World Precision Instruments) and recorded using Chart software on a PowerLab^{TM} system (sampling at 40 Hz, AD Instruments). Each strip was adjusted to a tension of 0.3 g and then allowed to equilibrate for at least 60 min, and then washed three times. All washes during this study were performed using the PSS HEPES solution [138].

2.2.4.1 Potassium Response

To measure the amount of contractile force generated by the vaginal strips, the tissue was subjected to seven varying concentrations of potassium (K^+: 5.88, 20, 30, 40, 50, 80, 124 mM). The force generated at 124 mM of K^+ was defined as the maximum force response of the tissue

to potassium. The forces generated were normalized to this maximum force response and a line was fitted to the linear portion of the dose response curve and utilized to calculate the effective concentration for 50% and 100% of the tissues response. The K^+ dose required to achieve 50% of the maximum response (EC_{50}) correlates to the sensitivity of smooth muscle to K^+, and the EC_{100} correlates to the lowest dose of potassium that resulted in 100% of the maximum contraction in the tissue sample. The EC_{100} is not necessarily the maximum dose given, and therefore along with the EC_{50} can help identify overall shifts in the potassium response curve between each group. The tissue was given 15 minutes to equilibrate at each K^+ dose when the load was recorded. The sample was then washed three times and given 15-20 minutes to recover.

2.2.4.2 Active Mechanical Properties

Next we wanted to examine how elongation affected the contractile properties of smooth muscle within the vagina. The tissue was contracted with the potassium concentration required to invoke the maximum contractile force response from the tissue in all groups, and elongated in 5mm increments until a maximum force of 20 g was achieved. The resulting force (load)-displacement graph represents the force resulting from the activated smooth muscle and passive elongation of the extracellular matrix components. The tissue was then returned to zero elongation and washed three times. A calcium free+papaverin buffer was applied to inhibit smooth muscle contraction and 15 to 20 minutes was allowed to ensure the sample was completely inactivated. The sample was again elongated in 5mm increments until a maximum force of 20 g was achieved. The resulting force (load)-displacement curve was referred to as the passive curve, which represents the force resulting from passive elongation of the tissue with no

active smooth muscle contribution. The maximum displacement required to generate 20 g of force was recorded for each specimen for both the activated and inactivated states of the smooth muscle. To estimate the force generated by the smooth muscle component of the vagina during elongation, the passive curve values were subtracted from the active curve to create a curve called the "active minus passive" curve, which was fit with an exponential in the form of:

$$F=C*e^{B*x} \qquad \textbf{2-1}$$

Where F represents the force generated per unit volume of tissue (mN/mm^3) and x represents displacement (mm). C (mN/mm^3) and B (1/mm) are the fit parameters. The parameter C represents the basal force at 0 mm of elongation. In the case of the active-passive curve, it should be similar to the force response at 80 mM of K^+ for each group from the potassium response portion of this study as the testing conditions are similar. Parameter B represents the nonlinearity of each curve, or how sharply the force increases during extension. A larger value for B relates to a more nonlinear force response (sharper increase) to the applied elongation.

The wet weight of each vaginal sample was recorded immediately after testing. To measure the volume of the tissue, the length (L) was measured using digital calipers (Mitutoyo Corp.), while the cross-sectional area (CSA) along the vagina was calculated after testing using the noncontact laser micrometer method described above. The length and cross-sectional area measurements were utilized to calculate the tissue volume of each specimen (L X CSA). All generated forces were normalized to tissue volume to account for changes in tissue size and muscle quantity.

2.2.5 Statistics

A power analysis on the preliminary data between the virgin and mid-pregnant animals was performed to assess the number of animals required to observe significant differences. To achieve a power of at least 80%, a minimum of 5 animals per group were needed to detect a 50% change in the tangent modulus, tensile strength, contractile force, EC_{50}, EC_{100}, maximum displacement, as well as parameter C. Passive mechanical properties were compared using a one-way ANOVA with a Sidak post-hoc ($p=0.05$), and presented as mean ± standard deviations. Active properties were compared using Kruskal-Wallis and Mann-Whitney post hoc tests where appropriate ($p=0.05$), and are presented as median (interquartile range). All data analysis was done using a statistical software package (12.0 SPSS Inc, Chicago, IL).

2.2.6 Results

As expected, the average weights of the animals increased from virgin 221 g to late pregnant 303 g (Table 2). TVL and GH values continuously increased from virgin, to mid-, and late-pregnant animals. These parameters began decreasing immediately postpartum (0-2 hours). At 4 weeks postpartum, the animal weights were decreased from the early post-partum period but elevated by 13% with respect to virgin animals (Table 2). The vaginal weight and volume from each tested sample for the active properties did not differ significantly between the groups ($p=0.4$ and $p=0.5$, respectively, Table 2).

Table 2 Baseline characteristics (weight, length, total vaginal length (TVL), and genital hiatus (GH)) of rodents including the tissue weight and volume of longitudinal vaginal sections used during the contractile assay. Data represented as median (interquartile range) [135].

	Weight (g)	Length (cm)	TVL (cm)	GH (cm)	Tissue Weight (g)	Tissue Volume (mm^3)
Virgin	221 (11.2)	29.0 (0.5)	2.1 (0.2)	0.5 (0.1)	0.25 (0.1)	51.8 (30.4)
Mid-Pregnant	246 (18.5)	29.5 (0.5)	2.5 (0.1)	0.5 (0.1)	0.24 (0.06)	69.4 (4.4)
Late-Pregnant	303 (13.7)	29.0 (0.8)	3 (0.1)	0.6 (0.25)	0.3 (0.03)	68.2 (33.4)
0-2 hour Postpartum	250 (36.7)	29.0 (0.8)	3 (0.2)	0.7 (0.15)	0.33 (0.06)	77.7 (12.5)
4 week Postpartum	243 (11.1)	30.0 (1.0)	2 (0.2)	0.5 (0.1)	0.28 (0.06)	58.8 (25.6)
Overall p-value	0.003	0.3	<0.001	0.001	0.4	0.5
Virgin vs. Mid-Pregnant	0.3	N/A	0.002	0.4	N/A	N/A
Virgin vs. Late-Pregnant	0.001	N/A	<0.001	0.008	N/A	N/A
Virgin vs. 2 hr PP	0.1	N/A	0.004	0.003	N/A	N/A
Virgin vs. 4 wk PP	0.3	N/A	0.4	0.7	N/A	N/A

2.2.6.1 Passive Properties

All stress-strain curves were nonlinear with the characteristic toe, linear, and failure regions typical for soft tissues. The vaginal samples from mid-pregnant, late-pregnant, and 0-2 hour postpartum animals were considerably less non-linear compared to all other time points (Figure 11).

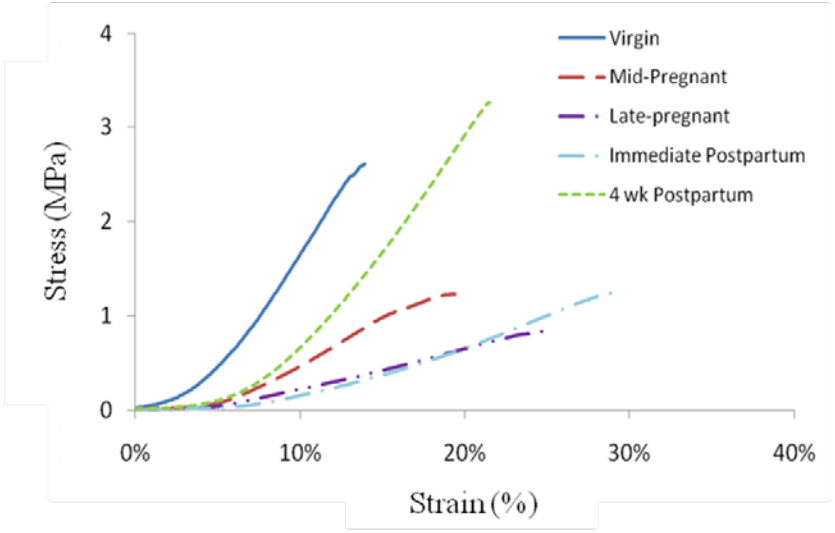

Figure 11 Representative stress-strain curves of the passive mechanical response from virgin, mid- and late-pregnant, immediate (0-2 hr) and 4 week postpartum animals [135].

This is reflected by the 53-68% decrease in the tangent modulus from longitudinal sections of the vagina during pregnancy and immediately postpartum ($p<0.001$; Table 3). By 4 weeks postpartum, the tangent modulus recovered to virgin levels (30.0±13.7 MPa, $p=1.0$). The tensile strength followed a similar trend, decreasing 47% in mid-pregnant ($p=0.04$) and 55% in late-pregnant ($p=0.01$) compared to virgin animals. However, unlike the tangent modulus, a significant difference was not detected in the tensile strength between virgin and immediate postpartum ($p=0.1$) groups with complete return to virgin levels by 4 weeks postpartum (Table 3, $p=1.0$).

Table 3. Passive mechanical properties of longitudinal vaginal sections subjected to a uniaxial tensile test. Data is represented as mean ± standard deviation [135]

	Tangent Modulus (MPa)	Tensile Strength (MPa)	Strain (%)	Strain-Energy Density (MPa)
Virgin (n=8)	25.0 ± 5.1	2.1 ± 0.65	14.0 ± 4.1	0.12 ± 0.06
Mid-Pregnant (n=7)	12.0 ± 7.7	1.1 ± 0.47	18.0 ± 5.6	0.08 ± 0.04
Late-Pregnant (n=7)	7.9 ± 4.0	0.95 ± 0.51	21.0 ± 6.9	0.09 ± 0.06
0-2 hour Postpartum (n=8)	8.5 ± 4.7	1.3 ± 0.46	24.0 ± 5.3	0.12 ± 0.04
4 week Postpartum (n=6)	30.0 ± 14.0	3.1 ± 1.7	20.0 ± 7.1	0.25 ± 0.18
Overall p-value	<0.001	0.001	0.01	0.2
Virgin vs. Mid-Pregnant	0.003	0.04	0.7	N/A
Virgin vs. Late-Pregnant	<0.001	0.01	0.2	N/A
Virgin vs. 2 hr PP	<0.001	0.09	0.007	N/A
Virgin vs. 4 wk PP	1.0	1.0	0.9	N/A

The ultimate strain increased from 33% to 77% during pregnancy compared to virgin animals (Table 3). The ultimate strain was largest in the immediate postpartum group (24±5 %) where it was found to be significantly higher than in virgin animals (14±5 %, $p=0.007$); indicating that tissue changes allowing for maximal distension are present at the time of delivery. There were no significant differences in strain energy density between each group ($p=0.25$; Table 3).

2.2.6.2 Active Properties

Response to Potassium

The normalized force response (mN/mm^3) of each tissue to varying doses of K^+ (mM) is illustrated in Figure 12.

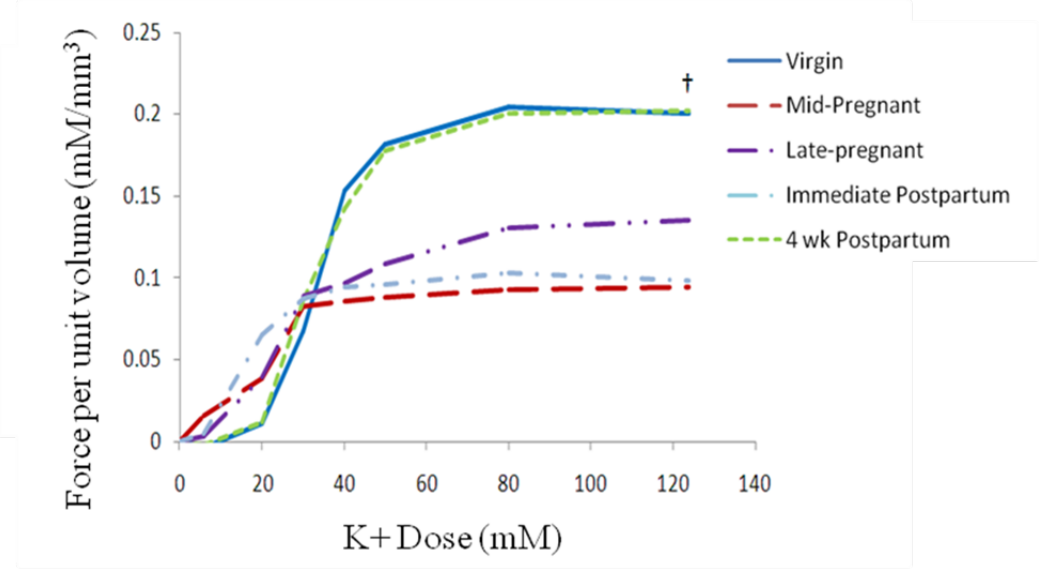

Figure 12 Force normalized to the volume of tissue at varying potassium doses. The † represents an overall p-value between the groups (p=0.033). Virgin and 4 week postpartum animals had similar higher force response to K^+ than mid-pregnant (p = 0.006), late-pregnant (p=0.04) and immediate postpartum animals (p=0.04) at 124 mM [135].

For the contractile properties, we observed a 56% decrease in contractile force (load) generated by mid-pregnancy (p=0.02); however, only a 36% decrease by late-pregnancy (p=0.3) compared to virgin animals. This may reflect some change in the distribution, quantity, or phenotype of the smooth muscle during pregnancy, because immediately postpartum (0-2 hours) animals again had a 54% decreased capacity to generate force in response to potassium compared to virgin animals (p=0.05, Table 4). Sensitivity of longitudinal vaginal strips to K^+ increased (lower EC_{50}) in mid-pregnancy and immediate postpartum period compared to virgin animals (p=0.002 and p=0.04, respectively). Late-pregnant rats had EC_{50} and EC_{100} values that fell between virgin and

mid-pregnant animals. At 4 weeks postpartum, the contractile force response returned to virgin levels (p=0.4, Table 4), but the EC_{50} and EC_{100} remained 17% and 24% lower than virgin animals (p=0.04 and p=0.002, respectively) suggesting that the heightened sensitivity to K^+ is maintained long-term.

Table 4. Active properties of longitudinal vaginal sections. The data is presented as medians (interquartile range) [135].

	Contractile Force (mN/mm^3)	EC_{50} (mM)	EC_{100} (mM)	Max. Dispalcement (mm)
Virgin (n=9)	0.18 (0.07)	40 (4.3)	74 (5.3)	2.5 (1.0)
Mid-Pregnant (n=5)	0.076 (0.009)	15 (9.2)	34 (9.6)	3.5 (1.5)
Late-Pregnant (n=7)	0.11 (0.09)	28 (12)	71 (20.9)	3.5 (1.0)
0-2 hour Postpartum (n=6)	0.063 (0.1)	24 (7.2)	68 (16.3)	3.0 (1.4)
4 week Postpartum (n=9)	0.21 (0.07)	34 (7.3)	57 (10.5)	2.0 (0.5)
Overall p-value	0.01	0.003	0.002	0.001
Virgin vs. Mid-Pregnant	0.02	0.002	0.001	0.004
Virgin vs. Late-Pregnant	0.3	0.04	0.4	0.003
Virgin vs. 2 hr PP	0.05	0.04	0.1	0.05
Virgin vs. 4 wk PP	0.4	0.04	0.002	0.7

Smooth Muscle Contribution with Elongation

The maximum displacement achieved in virgin animals following the application of 20 g of force was 2.5 (1.0) mm. The tissue distended 29% more during mid-pregnancy (p=0.004), 29% in late-pregnancy (p=0.003), and 17% in the 0-2 hrs postpartum animals (p=0.05). By 4 weeks postpartum, the tissue was less distensible returning to virgin values (Table 4, p=0.7). Examining the active-passive curve parameters allowed us to gain insight into the role of vaginal smooth muscle changes during elongation. The basal force prior to elongation (parameter C) followed a trend similar to the contractile force (Table 5). Virgin animals had a 53% and 54% larger baseline force generated compared to mid-pregnant (p=0.007) and 0-2 hr postpartum (p=0.03) rats (Table 5). Lastly the active-passive curve showed no significant differences in the

B parameter, or nonlinearity (p=0.15), between each group. This indicates that the smooth muscle contraction did not change with elongation of the tissue.

Table 5 The Active-passive curve was fit with an exponential equation resulted in basal force (C, mN/mm^3) and slope (B, 1/mm). The data for each group is represented as median (interquartile range) [135].

	C (mN/mm^3)	B (1/mm)
Virgin (n=9)	0.26 (0.04)	0.82 (0.6)
Mid-Pregnant (n=5)	0.17 (0.04)	0.38 (0.3)
Late-Pregnant (n=7)	0.26 (0.04)	0.35 (0.1)
0-2 hour Postpartum (n=6)	0.13 (0.08)	0.49 (0.3)
4 week Postpartum (n=9)	0.30 (0.1)	0.74 (0.3)
Overall p-value	0.006	0.03
Virgin vs. Mid-Pregnant	0.007	0.03
Virgin vs. Late-Pregnant	0.3	0.008
Virgin vs. 2 hr PP	0.03	0.09
Virgin vs. 4 wk PP	0.7	0.7

2.2.7 Discussion

The vagina must undergo significant changes during pregnancy to allow passage of a fetus at the time of delivery. Although clinically it is understood that these maternal adaptations occur, this study quantified how these adaptations are manifested in terms of the mechanical function of the vagina. The data confirmed clinical impressions by demonstrating significant changes in the passive mechanical properties and contractility of the vagina throughout pregnancy and into the postpartum period. The critical findings in this study include the significant changes in the passive (tangent modulus and ultimate strain) and active (contractile force and sensitivity to K^+) mechanical properties during pregnancy and ability to recover by 4 weeks postpartum. Based on the uniaxial tensile test protocol, the rodent model may not be an ideal model to study the effect of mesh implantation on vaginal tissue. An appropriate animal model would have had a negative impact due to parity making the vaginal tissue likely to prolapse overtime.

As we hypothesized, during pregnancy there was an increase in vaginal distensibility resulting from changes in both the passive mechanical and active contractile properties. In terms of the passive properties, a conceptual figure depicts the changes observed in the tensile behavior of longitudinal tissue samples throughout pregnancy and during the postpartum period

We observed a significant amount of variability in the passive mechanical properties in the 4 week postpartum group. This was largely due to two samples whose values were substantially higher than others in the group relative to virgin controls. While it is unclear why this was observed, one possible explanation was that these rats sustained some degree of vaginal injury resulting in a grossly unobservable, but mechanically measurable change resulting in stronger, stiffer, and tougher tissue (i.e. scar). The rats that suffered from a maternal birth injury may serve as a better animal model; however, additional methods to ensure a maternal birth injury were performed in the following study (Section 2.2.8).

The active smooth muscle properties were significantly altered throughout pregnancy in preparation for vaginal delivery. The 56% decrease in the contractile force generated during mid-pregnancy confirms the previous changes observed by us in smooth muscle phenotype of the vagina [139]. Interestingly, there was a slight increase in the contractile force during late-pregnancy, and may reflect previous findings which illustrated that between mid-pregnancy and late-pregnancy there is an increase in the percentage of smooth muscle cells that assume the contractile (vs. synthetic) phenotype [139].

Some important limitations of this study should be noted. First, it utilized only 4 week postpartum animals to examine any long-term effects due to pregnancy and vaginal delivery. Therefore, we felt it was a reasonable time point to examine the recovery of the passive and active properties of the vagina postpartum. A second limitation was the degree of variation

within the contractility data; however, this is consistent with previously published studies on vaginal tissue, indicating a natural variation in the contractile ability of the vagina between specimens [140, 141]. Finally, this study was limited to understanding the passive and active mechanical properties of longitudinal sections of vaginal tissue. Uniaxial tensile testing has proven to be an invaluable tool for understanding how mechanical properties change during pregnancy and postpartum, yet the function of the vagina is more complex and not loaded in a single direction *in vivo*.

In summary, this study examined how the passive and active longitudinal mechanical properties of the vagina change due to pregnancy related maternal adaptations and vaginal delivery. We found both passive and active properties are significantly altered during pregnancy likely as a mechanism to increase vaginal distensibility and reduce the risk of a birth injury to the mother and fetus. Most of these parameters were found to recover to pre-pregnant values by 4 weeks postpartum illustrating minimal effect of vaginal delivery on the active and passive properties of longitudinal samples in the rodent model. Based on the present study inducing a maternal birth injury may improve the parallels between the vaginal tissue properties of female patients and the rodent animal model. In addition, subjecting the vagina to biaxial, or bi-directional, testing protocols would better characterize the mechanical properties of the vagina, and may be more sensitive to detecting the effects of parity on vaginal tissue.

2.2.8 Rodent Injury Model

Maternal birth injury is by far the greatest risk factor for the development of pelvic floor dysfunction (PFD) later in life [14, 15, 18, 20, 142, 143]. Despite the morbidity, damage to the

vagina at the time of childbirth has received little attention [20, 142, 144, 145]. Based on previous studies utilizing the rodent model it has been shown that this animal model suffer minimally from a maternal birth injury. At four weeks parous rodents were shown to have minor differences in their active or passive biomechanical properties of vaginal tissues. However, this may make the rodent animal model advantageous for understanding how a controlled simulated birth injury affects the biochemical and biomechanical properties of the vagina. Clinically, the mechanical properties of the vaginal wall are thought to be weakened causing them to prolapse. The initial decrease in mechanical properties is thought to be related to injury or trauma at the time of vaginal delivery. This initial injury is suspected to make patients present with prolapse later in life.

We hypothesized that when applied at the time of injury incurred after a simulated maternal birth injury vaginal tissue heals incompletely, which is exhibited as an inferior mechanical properties due to elevated levels of collagen types III and V relative to type I collagen when compared to the uninjured vagina. Further, we believe that after suffering a maternal birth injury, the rodent vaginal properties will mirror those previously published from prolapsed patients. In this study, we therefore, sought to characterize changes in vaginal collagen ratios and tissue micro-architecture as well as changes in the mechanical properties of the vagina that occur following simulated birth injury [146-149].

2.2.8.1 Methods

Animals

Approval for this study was received from the Institutional Animal Care and Use Committee from the University of Pittsburgh (IACUC # 0911806). A total of 36 Long-Evans 3-month old

virgin rats were used in this study. Animals were divided into the following groups: control (N=18) and injured (N=18). Injured rats underwent a simulated birth injury via balloon distension and recovered for 4 weeks. Control and injured virgin animals were in similar phases of the menstrual cycle (estrous and metestrous) as determined by vaginal smears. Demographic variables such as total weight, genital hiatus (diameter of vaginal opening), and total vaginal length were obtained. Measurements of the genital hiatus (GH) and total vaginal length (TVL) were recorded before and after injury. After sacrifice, the weights and diameters of excised vaginas were measured.

Simulated Birth Injury

We utilized an established model of simulated birth trauma [150-152]. A 16 Fr Foley catheter was custom fit with a balloon. The tip of the catheter was trimmed so that it is flush with the end of the balloon. Experimental animals were anesthetized and the catheter-balloon construct was placed in the vagina. Following filling of the balloon, the animal was placed supine on the edge of a table and the Foley catheter was allowed to hang with 130g weight attached to its free-hanging end. The catheter with inflated balloon stayed in place for 2 hours. The balloon was then deflated and the catheter removed. Gross examination of vaginas was performed to assess the extent of injury. Balloon distention with 5 cc volume produced full thickness tears in all animals (Figure 13).

Figure 13 A representative photograph taken after immediately simulated birth injury. Urethra is located at 12 o'clock. Full thickness vaginal tear is visible, extending from 7 to 10 o'clock [116].

Histological Analysis

Thirty rats were utilized for the histological and immunofluorescence portions of the study: control (n=10) and injured untreated (n=10). Following sacrifice, the vagina was dissected away from its attachments to the pelvic sidewall, pubic symphysis, levator ani muscles and sacrum. The full thickness mid portions of the vaginas were excised, imbedded in Optimal Cutting Temperature media (Sakura Finetek Inc., Torrance, CA), cut into 5–7-µm sections with a Cryostat and stained with Masson's trichrome for examination of gross morphologic features. Histopathologic examination was carried out to assess the extent of tissue injury. Our histologic endpoints included – vaginal thickness on a cross section (epithelium to inferior margin of the muscularis), presence of a cellular infiltrate (absent, present, present-robust), tissue fibrosis (present/absent), and disruption of tissue architecture (yes/no). The transverse diameter of the cross-section of the mid portion of the vagina was measured across from one to another antilumenal side of the epithelium.

Immunofluorescence

Frozen embedded tissues were cut into serial sections of 5 to 7 µm and stored at -20^{o}C until they were ready for use. The sections were incubated with either collagen I and collagen III or collagen I and collagen V primary antibodies at room temperature for 1 hour. The primary antibody to collagen I is rabbit anti-collagen I ((1:100) Abcam, Cambridge, MA) collagen III is mouse anti-collagen III ((1:1000), Sigma, St. Louis, MO), and collagen V is mouse anti-collagen V ((1:1000), Chemicon, Billerica, MA). Optimal dilutions of primary antibody were determined by a series of previous titration experiments. The secondary antibodies for collagens I, III, and V are goat antimouse Cy3 (Jackson, West Grove, Pa), goat antirabbit Alexa 488 (Molecular Probes, Eugene, Oregon), and goat antimouse Cy5 (Jackson, West Grove, Pa). Smooth muscle F-actin was labeled with Alexa 647 Phalloidin (1:500, Molecular Probes, Eugene, Oregon). Sections were incubated with secondary antibody for 60 minutes, followed by five washes of bovine serum albumin (BSA) and five washes of phosphate buffered saline (PBS). Slides were stained for 30 seconds with Hoescht stain, followed by five washes of PBS. Sections were then mounted with gelvatol and a coverslip and dried overnight at 4 degrees C in the dark. Samples simultaneously labeled with three different primary antibodies (collagens I, III, and smooth muscle actin or collagen I, V, and smooth muscle actin) were scanned with an Olympus Fluoview BX61 confocal scanning laser microscope with a 60X objective. One of the authors (MA), blinded to the identity of the slides, performed all the analysis. Each specimen was analyzed at 10 random sites of the subepithelial and muscularis layers of the vagina. Fluorescence microscopy was interfaced to a quantitative computer program (MatlabTM). Results are represented as mean pixel intensity ratios per square area. The ratio of collagen I/III or I/V was used as an indicator of remodeling and the quality of the healing response. Regions

of interest (ROI) were drawn around vessels, which were identified by their morphology and positive staining of vascular smooth muscle F-actin, labeled with Alexa 647 Phalloidin (1:500, Molecular Probes, Eugene, Oregon). Initial studies showed no significant difference in mean pixel intensity ratios of collagens I/III and I/V with and without ROI containing vascular structures. Therefore vascular structures were not excluded in the final analysis.

Biomechanics

To characterize the biomechanical properties of vaginal tissue a uniaxial tensile test in the longitudinal direction was performed. Sixteen rats were utilized for this portion of the study: control (n=8) and injured untreated (n=8). Following a similar protocol as described in Section 2.2.3, vaginal tissue was isolated clamped in custom designed soft-tissue clamps. Cross-sectional area measurements were made for stress calculation, and strain was calculated by markers placed on the tissue. The tissue was then subjected to the aforementioned uniaxial load to failure protocol: a preload, preconditioning, and load to failure. Here, the slope of the linear region of the stress-strain curve was defined as the tangent modulus (a measurement of stiffness), while the tensile strength and maximum strain were recorded at failure (point at which the specimen breaks apart). The strain energy density was calculated by taking the area underneath the stress-strain curve until the point of failure.

Data Analysis and Statistics

All statistical analyses were performed using SPSS statistical software version release 17.0 (SPSS Inc., Chicago, IL). Our sample size was calculated based on preliminary data from virgin rats. Based on previously determined collagen ratios, we calculated that 10 rats per group would

have 80% power at the 2-sided 0.05 significance level to detect at least a 35% difference in the collagen I:V ratio and 50% difference in the ratio of collagen I:III between injured and uninjured animals. For mechanical data 6 rats per group would have 80% power at the 2-sided 0.05 significance level to detect at least a 45% difference could be observed in the tensile strength and a 30% difference in the tangent modulus. Since the values of the skewness and kurtosis statistics did not indicate a departure from symmetry in the data distribution, a Student's t-tests was used to evaluate differences in the mean collagen ratios (I to III and I to V), mechanical properties (tensile strength, maximum strain, tangent modulus, and strain-energy density), as well as the continuous variables of the anatomical and demographic data between the injured and uninjured rats. Since the variances for vaginal diameter were not equal based on Levene's test, post-hoc p-values were determined using Student's t-test for an unequal variances correction. Statistical tests were evaluated at the two-sided significance level of 0.05.

2.2.8.2 Results

Baseline characteristics obtained for the animals used in the study are listed in Table 6. Injury induced changes were reflected by a 1.2 - 1.5 fold increase in vaginal diameter despite 4 weeks of healing in the injured untreated group when compared to the controls ($p<0.001$). Total vaginal length (TVL) was 28% shorter in the injured rats after 4 weeks of healing compared to control animals, ($p<0.001$). When compared to controls, vaginal wet weights demonstrated a 36% increase in the injured rats ($p<0.001$) suggesting a global tissue response to the injury (Table 6).

Table 6 Variables at the time of sacrifice, demonstrating significant increase in vaginal wet weights, GH, and vaginal diameter after the injury compared to controls. TVL- Total Vaginal Length. GH-Genital Hiatus [116].

	Weight (g)	Vaginal Weight (gm)	TVL (cm)	GH (cm)	Vaginal Diameter (cm)
Virgin Control (n=10)	235.5 ± 22	0.25 ± 0.03	2.25 ± 0.24	0.28 ± 0.08	0.46 ± 0.07
Simulated Birth Injury (n=10)	236.2 ± 14.1	0.34 ±0.04	1.61 ± 0.22	0.61 ± 0.1	0.71 ± 0.22
p-value	1.0	<0.001	<0.001	<0.001	<0.001

Histology

Sectioned and Masson's Trichrome stained full thickness vaginal tissues were examined for overall histomorphology with light microscopy. The four layers of the vagina were well delineated in the control rats. For injured animals, disruption of the fibromuscular layer was noted on histological examination. The injury induced healing response resulted in notable tissue fibrosis and increased cellular infiltrate in the fibromuscular layer of the untreated injured rats, corresponding to the increased vaginal weights in this group (Figure 14).

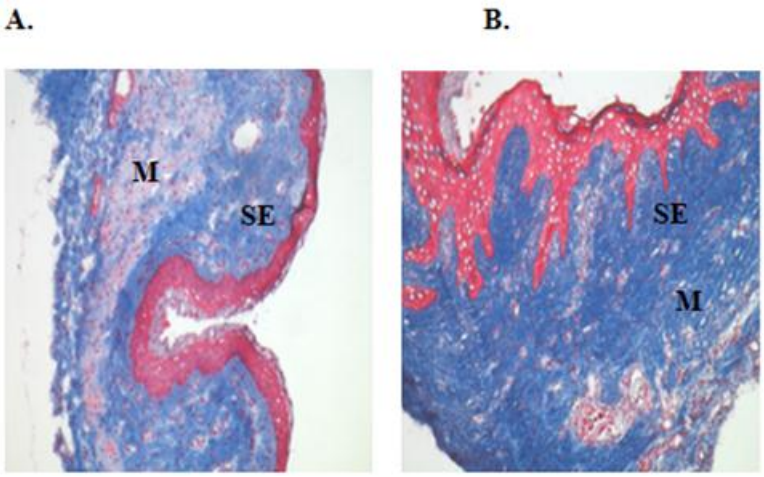

Figure 14 Light micrographs of vaginal wall of control (A), demonstrating well delineated layers of the vagina; 4 weeks after simulated birth injury (B), demonstrating disruption of the fibromuscular layer. Stain = Masson's trichrome. Magnification = x 10. SE, subepithelium; M, muscularis [116].

The transverse diameter of the cross-section of the mid portion of the vagina, measured across from antilumenal side of the epithelium to the other, was significantly smaller (0.46 cm) in the control animals when compared to injured rats (0.71 cm; p=0.001).

Immunofluorescence

Scanning confocal microscopy was used to simultaneously examine and quantify the relative amounts of two different antigens present in a fluorescent micrograph (Figure 15). Using this technique, we demonstrated that, the ratio of collagen I/V decreased 44% in rats after simulated birth injury relative to the controls (p=0.001), indicating persistent injury after 4 weeks of recovery.

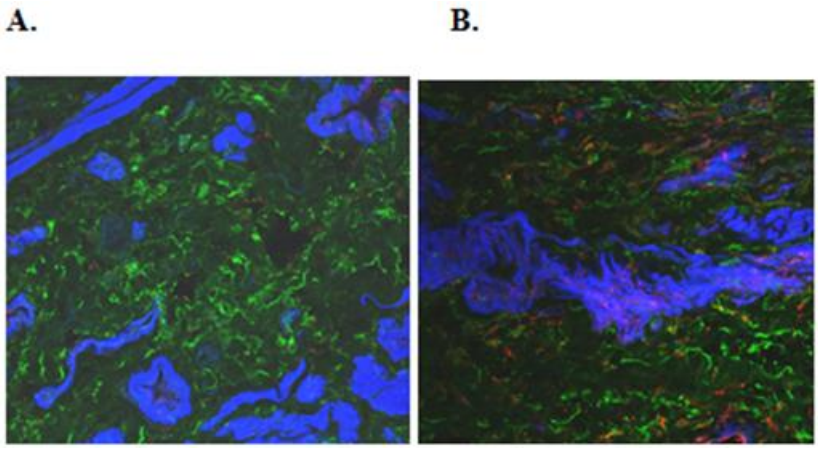

Figure 15 (A), A representative fluorograph of collagen subtypes: collagen I (green), collagen V (red) in the vagina of an uninjured rat. Blue represents smooth muscle F-actin. Five to seven micrometer sections of full-thickness vagina were labeled with primary antibodies against collagen I, V, and smooth muscle actin. Secondary antibodies linked to three different fluorophores were added at the appropriate dilutions. Quantitative analysis was performed using scanning confocal microscopy showing that the ratio of collagen I (green) to collagen V (red) is decreased after simulated birth injury. (B), a representative fluorograph of collagen subtypes: collagen I (green) collagen V (red) in the vagina of an injured rat, prepared similarly [116].

The ratio of collagen I/III, however, was not different 4 weeks post simulated birth injury (P=0.98) (Table 7).

Table 7 Comparison of ratio of collagen I/III and collagen I/V in the vaginal tissue of uninjured control, simulated birth injured rats. Simulated birth injury resulted in significant decrease in collagen I/V at 4 weeks suggests a persistently injured tissue with inferior mechanical properties [116].

	Relative Collagen I/III Ratio	Relative Collagen I/V Ratio
Virgin Control (n=10)	2.01 ± 0.63	4.95 ± 1.56
Simulated Birth Injury (n=10)	1.88 ± 0.91	2.75 ± 0.96
p-value	0.98	0.001

Biomechanics

Comparing the biomechanical properties of the vagina between uninjured controls and injured rats revealed significantly inferior results; with a 44% decrease in the tensile strength (force per cross sectional area required to disrupt the vagina) and a 38% decrease in the tangent modulus (a measurement of the resistance of the vagina to deformation) after simulated birth injury (Table 8).

Table 8 Biomechanical properties of the vaginal tissue, demonstrating significant decrease in tensile strength and tangent modulus after simulated birth injury [116].

	Tensile Strength (MPa)	Ultimate Strain (%)	Tangent Modulus (MPa)	Strain-energy Density (MPa)
Virgin Control (n=8)	2.1 ± 0.65	14 ± 4.1	25.1 ± 5.1	0.12 ± 0.06
Simulated Birth Injury (n=8)	1.2 ± 0.67	14 ± 4.6	15.3 ± 8.6	0.06 ± 0.03
p-value	0.018	0.95	0.018	0.049

The control animals had an average tensile strength and tangent modulus of 2.1 ± 0.65 MPa and 25.1 ± 5.1 MPa, respectively. Each of these mechanical properties were significantly higher when compared to the injured animals, which had a tensile strength of 1.2 ± 0.67 MPa (p=0.018) and tangent modulus of 15.3 ± 8.6 MPa (p=0.018).

2.2.8.3 Discussion

The rodent model for simulating childbirth injury has been utilized extensively for the study of stress urinary incontinence [150, 153, 154]. Simulated birth injury has been also shown to result in hypoxic injury to the vagina [153, 155]. However, no previous studies performed a comprehensive evaluation of the effect of simulated birth injury on the vaginal tissue by correlating the gross anatomical findings, biochemical transformations, and alterations in biomechanical behavior. In this study we examined the specific histomorphological, biochemical, and biomechanical changes that take place within the vagina after simulated birth injury. The primary findings of these experiments were that simulated birth injury resulted in long-term injury as measured by a combination of the above endpoints: an increased genital hiatus and persistently low ratios of collagen I/V despite 4 weeks of healing. The results of the biomechanical tests were consistent with the biochemical findings demonstrating persistent long-term injury (namely inferior biomechanical properties) in injured animals. With inferior mechanical properties, significantly less force was required to disrupt the vagina in this group (decreased tensile strength) when compared to the controls. The vaginal tissue in the injured rats was more compliant when compared to the controls (a decreased tangent modulus) indicating inferior tissue quality and increased vulnerability to deform in response to increases in force, eg. increases in intra-abdominal pressure.

The results of injury on the vaginal biomechanical properties develop the rodent into a better animal model for mesh implantation. Maternal birth injury at the time of delivery is thought to result in inferior biomechanical properties of female vaginal tissue and supportive structures and overtime lead to the development of symptomatic prolapse. To repair prolapse, surgery is often performed by grafting vaginal tissue that have these substandard biomechanical

properties. Therefore, to assess the effect of mesh implantation it is important to have similar biomechanical properties between the animal model and human tissue. Previous literature on the biomechanical properties of parous female illustrate that the tangent modulus ranges from 9.5 to 12 MPa and the tensile strength is roughly 1.4 MPa [106, 156]. After a simulated birth injury, the mechanical properties of the rodent vagina have comparable at a mean value of 15.3 MPa and 1.2 MPa for the tangent modulus and tensile strength respectively. In terms of biomechanical properties, after a simulated birth injury the rodent biomechanical properties may closely resemble parous women.

One of the limitations of our study is a relatively short (4 weeks) recovery period which is roughly equivalent to one to three years in humans. We chose this endpoint based on previous qualitative studies examining ultrastructure of the vaginal fibromuscular layer in a rodent model, in which it was demonstrated that collagen structure recovered 4 weeks after normal vaginal delivery [155]. The latter study however, focused on the fibril area fraction (the amount of matrix relative to collagen fibers) and did not distinguish between collagen subtypes. Studies examining the healing response of the medial collateral ligament after injury have demonstrated a decrease in collagen I/V ratio during the early healing phase that persists even after 52 weeks, indicating that this change may be a permanent indication of prior injury [55]. A second limitation was the method of uniaxial testing. Even though it allowed us to characterize and compare the longitudinal properties of the vagina and observe changes due to a simulated birth injury.

To overcome the above limitations, we have currently begun to examine an *in vivo* testing as well as multi-axial testing methods which would allow us to more fully characterize vaginal behavior in the longitudinal and circumferential axes of controls and injured animals.

This would allow us to draw stronger conclusions about the similarities of the injured rodent model to parous women.

In conclusion, birth injury persists long term with similar biomechanical properties reported for parous women. The negative affect of birth injury on the vaginal biomechanical properties enhances the rodent as a potential animal model; however, this animal model is still limited to perform mesh implantation because it is undersized. To overcome this limitation the abdominal wall, or hernia model, has been utilized to implant various meshes into the rodent. Differences in the loading conditions and biomechanical properties may affect the mesh-tissue interaction and host response; therefore, further evaluation of abdomen and mesh-tissue biomechanics compared to relevant animal models is required to assess its validity of the abdominal wall as an appropriate implantation site for studying prolapse meshes.

2.3 NONHUMAN PRIMATE

2.3.1 Introduction

Previously we illustrated how the rodent model may be used to assess changes that occur during pregnancy and postpartum. These studies have proved to be invaluable in our understanding of how the vagina supportive tissue complex adapts during pregnancy, but have been limited in illustrating the long-term effects of vaginal delivery on vaginal mechanical properties as the rat does not sustain a large degree of maternal birth trauma and completely recovers after a vaginal birth [8, 134, 139]. The following study illustrated that after suffering a simulated maternal birth

injury the mechanical properties of the rat matched published values for parous female patients (Section 2.2.8.3). Although we were able to create an injury and mimic the uniaxial mechanical properties of human vaginal tissue this animal model is still difficult to utilize for mesh implantation studies. Again, this is due largely to the limited amount of vaginal tissue to graft and perform biomechanical analysis on. Second, the rodent models lack muscular support and are quadrupeds which make the loading environment of the vagina and therefore mesh-vagina complexes very different than what is experienced *in vivo* for women. Further, this limited access and small changes in anatomy make it difficult to perform clinically relevant surgical procedures.

In contrast, the rhesus macaque is an established model to study the impact of vaginal delivery on vaginal tissue behavior because it has similar reproductive physiology to humans and spontaneously develops prolapse. More importantly, the size of the fetal head relative to the vaginal diameter places the mothers at a high risk to sustain an injury at the time of vaginal delivery, similar to humans [157]. It also has a district advantage of having similar gross and microanatomy to humans, and is more bipedal compared to the rodent. The parallels in the gross anatomy between the human and NHP make it possible to perform surgical repairs to vaginal tissue in a similar procedure to those performed clinically.

Based on the distinct advantageous of the NHP animal model we aimed to examine the native vaginal properties pre-and post vaginal delivery. In this study, we hypothesized that vaginal delivery results in long term changes in the vagina that predispose to the development of prolapse. Specifically, we believe that parity induced changes manifest as inferior mechanical properties associated with altered collagen structure. To test this hypothesis, we compared collagen alignment, the amount of the fibrillar collagens I, III and V, and mechanical properties

(tangent modulus or stiffness and tensile strength) in nulliparous and vaginally parous rhesus macaques. We focused our studies on the vagina because it is area that is grafted during prolapse repair and is the site of the multiple complications after mesh implantation.

2.3.2 Methods

2.3.2.1 Animals

The animals used in this study were maintained and treated according to experimental protocols approved by the Institutional Animal Care Utilization Committee of the University of Pittsburgh (IACUC # 0904403), and in adherence to the National Institutes of Health Guidelines on the use of Laboratory Animals. Accordingly, a minimum number of rhesus macaques (macacca mulatta) were utilized to answer our research question (see power analysis below) comprised of 14 cycling animals between 9 and 19 years of age. Parous animals (N=7) were a minimum of 12 months after their last delivery to allow adequate time to recover from short term birth injuries. Seven nulliparous control nonhuman primates (NHPs) were used for comparison. Routine laboratory tests and regular examinations by veterinarians during a quarantine period were used to certify that these experimental animals were pathogen-free and in good physical condition. Animals were maintained in standard cages with ad libitum water, and scheduled monkey chow supplemented with fresh fruit, vegetables, and multiple vitamins daily. A 12-h light/dark cycle (7am to 7 pm) was used and menstrual cycle patterns were recorded daily.

Available demographic data was collected including age, body mass index, gravidity, and parity of each NHP. A modified Pelvic Organ Prolapse Quantification (POP Q) exam was developed to take into account the smaller vaginal size in sedated NHP – rhesus macaque. Our

values are based on 10 previously examined nulliparous NHPs. Utilizing these exams, we calculated the urethrovesical junction to be 2 cm proximal to the vaginal introitus. Thus, in the fully supported vagina this position corresponding to point Aa of the POP-Q exam is -2 cm. The corresponding position on the posterior vagina wall (Ap) is -2 cm from the introitus. The gh, pb, Ba, Bp, C, D and TVL are measured similar to humans. In addition, the descent of the organs in all compartments is reported relative to the vaginal introitus as the hymen is less prominent in these animals. Prior to harvesting the vagina, a POP-Q exam was performed as described using a pediatric speculum. A crede maneuver was employed to mimic valsalva as a proxy for strain.

Following a POP Q exam, the vagina and supportive tissues were excised en bloc using a transabdominal approach. After the vaginal tissue had been isolated, the middle 2/3 was divided for (1) histomorphology, (2) biochemical, and (3) biomechanical analyses. Tissue samples obtained for all analyses avoided the urethra to reduce the influence on collagen alignment, composition, and its effect on the mechanical properties. Due to limited vaginal sizes, of several animals were unable to be examined using all described experimental protocols. Each section of this study was performed by one of the researchers who were blinded to the identification of the samples.

2.3.2.2 Trichrome Staining

For histomorphological imaging, tissue was embedded and frozen in optimal cutting temperature compound (OCT, Sakura, Tokyo). Sections of the vaginal cross-section were cut onto slides roughly 5-8 µm thick. Trichrome slides were used to ensure full thickness samples of the vaginal cross-section (epithelium, sub-epithelium, muscularis, and adventitia). These images were used to qualitatively assess differences between the vaginal cross-sections that may be

associated with vaginal parity. Blinded researchers examined each slide for any large changes in cross-sectional area composition, e.g. increases in smooth muscle or collagen composition.

2.3.2.3 Immunoflorescence

To assess the relative amounts of collagen I, III and V and the ratio of collagen I/(III+V), we followed an established protocol [52]. Briefly, sections used for immunofluorescence were also oriented along the longitudinal axis of the vagina, consistent with trichrome staining. All animals had three separate serial sections (5-7 μm) analyzed per assay, with 5-7 sites were quantified per section. Blocks were fixed, rehydrated, and placed into normal donkey serum for 45 minutes. Primary antibodies for collagen type I (mouse anti-Human 1:200;Biodesign, Saco, ME), collagen type III (goat anti-Human 1:500;Biodesign, Saco, Me), and collagen V (rabbit anti-Human 1:1000; Biodesign, Saco, Me) were first applied followed by incubation with secondary antibodies for 60 minutes. Each sample was imaged using an Olympus Fluoview microscope (DSS Imagetech, New Dehli, India). Fluorescence signals were digitalized to form a pixel based image displayed on a monitor and quantitated using Metamorph (v5.0, Universal Imaging Corporation) and represented as a relative collagen I/(III+V) ratio for each specimen. Three slides per animal were analyzed in five to seven randomly selected sites within the subepithelium (dense connective tissue layer of the vagina). Results for each collagen sub-type (I, III, and V) were represented as a threshold area for that particular collagen per total area, along with the collagen I/(III+V) ratio.

2.3.2.4 Collagen Alignment

Picrosirius red staining was performed to assess the overall alignment of the vaginal collagen matrix within the cross-section [158, 159]. Circularly polarized light and image-analysis software, was utilized to quantify collagen alignment by assessing fiber hue. To do this, 5 to 10 mm full thickness mid-vagina sections from 4 nulliparous and 6 parous animals were oriented along the longitudinal axis, embedded in OCT, and placed in liquid nitrogen. Blocks of tissue were then sectioned (7μm), placed on glass slides and stored at -70^{o}C. Seven to eight frozen sections per animal were hydrated briefly in dH_2O and imaged using a BX51 Olympus microscope. Five polarized light images per sample were taken at 20X in both the vaginal subepithelium and the muscularis. An area analysis was performed using Metamorph 5.0, where the hue component of the resulting image was obtained, and the number of red, orange, yellow, and green (the colors of collagen fibers in order of decreasing thickness and organization) pixels were calculated.

2.3.2.5 Passive Mechanical Properties

For biomechanical analysis, vaginal tissue samples from each NHP were carefully isolated from the surrounding connective tissue and wrapped in saline soaked gauze, placed in a plastic bag, and stored at -20^{o}C [106, 124]. On the day of testing, the tissue was thawed and a longitudinal section of tissue was isolated (18.2 ± 3.1 mm). The NHP vaginal tissue was subjected to a similar uniaxial tension protocol described in Section 2.2.3. In short, the vaginal tissue was clamped into custom designed soft tissue clamps, the cross-section area was measured, and strain markers were placed about the mid-substance of the tissue. After which the tissue was preloaded to 0.5 N, preconditioned, and loaded to failure. Each of the mechanical properties were

calculated from the stress-strain relationship as previously described [55]. Importantly, the loading conditions used in these experiments were not meant to recapitulate the physiology of vaginal delivery but rather to provide insight into fundamental differences in tissue behavior between nulliparous and parous animals.

2.3.2.6 Statistics

All statistical analyses were performed using SPSS (SPSS Inc, Chicago, Ill version 12.0.1). All data was examined to determine if it was normally distributed using a one-sample Kolmogorov-Smirnov test. A Student's t-test was used to compare all demographic data (age, height, weight, BMI, and total vaginal length (TVL)), collagen subtypes (collagen I, collagen III, collagen V, and collagen I/(III+V)) , collagen orientation (red:green ratio), and biomechanical properties (tangent modulus, tensile strength, maximum strain, and strain-energy density).

Statistics were aimed to answer our primary hypothesis which states that the mechanical properties of the tangent modulus and tensile strength would be inferior in parous NHP compared to nulliparous animals. Based on a preliminary study done within our lab on the biomechanical properties in the rodent model 7 animals would be required per group to detect at least a 30% difference between nulliparous and parous animals with an 80% power. Significant differences were found between these parameters with five and six samples in the nulliparous and parous groups, respectively, which indicates that we had reached 100% power for our primary outcomes as discussed below. The non-parametric Mann-Whitney test was used to compare POP-Q measurements. A Spearman's Rho rank correlation was performed to assess if the number of vaginal deliveries in the parous group correlated with any changes in collagen ratios, collagen subtypes, alignment, or biomechanical properties. All statistical tests were

evaluated at a significance level of 0.05. For normally distributed parameters, data is represented as mean (standard deviation) and for non-normally distributed data as median (interquartile range).

2.3.3 Results

Of the 12 animals used in this study, two were part of a shared study and had sufficient tissue for only a single analysis leaving one animal in each group without combined biomechanical and biochemical data. The demographical data of all 12 animals is shown in Table 9. Age in the nulliparous group had a mean of 11.0 ± 1.2 years which was significantly lower ($p=0.04$) than the parous group (13.0 ± 3.1 years). Parous animals had a median parity of 7 (range 1-8) which is relatively low for this species. The height (m) and weight (kg) of each animal was collected and used to calculate individual BMI values. There was no statistical difference found between the BMI of each group ($p=0.37$, Table 9).

POP-Q scores were compared between nulliparous and parous animals based on a modified exam (see Methods 2.3.2.1). All POP-Q measurements can be seen within Table 9. Nulliparous animals were observed to have a well supported vagina, as reflected in their superior POP-Q scores. The distance from the hymen to the cervix (C, $p=0.02$) and the hymen to the most dependent portion of the posterior fornix (D, $p=0.006$) was greater in parous relative to nulliparous animals indicating greater descent. No statistical differences were found in the remaining POP-Q measurements: genital hiatus (GH), perineal body (PB), anterior wall (Aa and Ba), and posterior wall (Ap and Bp), or the total vaginal length (TVL) (Table 9).

Table 9 Demographical and modified POP-Q variables from nulliparous and parous NHP.. Statistical differences were determined using a Mann-Whitney or Student's t-test (normally distributed data indicated by n). Non-parametric data is represented as median (interquartile range) while the remaining data is presented as mean ± S.D. [160]

	Nulliparous (n=7)	**Parous (n=7)**	**p-value**
Age (years)	11.0 ± 1.2	13.0 ± 3.1	0.04^n
BMI (kg/m^2)	16.0 ± 3.9	19.0 ±4.4	0.37^n
Parity	0 (0)	7.0 (2.0-8.0)	-
GH (cm)	0.5 (0.5 – 1.0)	2.0 (0.8 – 2.3)	0.12
PB (cm)	1.5 (1.0 – 1.5)	1.0 (1.0 – 1,8)	0.69
C (cm)	-6.0 (-6.0 – -6.0)	-3.5 (-5.5 – 2.3)	0.02
D (cm)	-7.0 (-7.0 – -6.3)	-4.0 (-5.8 – -2.8)	0.00
Aa (cm)	-2.0 (-2.0 – -2.0)	-2.0 (-2.0 – -1.0)	0.69
Ba (cm)	-2.0 (-2.0 – -2.0)	-2.0 (-2.0 – -1.0)	0.69
Ap (cm)	-2.0 (-2.0 – -2.0)	-2.0 (-2.0 – -1.0)	0.69
Bp (cm)	-2.0 (-2.0 – -2.0)	-2.0 (-2.0 – -1.0)	0.69
TVL (cm)	6.4 ± 0.79	6.1 ± 1.1	0.34^n

All specimens analyzed were corroborated to be full thickness vagina by trichrome staining. Similar to humans, the NHP vagina is comprised of 4 layers including a cellular epithelium (stained pink), sub-epithelium which consists of predominately collagen III (stained blue), muscularis layer (stained pick) comprising 40-50% of the total volume, and an adventitia tissue layer comprised of loose connective tissue layer (stained blue). There was not a gross difference in histological appearance between nulliparous and parous animals (Figure 16).

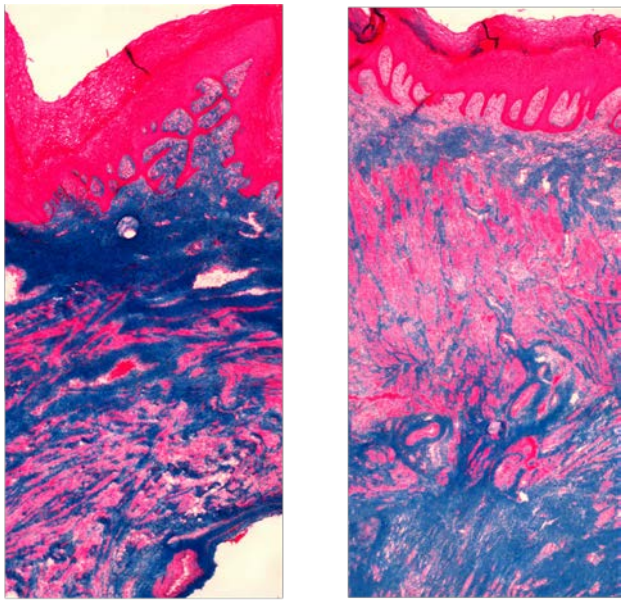

Figure 16 Trichrome images of nulliparous (A) and parous (B) NHP. Stained bright pink is the epithelium layer, followed by the sub-epithelium layer (blue), which contains a majority of the collagen matrix of the vaginal cross-section. The muscularis bilayer consists of a layer of circumferentially oriented and a layer of longitudinally oriented muscle fibers, which are stained pink. The adventitia, which is a loose connective tissue layer stained blue [160].

The ratio of collagen I/(III+V) was similar in the vaginal sub-epithelium between nulliparous and parous animals (Table 10; p=0.26). Individual collagen subtypes per area were also similar with nulliparous NHP having a collagen I (0.04 ± 0.02), collagen III (0.5 ± 0.04) and collagen V (0.2 ±0.06) and parous with collagen I (0.04 ± 0.03, p=0.83), collagen III (0.4 ± 0.2, p=0.11), and collagen V (0.07 ± 0.09, p=0.09).

Table 10 Relative collagen I/(III+V) ratio and individual collagen sub-types (I, III, and V) per area for nulliparous and parous NHP. All data is represented as mean ± S.D. Significance was determined using a Student's t-test ($p<0.05$) [160].

	Nulliparous (n=5)	**Parous (n=6)**	**p-value**
Collagen I/(III+V)	0.07 ± 0.03	0.09 ± 0.03	0.26
Collagen I	0.04 ± 0.02	0.04 ± 0.03	0.83
Collagen III	0.5 ± 0.04	0.3 ± 0.2	0.08
Collagen V	0.2 ± 0.06	0.07 ± 0.09	0.09

In contrast, quantitative analysis of picrosirius red stained sections showed an overall higher red:green ratio indicating more aligned collagen fibers in nulliparous vs parous animals. Indeed, nulliparous NHP had a red:green ratio of 2.7 ± 1.3 compared to parous NHP with a ratio of 1.4 ± 0.64 (p=0.06, Figure 17). Although these values were not statistically different, we found this was attributable to a single outlier in the parous group. After removing this single parous animal from the data analysis, the collagen alignment was significantly lower in parous compared to nulliparous NHPs (p=0.02).

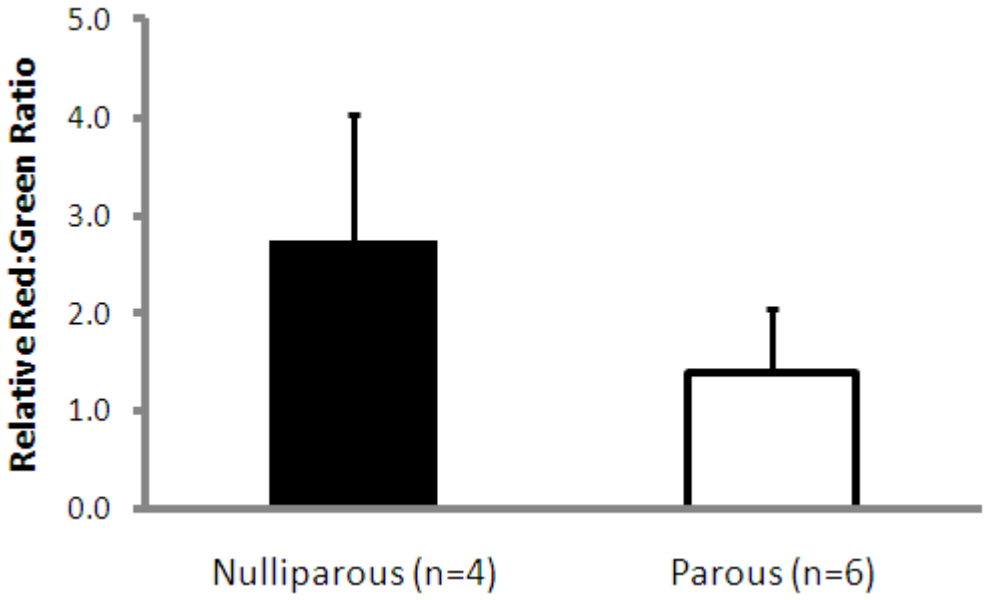

Figure 17 Relative red:green ratio for nulliparous and parous animals. A higher red:green ratio indicates a higher degree of alignment within the cross-section. We observed a decrease in collagen alignment associated with parity [160].

The parameters describing the mechanical properties of nulliparous versus parous primate vagina were determined from their stress-strain relationship (Figure 18). Both curves demonstrated nonlinear behavior with distinct toe, linear, and failure regions. However, the nulliparous group was more nonlinear beyond 3% strain, which is reflected by the higher tangent modulus (slope of

the stress-strain curve corresponding to the stiffness of the specimen; p=0.03) with nulliparous NHP having 52% higher tangent modulus as compared to parous animals (Table 11).

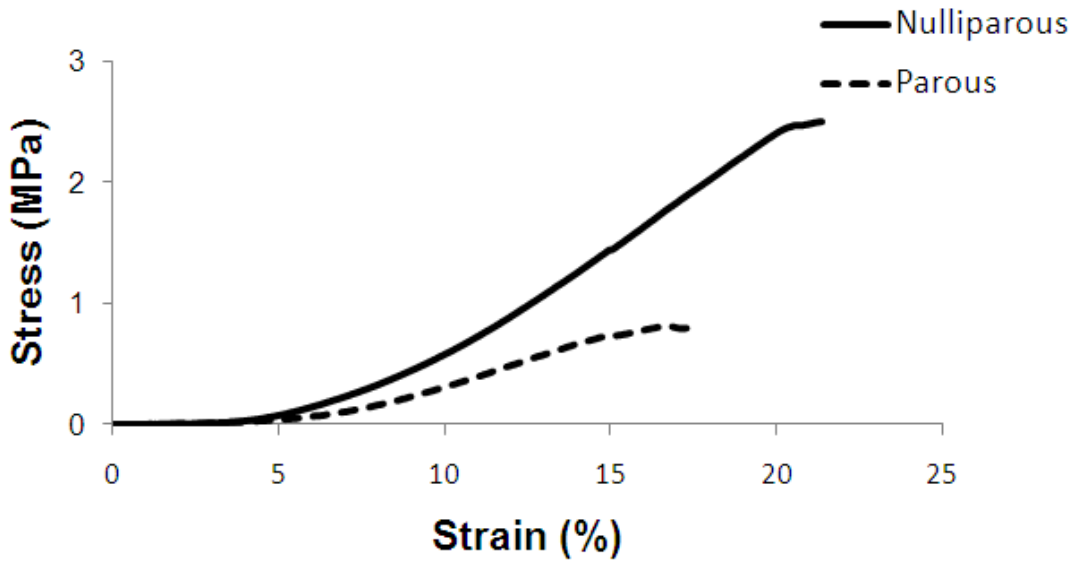

Figure 18 Representative stress-strain curves for nulliparous and parous animals from a uniaxial tensile test to failure. Both curves demonstrated nonlinear behavior with a distinct toe, linear, and failure regions. However, the nulliparous group was more nonlinear beyond 3-5% strain characterized by significant differences in the tensile strength, tangent modulus, and strain-energy density (Table 11) [160].

The nulliparous group also displayed a significantly higher tensile strength, which measured almost 3 times that of the parous group (Table 11; $p<0.001$). Correspondingly, it was found that the strain energy density of nulliparous samples was roughly 3 times greater than that of the parous group (Table 11, p=0.006). No statistical differences were detected between each group for ultimate strain (p=0.26). Thus, the data indicate that nulliparous tissue is stronger, more difficult to deform, and tougher than parous tissue.

Table 11 The biomechanical properties (tensile strength, maximum strain, tangent modulus, and strain-energy density) of nulliparous and parous NHP are presented as mean ± S.D. A Student's t-test ($p<0.05$) was used to determine statistical significance between each group [160].

	Nulliparous (n=5)	**Parous (n=6)**	**p-value**
Tangent Modulus (MPa)	27.0 ± 11.5	12.8 ± 6.6	0.03
Tensile Strength (MPa)	2.4 ± 0.53	0.96 ± 0.26	<0.001
Maximum Strain (%)	19.0 ± 5.4	16.0 ± 5.0	0.24
Strain-Energy Density (MPa)	0.18 ± 0.08	0.07 ± 0.02	0.006

Further analysis demonstrated no significant correlations between the number of vaginal deliveries and collagen sub-types, collagen I/(III+V) ratios, alignment, and biomechanical properties. Animals were then separated into three categories: nulliparous, parous no prolapse, and parous prolapse. For inclusion in the parous prolapse group one of the following POPQ parameters were required: C > -1, Aa,Ba >-1 or Ap, Bp >-1 with 3 animals meeting one of these criteria. By this method, we found significant negative correlations between prolapse and tangent modulus (r2= -0.53; p=0.01), tensile strength (r2= -0.67 p=0.002), strain-energy density (r2= -0.71; p=0.001), and collagen alignment (r2= -0.66; p=0.005; Table 12). Interestingly, the parous prolapse NHPs had the lowest red:green ratio (1.0 ± 0.07) compared to well supported parous NHP (1.8 ± 0.8) and nulliparous animals (2.7 ± 1.3), suggesting an association between a loss of collagen architecture and the development/progression of prolapse. This also correlated very well with the biomechanical properties. Animals with prolapse displayed a lower tangent modulus (9.5 ± 1.0 MPa), tensile strength (0.9 ± 0.2 MPa), and strain-energy density (0.06 ± 0.01 MPa) compared to normally supported parous animals (values = 1.0 ± 0.4 MPa, 16.0 ± 8.7 MPa, and 0.08 ± 0.03 respectively).

Table 12 Relationship between degree of pelvic organ support (categorized as nulliparous, parous supported, and parous prolapsed) and tangent modulus, tensile strength, strain-energy density, and collagen alignment. All data is represented as mean ± S.D. Significance correlations were assessed using a Spearmen Rho ranks test ($p<0.05$) [160].

	Nulliparous (n=5)	**Parous, Supported (n=3)**	**Parous, Prolapse (n=3)**	**Correlation (R^2)**	**p-value**
Tangent Modulus (MPa)	27 ± 11.5	16.0 ± 8.7	9.5 ± 1.0	-0.53	0.01
Tensile Strength (MPa)	2.4 ± 0.53	1.0 ± 0.4	0.9 ± 0.2	-0.67	0.002
Strain-Energy Density (MPa)	0.18 ± 0.08	0.08 ± 0.03	0.06 ± 0.01	-0.71	0.001
Collagen alignment	2.7 ± 1.3	1.8 ± 0.08	1.0 ± 0.07	-0.66	0.005

2.3.4 Discussion

The vagina is central to pelvic organ support such that a normally supported vagina will resist downward descent of the uterus, urethra, bladder, and rectum. After a substantial decrease in biomechanical properties the vagina can no longer support these loads and prolapse develops.

To adequately study how prolapse mesh implantation affects the grafted tissue, it is important that the animal model examined consist of several criteria.

Maternal birth injury subsequent to vaginal delivery is considered the greatest risk factor for the development of prolapse. In this study, we therefore, examined the impact of vaginal delivery on the vagina using histomorphologic, biochemical, and biomechanical outcomes in a non-human primate (NHP) model. The most important findings of the study were that vaginal parity was associated with decreased collagen alignment and inferior biomechanical properties without impacting overall tissue histomorphology. The loss of collagen alignment and progression to inferior mechanical properties was highly correlated with the presence of pelvic organ prolapse. A noteworthy result of this study was the effect of parity on the biomechanical

properties of the NHP vagina. First, we can recall the literature values for the tangent modulus and tensile strength of vaginal tissue parous human (9.5-12 MPa and 1.4 MPa, respectively) [106, 156]. Next, we can see that after delivery the mechanical properties of the NHP are analogous to these published values.

In this study, we assumed that the composition and structural organization of the dense connective tissue layer of the vagina was the major determinant of the overall tissue's biomechanical function. However, we found no differences in the relative amount of collagen subtypes of the subepithelium in nulliparous and parous animals. Here, we proposed that a change in a collagen subtypes or the collagen I/III+V ratio would be a marker of injury to and/or remodeling of the vagina subsequent a maternal birth injury. This collagen ratio has been previously shown to decrease in prolapse patients [51], and an ideal animal model for mesh implantation would reflect similar changes in the vaginal composition. However, there are several explanations why a parallel change was not observed in the collagen ratios that was observed in the mechanical properties. First, a change in collagen subtypes is not a marker for maternal birth injury at the time of delivery. Second, that an altered collagen supermolecular structure (i.e. alignment) precedes changes in collagen subtypes in the course of prolapse progression.

As an indication of altered molecular packing topology of collagen or its super-molecular structure, we measured collagen fiber alignment. We found that collagen fibers were less aligned in parous primates and that this correlated with a significant decrease in the parameters describing the mechanical properties of the tissue (tangent modulus, tensile strength, and strain-energy density). The packing topology or alignment of the collagen fibers within the extracellular matrix (ECM) is also an important contributor to the structural integrity of a tissue.

In general, a more aligned matrix (ECM) has superior mechanical properties when compared to a disorganized unaligned matrix assuming similar collagen composition and the aligned specimens are tested along the direction of collagen alignment [161-163]. The decrease in collagen alignment in parous animals provides tremendous insight into the biochemical basis for the inferior mechanical properties associated with parity. Moreover, we identified a correlation between the presence of prolapse, inferior biomechanical properties (tangent modulus, tensile strength, and strain-energy density), and a lower degree of collagen alignment in the vaginal cross-section. The degree of collagen alignment within the parous and prolapsed female population would help confirm if these changes are observed clinically and if the pathophysiology of prolapse development is the same in the NHP as it is in women. However, since only several of the NHP had prolapse, we can only speculate how parity and the development of prolapse may be related, but it is an interesting finding that warrants further investigation in future studies. Indeed, better characterization of the collagen matrix of vaginal tissue would help us better understand changes that occur with mesh implantation. A further decrease in collagen alignment after implantation may be a sign of a degenerative remodeling host response.

The major strength of this study is that we utilized the non-human primate animal model to answer our research question. By using the NHP model, we were able to overcome some of the problems associated with obtaining tissue biopsies in humans including inconsistent tissue quality from manipulation during procurement and variable exposures including smoking, hormone use and physical/occupational activity. We have illustrated that the parous NHP and parous women have similar vaginal biomechanical properties which is important for assessing how the structural properties of the mesh affect the host response.

However, our study also has several limitations. First, age was lower in the nulliparous animals. As age is also cited as a risk factor for the development of a pelvic floor disorders, it is possible that the changes in collagen alignment and biomechanical properties occurred as a result of age independent of parity; however, the difference in mean age was only 2 years which is unlikely to be clinically significant. Moreover, no correlations were found between age and any biochemical or biomechanical properties examined in this study. It is noteworthy that NHPs are relatively difficult to obtain and due to the expense and limited quantity, studies with large sample sizes are virtually impossible to perform. This is a key limitation when designing studies to evaluate the host response of prolapse repair of various used meshes. A second limitation is that in the current study design, we are unable to distinguish changes due to an injury at the time of delivery from those incurred as a result of pregnancy tissue adaptations. Finally, as alluded to previously, we cannot provide a definitive relationship between the changes observed with parity and those seen in animals with prolapse. Therefore, we can speculate that the decrease in biomechanical properties (e.g. tangent modulus and tensile strength) would lead to the progression and development of prolapse over time which is clinically observed in parous women.

In summary, parity has a significant long-term negative impact on collagen alignment and biomechanical properties of the vagina. The data provide a mechanism for the increased risk for prolapse in women after vaginal delivery due to altered collagen arrangement and mechanical properties. Further, due to the similar biomechanical properties of the NHP and female vagina, it supports the use of the NHP animal model for examining the effect of mesh implantation on vaginal tissue.

2.4 SHEEP

2.4.1 Introduction

The current lack of knowledge is largely due to the limitations in accessing tissue from human patients for obvious moral and ethical concerns. Previous research has examined the rodent and NHP as possible models for the effects of parity and mesh implantation [135, 160, 164]. These studies have shown that parity led to inferior uniaxial tensile mechanical properties of the vagina and modified POPQ scores in the NHP. However, the monetary expense of utilizing makes it challenging to utilize the NHP model to study mesh implantation of many current and next generation prolapse meshes. The sheep is a commonly used urogynecological animal model for study reproduction; however, little research has been done to examine the sheep as a valid animal model for examining mesh implantation into parous animals.

Sheep can naturally develop prolapse later in life therefore we hypothesize that vaginal delivery will significantly impact the passive support of the pelvic floor in the sheep model predisposing it to the development of prolapse later in life. Specifically, we hypothesize that parity will lead to inferior connective tissue support and biochemical and mechanical properties of vaginal tissue and reflect similar biomechanical properties reported for parous female patients. Unlike the rodent and NHP, sheep contain a multiple component stomach classified as the ruminant. This large ruminant makes it difficult to apply the typical valsalva maneuver required to accurately measure pelvic floor support. Therefore, a custom designed colpometer was developed as a secondary method for measuring pelvic floor support. Our objective was to examine the connective tissue support via a colpometer device and examine the fibrillar

collagens I, III, and V ratios and uniaxial mechanical properties of the vagina in nulliparous and parous mixed doreset ewe. The effect of parity was examined focusing mainly on the vaginal tissue due to its ease of access, isolation, and for comparisons with previous studies.

2.4.2 Methods

2.4.2.1 Animals

For this study, tail docked mixed Dorset ewe were utilized in accordance to the Institutional Animal Care Utilization Committee of the University of Pittsburgh (IACUC # 1006281), and in adherence to the National Institutes of Health Guidelines on the use of Laboratory Animals. Eight nulliparous (7-9 months) and eight parous (18 months) sheep were examined in this study. All animals were cycling, and parous sheep were 8 months from their last, and only, vaginal delivery and is primiparous. The weight of each animal was also recorded. To assess the pelvic floor support we utilized the standard Pelvic Organ Prolapse Quantification (POPQ) exam. All POPQ values were taken similar to female patients, and valsalva was performed as a proxy of the crede maneuver.

Due to the large abdominal cavity and ruminant of the sheep model, a secondary method for measuring pelvic floor support was developed. Here, connective tissue support was assessed utilizing a custom designed colpometer device. Our device consisted of a spring scale attached in series to a long cervical clamp that passes through a platform. A standard ruler was then used to measure the position of the cervical clamp relative to the platform when it is placed against the perineum. Animals were placed in the supine position and the colpometer was fixed to the cervix. A reference position was established by reducing the cervix to its normal anatomical

position and the displacement required to zero the force on the spring scale, or when the supportive tissues began to resist extension was recorded. This position was coined the native laxity of the pelvic floor. Subsequently, a maximum of 20 N was applied in ~5 N increments and the corresponding displacements were measured with respect to the reference position. This created a force-displacement relationship. The slope, which equates to the stiffness (N/mm) of the passive supportive structures in the pelvic floor was calculated from these data. The displacement at 20 N was recorded as the maximum displacement of the pelvic floor. To account for differences in each animal's vaginal length the native laxity and maximum displacement were normalized to the total vaginal length (TVL) of the respective animal. These are reported as the normalized laxity and normalized pelvic floor (PF) descent.

POPQ measurements were made prior to colpometer measurements and harvesting of the vagina. After colpometer measurements, a dissection was performed to expose the entire pelvic floor anatomy. The uterus, bladder, and vagina were harvested together. A further dissection was performed to isolate the vagina, and for this study the posterior vaginal tissue was utilized and divided for 1) histological 2) biochemical, and 3) biomechanical analysis.

2.4.2.2 Collagen Sub-Typing

The assay was performed by one of the researchers who was blinded to the identification of the samples following a protocol detailed previously [56]. In brief, a small portion of full-thickness vaginal wall was imbedded for histological confirmation and was done with a Trichrome stain. Under a dissecting microscope, epithelium of full-thickness vaginal wall was excised leaving the subepithelium, muscularis and adventitia for collagen extraction and analysis. An approximate 200 mg of the remaining dissected tissue were ground and dried. The weight of the dried tissue

was measured. The dry tissue was then incubated in 1ml 0.5M acetic acid for 24 hours at 4^{o}C. Pepsin (5mg/ml) was added at a ratio of 1:30 then 1:10 (by weight), stirring at 4^{o}C for 24 hours, respectively. After spinning at 14000 rpm for 1 hour at 4^{o}C, the supernatant was collected. One ml of 0.5M acetic acid was added and vortexed for 24 hours at 4^{o}C, followed by a centrifugation at 14000 rpm for 1 hour at 4^{o}C, then the supernatant was collected and combined with prior supernatant. The combined supernatant was neutralized with 0.5M NH_4HCO_3 and concentrated and stored at -80^{o}C for further analysis. Ten µl of the supernatant were separated by 5% SDS-gel electrophoresis under reducing conditions and stained with 0.5% Coomassie brilliant blue. Purified collagen type I, III and V (Sigma-Aldrich) and a pre-stained SDS-PAGE Standards (Bio-Rad) were loaded on the gels as controls. The intensity of the scanned bands was simultaneously quantified with software of UN-SCAN-IT gel (version 4.3, Silk Scientific Co, Orem, Utah) on the same gel to determine the relative quantity of each. The data were represented as ratio of I/III and I/III+V, equal loading was insured by normalizing to the dry weight of the sample. All experiments were performed in duplicate on nulliparous (n=6) and parous (n=4) animals.

2.4.2.3 Mechanical Properties

For biomechanical samples, tissue was placed in saline soaked gauze, placed in a sealed bag, and kept at -20^{o}C. This storage method has been shown to have minimal effects on the passive mechanical behavior of soft tissue under uniaxial tension [124]. For characterizing the uniaxial tensile properties we followed a previously established protocol described in Section 2.2.3[135, 136]. Briefly, the tissue was thawed at room temperature the day of testing and placed in custom designed soft tissue clamps to form a clamp-vagina-clamp complex. Each sample was preloaded

(0.1 N), preconditioned (10 cycle to 7% the clamp to clamp strain), and loaded to failure along the longitudinal axis of the vagina.

Defining the tensile strength as the maximum stress achieved at failure and the ultimate strain was the strain corresponding to the tensile strength. The tangent modulus was the slope within the linear region of the stress-strain curve. Lastly, the strain energy density was taken as the area underneath the stress-strain curve until failure.

2.4.2.4 Statistics

Statistics were done using the SPSS statistical package (SPSS Inc. Chicago, Il. Version 18.0). Data were examined to determine normality. POP-Q measurements excluding genital hiatus (gh), perineal body (pb), and total vaginal length (TVL) were considered non-parametric. In addition stiffness of the passive supportive structures, collagen I/(III+V), and collagen I/III ratio were found to not be normally distributed. For these comparisons a non-parametric Mann-Whitney test was performed between nulliparous and parous animals. The GH, PB, TVL, weight, normalized laxity and descent of the pelvic floor were considered parametric data. Including these parameters all mechanical properties were found to be normally distributed (tensile strength, ultimate strain, tangent modulus, and strain-energy density). These parameters were compared using a Student's test. All non-parametric data is represented as median (interquartile range) while all parametric parameters are displayed as mean ± standard deviation. All statistical tests were evaluated with a significance level of 0.05.

2.4.3 Results

Of the 8 nulliparous and 8 parous sheep, the age and weight of these animals were found to be significantly different between these two groups. The age of the nulliparous animals ranged between 7-9 months while the parous sheep had an average age of 18 months. Second, the weight of the nulliparous animals (55.3 ± 4.5) was significantly higher than the parous animals (38.4 ± 1.7; $p<0.001$). POP-Q scores for each group are listed within Table 13. The gh of the nulliparous sheep was 18% larger compared to parous animals ($p=0.024$). Even though there was a significantly larger gh for the nulliparous animals, overall the nulliparous vagina was more supported compared to parous animals. The distance from the hymen to the posterior fornix was significantly longer in nulliparous animals (D, $p=0.024$), while there was no change in the distance from the hymen to the cervix (C, $p=0.16$). However, in terms of anterior and posterior vaginal support the nulliparous animals had a less degree of vaginal wall laxity. The anterior wall support for the proximal (Aa) and distal (Ba) portions of the vagina were significantly lower in the parous sheep ($p=0.015$ and $p=0.015$ respectively). While no statistical differences were observed for the proximal (Ap, $p=0.065$) or distal (Bp, $p=0.065$) posterior wall, the parous sheep tended to have a more lax posterior wall (Table 13). Interestingly, with a difference observed in posterior fornix, there was no statistical difference in the TVL ($p=0.12$).

Table 13 POPQ scores from nulliparous and parous sheep. Anterior support was found to be significantly different after vaginal delivery

	GH (cm)	PB (cm)	C (cm)	D (cm)	Aa (cm)	Ba (cm)	Ap (cm)	Bp (cm)	TVL (cm)
Nulliparous (n=8)	2.3 ± 0.35	1.4 ± 0.56	-8.8 (4.4)	-10 (5.1)	-3 (1.9)	-3 (1.9)	-1 (2.4)	-1 (2.4)	10.4 ± 1.2
Parous (n=8)	1.9 ± 0.34	1.6 ± 0.34	-7.8 (3.9)	-6 (2.5)	-1.5 (0.63)	-1.5 (0.63)	0 (0.38)	0 (0.38)	9.4 ± 1.2
p-value	0.024	0.25	0.16	0.024	0.015	0.015	0.065	0.065	0.12

The colpometer revealed several interesting things about the passive support of the pelvic floor (Figure 19). The normalized laxity of the pelvic floor was 46% greater in the parous animals (p=0.008). These results suggest a change in resting position of the pelvic floor following vaginal delivery. The normalized descent of the pelvic floor was still 28% higher in parous animals (p=0.039) compared to nulliparous animals. However, the stiffness of the passive supportive structures was not significantly different between the two groups (p=0.065). The lack of a significant difference in the stiffness of the passive supportive structures suggests that once the supportive structures did begin to resist pelvic floor descent, there was no difference in their ability to do so.

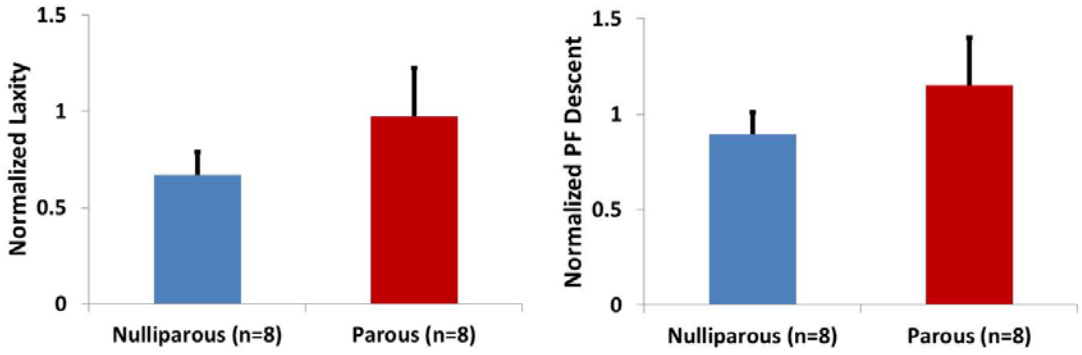

Figure 19 Normalized laxity (left) and normalized pelvic floor (PF) descent (right) were found to be significantly different between nulliparous and parous sheep (p=0.008 and p=0.039, respectively)

The collagen ratios of the vagina for nulliparous and parous animals are reported in Table 14. The collagen I//(III+V) and collagen I/III ratios were similar between each group (p=0.914 and p=0.914, respectively). Similarly, the mechanical properties of the vagina were not found to significantly different between each group (Table 14). There was only an 8% decrease in the tensile strength (p=0.66) and a 6% difference in the tangent modulus (p=0.76). While a 22% and 28% difference were calculated for the ultimate strain and strain-energy density between

nulliparous and parous animals, no significant differences were found in either of these parameters.

Table 14 Collagen ratios and mechanical properties of nulliparous and parous sheep. No differences were found due to parity between each groups regarding the collagen ratios or mechanical properties.

	Collagen I/(III+V)	Collagen I/III	Tensile Strength (MPa)	Ultimate Strain	Tangent Modulus (MPa)	Strain-Energy Density (MPa)
Nulliparous	1.2 (0.26)	1.4 (0.33)	2.8 ± 0.95	0.31 ± 0.11	20.0 ± 9.2	0.32 ± 0.14
Parous	1.1 (0.23)	1.4 (0.26)	2.5 ± 0.95	0.24 ± 0.95	21.1 ± 5.8	0.23 ± 0.14
p-value	0.914	0.914	0.662	0.177	0.764	0.238

2.4.4 Discussion

The goal of this study was to evaluate the effects of parity on pelvic floor support and the vaginal biochemical and biomechanical properties in the sheep animal model. The vagina plays a focal role in the support of the pelvic organs. In prolapsed women, the vaginal tissue is prone to failure which has lead clinicians to use permanent synthetic meshes to restore the lost structural support. Here we examined the sheep as a possible animal model to examine the effects of mesh implantation onto the vaginal tissue. At the moment, we are interested in evaluating the mechanics of the host response and consequently require an animal model with a similar biomechanical behavior and loading environment to the female prolapse patient.

First, we evaluated the pelvic floor support through the standard POP-Q measurements and then quantitatively examined pelvic floor support via the colpometer device. From these results we found that parity significantly affected the pelvic floor. The normalized laxity of the pelvic floor was much lower after pregnancy and vaginal delivery compared to nulliparous

animals. This can be interpreted as an effect of parity on the resting position of the pelvic organs.

Contradictory to our original hypothesis, the sheep animal model had no changes in the collagen ratios and a lack of significant differences in all biomechanical properties. We expected that parity would have a negative effect on the vaginal tissue leading to inferior mechanical properties postpartum. This was similar to our previous finding on the effect of parity on the mechanical properties of the vagina in the rodent model; however, even though we could detect a significant effect on the passive supportive structures of the pelvic floor via POP-Q measurements and our colpometer protocol, these changes were not manifested in vaginal mechanical properties. The absence of a reduction of mechanical properties of the vagina in the sheep constrains its use as an animal model for mesh implantation. The biomechanical properties of the female vagina are impaired after delivery and at the time of prolapse and these similar biomechanical properties need to be present in an appropriate animal model.

The inability to detect significant effects of parity in the mechanical properties of the vagina could be attributed to the limitations of the current study. First is the difference in age and weight of the nulliparous and parous sheep. Since age plays a role on the maturation of the pelvic floor support and weight is important in the level of intra-abdominal pressure applied to the pelvic organs both could significantly affect the outcomes of this study. Interestingly, even though the parous sheep were significantly smaller we were still able to show a decrease in the level of anterior vaginal wall support indicated by the POP-Q measurements. We were also able to identify that the normalized laxity of the pelvic floor was greater in parous animals compared to their larger nulliparous counterparts. However, it is important to have age and weight controlled studies to make better comparisons between nulliparous and parous animals and future

studies will aim at examining such groups. The lack of significance observed in the mechanical properties between nulliparous and parous animals could be attributed to several additional limitations. The first is that these animals were only eight months from giving birth. Here, we assumed that the vagina, as a supportive structure in the pelvic floor, will have inferior mechanical properties after pregnancy and vaginal delivery. This was reflected by POP-Q measurements and colpometer data, but it did not translate to significant differences in the collagen ratios or mechanical properties. Therefore, it is possible that eight months after vaginal delivery was not enough time for changes in the mechanical properties of the vagina to manifest. Longer time points may be required to observe the remodeling effects due to a change in loading conditions (native laxity) of the pelvic floor on the mechanical properties of the vagina.

In conclusion, parity was found to only affect the passive support of the pelvic floor. By comparing POP-Q and normalized laxity, it was clear that parity increased the normal resting position of the pelvic organs. However, these alterations in pelvic floor support did not result in a negative effect on the collagen ratios and biomechanical properties of the vagina eight months after vaginal delivery. Future studies will examine the result of a simulated maternal birth injury on the vaginal mechanical properties. A birth injury may deteriorate the vaginal mechanical properties similar to those observed in the rodent model (Section 2.2.8), and make it a better model that would assimilate more closely to the clinically grafted vaginal tissue of the.

2.5 CONCLUSION

In Section 2.0 we examined three of the commonly used animal models for pelvic floor research: rodent, NHP, and sheep. Parity, a considerable risk for developing prolapse, is thought to negatively affect the mechanical properties of the vaginal tissue: weakening the vaginal tissue and making it prone to prolapse later in life. Here, our overall goal was to characterize and compare the native properties of the vaginal tissue between nulliparous and parous animals via collagen ratios and mechanical properties and how well they reflected published literature on parous and prolapsed women [51]. The motivation for this investigation was to determine an animal model that would be suitable to evaluate the biomechanics of the host response to prolapse meshes. Surgical repair of prolapse often involves the implantation of a permanent synthetic graft.

An interestingly finding from these studies was the lack of change in the collagen I/III ratio after vaginal delivery in the rodent, NHP, and sheep animal models. While we were not able to distinguish any significant differences in the mechanical properties between nulliparous and parous rodents, the rodent has provided relevant information concerning the maternal adaptations of the mechanical and contractile properties of the vagina throughout pregnancy. Therefore, rodent would be advantageous as an animal model because it is small, inexpensive, and easier to work with compared to the NHP and sheep.

Parity did not negatively impact the vaginal biomechanical properties as hypothesized. In a follow up study, we examined the outcome of a simulated birth injury in the rodent model. This study allowed us to assess the persistent effects of an injury by observing a 44% decrease in the tangent modulus and lowered the tensile strength by 38%. After a simulated injury the

tangent modulus and tensile strength of the rodent reflect values previously published for the parous human.

Parity in the NHP was found to have a negative effect on the biomechanical properties of vaginal tissue. After parity, the tangent modulus and tensile strength decreased by an average of 53% and 60%, respectively. The mechanical properties of the vaginal tissue from parous NHP mirrored those previously published for parous women. This finding indicates that NHP suffer a permanent affect due to parity and has similar biomechanical properties as those women suffering from vaginal wall laxity and possible including women undergoing prolapse repair surgery.

The sheep offers the opportunity to evaluate a larger animal model compared to the rodent, but is more affordable than NHP animal studies. When examining the mechanical properties of this animal model, parity did not result in inferior biomechanical properties of the vaginal wall. Therefore, the sheep currently needs additional studies to examine it potential as an adequate animal model for examining the biomechanical response to mesh implantation. These studies may include performing weight and aged matched sheep studies to remove the effects of confounding risk factors. In addition, if these studies remain fruitless at identifying a lack of poor biomechanical properties due to parity, it may be beneficial to utilize a simulated birth injury. Developing a birth injury in the sheep may improve this animal model for the evaluating the host response to mesh implantation. First, the injured vaginal tissue may have similar biomechanical properties as the parous female patient; and, more importantly, it would offer a relatively inexpensive means to evaluate mesh implantation compared to the NHP.

This simulated birth injury has been shown to improve the rodent as a vaginal model for examining the effects of mesh implantation. However, this animal model is still limited due to

the size of the vagina and implantation site. This limitation has forced researchers to examine the rodent abdominal hernia model as an alternative [73, 165-167]. These studies have shown important finds regarding the biochemical and biomechanical properties after implantation. Further, this abdominal model has the ability to provide a great amount of baseline data of mesh incorporation. Utilizing the rodent abdominal implants as a replacement for a vaginal implantation model requires additional evaluation of the mechanics of the host response *in vivo*. In short, the effect of mesh implantation on this surrogate model needs to be characterized relative to an appropriate vaginal model.

In summary, it was found that the NHP vaginal model was the most suitable to evaluate the biomechanics of the host response to prolapse meshes. The NHP has similar gross and microanatomy and physiology as females. The comparable pelvic floor support and vaginal mechanical properties of the NHP that parallel those of parous women make it the best choice to perform *in vivo* studies of the mesh-tissue complex.

3.0 CHARACTERIZING THE *EX VIVO* PROPERTIES OF SYNTHETIC PROLAPSE MESHES

3.1 OVERVIEW

Synthetic meshes are commonly used as a permanent structural support to repair POP as autologous tissue repair has been associated with failure rates in excess of 30% [5, 51, 68, 168]. This is thought to be because native tissue repairs utilize already weakened tissue and consequently fail to address the mechanism that initially caused failure. Thus, it is not surprising that the use of synthetic meshes was reported in 93% of abdominal sacral colpopexies and 58% of vaginal reconstructive procedures [63].

Despite its widespread acceptance and use, synthetic meshes have had little regulatory oversight. While federal laws have mandated oversight and pre-market approval of medical devices through the 1976 Medical Devices Amendment Act, most meshes used in pelvic surgery are not subject to this jurisdiction as they are considered 510 (k) devices, i.e. a device that is based on a similar device that was in use prior to 1976 in this case, hernia meshes. This is especially alarming since the FDA released a public health warning on October 21, 2008 citing a high rate of complications with the use of synthetic meshes following urogynecological implantation. The list of complications includes acute and chronic infection, tissue contraction due to mesh shrinkage, erosion of the mesh into adjacent structures, and dyspareunia [60, 80,

169, 170]. As previously mentioned erosion is a particularly startling complication as it involves the implanted mesh, or designed treatment for prolapse, to physically corrode through the neighboring bladder, urethra, or rectum. These complications are caused by the limited understanding of the textile and structural properties of commonly used prolapse meshes. Thus, research on the impact of synthetic meshes on clinical outcomes is profoundly needed starting with lab-based studies, especially on newer mesh products and designs for which there is little clinical data. Currently, a large degree of attention has been to describe the specific weight and pore size of these prolapse meshes (Table 15).

Table 15 The **i**ndustry reported specific weight and pore size of five prolapse meshes

Synthetic Mesh	Specific Weight (g/m^2)	Pore Size (µm)
Gynemesh	42	2440
UltraPro	31	4000
SmartMesh	19	2370
Novasilk	21	1121
Polyform	41	1730

Gynemesh was one of the earliest polypropylene grafts utilized in prolapse repair surgeries and is often considered the "gold standard" of meshes. Newer generation meshes (UltraPro, SmartMesh, Novasilk, and Polyform) were designed to help decrease the overall morbidity associated with mesh implantation. However, characterizing the *ex vivo* properties will help us gain insight into the innate differences between these prolapse meshes prior to implantation in an animal model. Previous studies have exploited uniaxial and ball-burst load to failure protocols to reveal significantly different *ex vivo* structural properties of older generational meshes for incontinence repair, prolapse surgery, and abdominal hernia grafts [77, 80, 83]. These studies highlight specific differences in the structural properties of polypropylene

meshes; however, many of the structural properties of these grafts are affected by their respective textile properties. The fiber pattern (knit or woven), multi- or monofilament, pore size, specific weight, porosity, and degree of anisotropy are all textile properties that can affect the overall global structural response of the mesh. Porosity and the degree of anisotropy are very important for describing the properties of these meshes and little published or reported data exists on these parameters for prolapse meshes.

In the presented studies, we aimed to examine these additional textile features (porosity and degree of anisotropy) and utilize a uniaxial and ball-burst testing protocol to compare the structural properties of prolapse meshes. Again, Gynemesh is an older mesh because which is often referred to as the "gold standard" based solely on the fact that it was the original prolapse mesh to appear on the market against which all other meshes are compared. In addition to Gynemesh, we examined the newer generational meshes of UltraPro, SmartMesh, Polyform, and Novasilk.

3.1.1 Porosity

One of the main textile properties often examined in these prolapse meshes is the pore size. The pore size is important for host tolerability specifically regarding tissue ingrowth and rejection. Pore size may be measured by averaging the two largest perpendicular lines of a single pore [171]. Previous urogynecological meshes with small pores had reported high rates of infection and a lack of tissue incorporation [171]. This type of infection is related to the inability of immune cells (e.g. macrophages) to penetrate pores <10 μm. Bacteria can grow within these

small pores, eventually leading to serious clinical complications. Pore size has also been shown to affect the degree, type, and rate of tissue ingrowth [76, 171, 172].

Examination of pore size may help identify meshes that are more prone to infection; however, there is not a standard method to report pore size which is problematic for evaluation and comparison. For example, the maximum, median, or minimum pore size of a mesh may be reported to clinicians upon the development of a new mesh; however, this can provide little information about the overall porosity of the material and may lead to biased reports on a material's pore size. Therefore, a measurement of the material's porosity, in conjunction with pore size data, may prove to be a better method for providing accurate information about these meshes.

By definition, porosity is the measurement of openness or void spaces relative to the solid material. Porosity typically ranges from 0-100%, with 0% relating to a completely uniform or nonporous material and 100% to a completely open material. Porosity can be accurately measured using a scanning electron microscope (SEM), or can be quantified following methods previously described for trabecular bone and relative material composition of composites (material 1 relative to material 2). Here, we will discuss the methods we used for calculating porosity, following a similar method to that used with trabecular bone [173].

Below is an illustration of a synthetic mesh that may be may be used for porosity calculated (Figure 20).

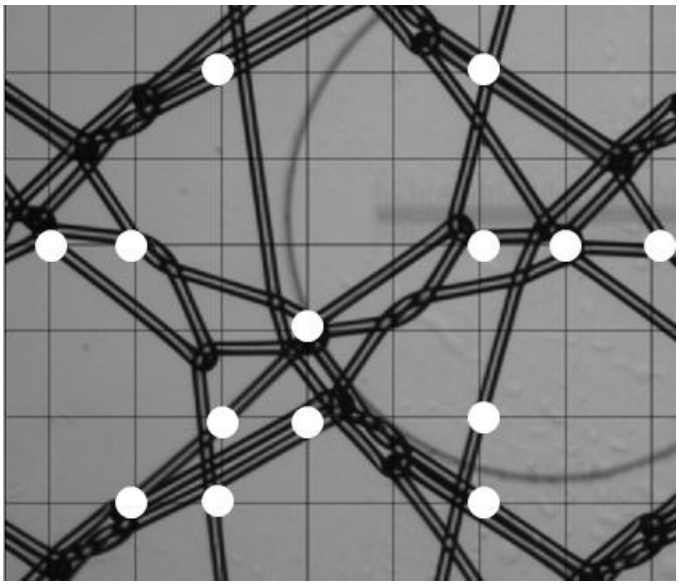

Figure 20 Image used to calculate porosity of a synthetic mesh (Novasilk)

For simplification, this example image uses a reduced number of grid lines (8 x 6) to illustrate the ideas behind this methodology. Each point that the crosshairs of the grid intersect with the mesh is highlighted by a white dot. The sum of all these points is then calculated (M) to produce the mesh to the total number gridline intersections (M:V). Only points at the inner gridline intersections were considered in the calculation for porosity. After this value has been calculated, the mesh's porosity can be calculated using the following equation: Porosity = 1 – M:V. In the pictured image the sum of intersection points is 14 (M), the total number of possible points is 48 (V), and the mesh to intersection ratio is ~0.29. For this example the porosity of the material was determined to be 71% (Porosity = 1 –M:V).

3.1.2 Microstructural Architecture

While the previous measurement is a valuable tool for determining the sheer porosity of a material, or percentages of different composites within a material, it cannot provide any

information about the microstructural architecture of the material. Stereology is the quantification of three-dimensional (3D) information from two-dimensional (2D), or planar, data [174-178]. It is often used to help understand the elastic symmetry of a material or biological structure (e.g. trabecular bone). This elastic symmetry can help us identify the degree of anisotropy of the prolapse meshes. For example, a mesh that would be elastic symmetric could be assumed to be an isotropic material. A prolapse mesh labeled as an isotropic material has the same structural and mechanical properties along all loading directions. In contrast, anisotropic meshes have directionally dependent or contingent on the loading direction structural and mechanical properties.

For our purposes, we utilized the mean intercept length (MIL) fabric tensor to model the planar prolapse mesh. Other methods commonly used to model a specimen's microstructure are the star length distribution (SLD) and star volume distribution (SVD) which have been developed for more 3D studies [175, 176]. However, the MIL theory can easily model a planar material's microstructure using second order tensors, coined fabric tensors, for determining the degree of anisotropy [178].

These fabric tensors are derived from 2D images of a material or specimen. However, a couple assumptions must be made. The first is that the image is a representative volume element (RVE) of the entire sample. The second is that this RVE is greater than the largest microstructure (e.g. pore). As you can see in Figure 21, a line at a specific angle (θ) is placed onto the image.

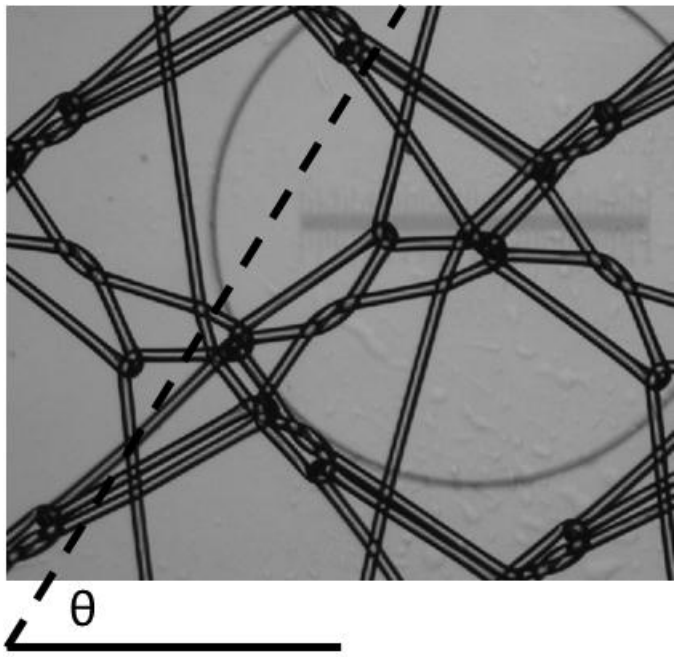

Figure 21 Representative line used in calculating a MIL fabric tensor at angle θ

The number of times this line crosses over constituents (i.e. from mesh to void or from void to mesh) is divided by the total length of their respective lines to calculate the MIL, or L(θ). This is typically done at multiple angles which can then be found to fit the equation of an ellipse, with the subscripts of M_{11}, M_{22}, and M_{12} corresponding to the x_1 and x_2 axes of the specimen and θ relating to the respective angle (Equation 3-1).

$$\frac{1}{L(\theta)^2} = M_{11}\cos^2\theta + M_{22}\sin^2\theta + M_{12}\sin\theta\cos\theta \quad \text{3-1}$$

This creates a positive symmetric second rank tensor where $M_{12} = M_{21}$. The eigenvectors of this fabric tensor correspond to the direction of the microstructural architecture. The fabric tensor's eigenvalues relate to the distribution of the microstructure along the eigenvector. The determinant of the fabric tensor is a scalar value representation which also correlates to the distribution of the microstructure along the eigenvector.

The fabric ellipsoids that are created from Equation 3-1 can provide additional information about material symmetry. Assuming the material involved is isotropic, the fabric ellipsoid can be used to define the elastic symmetry and by calculating the ratio of the eigenvalues can determine if the material isotropic or anisotropic. For example, a material will be shown to be orthotropic, transversely isotropic, or isotropic based on the shape of the fabric ellipsoid [178]. Typically, these are done along three different axes of the specimens to compile a full second order tensor; however, for the 2D case, it can still be useful for identifying isotropic materials. For example, if the fabric ellipsoid of a material evolves into a sphere and the eigenvalue ratio approaches a value of 1, then the material is elastically symmetric, or isotropic. Cowin and Doty provide a more detailed definition and outline of the formation of the fabric tensor [178].

3.1.3 Structural Properties

The porosity and degree of anisotropy are additional textile properties that impact the biomechanical behavior of these prolapse meshes. The biomechanical properties of these prolapse meshes can affect the host responses following implantation. Therefore, it is important to determine the biomechanical properties of prolapse meshes prior use for surgical repair. These biomechanical characteristics are often broken into mechanical and structural properties. Structural properties describe how a tissue or material, or a group of tissues or materials, responds to an applied force (load) in terms of displacement or elongation. However, structural properties generally do not take into account any geometric characteristics of a tissue (e.g. area, length, etc.). Thus, if two tissue samples are identical in every way except for their size, the

structural properties of the larger sample will be superior to that of the smaller sample, because the load will be dispersed over a larger area. While a variety of testing methodologies can be employed to reveal the structural properties of a sample, one of the most conceptually simple tests is a uniaxial load-elongation test to failure [25]. During this test, one end of a sample is rigidly attached to force sensor (load-cell), which is connected to the moveable crosshead of a material testing machine. The other end of the sample is rigidly attached to the machine's base. Following a protocol to remove slack and minimize viscoelastic effects, the crosshead is then moved at a constant rate until the specimen is elongated to the point of failure, or material rupture. These data can then be plotted as shown in Figure 22.

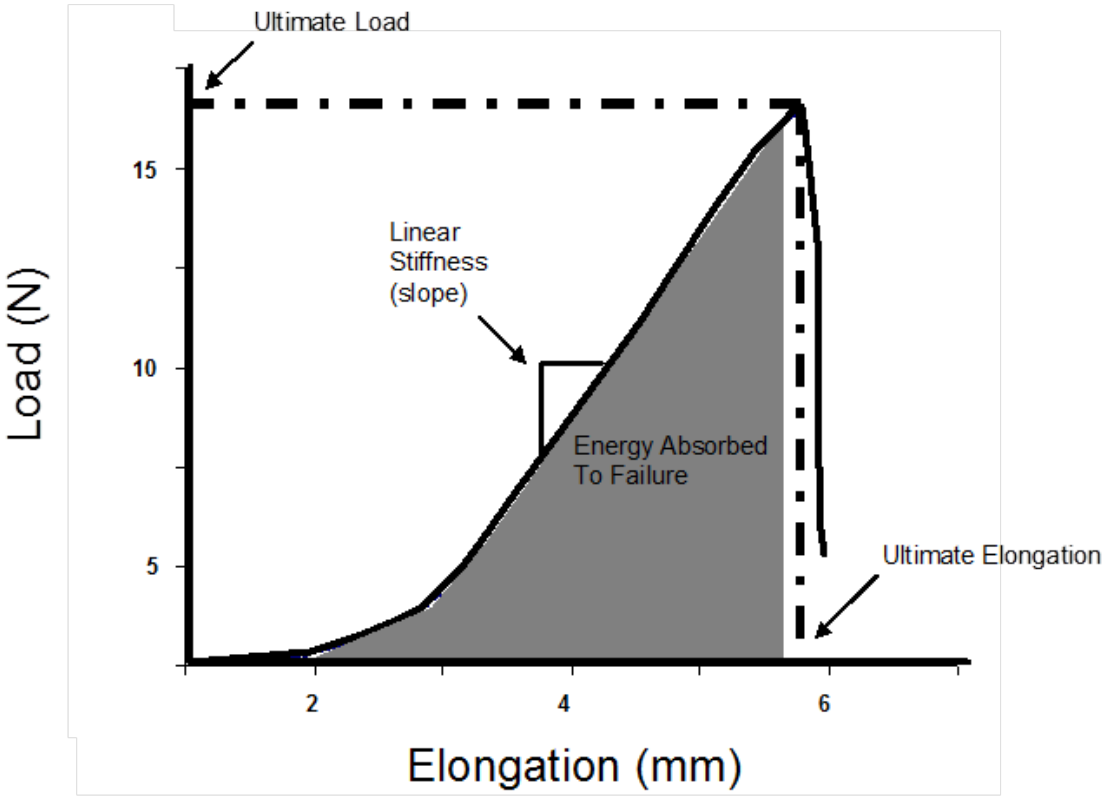

Figure 22 A typical load-elongation representation from a uniaxial tensile test to failure illustrating how each of the parameters describing the structural properties (ultimate load, ultimate elongation, linear stiffness, and energy absorbed) of a tissue complex are determined.

This curve typically has a non-linear shape for biological tissues and synthetic meshes, which can be divided into 3 regions- the initial nonlinear toe region, the linear region, and the failure region. The parameters that describe the structural properties of the specimen include the ultimate load (the maximum force applied to achieve failure), ultimate elongation (the displacement that the specimen elongated up until failure, which is also the elongation that corresponds with the ultimate load), linear stiffness (slope of the load-elongation curve within the linear region), and energy absorbed prior to failure (the area underneath the load-elongation curve). This uniaxial tensile testing is often used for characterizing the structural properties of prolapse meshes because it replicates the physiological loading direction after implantation following the clinical abdominal sacrocolpopexy prolapse repair procedure.

3.2 TEXTILE PROPERTIES

3.2.1 Introduction

A wide range of biomaterials are available to clinicians for incontinence and prolapse procedures with little quantitative data on which to base the selection of a particular material. Although limited data suggests that synthetic polypropylene meshes are superior to biologic meshes in terms of anatomical [69] and biomechanical [70] outcomes, there is evidence that the complications associated with synthetic meshes can cause a great degree of morbidity including infection, erosion, exposure, and pain [69, 71]. In addition, the vaginal tissue to be augmented is often structurally compromised, atrophic and devascularized. Such poor tissue quality increases

the risk of poor tissue incorporation into the mesh potentially resulting in suboptimal healing and mesh exposure or erosion into an adjacent viscous.

Due to the high rate of unreported complications of the currently used meshes, the FDA recently released a warning against their use in urogynecological procedures [FDA Public Health Notification: Serious Complications Associated with Transvaginal Placement of Surgical Mesh in Repair of Pelvic Organ Prolapse and Stress Urinary Incontinence: Issued October 21, 2008]. This has fueled the development of the next generation meshes, which tend to be more lightweight and have larger pores. The theory behind this trend is governed by the thought that stiffness, pore size, and mesh density affect host incorporation and complication rates [80, 171, 179]. For example, Gynemesh PS^{TM} (Ethicon) was originally designed to be a lightweight mesh (45 g/m^2) for prolapse repair but is now considered to be a mid-weight material (40-60 g/m^2). This has led Ethicon to develop the next generation of prolapse mesh UltraPro^{TM}. UltraPro has a specific weight of roughly 57g/m^2 with a monofilament dissolvable suture designed to reduce permanent deformation and increase ease of handling prior to implantation. After implantation, this monofilament within the mesh dissolves and the remaining mesh has a specific weight of 28g/m^2. Moreover, other companies have developed meshes with lower specific weights than Gynemesh. For example, Smartmesh^{TM} (Mpathy) is an ultra-lightweight material (19 g/m^2) designed for maximum tissue incorporation and patient comfort. Novasilk^{TM} (Coloplast) also has a much lower specific weight (21 g/m^2), while Polyform^{TM} (Boston Scientific) has a similar (40 g/m^2) specific weight compared to Gynemesh.

Along with specific weight, companies often report a single pore size value for each mesh; however, it is difficult to interpret what this pore size means. Typically, pore size is reported as a mean, median, or maximum value, but it is difficult to relate this single value to the

overall porosity of the mesh. This reported pore size of Gynemesh, UltraPro, SmartMesh, Novasilk, and Polyform can be found in Table 15. However, these synthetic meshes are often knitted and can contain pores significantly smaller than the reported pore size. Therefore, it may be helpful to examine the overall porosity of these meshes in addition to a single pore size value. Lastly, the anisotropic behavior of these meshes can affect the structural properties and may have different results when implanted along one orientation versus a second orientation. Therefore, determining if a mesh has specific directional properties is important for considering prior to implantation.

The specific weight, pore size, and porosity are all textile properties of the meshes. Research examining these textile properties along with the architectural microstructure to determine the anisotropy of synthetic meshes would help further characterize these meshes *ex vivo*. A material's microstructure has been shown to be easily modeled using the previously described method to formulate a fabric tensor (Section 3.1.2). Based on the mean intercept length (MIL) method and assuming orthotropy these fabric tensors can quantify the anisotropy of a material, which is more directly related to the mechanical properties of these synthetic meshes. This information would provide valuable insight into how the knit pattern of these meshes affects the mechanical response *ex vivo*. Further, by improving our knowledge of the *ex vivo* properties of synthetic prolapse grafts, it may help us predict how these grafts will perform *in vivo* prior to implantation.

3.2.2 Methods

Each mesh [Gynemesh, UltraPro, SmartMesh, Novasilk, and Polyform] was removed from the sterile packaging and divided for imaging and structural analysis (described below). Specific weight measurements (g/m^2) and industry reported pore sizes (μm) were provided from each company (Table 16). For imaging, a small 10 by 10 mm square section of mesh was removed. Textile properties of each mesh (n=4 per mesh) were examined by viewing a 6.5 by 5.2 mm section via light microscopy (Olympus MVX10 MacroView). All images were taken by a blinded technician.

3.2.2.1 Porosity

Images were analyzed using ImageJ software (1.36b NIH, USA). Porosity was calculated by overlaying a 10-by-12 grid of perpendicular lines overlaid on each image. The points of intersection of the grid were determined to be either above the mesh or empty space. The number of points overlaying the mesh was then divided by the total number of intersection points. This provides the ratio of mesh:total volume (M/V). The porosity metric was then calculated (porosity = 1 - M/V) and reported as a percentage of empty space.

3.2.2.2 Degree of Anisotropy

To quantify each mesh's architectural microstructure, we utilized the mean intercept length (MIL) theory previous described in Section 3.2.2.2. Briefly, images were imported into ImageJ, and the number of intersections between the mesh and empty space were counted along each line at a specified angle (θ). This task was performed at several angles ($\theta = 0^o$, 30^o, 45^o, 60^o, and 90^o)

and used to calculated the mean intercept lengths, $L(\theta)$. The MIL produces an ellipse on a polar plot (Equation 3-1), and with the assumption that the examined materials are isotropic, the degree of material symmetry based on the structural arrangement of the isotropic material, ranging from orthotropic to isotropic, can be determined from this fabric ellipsoid [177, 178].

Here M_{11}, M_{12}, and M_{22} are determined from $L(\theta)$ at the varying angles (θ) using a custom designed program (Appendix B). These values constitute the material tensor M, which can be quantified using the fabric tensor H (H=M-1/2). The eigenvalues of the fabric tensor relate to the magnitude of the microstructure distribution along the principle direction [178]. For the two-dimensional case, the eigenvalues of the fabric tensors will be denoted τ_1 and τ_2, where $\tau_1 \geq \tau_2$. Through eigenvalue analysis, the degree of anisotropy (DA) was calculated from the ratio of the 1st and 2nd eigenvalues ($DA = \tau_1/\tau_2$) with a value of 1 representing an isotropic material. The DA is an indicator of the geometric anisotropy of these prolapse meshes, and for the present study is limited to categorizing a material as isotropic or anisotropic.

3.2.2.3 Statistics

The porosity of each mesh was compared using a one-way ANOVA test. A Dunnett's T3 post hoc was performed ($p<0.05$). The DA was examined using a one sample t-test ($p<0.05$); the degree of anisotropy of each mesh was compared to an isotropic material (DA=1). All statistical analysis was performed in SPSS (Version 12.0, Chicago, IL).

3.2.1 Results

Gross examination revealed that each mesh had a unique knit pattern (Figure 23-Top). SmartMesh was found to have a porosity of 78% ± 1.4% which was significantly higher than Gynemesh (62% ± 3.2%; $p<0.001$), UltraPro (67% ± 1.5%; $p<0.001$), Novasilk (67% ± 3.8%, $p=0.001$) and Polyform (56% ± 3.2 %; $p<0.001$). Polyform was found to be least porous and significantly less than UltraPro ($p=0.001$), SmartMesh ($p<0.001$), and Novasilk ($p<0.001$) meshes. The fabric ellipsoid of each mesh is displayed in Figure 23– Bottom.

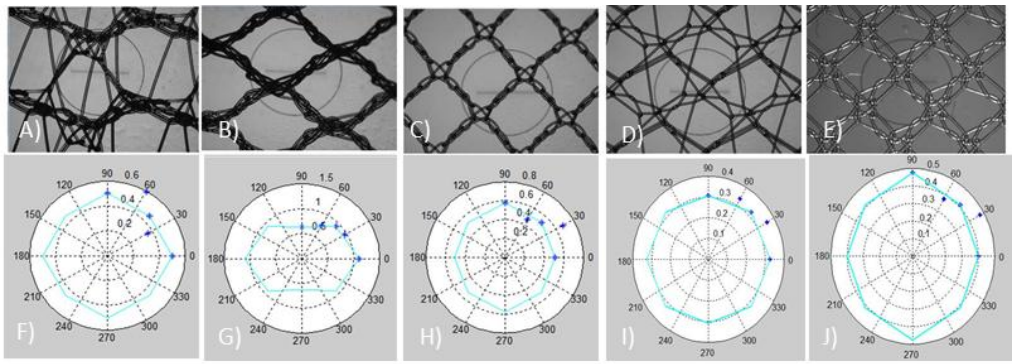

Figure 23 Figure the macroscopic images of the meshes (A-J) and the respective fabric ellipse for F) Gynemesh, G) UltraPro, H) SmartMesh, I) Novasilk, and J) Polyform

SmartMesh and Polyform were found to have more circular ellipsoids which corresponds to a more isotropic material. This is further quantified by the DA calculated for the SmartMesh (1.4 ± 0.31) and Polyform (1.4 ± 0.41) meshes. The DA revealed that these meshes did not significantly differ from the assumption of isotropy ($p=0.1$ and $p=0.12$, respectively). However, Gynemesh ($p=0.004$), UltraPro ($p=0.007$), and Novasilk ($p=0.02$) were all shown to have some degree of anisotropy (Table 16). This information, along with the planar geometry of these meshes, indicates that Gynemesh, UltraPro, and Novasilk behave like a transversely isotropic material.

Table 16 Table of textile properties for each mesh

Synthetic Mesh	Porosity (%)	Degree of Anisotropy (DA)
Gynemesh (n=4)	62 ± 3.2	1.5 ± 0.12
UltraPro (n=4)	67 ± 1.5	1.6 ± 0.18
SmartMesh (n=4)	78 ± 1.4	1.4 ± 0.31
Novasilk (n=4)	67 ± 5.7	1.2 ± 0.11
Polyform (n=4)	56 ± 5.7	1.4 ±0.41

3.2.2 Discussion

This study examined the porosity of each mesh and found that all meshes were >50% porous. Compared to Gynemesh, the original polypropylene prolapse mesh, newer generation meshes were more porous except for Polyform (56% ± 5.7). We also determined the DA by examining the architectural microstructure of each mesh. Based on their structural geometry, only SmartMesh and Polyform were found to have a DA that was not significantly different from an isotropic material. Gynemesh, UltraPro, and Novasilk all exhibited significantly different DA away from isotropy as compared with SmartMesh and Polyform. The meshes that were found not to be geometrically isotropic may be considered transversely isotropic due to the planar structure of these materials.

3.3 UNIAXIAL TENSILE PROPERTIES

3.3.1 Introduction

Gynemesh was the original polypropylene (PP) mesh commonly used in prolapse repair, but despite its popularity, it has a relatively high complication rate. While we do not currently know the optimal biomechanical properties for urogynecological meshes [165, 180], the industry appears to be moving in the direction of lighter weight, and presumably less stiff, designs with their newer generation meshes and mesh kits. This trend includes UltraPro, SmartMesh, Novasilk, and Polyform meshes. Some even use additional technology to reduce the resultant mesh burden, such as Ultrapro™ used in Prolift +M™ (Gynecare, Somerville, NJ) which includes interwoven poliglecaprone 25 fibers which will resorb in the process of mesh incorporation by the host tissue.

Here, we contend that prior to determining the behavior of a mesh *in vivo,* one must have a comprehensive understanding of its mechanical behavior *ex vivo,* using a previously published protocol [80, 83]. In this study, we describe the uniaxial properties of vaginally implanted pelvic organ prolapse meshes under a load-to-failure protocol. The uniaxial tension test mimic the loading directions after an abdominal sacrocolpopexy procedure for prolapse mesh implantation. We also describe the permanent deformation of the meshes after sub-maximal repetitive cyclic loading seen at loads comparable to those seen in the immediate post-op period [181]. Our hypothesis is that newer generation meshes will demonstrate less stiff uniaxial properties than older meshes. We also believe there will be considerable differences in structural properties amongst the meshes used for vaginal repair of pelvic organ prolapse because of their distinct

textile manufacturing properties. It is our goal that this data will provide the baseline information required for future studies of the mesh-tissue complex *in vivo* eventually leading to the development of improved meshes to reduce their health burden for women. Utilizing a uniaxial tension protocol will determine the structural properties (i.e. stiffness) that may impact the host response following implantation of prolapse mesh into an animal model developed in Section 2.0

3.3.2 Methods

3.3.2.1 Tensile Testing Protocol

The methods for tensile testing have previously been described [80, 83]. Mesh samples were attached to a custom set of clamps to form a clamp-mesh-clamp construct. Clamp to clamp distances were measured. To ensure that samples were tested consistently, an aspect ratio (width to height ratio) of five was maintained for all samples. An average clamp-to-clamp length was 75.2 mm with a width of 15.2 mm.

Once the meshes were properly affixed in the clamps, each sample was placed in a 37°C saline bath with one clamp rigidly affixed to the base of the Instron TM 4502 (Instron, Norwood, MA) screw driven testing apparatus and the other clamp fixed to a load cell that was attached to the crosshead of the testing apparatus. After allowing ten minutes for equilibration to the saline bath, a preload of 0.1 N was applied using an elongation rate of 10 mm/min. This removes all slack within the sample allowing for measurements of the clamp to clamp distance for calculations of relative elongation. After this procedure, the samples were loaded to failure along the longitudinal axis at a rate of 50 mm/min. The load at failure (N) and the elongation prior to

failure (mm) were obtained. The relative elongation of the samples was calculated by dividing the elongation achieved by the clamp to clamp distance measured after the preload.

Load versus relative elongation curves were plotted and analyzed. Curves were bilinear, with an initial region of low stiffness that transitioned into a high stiffness region at the point of inflection (defined below; Figure 24). The low stiffness region (N/mm) was defined as the minimum slope over a 15% interval of relative elongation. The high stiffness region (N/mm) was defined as the maximum slope over a 30% interval of relative elongation. The inflection point was defined as the intercept of the tangent lines fit in these two regions. The load (N) and relative elongation (%) at failure were also recorded.

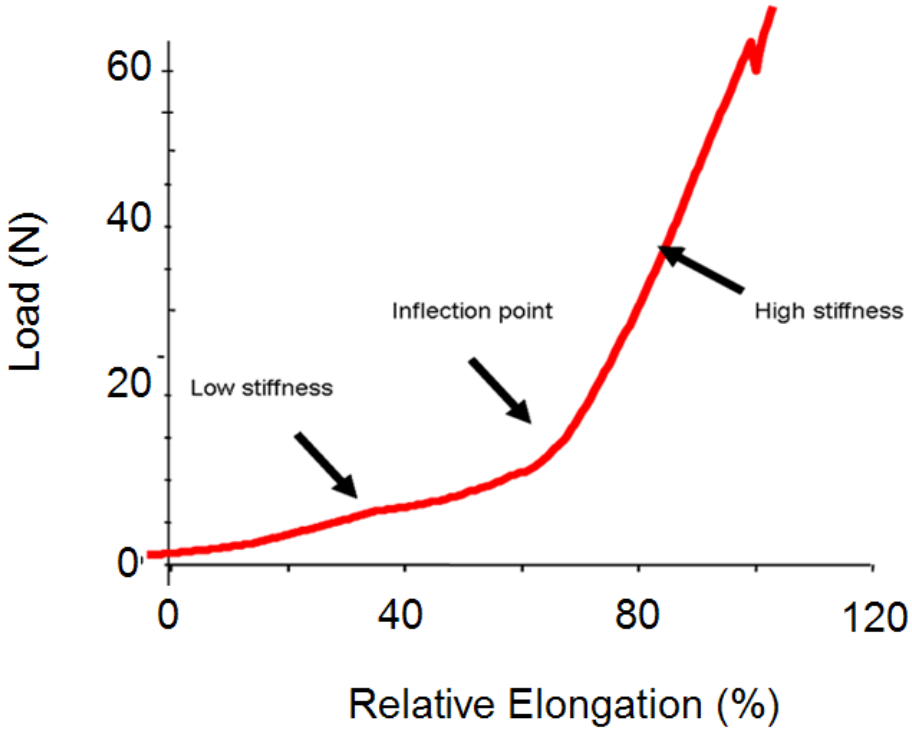

Figure 24 Typical load-relative elongation curve demonstrating the non-linear behavior of the meshes. The inflection point represents the transition from low to high stiffness [80].

An additional three samples per mesh type (N=3) were cyclically tested using three protocols (C1-C3) in order to assess permanent elongation of the mesh that has been previously described [80, 83]. This test is designed to assess how the meshes will respond to repetitive loading, i.e. under the assumption that the prolapse meshes will sustain repetitive sub-failure loads *in vivo* as a result of activities that increase intra-abdominal pressure during the early post-operative period. Briefly, samples were preloaded to 0.1 N at a rate of 10 mm/minute and the cross-head position was set to zero. The clamp-to-clamp distance was measured; meshes were then cycled from 0.5-5 N (C1), 0.5-15 N (C2), and finally 0.5-5 N (C3), each for ten cycles. The relative elongation after each portion of the cyclical loading protocol (C1-C3) was again measured by applying a 0.1 N preload and measuring the difference between the current crosshead position from its initial position. This represented the permanent deformation of the mesh in response to cyclical loading.

3.3.2.2 Statistics

Sample size calculations were based on initial data from a previous study [83] that tested Gynecare TVT^{TM} slings. Five samples per group were needed to detect a minimum of 100% difference in low stiffness, 15% difference in the inflection point, and 75% difference in permanent elongation between Gynecare and other brands with 80% power. A one-way analysis of variance was used to assess differences between groups and a post hoc comparison was performed using Dunnett's multiple comparison procedure.

A Pearson Correlation test was performed to examine if any of the textile properties (specific weight, pore size, porosity, and DA) to the *ex vivo* uniaxial structural results. For these correlations the *in vivo* specific weight of UltraPro (28 g/m^2) was used because it is assumed that

the single monofilament does not significantly contribute to the overall *ex vivo* properties. This assumption is based on preliminary work shown in Appendix C. Here, correlations are defined as strong (R^2=0.7-1.0), mild (R^2=0.4-0.7), or weak (R^2=0.2-0.4).

3.3.3 Results

Uniaxial properties yielded significant differences between these prolapse meshes. Upon examining the low stiffness of these meshes, Gynemesh (0.29 ± 0.015 N/mm) was significantly higher than UltraPro (0.009 ± 0.0016 N/mm; p<0.001), SmartMesh (0.18 ± 0.026 N/mm; p=0.001), Novasilk (0.072 ± 0.05 N/mm; p=0.002), and Polyform (0.13 ± 0.008 N/mm; p<0.001). The low stiffness UltraPro was 32, 20, and 14 times less stiff compared to Gynemesh (p<0.001), SmartMesh (p=0.001), and Polyform (p<0.001) respectively (Table 17). SmartMesh and Polyform were shown to have close low stiffness values (p=0.08), which were both below Gynemesh (p<0.001), yet larger than UltraPro (p=0.001 and p<0.001). Novasilk had the largest variance in the calculated low stiffness. It was significantly lower than Gynemesh (p=0.002) and SmartMesh (p=0.04) but no differences were found compared to UltraPro (p=0.3) and Polyform (p=0.3). Interestingly, Polyform was found to have the largest high stiffness (1.4 ± 0.11 N/mm). Gynemesh was only 4% less compared to Polyform (p=1.0), while UltraPro was 83% (p<0.001), SmartMesh was 58% (p<0.001), and Novasilk was 64% (p<0.001) less than Polyform. UltraPro was found to have the smallest high stiffness, over 5.8 times less than Gynemesh (p<0.001) and Polyform (p<0.001). It was also found to be over 50% lower as compared with SmartMesh (p<0.001) and Novasilk (p=0.01; Table 17).

Table 17 Structural properties derived from a uniaxial load to failure test of the synthetic prolapse meshes: Gynemesh, UltraPro, SmartMesh, Novasilk, and Polyform

Uniaxial Tensile Properties					
Mesh	Low Stiffness (N/mm)	High Stiffness (N/mm)	Failure Load (N)	Extension (mm)	Energy Absorbed (N/mm)
Gynemesh (n=5)	0.29 ± 0.015	1.4 ± 0.093	46 ± 0.89	50 ± 3.3	874 ± 108
UltraPro (n=5)	0.009 ± 0.0016	0.24 ± 0.019	8.0 ± 0.69	74 ± 3.4	165 ± 16
SmartMesh (n=5)	0.18 ± 0.026	0.59 ± 0.04	23 ± 1.8	52 ± 1.9	482 ± 48
Novasilk (n=5)	0.072 ± 0.045	0.51 ± 0.09	20 ± 4.5	67 ± 17	459 ± 219
Polyform (n=5)	0.13 ± 0.008	1.4 ± 0.075	54 ± 4.8	67 ± 3.0	1134 ± 124

Polyform also failed at the highest uniaxial load. It was 14%, 85%, 58%, and 64% greater than Gynemesh ($p=0.015$), UltraPro ($p<0.001$), SmartMesh ($p<0.001$), and Novasilk ($p<0.001$; Table 17) respectively. UltraPro failed at a significantly lower load than all other meshes ($p<0.001$ for each mesh). Only SmartMesh and Novasilk failed at loads without statistical difference ($p=1.0$). The energy absorbed followed the same significant trends as the failure loads, with Polyform absorbing the most compared with Gynemesh ($p=0.036$), UltraPro ($p<0.001$), SmartMesh ($p<0.001$), and Novasilk ($p<0.001$). UltraPro required the least amount of energy to achieve failure (Table 17). The uniaxial extension was greatest in the least stiff mesh (UltraPro) at 74 ± 3.4 mm. This was 33% and 29% higher than Gynemesh ($p<0.001$) and SmartMesh ($p<0.001$); however only 9% difference was calculated from Novasilk ($p=0.4$) and Polyform ($p=0.08$).

The textile properties of these meshes were found to have several correlations to their respective uniaxial properties. A mild correlation existed between the specific weight and the uniaxial high stiffness ($R^2=0.69$, $p<0.001$), failure load ($R^2=0.61$,$p<0.001$), and energy absorbed

((R^2=0.48, p<0.001). A significant but weak correlation was found between specific weight and low stiffness (R^2=0.26, p=0.009) and no correlation was found with the uniaxial extension (p=0.47). The pore size reported for each of these meshes was found to be weakly correlate with the uniaxial failure load (R^2= -0.2, p=0.027) and energy absorbed (R^2= -0.25, p=0.012). However, porosity measurements were found to have a negative mild uniaxial high stiffness (R^2= -043, p=0.002), failure load (R^2= -0.43, p=0.002), and to energy absorbed (R^2= -0.41, p=0.003). DA did not correlate with any uniaxial properties.

3.3.4 Discussion

The results from our uniaxial testing protocol demonstrated that there was heterogeneity among the structural properties of meshes designed for vaginal implantation for repair of pelvic organ prolapse. We were able to show that most meshes were less stiff than the prototypical pelvic mesh, Gynemesh. This finding was anticipated, as meshes with higher stiffness values have been associated with higher rates of complications, and newer meshes have been engineered to be less stiff than their older counterparts. It is also interesting that UltraPro was the least stiff mesh. It is manufactured by Gynecare who also manufactures the prototypical pelvic mesh, Gynemesh, which is one of the stiffer meshes tested.

Our lab has previously published similar data for mid-urethral slings and abdominal prolapse meshes [80, 83]. Notably, some of the meshes used for abdominal prolapse repair are made of the same materials used in vaginal prolapse repair, although many newer products were tested in this study. However, it is important to note that this testing was done *ex vivo* and in a single dimension. Physiologic stresses are applied in more than a single dimension and expose

these synthetic meshes to a complex loading environment. After implantation, meshes are typically incorporated into the host tissue, thereby creating a mesh-tissue complex. This makes understanding the *in vivo* scenario difficult as each mesh originally exists as a separate structure approximated to tissue with sutures, but later becomes incorporated after tissue ingrowth and becomes a mesh-tissue complex. As such, this experimental set-up allows us to draw only preliminary conclusions about the various meshes. Additional studies subjecting these meshes to structural testing via a 2D ball-burst apparatus will allow us to better understand the behavior of these meshes under different loading conditions. Additionally, we are currently implanting these meshes into a rodent model with plans for subsequent testing of the mesh-tissue complex in both the uniaxial and biaxial planes, which will help us characterize the *in vivo* properties of the mesh-tissue complex after tissue incorporation.

Further research will be needed to understand how these differences in biomechanical performance in the lab impact clinical outcomes. Historical data has shown that stiffer meshes have led to higher erosion rates. This has been seen with Nylon, Marlex, and Gortex meshes. While the erosion rates of these products is likely related to textile qualities other than stiffness such as pore size and braided/woven construction, we were able to show the continuing trend towards lighter weight, less stiff mesh in newer products with this study. In contrast to this, Deffieux, *et al.* were unable to show a difference in erosion rates between Gynemesh™ (Gynecare, Somerville, NJ) and the second-generation product Gynemesh after mesh-augmented transvaginal cystocele repair [179]. Although no differences in erosion were found in this study, here we reported the structural properties for Gynemesh subjected to uniaxial tension and found it to be one of the stiffer meshes. This is particularly important when considering the host

response following mesh implantation. A stiffer prolapse mesh may result in a degeneration host response and erode through the vaginal tissue.

In conclusion, we have shown that there are marked differences amongst the meshes used for vaginal repair of pelvic organ prolapse. Most newer generation meshes are less stiff than the prototypical pelvic mesh, Gynemesh PS™, in both the high and low stiffness areas of the load elongation curve. The one exception to this is Boston Scientific Polyform™ which was not significantly different in the high stiffness region compared to Gynemesh. Studies in our laboratory are examining the *ex vivo* structural properties from a ball-burst protocol of these meshes along with characterizing the *in vivo* properties after mesh implantation. However, the structural properties from this uniaxial protocol have identified meshes with varying stiffness. The next step is to study how these textile and structural properties correlate with clinical outcomes such as mesh erosions and surgical failures.

3.4 BALL-BURST PROPERTIES

3.4.1 Introduction

Structural properties of meshes are often examined using uniaxial or ball-burst (BB) testing protocols. Previously, studies examining the structural properties of commonly used prolapse meshes under uniaxial tension have observed that each mesh has significantly different structural properties, even though all of these meshes were made from type I polypropylene [80]. While uniaxial testing may utilize different sized samples which are normalized for length and width,

current American Society of Testing and Materials (ASTM) ball-burst standard testing devices require relatively large square samples (70×70 mm). Although this is typically not an issue in the textile industry, obtaining biological samples or mesh samples post-implantation of this size is difficult because studies of this nature utilize small animal models. Therefore, a scaled version of the ball-burst device must be used to test excised biological samples. A study on abdominally placed meshes in the rodent model utilized a scaled down version of a ASTM standard ball-burst test [111]. This early work on the development of a modified ball-burst test allowed for biomechanical testing of the mesh-tissue complex. Although failure loads and elongations will change with an altered sample size (differ by the scaling factor), stiffness measurements of a sample will theoretically remain constant between the ASTM and scaled ball-burst tests.

The objective of this study was to rigorously characterize the *ex vivo* structural properties of five commonly used synthetic meshes (Gynemesh, UltraPro, SmartMesh, Novasilk, and Polyform) via a scaled ball-burst apparatus.

3.4.2 Methods

3.4.2.1 Preliminary Studies

Current ASTM ball-burst standard testing devices require large square samples (70×70mm). Since a scaled version of the ball-burst device must be used to test excised biological samples, a preliminary study was performed between the ASTM standard and our custom scaled ball-burst devices. Although failure loads and elongations will change with an altered sample size (differ by the scaling factor), stiffness measurements of a sample should theoretically remain constant between the ASTM and scaled ball-burst tests. The aim of this study was to validate the device

by comparing stiffness measurements of mesh samples tested using the scaled down device and the ASTM standard device.

Briefly, Gynemesh, SmartMesh, Novasilk, and Polyform were examined (n=5 per mesh) on the ASTM standard ball-burst apparatus and compared to the scaled ball-burst results. There was no significant difference in the stiffness between the ASTM standard and scaled ball-burst protocols ($p=0.86$). Gynemesh and Novasilk had the largest variability with an 11% and 9.8% difference between ball-burst setups, respectively. Polyform was found to have a 5% difference while SmartMesh had only a 0.6% difference between the ASTM standard and scaled ball-burst. The ASTM standard failure load was significantly higher ($p<0.001$) when compared to the loads resulting from the scaled ball-burst protocol. The difference in the reported failure load was roughly 2.5 and can be attributed to the scaling factor of the ball-burst setup. A significant difference was also observed in the extension ($p<0.001$) and energy absorbed ($p<0.001$; data not shown). These differences were accounted for by the scaling factor of the ball-burst setup or the sample surface area. A more in-depth comparison between ASTM and scaled ball-burst experiments are displayed in Appendix D.

3.4.2.2 Methods

3.4.2.3 Ball-Burst Protocol

The scaled ball-burst was made from 304 stainless steel and had a ball diameter of 9.52 mm: the sample would have a 16.6 mm diameter and ~216 mm^2 surface area. For structural ball-burst properties, Gynemesh (n=8), UltraPro (n=5), SmartMesh (n=5), Novasilk (n=5), and Polyform

(n=5) were cut into 25x25 mm squares. Each sample was soaked in physiological saline solution (0.9% NaCl) at room temperature prior to testing.

The mesh was then secured between two flat clamps with interlocking triangular grooves which were tightened to secure each sample. The clamps were mounted onto a custom stand, which attached to an x-y translational table at the base of an InstronTM 4502 (Instron, Norwood, MA). The ball was connected in series with a load cell (Honeywell, 5 kN) and moveable cross-head. The ball was then centered over the mesh sample using the translation table. A small preload of 0.5 N was applied to ensure contact between the mesh and the ball, while minimizing mesh deformation prior to testing. Each sample was then loaded to failure at a rate of 10 mm/min.

The resulting load-elongation curves were then analyzed to determine the structural properties of each mesh. The failure load (N) and the maximum extension (mm) corresponding to the ball breaking through the specimen were recorded. To calculate stiffness (N/mm) the maximum slope over a running window of 20% of the failure elongation was used. Lastly, the energy absorbed was calculated as the area underneath the curve until failure (N/mm).

3.4.2.4 Statistics

Power analysis of the structural properties for sample size calculations were done on a preliminary data between Gynemesh and SmartMesh (G*Power 3.1.2). It was found for ball-burst testing that a minimum of three samples per group were needed to detect a minimum difference of 4% in stiffness, 21% in failure load, 2% in maximum extension, and 5% in the energy absorbed at 80% power.

A one-way analysis of variance (ANOVA) test was used to assess differences in porosity and ball-burst structural properties between groups. Based on the Levene test of variance, either a Bonferroni of Dunnett's T3 post hoc test was performed. All statistical tests were performed with a significance value of $p<0.05$ using a statistical package software (PASW Statistics 18.0)

It was important to consider if there were any correlations between the textile and *ex vivo* structural properties; therefore, a Pearson Correlation test was performed to examine if any of textile properties (specific weight, pore size, porosity, and DA) and *ex vivo* structural results from the ball-burst protocol where associated. Again we defined correlations as strong (R^2=0.7-1.0), mild (R^2=0.4-0.7), or weak (R^2=0.2-0.4). Negative signs (-) in front of the R^2 indicate a negative correlation.

3.4.3 Results

Comparisons between the structural properties of each of these meshes from a ball-burst test revealed that Gynemesh and Polyform were roughly 60% and 42% stiffer than SmartMesh ($p<0.001$) and Novasilk ($p<0.001$), respectively. No significant differences between UltraPro were found when compared to Gynemesh ($p=0.1$) or Polyform ($p=0.12$; Table 18). SmartMesh, the least stiff mesh, also failed at the lowest load. SmartMesh failed at a load that was 143% smaller than that of Gynemesh ($p<0.001$), 70% lower than UltraPro ($p=0.003$), and 144% lower compared to Polyform ($p<0.001$). Gynemesh and Polyform failed at comparable loads (0.4% difference), and both were significantly higher than UltraPro ($p=0.001$ and $p=0002$, respectively) and Novasilk ($p<0.001$). The maximum extension of Novasilk (Table 18) was 16% less compared to both Gynemesh ($p=0.002$) and UltraPro ($p=0.01$) and 24% less compared to

Polyform ($p<0.001$). Polyform also extended significantly farther than the SmartMesh ($p=0.002$), however no other significances regarding extension were found (Table 18).

The energy absorbed by these meshes displayed a trend similar to that of the ball-burst stiffness data. The energy absorbed of Gynemesh was found to be 41%, 62% and 61% greater than UltraPro ($p<0.001$), SmartMesh ($p<0.001$), and Novasilk ($p<0.001$) respectively. It was also found that the energy absorbed of the Polyform mesh was 35% greater than UltraPro ($p=0.002$), 58% higher than SmartMesh ($p<0.001$), and 57% larger compared to Novasilk ($p<0.001$).

Table 18 Structural properties of the individual meshes calculated from the load-elongation relationship from the ball-burst protocol

Ball-Burst Structural Properties				
Mesh	Stiffness (N/mm)	Failure Load (N)	Extension (mm)	Energy Absorbed (N/mm)
Gynemesh (n=8)	28 ± 2.7	108 ± 8.6	7.3 ± 0.31	288 ± 37
UltraPro (n=4)	22 ± 2.8	76 ± 12	7.3 ± 0.21	170 ± 11
SmartMesh (n=5)	11 ± 0.89	45 ± 3.8	6.7 ± 0.45	109 ± 11
Novasilk (n=5)	16 ± 5.5	54 ± 19	6.3 ± 0.56	113 ± 43
Polyform (n=5)	28 ± 0.43	108 ± 5.7	7.8 ± 0.05	261 ± 27

Textile properties of the meshes were found to correlate with ball-burst properties. The specific weight of the meshes strongly correlated with ball-burst stiffness ($R^2=0.78$, $p<0.001$), failure load ($R^2=0.85$, $p<0.001$), and energy absorbed ($R^2=0.89$, $p<0.001$). However, it only weakly related to extension ($R^2=0.38$, $p=0.001$). The provided pore size value of each mesh did not correlate with any of the ball-burst properties. However, porosity measurements were found to correlate with stiffness ($R^2= -0.64$, $p<0.001$), failure load ($R^2= -0.6$, $p<0.001$), energy

absorbed (R^2= -0.57, p<0.001) determined from the ball-burst load to failure test. A weak negative correlation between porosity and extension was also found (R^2= -0.34, p=0007). Interestingly, DA weakly correlated with ball-burst extension (R^2=0.22, p=0.037).

3.4.4 Discussion

In this study we have examined the *ex vivo* structural testing via ball-burst protocols of five commonly used prolapse meshes. Our focus was to improve our understanding of the properties of these meshes prior to their implantation *in vivo*. These synthetic meshes are designed to have large pore size and overall porosity to reduce the risk of infection and facilitate tissue ingrowth after implantation.

To better characterize the *ex vivo* properties of these meshes it is important to report the failure properties of these meshes; however, most meshes reach a clinical failure (e.g. erosion or prolapse recurrence) prior to experiencing a mechanical failure. It has been previously proposed that due to the lack of mechanical failure and the relatively small displacements experienced *in vivo*, that the stiffness of these meshes, specifically the stiffness values calculated from ball-burst and uniaxial protocols, play an important role in mesh complications. It is thought that a higher mesh stiffness may increase a woman's risk for erosion and exposure [80].

When examining the structural properties from a ball-burst test, we found that Gynemesh and Polyform behaved with only a 1% difference in stiffness. These meshes had the highest ball-burst stiffness, while SmartMesh was significantly less stiff than Gynemesh (p<0.001), UltraPro (p<0.001), and Polyform (p<0.001).

Next our group intends to investigate the relationship between these different properties acquired from the ball-burst test, the host response, and surgical outcomes in an animal model. The *ex vivo* ball-burst protocol data of these five commonly used synthetic prolapse meshes provides the baseline data for implantation studies, whereby we intend to utilize this scaled ball-burst device to examine properties of *in vivo* mesh-tissue complexes. However, it was important to obtain this data first to understand the *ex vivo* properties of prolapse meshes prior to examining the *in vivo* properties of the mesh-tissue complex after tissue incorporation.

3.5 CONCLUSION

Section 3.0 describes the characterizations of the *ex vivo* textile and structural properties of five commonly used synthetic prolapse meshes. This aim was designed to identify two additional textile properties (porosity and degree of anisotropy) that could affect the structural properties of these prolapse meshes. Here, we illustrated that while these meshes are quite similar, as being characterized as lightweight, macroparous and knit, monofilament meshes, there are significant differences in the porosity and DA of these materials which may have a significant effect on their *in vivo* properties. Porosity is important because it can better define the mesh burden, or the amount of mesh per void area for tissue in-growth, while DA can identify the directional dependence of the structural properties to the loading and implantation direction.

The uniaxial and ball-burst testing protocols help us determine the structural properties of these meshes in response to multiple loading conditions, which may be experienced *in vivo*. Here, we have shown that these meshes have significantly different structural properties under

uniaxial and ball-burst protocols. Under uniaxial tensile testing, each mesh was loaded along the same direction it is typically implanted. From this study, Gynemesh was found to be the stiffest mesh while UltraPro was the least stiff mesh. However, from our ball-burst protocol SmartMesh was found to be the least stiff mesh compared to all other meshes with the exception of Novasilk. The DA may be important for understanding how these meshes will behave *in vivo* under different loading conditions and may possibly explain differences observed between our uniaxial and ball-burst structural properties. For example, the UltraPro mesh when compared to Gynemesh was found to have a 97% and 82% difference in low and high stiffness in response to uniaxial tensile loading, but only a 15% difference in response to ball-burst testing. This indicates that a change in loading condition on the mesh, in this case constraining circumferentially along all sides, can significantly affect its behavior. This illustrates how drastically the structural properties can be affected by its loading environment and in conjunction with the textile characteristics may affect the host response.

These studies are only the first step in better understanding the textile and structural behaviors of commonly used synthetic prolapse meshes, but still can provide us with a more developed understanding of the *ex vivo* properties of these prolapse meshes. These studies provide the necessary baseline data on prolapse meshes for examining the *in vivo* properties after implanting these meshes and characterizing the biomechanical properties of the host response.

4.0 *IN VIVO* BIOMECHANICAL PROPERTIES OF MESH-TISSUE COMPLEX

4.1 OVERVIEW

As earlier mentioned, synthetic prolapse meshes have been shown to have a high rate of complications with a large percentage of women requiring repeat surgery [63, 80, 93, 94]. Therefore, it is important to understand how these *ex vivo* properties and mesh characteristics relate to *in vivo* mesh-tissue complex properties. However, prior to performing implantation studies, we had to examine several animal models and characterize the *ex vivo* properties of the commonly used synthetic meshes. From our first aim, we examined and compared several commonly used urogynecological animal models (Section 2.0). From this study, we identified that the non-human primate (NHP) vaginal model is the most suitable model to evaluate the biomechanics of the host response to prolapse meshes. Although this is possibly the most relevant animal model due to its anatomical, physiological, and biomechanical similarities, the expense of utilizing this animal model to evaluate multiple meshes over long periods of times is considerable. Therefore, many researchers utilize the abdominal wall of small animals, most notably the rodent, to evaluate the mechanical properties.

For the implantation studies in this section, we focused on the implantation of three prolapse meshes (Table 19) that had varying stiffness values based on the uniaxial tension load to failure protocol.

Table 19. Specific weight, pore size, and mean stiffness calculated in the low stiffness region from the uniaxial tension test

Synthetic Mesh	Specific Weight (g/m^2)	Pore size (µm)	Stiffness (N/mm)
Gynemesh	42	2440	0.29
SmartMesh	19	2370	0.18
UltraPro	31	4000	0.009

These meshes were examined to evaluate the host response to prolapse meshes with similar macroporous and light-weight properties, but significantly different stiffness values. Currently, the new generation of meshes are designed to decrease the mesh burden on vaginal tissue. This has caused a shift to use more lightweight, high pore size, and less stiff polypropylene meshes in prolapse repair procedures. This is based on the theory to help decrease patient morbidity, and specifically reduce the number of mesh erosions. As you can observe from the average characteristics (Table 19) of these three prolapse meshes, both SmartMesh and UltraPro have a lower specific weight and roughly similar or greater pore size to the "gold standard" Gynemesh. More importantly, from our *ex vivo* studies (Section 3.3), SmartMesh and UltraPro were found to be significantly less stiff under uniaxial tension compared to Gynemesh. Utilizing these meshes provides us with a means to evaluate how the current trend of mesh design (less stiff) affects the biomechanical properties of the host response.

In this aim, we examined how implantation of these prolapse meshes affected the functional properties of the mesh-tissue complex (MTC) following implantation into the vaginal and abdominal model.

4.1.1.1 Animal Controls

As described in Section 1.3.4 animal models are often used to examine how these grafts function *in vivo*. However, to appropriately evaluate the mesh-tissue complex it is important to utilize control animals [72]. These controls for *in vivo* studies can take several forms. The first is to use a contralateral control. When possible this allows for an animal to serve as a control for itself which helps improve the statistical methods a study can perform. For example, this is often done in knee injury studies; investigators may injury the left knee and provide some type of treatment and not injury the right knee [122, 182]. These types of controls are not always available depending on the site of implantation. Therefore, the use of sham-operated controls and non-operated control are also utilized. Here, we refer to sham-operated controls as following a similar method as implanted animals (e.g. dissection) without the placement of a synthetic graft. These types of control can provide valuable information on the effect of surgery on the biochemical or biomechanical properties of the implanted tissues. These animals will suffer from an injury due to the surgery and will have a host reaction (e.g. inflammation) without a foreign material. Lastly, a non-operated control can be useful to understand how the native tissue behaviors prior to injury (i.e. dissection) or implantation. Each type of control is useful and can provide meaningful data for a study, but it is important identify the type of control being utilized because each has its limitation.

4.1.2 Stress Shielding

These surgical control groups are required when performing surgical implantation to be able to compare the native, or underlying, biochemical and biomechanical properties of the tissue pre- and post-implantation. Due to the fact that there are many factors that can be affected by mesh implantation including collagen ratios, collagen alignment, degradation enzyme activity and differences in the inflammation response; it is important to identify which characteristic of the host response that you desire to compare to controls. In this dissertation, we were interested in evaluating the functional result of the host response. While remodeling of the tissue can often result in histological and biochemical changes, alterations in these properties typically result in changes in the mechanical properties of the tissue. Although the ideal mesh material has not yet been identified, we hypothesize that a more apt prolapse mesh would help augment the structural properties of the native vaginal wall and result in strengthened biomechanical properties compared to prolapsed tissue. Further, it is believed that a large mismatch in vaginal and mesh biomechanical properties will impair the vaginal tissue smooth muscle (active) and extracellular (passive) components, and it is not enough for the mesh to help maintain the properties of the control animals, but also preserve active contractile behavior after implantation.

Previous research has shown that a mismatch between the native tissue properties and the synthetic implant can have this negative impact on tissue remodeling [183]. It is this adverse host response to the mesh that is believed to be linked to the clinical complication of mesh erosion and exposure. This is related to the phenomenon coined stress shielding and stress-raising [72]. The larger the mismatch between the graft material and native tissue, the greater degree of stress shielding or stress-raising will have on the remodeling process. Stress shielding

is often described when the graft absorbs the loads and strains typically experienced by the surrounding tissues. In bone, this has been shown to lead to atrophy and degradation [72, 184-186]. However, other grafts may increase (stress-raising effect) the loads borne by the surrounding tissues and can result in cell hyperplasia and hypertrophy [72]. The effect of mechanical properties of implants on the surrounding tissue *in vivo* has been widely shown in various fields [185, 187, 188]. This has forced the expansion of how we characterize the host response to these synthetic grafts, beyond the biocompatibility and *in vivo* biochemical properties of the tissue after implantation, to include the functional mechanical response to synthetic grafts.

4.1.3 Estimated Tissue Contribution

Carefully evaluating the functional properties of the tissue is required to better understand how the graft is functioning after the host response and incorporation. The first functional properties to consider are the structural properties (i.e. stiffness, failure load etc.) of the mesh-tissue complex (MTC). As previously described, we intend to utilize a scaled ball-burst apparatus to determine the structural properties of the MTC after implantation. In order to better replicate the physiological loading environment, it is important that the MTC has similar structural properties compared to the native tissue. However, it is also important that the tissue formation after graft placement can actively function via smooth muscle contraction and also has some biomechanical integrity to prevent future complication or recurrence. The lack of the newly formed tissue to function is a result of the previously described “stress shielding” phenomenon. For a better

understanding the effects of stress shielding, it is important to quantify the contribution of the vagina to the structural properties of the MTC.

To calculate the estimated tissue contribution to the MTC stiffness and MTC failure load, several assumptions have to be made. The first assumption is that the innate structural properties of the mesh do not change overtime or after implantation. Therefore, the stiffness (k_{mesh}) and failure load (F_{mesh}) of the mesh prior to implantation are the same after implantation and tissue incorporation. Preliminary research utilizing the abdominal wall animal model has confirmed that this assumption holds [74, 77]. The next two assumptions are related: there is negligible interaction between the tissue and mesh and the mesh and tissue behave as a parallel system (e.g. two parallel springs). From these assumptions, we can derive that the equivalent failure force, or force of the MTC (F_{MTC}), is related to the force observed in the tissue (F_{tissue}) by the following equation:

$$F_{MTC} = F_{tissue} + F_{mesh} \quad \textbf{4-1}$$

The force of the MTC is recorded experimentally and from our first assumption and utilizing the determined *ex vivo* structural properties for the mesh, the failure load of the tissue can be calculated with simple algebraic rearranging. The stiffness of the tissue is derived following the same method. The equation for the estimated tissue contribution to the stiffness of the MTC is shown below:

$$k_{tissue} = k_{MTC} - k_{mesh} \quad \textbf{4-2}$$

These estimated tissue parameters (F_{tissue} and k_{tissue}) begin to provide us with some basic insight of how tissue below the synthetic mesh behaves, and is an initial step into characterizing the tissue's functional properties. This method will be utilized in the following sections to

determine the tissue's contribution to the explanted graft-tissue complex from the abdominal wall and vagina.

4.2 ABDOMINAL MODELS

4.2.1 Introduction

To assess commonly used urogynecological meshes, we initially examined the *ex vivo* properties of these synthetic meshes. We have shown significant differences in mesh stiffness under both uniaxial and ball-burst protocols Sections 3.3 and 3.4 [80]. However, studies examining how the *ex vivo* properties of these meshes relate to clinical complications are often limited due to the inability to perform rigorous experimental studies with adequate tissue acquisition in human patients. Therefore, researchers often times turn to animal models. The non-human primate (NHP) is considered one of the best animal models of the pelvic floor due to the similar anatomical and functional part the connective tissue, musculature, and vagina have in pelvic floor support. The limitation of NHP studies often is the low sample size and ethical issues associated with their use. Therefore, previous studies have examined the *in vivo* properties of these prolapse meshes largely using the abdominal wall model [40, 73, 75-77, 104, 105, 107, 108, 111, 167, 189, 190]. Subcutaneous implantations of grafts and other biomaterials have become relatively common for several reasons. It is an easily accessible site for implantation. Second, the desired location for implantation may be too small to access or explant mesh-tissue samples large enough to perform biochemical and biomechanical analysis of the mesh-tissue

complex. This is often the case for the rodent vaginal model as detailed in Section 2.2.8.3. Therefore, researchers have utilized the abdomen model because it can offer an implantation site large enough for multiple methods of analysis in a variety of animal models. And lastly, it allows for a general characterization tissue incorporation of a synthetic mesh material *in vivo*.

The rodent is an established abdominal model developed for studying hernia repairs and is commonly used to assess the biocompatibility and biomechanical properties of prolapse meshes in animal models. An abdominal approach is common because the rodent animal model would otherwise be limited to small pieces of vaginal mesh implantation, which would elude traditional biomechanical protocols and limit biochemical analysis. The presented works have significantly contributed to our understanding of the host response to different prolapse meshes, but the major limitation of the rodent model, and other quadrupeds, is the altered loading conditions relative to the pelvic floor. While a suitable animal model does not need to perfectly mirror the loading conditions of the pelvic floor, it should be useful to understand how these changes in loading conditions may impact results and interpretations. Therefore, it is important to examine how different abdominal models may affect the host response to these synthetic meshes. The rodent model arguably has minimum loading and moment within the abdominal wall when compared to the NHP, which is more bipedal and must use their abdominal muscles during daily activity. Since our goal is to evaluate the mechanics of the host response, it is important to determine if the rodent and NHP abdominal models behave as an appropriate alternative for the NHP vaginal model.

We hypothesize that meshes with a higher stiffness will shelter the native tissue from experiencing the normal stress and strain cues and produce the “stress-shielding” effect further reducing the tissue contribution to the mesh-tissue complex. Moreover, we believe that

differences in the loading condition may alter the host response by changing in the collagen deposition during tissue incorporation and decrease the tissue contribution to the biomechanical of the mesh-tissue complex. The current study examined the biochemical and biomechanical properties of the mesh-tissue complex after implantation into the rodent and NHP abdominal wall using three commonly used synthetic meshes [Gynemesh, UltraPro, and SmartMesh]. This study's aims were two fold 1) examine structural properties after mesh implantation between each mesh type within their respective animal models and 2) correlate the *in vivo* properties of each mesh to the *ex vivo* textile (i.e. porosity and specific weight) properties. In addition, we would like to correlate these *in vivo* properties to the uniaxial (i.e. low stiffness) and ball-burst (i.e. stiffness) structural properties.

4.2.2 Animals

4.2.2.1 Rodent

A total of 31 female Long Evans rats were utilized in this study. All rodents were aged 3-month old prior to implantation and were nulliparous. Normally cycling nulliparous rodents were anesthetized using isoflurane in combination with ketamine. A 2 cm incision was made through the skin and a 1 cm incision was made through the midline of the abdominal muscle and the ovaries were examined. Abdominal muscle was closed (4.0 polysorb) and a 3 cm by 3 cm piece of Gynemesh (n=9), UltraPro (n=9), or SmartMesh (n=7) was sown covering the abdominal incision overlying the anterior abdominal wall fascia (Figure 25).

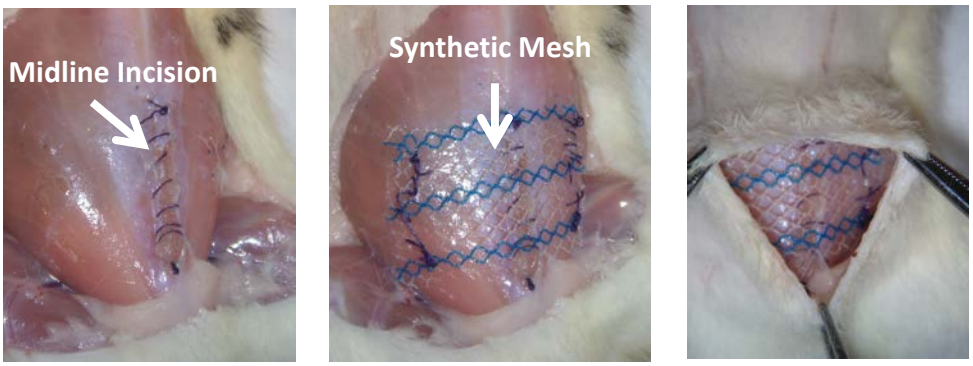

Figure 25 Abdominal implantation of synthetic meshes in the rodent animal model. A) identidifies the mid-line incision and closure B) highlights the 3 cm square piece of mesh implanted C) illustrates prior to dermis closure the location of the mesh with the skin pulled back over the abdomen.

An additional six age matched rodents served as non-operated controls. Each mesh was sutured along two opposite lengths of the mesh into the abdominal wall using 4.0 resorbable sutures (Polysorb). A subcutaneous closure of the dermas was performed and staples were used as a secondary closing method. Animals were allowed to heal for 24 weeks after implantation and non-operated aged controls were used in the rodent model. Upon explanting the abdominal wall mesh-tissue complexes (MTC) consisted of the abdominal fascia, muscle, and implanted mesh. The abdominal muscle layer was left intact due to the thin fascia layer of the rodent animal model. Ideally, the muscle layer would be removed to isolate the mesh fascia complex, similar to the protocol utilized in the following NHP study.

4.2.2.2 Non-human Primate

Twenty-one female rhesus macaques (macacca mulatta) between 10 and 15 years of age were utilized in this study. Animals were housed with a 12-h light/dark cycle (7am to 7 pm) with food access and water was provided ad libitum. Parous normally cycles NHP females were sedated

via incubation with isoflurane. Roughly a 10 cm incision was made along skin and midline of the abdominal muscle was found. The peritoneal cavity was accessed along midline and a hysterectomy with abdominal sacrocolpopexy was performed for a separate study. Closer of the abdominal muscle was made us using 3.0 resorbable sutures (Polysorb). The lateral abdominal cavity was accessed and two 2.5 cm by 2.5 cm square samples of Gynemesh (n=4), UltraPro (n=5), or SmartMesh (n=5) were secured on either the left or right abdominal wall overlaying the fascia similar to the rodent model. Sham operated controls (n=7) underwent the same dissection without the placement of mesh to assess the effects of surgery. Due to the increased size of the abdomen, contralateral abdominal walls were randomized within mesh implantation and sham-operated animals to serve as non-operated controls in six animals.

After surgery, animals were allowed to recover for 12 weeks prior to tissue harvesting. All surgical instruments used in these implantations were autoclaved sterilized and mesh samples were sterile and sealed prior to surgery. Abdominal walls were removed intact and divided for biomechanical analysis. The MTC tested from this animal model consisted of the abdominal fascia and incorporated mesh.

4.2.3 Methods

4.2.3.1 Biomechanical Properties

For biomechanical analysis abdominal mesh-tissue complexes were isolated from the surrounding tissue, wrapped in saline soaked gauze, and stored at -20^{o}C until the day of testing [106, 124]. This study was performed in accordance to the Institutional Animal Care Utilization Committee of the University of Pittsburgh for rodent (IACUC #0910805) and non-human

primate (IACUC #100867) implantation. For the rodent model due to the exceptionally thin fascia layer biomechanical properties were assessed with abdominal muscle attached, while this was removed in the NHP animal model. All samples were tested within 4 months of tissue collections. On the day of testing samples were thawed at room temperature and length and width measurements were made using digital calipers. To measure the thickness of the mesh-tissue complex a noncontact laser reflectance system was utilized [119]. A scaled version of the American Society for Testing and Materials (ASTM) ball-burst apparatus was used to characterize the biomechanical properties of the mesh-tissue complex. The ball-burst apparatus was scaled by a factor of 2.67, and has been previously shown to have minimal effects on the reported stiffness and other changes were accounted for by the scaling factor (Section 3.4.2.1).

For testing each mesh-tissue complex was secured between two flat clamps with interlocking triangular grooves. Each sample had a diameter of 2.5 cm, and the base of the ball-burst fixture was placed onto an x-y translation table fixed to a materials testing machine (Instron^{5565} Industrial Products, Grove City, PA). The ball was attached to a moveable crosshead in series with a 5kN load cell (2525-800 Drop-down Series; Instron, Canton, MA). After the tissue was secured into the base of the Instron the crosshead was lowered until the ball fell within 5 mm of the mesh-tissue complex. The sample was than centered under the ball utilizing the x-y translational table. The mesh-tissue complex was kept moist using 0.9% saline solution throughout the protocol. A preloaded of 0.5 N was applied and then the tissue was loaded to failure at a rate of 10 mm per minute. The resulting load (N) and elongation (mm) were recorded to create the load-elongation relationship of the mesh-tissue complex or sham specimens.

The ultimate load (N), or failure load, and the maximum displacement (mm) which corresponds to that point of failure are reported. The stiffness (N/mm), or resistance to

deformation, of the mesh-tissue complex was calculated using a running window of 20% of the load-elongation curve. A slope was calculated for each window and the maximum slope being defined as the stiffness of the complex.

To assess how the sham or native tissue properties compare the tissue contribution of the mesh-tissue complex estimated tissue stiffness and failure load were calculated. This estimated tissue contribution to the overall mesh-tissue complex properties was based on several assumptions. First, it assumes that the mesh and tissue are parallel nonlinear elastic springs. It further assumes that the tissue and mesh are non-interaction and that the mesh's properties do not change over the course of implantation. The *ex vivo* properties of Gynemesh, UltraPro, and SmartMesh were characterized on additional pieces of mesh (n=5 per group). The same protocol and data analysis methods used on the MTC were used to determine mesh load, displacement, and stiffness. With this additional data and utilizing the methodology from Section 4.1.3 we could determine the estimated tissue stiffness (N/mm) and estimated tissue load (N).

4.2.3.2 Statistics

A brief analysis of the data was performed to determine if the data violated the assumption of normality. In the rodent abdominal model the MTC stiffness, estimated tissue stiffness, and weight were found to be normally distributed. In contrast the MTC failure load, estimated tissue failure load, and length were found to not be normally distributed. Regarding the NHP abdominal model, MTC failure load and stiffness and estimated tissue failure load and stiffness were found to be non-parametric data. The age and BMI was also not considered parametric data while animal height and weight were found to be normally distributed.

All parametric data was statistically compared utilizing a one-way ANOVA. A test of homogeneity of variances was performed either a Bonferroni or Dunnett's T3 post hoc was performed when appropriate. To compare non-parametric data a Kruskal-Wallis comparison with a Mann-Whitney post hoc was performed.

Relationships of the estimated tissue contribution in the rodent and NHP abdominal wall to porosity, pore size, specific weight, low stiffness and stiffness via a uniaxial and ball-burst test respectively were made using a Spearman Rho correlation. Parametric data is represented as mean ± standard deviation, and non-parametric data is displayed as median (interquartile range). All statistical tests were performed using the software package SPSS (SPSS Inc. Chicago, Il. Version 18.0). All comparisons were made using a significant level of 0.05.

4.2.4 Results

4.2.4.1 Rodent

All rodent data is reported in Table 20. It was found that the length of these animals was not significantly different; however, the weight was significantly lower in the control group compared to Gynemesh ($p=0.007$), UltraPro ($p<0.001$), SmartMesh ($p<0.001$). Examining the biomechanical properties, we noted that the control and implanted animals displayed a typical load-elongation response with a clear non-linear "toe" region followed by the linear and failure regions.

Table 20 Table of the rodent demographical and biomechanical data Estimated tissue contribution to the MTC is described as tissue stiffness and tissue failure load.

	Weight (g)	Length (cm)	MTC Stiffness (N/mm)	MTC Failure Load (N)	Tissue Stiffness (N/mm)	Tissue Failure Load (N)
Control (n=6)	233 ± 11.1	29.5 (0.4)	8.5 ± 2.1	27.5 (11.0)	8.5 ± 2.1	27.5 (11.0)
Gynemesh (n=9)	288 ± 23.8	29.9 (0.7)	32.9 ± 6.1	147 (20.4)	5.4 ± 6.1	38.6 (20.4)
SmartMesh (n=7)	292 ± 13.8	30.2 (1.6)	17.4 ± 2.3	74.1 (28.7)	6.3 ± 2.3	29.6 (28.7)
UltraPro (n=9)	307 ± 31.5	30.3 (0.5)	31.4 ± 6.0	132 (12.9)	9.1 ± 6.0	77.7 (12.9)
Overall p-value	<0.001	0.073	<0.001	<0.001	0.37	0.015
Control vs. Gynemesh	0.007	N/A	<0.001	<0.001	N/A	0.22
Control vs. SmartMesh	<0.001	N/A	0.018	0.001	N/A	0.95
Control vs. UltraPro	<0.001	N/A	<0.001	<0.001	N/A	0.018

From the biomechanical properties we found significant differences between each group regarding the MTC stiffness and failure between each groups ($p<0.001$ and $p<0.001$, respectively). First, examining the MTC stiffness we found that compared to control animals there was a 3.8-, 3.7-, and 2-fold increase after implantation with Gynemesh ($p<0.001$), UltraPro ($p<0.001$), and SmartMesh ($p=0.18$) respectively. SmartMesh was also found to be 62% different then Gynemesh ($p<0.001$) and 58% different UltraPro ($p<0.001$), while no significant differences were observed between these two meshes ($p=1.0$). Assessing the failure load of the MTC a similar trend was observed. All grafted abdominal walls failed at a significantly higher load compared to control samples. Control samples failed at 24.5 (11.0) N which was significantly lower compared to Gynemesh ($p<0.001$), UltraPro ($p<0.001$), and SmartMesh ($p=0.001$) implants. Of the grafted abdominal walls SmartMesh failed at the lowest load. Gynemesh was 2.0-fold and UltraPro was 1.8-fold larger compared to the SmartMesh implanted group ($p<0.001$ and $p<0.001$, respectively).

Interestingly, by examining the estimated tissue contribution to the MTC we observed that many of the differences found between the control abdominal wall specimens and the

grafted samples may have resulted in the native mesh properties. Comparing the estimated tissue stiffness we found no significant differences between the control group and any grafted abdominal wall (p=0.37). Investigating the estimated tissue failure load we found that UltraPro remained significantly higher than control (p=0.018) and SmartMesh (p=0.012) groups. Significance was not observed between any of the comparisons. Utilizing the Spearman's Rho test for correlations, no relation between the estimated tissue stiffness and the *ex vivo* properties of the synthetic mesh. However, an association between the low stiffness, a structural properties derived from a uniaxial load to failure test, and the estimated tissue failure load was found (R = -0.438, p=0.029). A connection between the reported pore size of these synthetic meshes and the estimated tissue failure load was also revealed through this analysis (R = 0.583, p=0.002).

4.2.4.2 NHP

There were no differences between each of the NHP groups regarding demographical data: including age (p=0.56), BMI (p=0.69), height (p=0.24), or weight (p=0.29). Table 21 lists the reported values of each group. However, examining the biomechanical properties calculated from the ball-burst protocol we observed that the MTC failure load was significantly different between each group (p=0.005).

Table 21 Non-human primate demographical data.

	Age (years)	Weight (kg)	Height (m)	BMI
Sham (n=7)	15 (4.5)	7.6 ± 1.4	0.52 ± 0.03	27.5 (4.7)
Gynemesh (n=4)	14.5 (1.3)	8.6 ± 1.3	0.55 ± 0.02	27.9 (3.8)
SmartMesh (n=5)	13 (1..0)	9.5 ± 0.72	0.55 ± 0.02	29.6 (4.6)
UltraPro (n=5)	12 (3.3)	8.3 ± 0.78	0.54 ± 0.02	26.5 (6.2)
Overall p-value	0.56	0.29	0.24	0.69

No significant differences in the failure load resulted due to the dissection of the fascia layer during our sham surgeries compared to control animals (p=0.19). However, Gynemesh was failed at a significantly higher load compared to sham animals (p=0.024) but not the control group (p=0.067). UltraPro and SmartMesh implanted abdominal walls were also found to fail at a load which was 83% (p=001) and 68% (p=0.003) different than sham animals, respectively. Although close to reaching statistical significance (p=0.052) UltraPro and SmartMesh abdominal walls were not different compared to the biomechanical properties of the control abdominal wall. This could partially be related to the higher degree of variation in the control animals (Table 22).

Next we examined the tissue contribution to the MTC stiffness and failure load (Table 22). The estimated tissue stiffness of the abdominal wall was found to be significantly different between the studied groups (p=0.011). Compared to control abdomens after implantation there was a 90%, 46%, and 17% decrease in the stiffness after Gynemesh (p=0.019), UltraPro (p=0.25), and SmartMesh (p=0.79) implantation. A similar trend was observed comparing these mesh implantations to sham operated controls abdominal walls. The estimated tissue stiffness after Gynmesh implantation was 83% lower (p=0.042) compared to sham animals with no other

significant differences present. Gynemesh at 2.1 (13.9) N/mm grafted abdominal walls also had a roughly 8-fold smaller estimated tissue stiffness compared to SmartMesh 27.7 (5.4, p=0.016)

Table 22 Biomechanical properties of the MTC after mesh implantation into the abdominal wall. Estimated tissue contribution to the MTC is also reported below

	MTC Stiffness (N/mm)	MTC Failure Load (N)	Tissue Stiffness (N/mm)	Tissue Failure Load (N)
Control (n=6)	32 (18.7)	73.6 (38.2)	32 (18.7)	73.6 (38.2)
Sham (n=7)	18.5 (15.8)	50.9 (17.7)	18.5 (15.8)	50.9 (17.7)
Gynemesh (n=4)	29.5 (13.9)	126.4 (22.9)	2.1 (13.9)	18.3 (22.9)
SmartMesh (n=5)	38.8 (5.4)	110.6 (9.5)	27.7 (5.4)	66 (9.5)
UltraPro (n=5)	39.5 (18.3)	121.4 (56.7)	17.2 (18.3)	45.6 (56.7)
Overall p-value	0.068	0.005	0.048	0.05

Lastly, we correlated the estimated tissue contribution to the MTC with several of the reported (specific weight and pore size) and calculated (porosity and stiffness) parameters of these synthetic meshes. It was found that the estimated tissue stiffness correlated positively with the porosity (R=0.679, p=0.006) but negatively with the specific weight and stiffness calculated from the ball-burst protocol (R=-0.679, p=0.006). The estimated failure load of the tissue was also found to correlate with these same parameters. Again a negative correlation was observed with the specific weight and stiffness while a positive correlation appeared with the porosity (R=0.606, p=0.022).

4.2.5 Discussion

This study was designed to assess the *in vivo* biomechanical properties of the host response after synthetic mesh implantation in the rodent and NHP abdominal models. Here, our aim was to compare two newer generation light-weight meshes (SmartMesh and UltraPro) to the original

prolapse polypropylene mesh (Gynemesh). The implanted animals were compared to sham and/or control animals after 24 weeks and 12 weeks in the rodent and NHP, respectively. This study went a step beyond examining the MTC properties by calculating the estimated tissue contribution to the stiffness and failure load. The tissue contribution of each MTC property to the baseline biomechanical properties of the tissue allows us to assess the quality of the tissue that incorporated these synthetic grafts, and is a method to assess the biomechanical properties after the host response.

In the rodent model, we observed a significant increase in the stiffness of the MTC 24 weeks after implantation with Gynemesh, SmartMesh, and UltraPro. However, when we examined the estimated tissue stiffness, we noted that the biomechanical properties of the abdominal wall did not significantly change after implantation. This implies that the only differences observed in the MTC from control tissues and grafted abdominal walls were attributed to the *ex* vivo stiffness of each mesh calculated from the ball-burst load to failure protocol. Consequently, we can see that this may be the case when we revisit the structural properties derived from the ball-burst test in Section 3.4.3. Even though we did observe a small, but significant, change in the estimated load at which the abdominal tissue failed in the UltraPro graft, it is difficult to state why only this particular mesh observed an increase.

In the NHP animal model, we saw several different trends concerning the biomechanical properties of the grafted tissues. Interestingly, there were no significant differences between the sham and control animals with any of the MTC stiffness values. However, Gynemesh, the stiffest *ex vivo* mesh, displayed the lowest estimated tissue stiffness after implantation; neither the SmartMesh nor UltraPro grafted abdomens had significantly different biomechanical

properties from the sham or control groups. This may be the first evidence of "stress-shielding" after implantation of these prolapse meshes.

Evaluating the rodent and NHP animal model is important because the loading effects of the abdominal wall are different in each. The altered loading conditions of the abdominal wall may, in fact, be the reason that stress-shielding was not observed in the rodent but was observed in the NHP. The rodent, a quadruped, is often on four legs with the abdominal wall muscle perpendicular to the ground. While the abdominal muscles may provide support to the internal organs, little work is done by them on a daily basis. Conversely, this may not be true for the NHP, as it is more bipedal than the rodent and uses its abdominal muscles for posture and movement. These differences may affect how the host responds to the graft placed in the abdominal wall.

Direct comparisons between animal models were minimized in this study due to several limitations. The first limitation is that each of these animal models was implanted with meshes for different lengths of time: 24 weeks for the rodent and 12 weeks for the NHP. The difference in implantation time is related to cost of housing. The smaller rodent model is advantageous because it costs less to house than the NHP which allows for longer time points. The second limitation of this study is the specimens examined during ball-burst testing. In the NHP, the fascia and graft were completely isolated from the muscle and tested as a separate unit; however, the rodent fascia was extremely thin, making a clean dissection of the incorporated mesh fascia layer from the muscle nearly impossible. Therefore, we cannot make direct comparisons of the rodent and NHP and can only infer possible reasons for the differences in the estimated tissue properties.

Although direct comparisons could not be made, several general trends can be reviewed. First, implantation of Gynemesh did not affect the biomechanical properties of the abdominal wall in rodents, but did significantly lower the biomechanical properties of the underlying tissue in the NHP abdomen. The NHP abdominal model displayed precursors of a stress-shielding response, which was evident by the inferior tissue contributions after the stiffest mesh (Gynemesh) was implanted. An important finding from this study was that the biomechanical properties of the underlying tissue in the rodent and NHP abdominal models were different after mesh implantation. To evaluate the ability of these abdominal models to assess the mechanics of the host response the biomechanical properties of the abdominal models should be assessed relative to the changes vaginal tissue's biomechanical properties following implantation.

Future studies will examine the biochemical properties of these grafted tissues to help gain insight into the changes associated with graft implantation. These studies will aim to quantify the total collagen content and the collagen I/III and I/(III+V) ratio. The collagen content and ratios are important because collagen is a major component in the ECM that leads to the passive biomechanical properties of soft tissues.

In summary, this study highlighted that the estimated tissue contribution to the biomechanical properties of the MTC was significantly different based on which synthetic mesh (Gynemesh, SmartMesh, or UltraPro) and animal model utilized. The NHP model exhibited some early signs of stress-shielding which were not observed in the rodent model. Compared to the rodent abdominal wall, the NHP abdominal model may be a better model for evaluating the biomechanical properties of the host response following mesh implantation. This was the first step towards a better understanding of the host response to synthetic prolapse meshes; in the

future, these models will continue to be utilized to evaluate the next generation of prolapse meshes.

4.3 VAGINAL MODEL

4.3.1 Introduction

Clinical studies of how a synthetic mesh incorporates into the tissue are often difficult to conduct. This is related to the fact that large tissue samples are required for rigorous study, but cannot be obtained from humans except in the case of mesh removal do to surgical failure or a complication, cases which are likely not representative of the host response for the majority of patients. Moreover, it is difficult to control for confounding risk factors such as obesity, age, and hormonal status in humans.

As illustrated in Section 4.2, the abdominal wall is an appealing alternative to characterize the mechanics of the host response following mesh implantation; however, these abdominal models are not adequate replacement for studying the combined effects of anatomical, physiological, or replication of clinically relevant implantations as vaginal implantation. As described in Section 2.2.8, the vagina in the rodent animal model can have similar biomechanical properties as parous women after suffering from a simulated birth injury. Nonetheless, the majority of studies utilizing this animal model remain focused on evaluating mesh implanted to repair an abdominal wall defect due to the limited size of vaginal tissue. The rabbit has a sufficiently large vaginal site to implant mesh; however, anatomical and physiological

differences raise questions about the translation of these results to the human. As discussed in the conclusion of the first aim (Section 2.5), the NHP vaginal model is arguably the most appropriate to study mesh implantation onto vaginal tissue. Reiterating our earlier findings, the tangent modulus and tensile strength of the parous human vagina (9.5-12 MPa and 1.4 MPa, respectively) to be similar to that of the parous rhesus macaque (12.8 MPa and 0.96 MPa, respectively) [106, 156, 160]. While the abdominal wall is an appealing alternative model which has been utilized to characterize the biochemical and mechanics of the host response following mesh implantation [40, 73, 75-77, 104, 105, 107, 108, 111, 167, 189, 190], it has several significant limitations. The abdominal wall has a different composition, local physiology, and loading environment compared to the vagina. In addition, it is impossible to perform a clinically relevant prolapse repair procedure in the abdominal wall of an animal model. Utilizing the NHP vaginal model enables us to make more direct comparisons because this animal model has similar vaginal composition, micro- and gross anatomy, physiology, and mechanical properties of the vagina and pelvic floor compared to women. The aim of this study was to characterize the host response to implantation of three prolapse meshes with different stiffness values. Based on our previously developed uniaxial tension protocol, Gynemesh PS (Ethicon), the original polypropylene mesh for prolapse repair, was used as the prototype stiffest mesh (0.29 ± 0.015 N/mm). For comparison, we used UltraPro (Ethicon) a low stiffness mesh (0.009 ± 0.0016 N/mm) and SmartMesh (Mpathy) in intermediate stiffness mesh (0.18 ± 0.026 N/mm). Utilizing the NHP animal model (rhesus macaque), these meshes were implanted via sacrocolpopexy and the mesh-tissue complex (MTC) was assessed after 3 months for active contractile and passive structural properties relative to sham controls. We hypothesized that the stiffer Gynemesh, would be associated with an increased stress-shielding response, preventing the vagina from

experiencing the native loading conditions, resulting in inferior tissue incorporation and reduced tissue function following implantation.

4.3.2 Methods

4.3.2.1 Animals

Animals that were used in this study were maintained and treated according to experimental protocols approved by the Institutional Animal Care Utilization Committee of the University of Pittsburgh (IACUC #1008675) and in adherence to the National Institutes of Health Guidelines for the use of laboratory animals, and a minimum number of rhesus macaques (macacca mulatta) were used to answer our research question (see power analysis). Non-human primates (NHP) consisted of 17 cycling parous animals (9 to 16 years old) that were a minimum of 12 months after their last delivery. Routine laboratory tests and regular examinations by veterinarians during a quarantine period were used to certify that these experimental animals were pathogen-free and in good physical condition. Animals were maintained in standard cages with ad libitum water and a scheduled monkey diet supplemented with fresh fruit, vegetables, and multiple vitamins daily. A 12-hour light/dark cycle (7 AM to 7 PM) was used, and menstrual cycle patterns were recorded daily. Available demographic data of each NHP were collected prior to and after surgery including age, body mass index (BMI), gravidity, and parity.

Afterwards NHPs were randomly selected to be implanted, via abdominal sacrocolpopexy. Briefly, a midline incision was made through the abdominal wall. Each NHP had a hysterectomy performed with keeping the ovaries intact. An anterior and posterior dissection was performed to dissociate the vagina from the bladder and rectum respectively. A 3

cm wide by 10 cm long piece of mesh was placed on the anterior and posterior wall. Continuous sutures (Bison) were used to secure the mesh along each lateral edge. The anterior and posterior pieces of mesh were combined and anchored into the sacral spine with two resorbable sutures. Excess mesh was trimmed prior to closing the peritoneal cavity. The abdominal muscle layer was closed with a single continuous suture, while three to five interrupted sutures were used to re-approximate the borders of the skin. This was followed by a continuous suture subcutaneous closure. Animals were implanted with one of three commonly used synthetic meshes Gynemesh (n=6), SmartMesh (n=8), or UltraPro (n=7). A separate group of animals underwent a sham surgical procedure to control for the effects of surgery (n=9).

Animals were implanted for three months prior to vaginal tissue being explanted. Tissue samples were than divided for active and passive biomechanical characterization.

4.3.2.2 Active Properties

Smooth muscle contractility assays were performed on the anterior proximal vaginal. Of the NHPs implanted, only a sub-population were viable for contractile analysis: sham (n=5), Gynemesh PS (n=4), SmartMesh (n=8), and UltraPro (n=4). Tissue samples were cut into 1-2x6-10 mm^2 circumferentially oriented vaginal strips of the MTC. Two clips were used to secure each vaginal strip into the base of a biochamber and to a load cell (Honeywell). Load response data was recorded in grams continuously. Each strip was placed into a heated biochamber with Krebs solution to 37^oC and subjected to a ~10 mN preload. Samples were then allowed to equilibrate for an hour before exposing to a 120 mM dose of potassium (K^+) to determine maximum contractility. Each MTC was run in duplicate and averaged together to

obtain a single response from each specimen. The contractile force was converted to mN and then normalized to tissue volume (mm^3) as described in Section 2.1.3.

4.3.2.3 Passive Properties

To determine the passive biomechanical properties of the MTC, we utilized a custom designed scaled ball-burst apparatus. Samples for passive biomechanical analysis were obtained from the posterior and proximal vaginal wall. Of the total animals operated, only a subsection of animals were capable of undergoing biomechanical testing due to the required specimen size: sham (n=8), Gynemesh (n=3), SmartMesh (n=5), and UltraPro (n=7). The grafted vaginal tissue was then isolated from the surrounding ungrafted area (Figure 26).

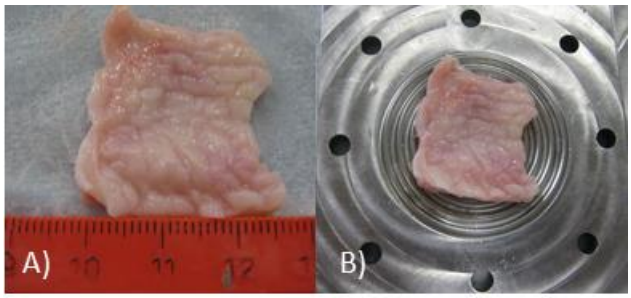

Figure 26 Isolated image of the lumen of a grafted vagina (A) Vaginal sample placed in the custom designed ball-burst clamp prior to testing (B)

Thickness measurements of the mesh-tissue complex were made utilizing a noncontact laser reflectance system [119]. For testing, each mesh-tissue complex was secured between two interlocking clamps. Grafted vaginal specimens had a minimum diameter of 2.2 cm. The base of the ball-burst fixture was placed onto an x-y translation table fixed to a materials testing machine (version 5565; Instron Industrial Products, Grove City, PA). The ball was attached to a moveable crosshead in series with a 5kN load cell (2525-800 Drop-down Series; Instron, Canton, MA). After the tissue was secured into the base of the Instron, the crosshead was lowered until

the ball fell within 5 mm and the sample centered underneath the ball. The mesh-tissue complex was subjected to a preloaded (0.5 N) and then was loaded to failure. All tests were performed at a rate of 10 mm/minute. The resulting load (N) and elongation (mm) were recorded to create the load-elongation relationship of the mesh-tissue complex or sham specimens.

The ultimate load (N), or failure load, and the maximum displacement (mm) was determined at the first point of failure. The stiffness (N/mm), or resistance to deformation, of the mesh-tissue complex was calculated using a running window of 20% of the entire load-elongation curve.

To determine the underlying tissue contribution to the mesh-tissue complex, an estimated tissue stiffness and failure load were calculated. This estimated tissue contribution to the overall mesh-tissue complex properties were based on several assumptions. These assumptions are detailed in Section 4.1.3. The estimated tissue stiffness (N/mm) and estimated tissue load (N) were compared to sham animals.

4.3.2.4 Statistics

All statistical comparisons were made using SPSS (SPSS Inc. Chicago, Il. Version 18.0). All data was examined to determine if it was normally distributed. All data was found to be non-parametric, therefore, a Kruskal-Wallis test with a Mann-Whitney post hoc was performed between each group. Correlations between the estimated tissue contributions (i.e. estimated tissue stiffness and failure load) to porosity, pore size, specific weight, low stiffness from uniaxial testing, and stiffness from the scaled ball-burst protocol were made using a Spearman's Rho test. All comparisons were made using a significant level of 0.05. Non-parametric data is presented as median (interquartile range).

4.3.3 Results

Animal demographical and POP-Q data was compared and highlighted in Table 23 and Table 24.

Table 23 Demographical data collected on each NHP. No statistical differences were observed in any of these confounding risk factors for POP

	Age (years)	Height (m)	Weight (kg)	BMI	Gravidity	Parity
Sham(n=9)	15 (5)	0.52 (0.032)	7.4 (2.5)	27.4 (6.4)	3 (4)	3 (4)
Gynemesh (n=6)	13.5 (1.8)	0.53 (0.041)	8.0 (1.1)	27.7 (3.8)	5 (0.75)	3 (3.5)
SmartMesh (n=8)	13 (3.3)	0.54 (0.025)	8.8 (2.7)	30.3 (4.7)	5 (1.5)	5 (2.3)
UltraPro (n=7)	11 (2)	0.53 (0.025)	6.4 (0.95)	22.3 (2.7)	2 (1)	2 (1)
Overall p-value	0.26	0.68	0.084	0.088	0.11	0.22

Examining the above demographics of the NHP groups and the general POP-Q scores at the time of euthanasia was important to consider prior to performing rigorous analysis on the active and passive biomechanical properties. Animals had similar age, BMI, gravidity and parity. Previous research in the NHP animal model has shown that a decrease in the mechanical properties of vaginal tissue is associated with parity and prolapse [160]. Therefore, it was essential to identify that all confounding risk factors, most importantly parity, that may impact vaginal biomechanical properties are not statistically different between each group.

Table 24 POP-Q scores taken at the time of euthanasia

	GH	PB	C	D	Aa	Ba	Ap	Bp	TVL
Sham(n=9)	1.5 (0.7)	1.3 (0.4)	-4 (0.75)	-5.25 (0.5)	-2 (0)	-2 (0)	-1.5 (1)	-1.5 (1)	5.5 (1.7)
Gynemesh (n=6)	1.6 (0.73)	1 (0)	-5.5 (0.5)	-5 (0)	-2 (0.38)	-2 (0.38)	-2 (0)	-2 (0)	5.65 (0.93)
SmartMesh (n=8)	2 (0.1)	1.1 (0.6)	-4.5 (0.75)	-5 (0.78)	-1.75 (1)	-1.75 (1)	-2 (0.63)	-2 (0.63)	5.9 (0.7)
UltraPro (n=7)	1.5 (0.4)	1 (0.5)	-5 (0.25)	-5.5 (0.45)	-2 (0.5)	-2 (0.5)	-2 (0.25)	-2 (0.25)	4.5 (1.1)
Overall p-value	0.203	0.412	0.242	0.243	0.51	0.51	0.185	0.185	0.286

POP-Q measurements are reported to indicate that the level of support from each NHP was not statistically different between the sham and experimental groups.

4.3.3.1 Active Properties

The contractile ability of vaginal tissue was significantly affected by mesh implantation. The contractility of the grafted vagina was significantly negatively impacted by mesh implantation. Relative to sham [0.31 (0.05) mN/mm^3], the stiffest mesh Gynemesh PS, had the greatest negative impact on vaginal contractility at 0.005 (0.01) mN/mm^3 (p-value=0.01) followed by SmartMesh 0.11 (0.04) mN/mm^3 (p-value=0.001; Figure 27).

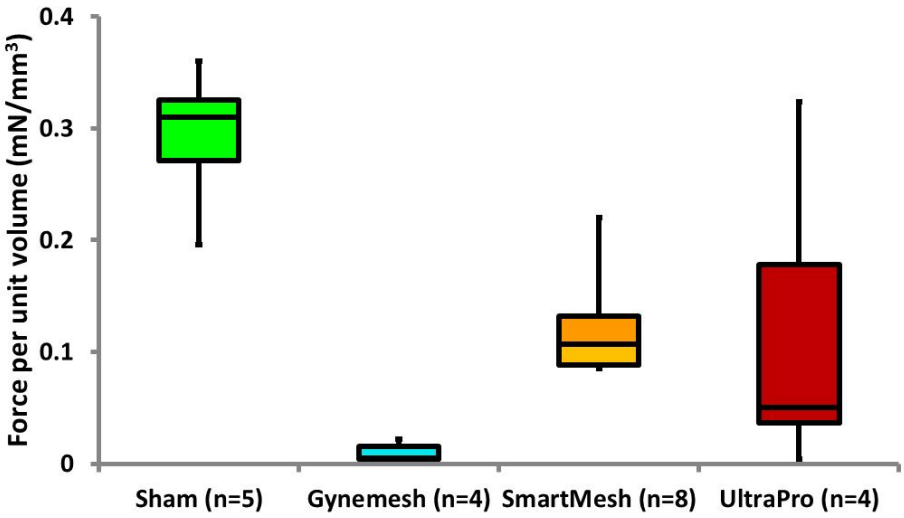

Figure 27 Box plot of the contractility assay results of sham and mesh implanted animals. Contractile force, or force per volume (mN/mm^3) is shown on the y-axis

Vagina grafted with SmartMesh had a significantly lower contractility relative to sham (p-value=0.001); however, the vaginal tissue still could generate a significantly higher load response compared to Gynemesh (p-value=0.004). UltraPro was found to not be significantly different from sham (p=0.26), Gynemesh (p=0.11), or SmartMesh (p=0.24). The inability to found statistical differences may be related to the higher degree of variance in the UltraPro group (0.05 (0.14) mN/mm^3).

4.3.3.2 Passive Properties

For the second aim of our study, we examined the passive structural properties of sham and mesh-tissue complexes (MTC) after implantation with Gynemesh, SmartMesh, and UltraPro. When comparing the MTC stiffness and failure loads, we observed no statistical differences

between any of the experiment groups (p=0.067 and p=0.25, respectively). However, examining the contribution of the underlying vaginal tissue to the stiffness, it was evident that the vaginal properties after implantation was different between each group (p=0.039, Table 25)

Table 25 Passive MTC and estimated tissue contributions to the stiffness and load at failure for sham control and NHP implanted animals. Statistical results below illustrate each group relative to sham, and the data is represented as median (interquartile range)

	MTC Stiffness (N/mm)	MTC Failure Load (N)	Tissue Stiffness (N/mm)	Tissue Failure Load (N)
Sham (n=7)	40.0 (18.7)	163.1 (48.4)	40.0 (18.7)	163.1 (48.4)
Gynemesh (n=3)	26.9 (3.2)	166.3 (21.0)	-0.57 (3.2)	58.2 (21.0)
SmartMesh (n=5)	42.4 (47.4)	166.3 (62.4)	30.0 (47.4)	133.7 (62.4)
UltraPro (n=5)	52.3 (16.8)	209.4 (97.6)	31.3 (16.8)	121.7 (97.6)
Overall p-value	0.067	0.252	0.039	0.076
Sham vs. Gynemesh	N/A	N/A	0.012	N/A
Sham vs. SmartMesh	N/A	N/A	0.833	N/A
Sham vs. UltraPro	N/A	N/A	0.281	N/A

The estimated tissue stiffness of Gynemesh implanted animals was roughly 0% which was significantly lower compared to sham (p=0.012), SmartMesh (p=0.036), and UltraPro (p=0.017). Contrary to the Gynemesh implanted animals, the contribution to the total MTC stiffness following SmartMesh and UltraPro implantation was roughly 80% and 58% respectively. From the amount of tissue contribution to the MTC stiffness in both SmartMesh and UltraPro implanted animals there was no statistical difference compared to sham operated controls (Table 25). Interestingly, unlike the statistical changes in the tissue stiffness, we did not see a corresponding significant change in the estimated tissue failure load (p=0.076). Even

though no statistical changes were detected, the tissue load did not greatly contribute to the MTC failure load, and Gynemesh implanted tissues contributed the smallest about to the failure loads.

From our correlation analysis we observed that several *ex vivo* properties correlated with the smooth muscle and estimated tissue contribution to the MTC stiffness after mesh implantation. The amount of contractile force generated by the smooth muscle negative correlated with the specific weight (R= -0.742, p=0.001) and stiffness calculated from the load-elongation created by the ball-burst test (R= -0.742, p=0.001). This smooth muscle response associated to a similar degree but in a positive manner with the porosity of each mesh (R= 0.742, p=0.001). Although not quite significant, it is interesting that pore size had a weak correlation to contractile behavior (R= -0.486, p=0.056). The estimated tissue stiffness correlated positively with porosity but negatively with the specific weight and stiffness when the mesh was subjected to the ball-burst protocol (R= 0.579, p=0.024).

4.3.4 Discussion

In this study, we compared the impact of 3 prolapse meshes on the functional properties of the vagina following sacrocolpopexy utilizing a NHP model. Specifically, we grafted the anterior and posterior vagina with one of three commonly used synthetic prolapse meshes (Gynemesh, SmartMesh, and UltraPro). From previous studies, these meshes were found to have varying stiffness values in response to uniaxial tension descending from Gynemesh, SmartMesh, to UltraPro. Our aim was to evaluate the effect of these prolapse meshes on the active and passive properties of the vaginal tissue *in vivo*. The most important finding of the paper was that mesh

implantation significantly impacts the underlying vaginal biomechanical properties. Further, it was found that with increased weight and stiffness more evidence of deterioration in the active and passive properties of the grafted vagina was present.

NHPs vaginal tissue that was grafted with Gynemesh, the stiffest mesh implanted, had the greatest negative impact on vaginal contractile (active) and passive mechanical properties following implantation. The effect of stiffness was distinct, as a correlation of *ex vivo* mesh stiffness was found with the ability of the MTC to contract. These combined results are preliminary evidence of a stress-shielding response suggesting that stiffer meshes are preventing the vaginal tissue from experiencing the typical loads it would be subjected to in its native state. Characteristic of implants that cause a stress-shielding response, grafting with Gynemesh led to a remodeling response which over time lessened the biomechanical properties of the vaginal tissue possibly making it more susceptible to erosion following prolapse repair. Further investigations are warranted to examine biochemical analysis of active and passive components of the vaginal tissue to confirm these findings. Although Gynemesh consistently lowered both the active and passive properties of the vaginal tissue, the two lighter weight and less stiff new generation synthetic meshes examined in this study did not exert the same magnitude of an adverse impact on vaginal properties. Previous studies have found similar result when grafting the patellar tendon with a stiff constructs. A rigid graft resulted in a degradation of the patellar tendons

structure evident by a decrease in collagen diameter and organization of the patellar tendon [184].

Interestingly, the ability of the body to incorporate these two new generation meshes while maintaining its native biomechanical properties may be important for an overall healthier response and reduced complication rates, specifically erosion of the mesh through the vagina. Implantation of each mesh had some degree of a negative impact on the contractile properties of the vagina. However, the lack of significance found after implantation with the UltraPro graft could be attributed to the large degree of variance. This variance in contractile behavior may be due to the *ex vivo* properties of the UltraPro graft. Previous studies have shown that UltraPro has very different mechanical properties depending on the direction of the applied force [84]. This is known as anisotropic behavior, or directional dependent properties, and needs additional investigation to determine how this directional dependence of UltraPro impacts the contractile behavior of the vagina. Understanding that the *ex vivo* mesh properties impact the host response are important for designing future prolapse meshes. In the present study, we performed a correlative analysis between the specific weight and stiffness values derived from uniaxial and ball-burst structural tests. Of these *ex vivo* properties, we found that better active and passive properties correlated with lighter meshes, higher porosity, and less stiff meshes (via ball-burst

protocol). These results are an early indication that *ex vivo* properties can be used to predict the host response and, therefore, vaginal properties post-implantation.

This study produced meaningful results, but is not without limitations. In the present study we assumed that mesh and tissue had negligible interaction to calculate the estimated tissue contribution of the vagina to the MTC. In the future, we aim to develop models that would be able to incorporate the interaction of the in-grown tissue and the synthetic mesh. These models would improve our understanding of how the structural properties of the meshes affect the mechanics of the host response. Another limitation of the current study is the small number of meshes examined. This is related to the cost of NHP studies, which make it difficult to perform studies with large sample sizes for extensive periods of time. Nevertheless, the lack of tissue contribution after implantation with Gynemesh PS suggests an adverse remodeling response. Lastly, the NHPs utilized in this study were parous and many of them did not suffer from prolapse, which is clinically the tissue that is often grafted with these prolapse meshes.

In summary, this study examined the *in vivo* active and passive properties of grafted vaginal tissue after implantation with three synthetic prolapse meshes. These combined results serve as preliminary evidence of a stress-shielding response and warrant further investigation including biochemical analysis of active and passive components of the vaginal tissue. Additionally, combining these results with those from future studies may shed light on the reason(s) behind the high rate of mesh-related complications from prolapse repair.

This phenomenon was particularly evident while examining the stiffest *ex vivo* mesh (Gynemesh PS) compared to two less stiff grafts (SmartMesh and UltraPro). Research is needed to characterize the biochemical properties (e.g. collagen ratios) of the vagina after mesh implantation to confirm the changes observed from our active and passive biomechanical analyses. Further studies of additional meshes with a different range of textile properties (e.g. porosity and specific weight) and structural properties (e.g. stiffness) will help us determine which individual or combination of properties can overt this stress-shielding response and lead to improved tissue incorporation after implantation.

4.4 CONCLUSION

These implantation studies have provided us with valuable information about the host response due to synthetic mesh implantation into *in vivo* animal models. First, we observed that the rodent and NHP abdominal models do not exhibit the same biomechanical profile after implantation. As previously eluded to (Section 2.2.8.3), the rodent abdominal model needed to be evaluated compared to other animals. The amounts of tissue contribution to the MTC properties in the rodent abdominal model were not negatively affected by mesh implantation; however, a degeneration of biomechanical properties was observed with the implantation of a stiff mesh in the NHP abdominal wall. This suggests that when implanting graft materials into the abdominal wall of these animals, the host response is unique to each model and should be respectively

considered when designing studies to evaluate the biomechanical response of tissues to mesh incorporation. This difference in host response should be considered when drawing conclusions from the rodent animal model regarding biomechanical relevance. Interestingly, comparing these abdominal results to those obtained from vaginally implanted prolapse meshes revealed a similar trend in tissue contribution of the NHP abdomen and NHP vaginal model. While Gynemesh was not observed to have an effect on the tissue contribution in the rodent model, additional research is required to ensure that this is not a species related response to these synthetic grafts.

In addition to the abdominal models, we utilized the NHP vagina to represent a more clinically relevant prolapse mesh implantation model. The NHP vaginal model is of great importance because it places the MTC under a physiological loading condition which is more similar to what would be experienced after clinical prolapse repair. From this study, we found that the tissue properties of the underlying vaginal wall were significantly different after mesh implantation. After implantation with Gynemesh, the active and passive biomechanical properties of the vaginal wall were inferior compared to sham and SmartMesh graft augmentation. Interestingly, a similar trend was observed after mesh implantation in both the NHP abdominal and vaginal models. Although the degree to which mesh implantation affected the passive biomechanical properties of the vaginal wall was variable, Gynemesh had the largest negative impact on the underlying tissue after both abdominal and vaginal graft implantation.

The data from these studies show the effect of mesh implantation on the biomechanical properties of the host response in two different animal models, as well as in separate locations within the NHP model. The rodent model illustrated little functioning tissue after mesh incorporation and minimal changes in the tissue contributions after mesh implantation. However, in both the NHP abdominal and vaginal models, early signs of stress-shielding were

observed. These studies are the first to suggest this possible degenerative remodeling response; this information could help us understand why older generation meshes, typically with greater stiffness, had such high complication rates. Furthermore, this data, in conjunction with that gathered from future investigations, can indicate which structural properties are most essential to ensure a positive host response in which anatomical support is restored, while native tissue integrity is maintained.

5.0 SYNTHETIC MESH MODELING

5.1 OVERVIEW

Synthetic polypropylene (PP) meshes are often used to restore anatomical and biomechanical support for women suffering from prolapse [80]. From our *in vivo* studies, we have assessed how three prolapse meshes affect the underlying abdominal or vaginal wall after implantation. The previous aims provide us with evidence that implantation of a stiff prolapse mesh can result in a negative remodeling response and inferior biomechanical properties. Modeling can help us evaluate how changes in the material properties, for example the stiffness, can affect the load-displacement behavior. Further, it can help us identify localized areas of increased stress and strain which may be related to eroding on the vaginal tissue. Lastly, future studies may provide us with insight of how the mesh parameters affect the biomechanical properties following implantation.

Previous research has shown that constitutive models in conjunction with finite element analysis (FEA) can predict the biomechanical behavior of synthetic meshes and biological tissues [86-88, 92]. Although previous research has begun to utilize these modeling approaches on abdominal grafts, little modeling and characterization has been performed on polypropylene meshes used in prolapse repair. The aim of this study was to develop a finite element model of

two newer generations meshes, SmartMesh and UltraPro, under a uniaxial tension testing protocol utilizing simple Timoshenko beam elements.

Additionally, we aimed to rigorously characterize the architecture of these synthetic meshes. Characterization of the pore size, aspect ratio, or fiber diameter of each mesh would greatly improve our ability to determine which textile properties are important for eliciting the *ex vivo* structural properties. Defining these parameters for each mesh would provide invaluable inputs into future constitutive models of synthetic grafts. Additionally, it would also provide a stronger basis to make comparisons between meshes regarding innate properties of the mesh pattern. Utilizing a custom designed Matlab (The MathWorks, Natick, MA) script, we wanted to define the *ex vivo* characteristics of the mesh patterns of Gynemesh, UltraPro, SmartMesh, Polyform, and Novasilk.

In the future, these modeling effects may be utilized through FEA to understand how the mesh and tissue interact at the time-zero implantation point and how fixation of these meshes may influence their biomechanical behavior following different surgical techniques.

5.1.1 Co-Rotation Theory

The co-rotational approach is often utilized to decompose rigid body motion and strain deformation [191, 192]. This is done by defining a local coordinate system where local rotations and deformations occur. This creates an elegant model that allows local geometry (segment level) to undergo linear deformations, while the global material may have some degree of non-linearity due to large rotations. Briefly, this means that when a linear stress-strain relationship is

defined, any non-linear behavior is a direct result of the rotation and aligning of the beam elements during displacement.

The main assumption of the co-rotational theorem is that there are small local strains but large global displacements and rigid body rotations [191]. From this assumption, simple relationships describing the local force and tangent stiffness matrices can be derived. This co-rotational definition allows for the development of relationships between the local internal forces and the tangent stiffness on a local and global scale. By determining the relative changes of each segment's displacements, rigid body rotation, and deformation from the original to current lengths, the global and local internal forces can be related by calculating the virtual work in both the local and global systems. Here, the global force (f_g) is related to the local internal force (f_l) by:

$$f_g = B^T * f_l \quad \textbf{5-1}$$

In this formula, B is defined as a transformation matrix which relates the global and local internal forces. The transformation matrix, B, is determined from the beam rotation and deformation via the co-rotational theorem. A more detailed formulation of the B matrix is detailed by Battini and Crisfield [192, 193]. In short, B accounts for the current length and rotation in the global force calculations. The local forces (f_l) are represented through three elements:

$$f_l = [N, M_1, M_2]^T \quad \textbf{5-2}$$

For the local forces, N represents the normal or axial load, while M_1 and M_2 are moment forces. The form which the local internal forces take depends on the beam element utilized: Euler-

Bernoulli or Timoshenko. The local stiffness matrix (K_l) is calculated by differentiating the local internal forces and is related to the global stiffness (K_g) via:

$$K_g = B^T * K_l * B + \frac{z * z^T}{l_n} N + \frac{1}{l_n^2} * (r * z^T + z * r^T) * (M_1 + M_2) \quad \textbf{5-3}$$

where z and r are vectors that account for the deformation and rotation of each segment, respectively, and l_n is the current length of the segment. The local internal forces and stiffness matrices are computed via integration over the cross-section of the beam element.

5.1.2 The Timoshenko Beam Element

Within the co-rotational theory, beam segments are often used to describe the stress-strain relationship between two connecting nodes. For example, a rectangular mesh (Figure 30) may be modeled using a representative skeletonized mesh. After computerized mesh generation, each line segment can be divided into n number of equally spaced nodes. Each individual line segment, represented by the area between nodes 1 and 2, can be modeled utilizing a beam element (Figure 30 C). The combination of all the beam elements constitute the framework of the mesh, and the locations where node elements between multiple beams overlap are termed joints. The joints are represented in Figure 28 by blue node elements.

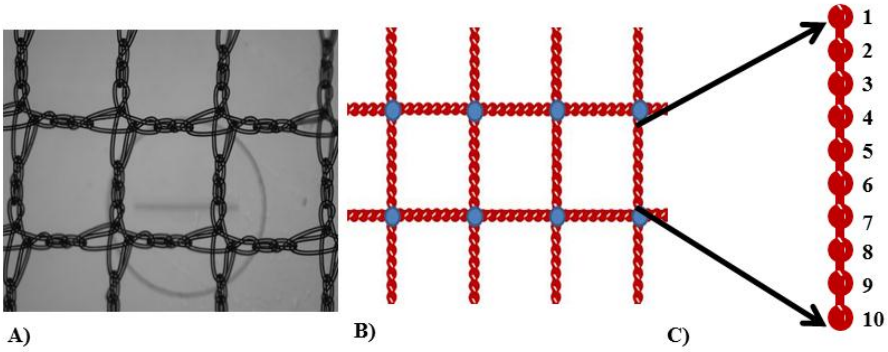

Figure 28 A macroscopic image of SmartMesh was taken (A) and the corresponding representative mesh (B) where each line segment is divided by 10 nodes (C). In between each nodal segment is modeled as a beam element.

For the purpose of this thesis, we will focus on the Timoshenko element. Briefly, the Timoshenko beam accounts for simple first-order shear deformation unlike the Euler-Bernoulli beam, which is considered to be shear indeformable [191, 192, 194]. The Timoshenko beam allows for infinitesimal strains of each node element in addition to large displacements and rotations along the framework of the material, in accordance with the co-rotational framework discussed in Section 5.1.1[193, 195]. This beam theory also assumes a constant cross-sectional area of each node element during elongation and deformation for the calculation of stresses. For a Timoshenko beam, the local internal forces are determined by performing a Gaussian integration along the cross-section of each element, as follows:

$$N = \int_v \frac{\sigma}{L} dv \quad \textbf{5-4}$$

$$M_1 = \int_v (\frac{\sigma * z}{L} - \frac{\tau}{2}) dv \quad \textbf{5-5}$$

$$M_2 = \int_v (-\frac{\sigma * z}{L} - \frac{\tau}{2}) dv \quad \textbf{5-6}$$

Here, N represents the normal or axial force while M_1 and M_2 are the bending moments. L denotes the length of the element, and z is the distance along the cross-sectional area. The normal stress (σ) is determined using the assumed stress-strain relationship within the beam element. For example, a simple linear relationship (Hooke's Law) can be assumed to describe the local stress-strain behavior:

$$\sigma = E * \varepsilon \quad \textbf{5-7}$$

The tangent modulus (E) of a material relates the stress (σ) and strain (ε) of the nodal element. Further, from Hooke's Law we can derive the shear stress (τ) as:

$$\tau = G * \gamma \quad \textbf{5-8}$$

where γ is the shear strain, and G is the shear modulus defined by:

$$G = \frac{E}{2 * (1 + v)} \quad \textbf{5-9}$$

In Equation 5-9, Poisson's ratio of the material (v) relates the tangent modulus to the shear modulus. Equations 5-7 and 5-8 can be substituted into the local force Equations 5-4, 5-5, and 5-6 for normal and shear stress (σ and τ). The local stiffness matrix (K_l) can then be determined from the local forces by differentiating these respective equations. Finally, the local stiffness matrix can be used to calculate the global stiffness (K_g) of the material by Equation 5-3. A more in-depth derivation and utilization of the classical Euler-Bernoulli and shear deformable Timoshenko beam elements can be found elsewhere [191-195].

5.1.3 Fiber Recruitment Model

The network of synthetic prolapse meshes often consists of multiple non-woven strands of polypropylene (PP). From examination of the mesh architecture, it is clear that each line segment actually consists of multiple strands of polypropylene. However, the artificially rendered geometric framework of these synthetic meshes utilizes the assumption that each bundle of fibers behaves as a single line segment which may be an idealized system (Figure 29).

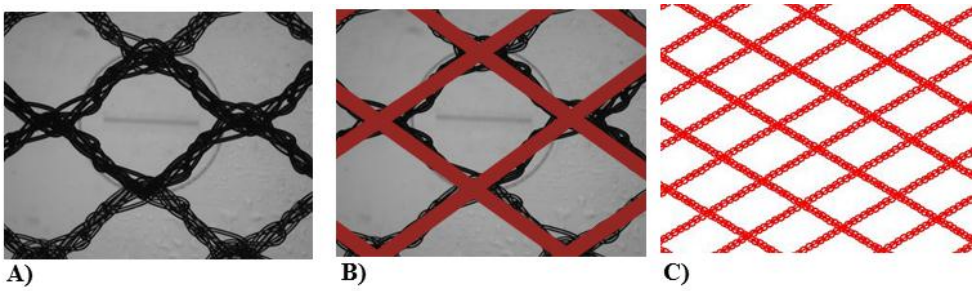

Figure 29 Magnified image of the UltraPro mesh (A) illustrating the multiple polypropylene fibers compared to a representative image of the generated mesh pattern (B) and an image of the mesh generated and divided into node segments (C).

The numerous fibers within each segment may not all be loaded simultaneously, resulting in inaccuracies of the predicted load response, as simulated utilizing the co-rotational theorem. Therefore, examining models developed to simulate the behavior of collagen within the extracellular matrix (ECM) is beneficial.

Uncrimping and recruitment of collagen fibers within the ECM is common among many biological soft tissues [34, 136, 196]. As a biological soft tissue is elongated, the collagen fibers lose their crimped pattern and become taut; as the elongation continues, additional fibers are recruited to resist the load through rotation. Additionally, fibers that have different lengths and were previously not stretched are recruited to resist deformation of the tissue. These properties

of collagen are often attributed to the early non-linear "toe region" from uniaxial load-elongation protocols. To characterize this non-linear behavior of soft tissues, structural and phenomenological models have been utilized [136, 197-200]. One the most widely used methods for modeling the elastic response of collagen during this uncrimping and recruitment is the two parameter exponential model:

$$\sigma = A * \left[e^{B*\varepsilon} - 1 \right] \quad \textbf{5-10}$$

Here, A and B are fitting parameters determined from experimental data [136, 199]. From this formula, the modulus at each strain increment can be calculated by:

$$\frac{\partial \sigma}{\partial \varepsilon} = A * B * e^{B*\varepsilon} \quad \textbf{5-11}$$

Even though additional, more complex structural models exist for describing this non-linear behavior, there are advantages to using this simplistic model. First, it is only a two parameter method with A as a scaling factor and B solely governing the degree of non-linearity. Second, this phenomenological approach is also easily incorporated into more complex structural or viscoelastic models, making it a versatile model for the stress-strain relationship [136, 197, 199].

Although the biomechanical properties of biological soft tissues and polypropylene meshes are significantly different, both have similar traits that have been observed experimentally. Like many soft tissues, light-weight deformable meshes can undergo large deformations with relatively small increases in load. The majority of polypropylene meshes have also been shown to display non-linear behavior under uniaxial loading, regardless of knit pattern or pore size [80, 83]. Therefore, this model may be useful in describing the large degree of non-linearity that these polypropylene meshes can display.

5.2 CONSTITUTIVE MODELING

5.2.1 Introduction

Synthetic polypropylene (PP) meshes are commonly used to restore anatomical support in prolapsed patients; however, little is understood about the properties of these synthetic grafts. Previous research has examined the use of constitutive models to help describe and predict the behavior of different graft materials [92, 176, 201, 202]. The textile field is old and has often utilized constitutive and finite element modeling techniques; however, the application of these approaches to the field of urogynecology and the commonly used synthetic meshes utilized in prolapse repair is relatively new. Peirce had previously described his method of modeling woven fabrics as rods, which laid much of the groundwork for the future development of theorems connecting geometric and mechanical behaviors [201, 202], while a more general history of various modeling techniques is portrayed by Yeoman *et al.* [203]. Recently, the further development of the co-rotational theorem detailed in Section 5.1.1 allows for modeling of mesh materials under the assumption of large rotations and deformations but infinitesimal strains [191-193, 195]. This approach may be better suited for prolapse meshes that are macroporous and undergo large strand rotations during uniaxial deformation [80]. The co-rotational theorem is an advantageous theory to utilize when initially modeling these prolapse meshes because it is a model that considers the meshes geometry playing a role in the mesh structural behavior. In this study, we aimed to examine the use of the co-rotational approach to model the *ex vivo* structural properties of two newer generation meshes (SmartMesh and UltraPro) subjected to a uniaxial load to failure protocol. Here, each segment was described using a Timoshenko beam element.

5.2.2 Methods

For this study, we wanted to examine the *ex vivo* properties of SmartMesh and UltraPro undergoing uniaxial tension. The uniaxial simulation will be compared to the load to failure data collected from each mesh; however, the overall goal of this method is not to model the failure of the mesh during extension. Nonetheless, it is important to be able to characterize the full range of mesh behavior by examining multiple loading conditions. Figure 30 illustrates the differences in geometry along orientation 1 and orientation 2 (O1 and O2, respectively).

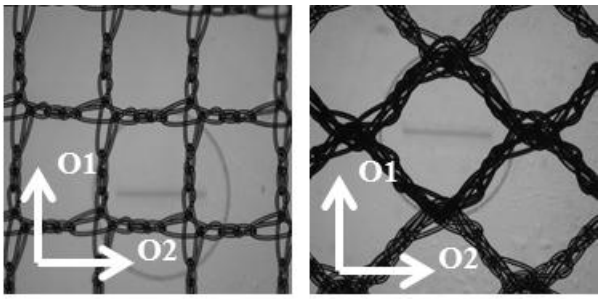

Figure 30 Macroscopic images of SmartMesh (left) and UltraPro (right) meshes illustrating the referred to orientation 1 (O1 or warp) and orientation 2 (O2 or weft).

From our previous study, we can assume that SmartMesh behaves as an isotropic material (Section 3.2.1). Based on this assumption, the structural properties of SmartMesh along O1 and O2 are expected to have similar load-elongation profiles and do not need to be independently evaluated. However, based on these earlier results, UltraPro violates the isotropic assumption and needs to be modeled separately in each direction (along O1 and O2). To determine the structural properties along the second orientation (O2) axis, additional pieces of UltraPro mesh (n=3) were isolated following the previously described protocol in Section 3.3.2.1. The average failure load and elongation values of these three loading conditions (SmartMesh and UltraPro

along O1 and O2) are presented in Table 26. Briefly, UltraPro O1 refers to the UltraPro mesh being loaded along the first orientation (Figure 32). SmartMesh was assumed to be isotropic based on the DA results and is loaded along an arbitrary axis (O1=O2). For these finite element predictions, we desired to have accurate predictions compared to our experimental data defined by the goodness-of-fit parameters of R-squared ($R^2 > 0.9$) and the root mean squared error (RMSE < 5).

Table 26 Average failure load (N) and displacement (mm) values of SmartMesh and UltraPro (O1 and O2) from a uniaxial tensile test

	Failure Load (N)	Maximum Extension (mm)
SmartMesh (n=5)	23.7 ± 1.8	53 ± 1.2
UltraPro (O1) (n=5)	8.6 ± 1.2	75.4 ± 2.7
UltraPro (O2) (n=3)	77.5 ± 10.1	38.4 ± 4.2

5.2.2.1 Mesh Generation

Prior to simulation, each mesh had a representative mesh generated from a custom made Matlab script (MathWorks Version 7.11, 2010). Figure 33 illustrates the final product after generation of each mesh for each mesh. In short, two populations of fibers, with a similar diameter, were assumed for each of these meshes. A representative generated mesh and actual Matlab generated mesh framework is shown in Figure 31.

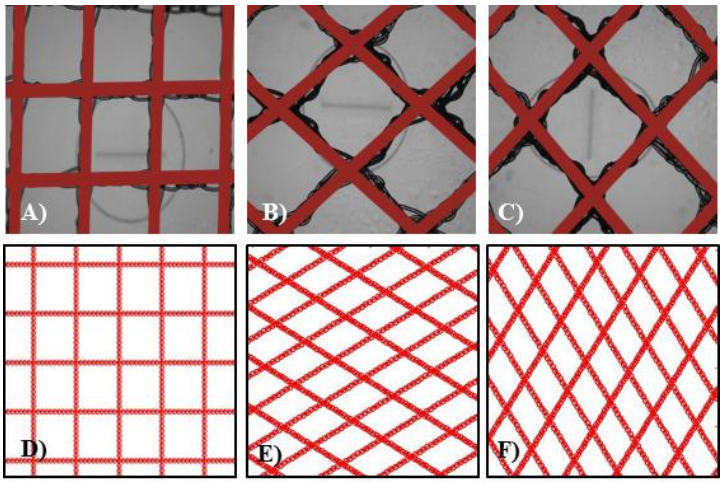

Figure 31 Top panels are macroscopic images of each mesh with an overlaid image of the skeletonized mesh of SmartMesh (A), UltraPro along orientation 1 (B), and UltraPro along orientation 2 (C). Bottom panels are representative area during the Matlab rendering of each mesh (D-F).

All generated mesh images were standardized to the average size of each sample mesh tested under uniaxial tension conditions (75 mm long x 15 mm wide). Lastly, the number of nodes along each line segment was set to 10; however, it should be noted that negligible changes occurred in the load-elongation response after increasing the number of nodes to 15 or 20. Due to the increased computational cost, a standard number of 10 nodes were utilized in all simulations.

5.2.2.2 Moment Transfer and Diameter Calculations

Aside from the stress-strain relationship, fiber geometry and node interaction terms were included in our simulations. Here, the node interaction term affects the degree which overlapping nodes, or joints, can transfer the moment forces (M_1 and M_2) generated between the nodes during rotation of the mesh. Since these meshes are not rigidly locked at the overlapping knits, it is important to consider the bending that occurs at these joints. Therefore, we implemented a 'hinge' parameter that can range from 0, or no moment transferred, to 1,

indicating that all of the moment transferred. At a value of 1, the joint behaves as a rigid interaction, whereas at 0, no moment forces are transferred between nodes and only the axial force would be transmitted across each joint. Although it is unclear how much of the moment is transferred between nodes, it is known that these are not rigid interactions. Therefore, for much of the present study, this 'hinge' parameter was set to 0.5 allowing 50% of the moment forces to be transferred at the joints.

The second parameter accounted for is the diameter of these representative fibers. Upon closer examination of Figure 32, we can see that both SmartMesh and UltraPro segments would consist of multiple fibers within creating a thick bundle instead of the originally assumed single polypropylene fiber utilized in the previously used model. For example, each thick bundle in UltraPro mesh is comprised of five strands of polypropylene. Since this linear stress-strain relationship relied on a modulus value for a representative fiber, we were unable to incorporate the multiple fiber bundle information into modeling of the *ex vivo* diameter of each mesh. Therefore, we needed to develop a method to accurately represent the multiple fibers of polypropylene into a single fiber diameter measurement. If we were to take a cross-sectional image, we may observe something similar to what is shown in Figure 32:

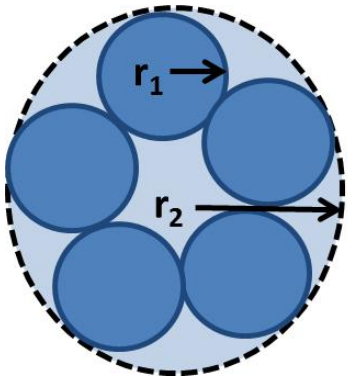

Figure 32 Schematic cross-sectional view of a thick PP fiber bundle. In this bundle, five individual fibers make up the larger bundle's circumference (represented by the outer dashed line)

Here we can easily see that using the radius measurement for the larger bundle (r_2) would provide us with an overestimate of the actual cross-sectional area of PP within the bundle (indicated by the shaded area). Therefore, the total number of fibers per bundle (n) was determined for each mesh, and the average radius of a single PP strand for each mesh was measured. The total area of the individual fibers was calculated by the following expression:

$$A_{total} = n * \left(\pi * r_1^2\right) \textbf{4-12}$$

From the total area of the total fiber cross-sectional area, a single representative fiber diameter (d_{rep}) could be calculated:

$$d_{rep} = 2 * r_{rep} = 2 * \sqrt{\frac{A_{total}}{\pi}} \textbf{4-13}$$

This representative diameter is a more accurate measurement of the cross-sectional area of the bundle which could then be implemented into the program prior to simulations. The d_{rep} of SmartMesh and UltraPro were found to be 0.11 mm and 0.19 mm, respectively. These values are different from outer diameter values of each mesh which were measured as 0.24 mm and 0.43 mm for SmartMesh and UltraPro. The effect of diameter on the load-elongation predictions

is shown in Appendix G. Simulations for each mesh and orientation were compared to the average load-displacement from the experimental data utilizing the R-squared (R^2) and root mean square error (RMSE) parameters.

5.2.2.3 Linear Stress-Strain Model Fiber

Within the context of co-rotational theory, we made the first attempt to simulate the *ex vivo* properties of two new generation synthetic prolapse meshes assuming a linear stress-strain relationship (Equation 4-7) on the local level. For mathematical predictions, rendered mesh frameworks were imported into a custom design solver which required three material inputs: modulus, diameter, and hinge parameter. Other user inputs included the step size and final displacement, or point to simulate towards. For all simulations, meshes were loaded along the referred direction. The appropriate representative diameter measurement was used for each mesh (d_{rep}=0.11 and d_{rep}=0.19). In addition, the hinge parameter has been shown to have only a minor effect on the inflection point (Appendix G). Therefore, this parameter was set to an arbitrary value of 0.5. First, we will examine the SmartMesh results. For this simulation, a modulus value of 200 MPa was used, and the simulation was run to a displacement of 52 mm with 1500 steps (Figure 33).

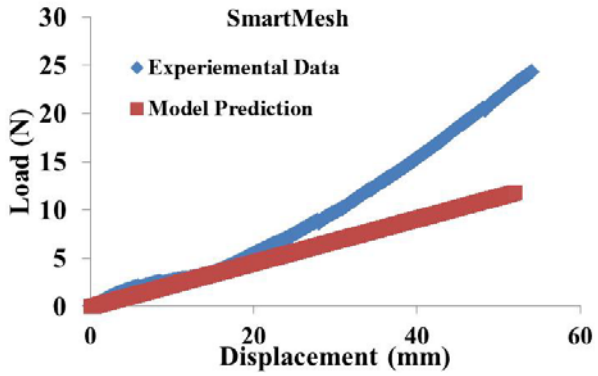

Figure 33 Experimental and model predictions of the load-displacement relationship of the SmartMesh subjected to a uniaxial tensile test loaded along an arbitrary axis (O1=O2)

The initial portion of the load-displacement curve match quite well but the overall quality of fit resulted in an R^2 of 0.5 and a RMSE of 4.79. For the UltraPro simulations, testing for each orientation was run separately. Nonetheless, a single modulus (90 MPa), moment transfer (0.5), and representative fiber diameter (d_{rep}=0.19) value was used for each simulation. UltraPro simulations testing along the orientation 1 direction were displaced 88 mm, while those loading along orientation 2 were set to 68 mm (Figure 34).

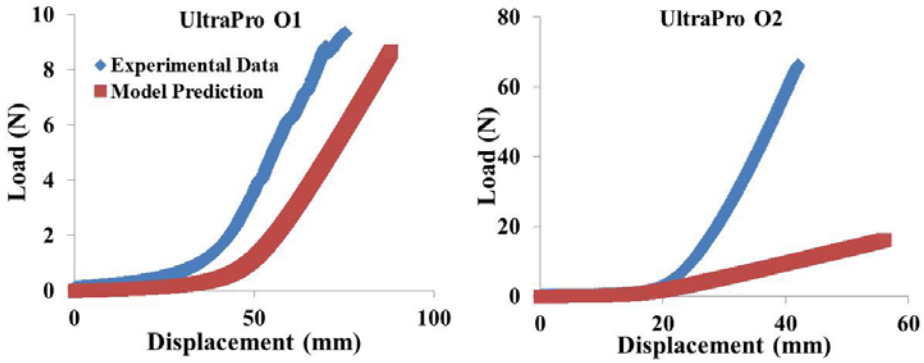

Figure 34 UltraPro simulations along orientation 1 (left) and orientation 2 (right) plotted against experimental data

Due to the geometry of SmartMesh, there was no rotation of the mesh during elongation resulting in the absence of non-linearity in the prediction of the load-displacement response (Figure 33). SmartMesh is square, so there is no rotation of the fibers during a simulated elongation test. Although SmartMesh does not display the same degree of non-linearity as other prolapse meshes, it does show a small degree in the experimental data which is not captured by this linear local stress-strain relationship. Alternative modulus (100 MPa) and diameter (d=0.24) values could have been implemented to achieve a better fit; however, none could account for the degree small degree of non-linearity. Simulation along orientation 1 (O1) for UltraPro resulted in a good match between experimental and predicted loads (R^2 = 0.91 and RMSE = 0.807). However, the finite element simulations along the perpendicular orientation (O2) of the UltraPro mesh could not account for the sharp increase in load-displacement curve after ~ 20 mm (R^2 = 0.27 and RMSE = 20.65; Figure 34).

One major advantage of these early simulations is that they can identify the importance of mesh geometry on the load-displacement profile. This approach had a linear stress-strain relationship; therefore, the anisotropic behavior of UltraPro can be attributed to the degree of non-linearity resulting from changes in geometry.

A second benefit of this approach is that its predictions were based largely on two input parameters: the fiber diameter and modulus of polypropylene. However, a key limitation of this approach was the use of an arbitrary modulus value. Utilizing a modulus value of polypropylene taken from the literature which range from 3.1 to 3.8 GPa, would have greatly improved its relevance [72]. The large range for the moduli values of polypropylene can be credited to the variations in manufacturing and pretreatment of the fibers prior to packaging. Implementing a modulus near the previously published values caused load predictions were orders of magnitude

higher as compared to experimental results (Appendix G). Therefore, a subsequent aim was developed to determine the modulus the individual polypropylene strands utilized in the fabrication of these prolapse meshes.

Individual polypropylene strands (n=4) were removed from the UltraPro mesh and tested via a uniaxial load to failure protocol. To investigate the effect of multi-fibers in a bundle, single mesh strands (n=4) that consisted of roughly 5 interknit fibers were excised from the mesh framework and tested in a similar fashion: 0.1 N preload and then loaded to failure. There was roughly a 50% decrease in the modulus of the knitted strand opposed to the single fiber (1.5 ± 0.03 GPa vs. 3.3 ± 0.4 GPa). Here, are modulus values for a single strand of PP was on the same magnitude as those previously published in literature, but there also appeared to be a degree of non-linearity within the stress-strain curve of the knitted strand which was absent from the single fiber results (Figure 35).

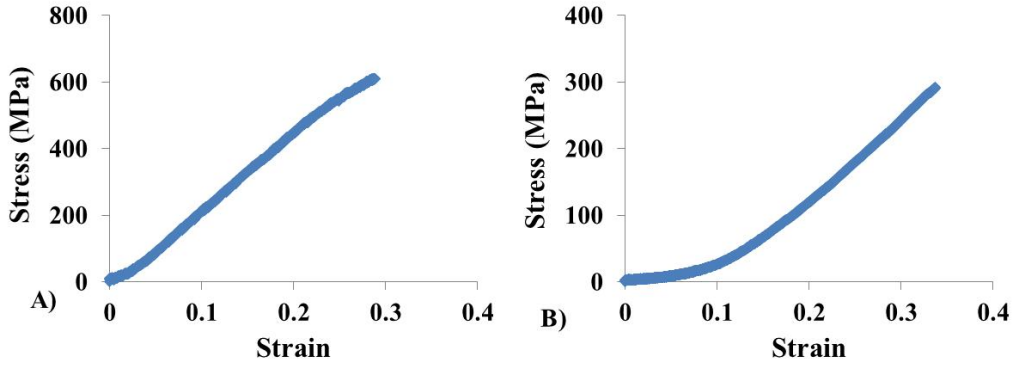

Figure 35 Representative stress-strain relationship plots for a a single polypropylene strand (A) and an isolated knitted strand comprised of 4 single strands (B) as calculated from a uniaxial load to failure test.

The inability of the linear stress-strain relationship to fully capture this non-linear behavior, especially while examining the second orientation of the UltraPro mesh, could be seen

as a limitation of the current model. Therefore, alternative models may be able to account for this additional degree of non-linear behavior observed by a single knitted strand.

5.2.2.4 Fiber Recruitment Model

The preliminary results from the above study provided insight into how the properties of a single strand of polypropylene may be orders of magnitude higher than the complete mesh. This type of behavior has been previously observed in studies examining the ECM component of collagen, as derived from the individual fiber's ability to rotate and straighten (uncrimp) prior to experiencing significant load levels. In fact, many biological soft tissues display a non-linear toe region prior to point at which all of the fibers are engaged in resisting deformation, and this phenomenon is often characterized through recruitment models. A common recruitment model used in biological studies is illustrated in Equation 4-10. This function describing the stress-strain relationship can be substituted for local internal force (Equations 4-4, 4-5, and 4-6) to account for polypropylene fiber uncrimping and rotation within the polypropylene mesh framework. This model allows for an additional degree of freedom by having two parameters. Here, A is a scaling factor and B governs the non-linearity of the curve.

The experimental knitted data was fit with this recruitment function to define a range of A and B parameters. Briefly, pooled data from each knitted strand test (n=4) was the UltraPro mesh were fit with an exponential function, and it was found that A=50 and B=6. Based on this information, ranges of A (25, 50, 75, 100, and 200) and B (1, 2, 3, 4, 5, and 6) values were utilized to simulate the load displacement response. All simulations utilized a minimum of 20,000 steps. The step size was increased from the original 1,500 steps used to better simulate the non-linearity in the local stress-strain relationship. Again, the hinge parameter was set to 0.5,

and the representative fiber diameters for SmartMesh (d_{rep}=0.11) and UltraPro (d_{rep}=0.19) were used. All simulations were performed within one standard deviation of the average mesh value data previously obtained (Table 26). SmartMesh was simulated to 52 mm, while UltraPro was predicted until 73 mm and 41 mm for Orientations 1 and 2, respectively.

To determine how these simulations could predict the experimental data, load-displacement data from each uniaxial experiment was averaged. This average load-displacement curve was fit with a spline function. This was utilized to create a spline function with x and y values of equal number of steps to the finite element predicted force and displacements. To determine which A and B parameter would best describe the experimental data we utilized a reverse finite element approach. The R-squared (R^2) and root mean square error (RMSE) for the predicted load-displacement curve were compared to the average experimental curves.

Fiber Recruitment Model Results

Simulations for SmartMesh (single arbitrary axis) and UltraPro (O1 and O2, individually) were examined for each combination of A and B values. Out of each possible combination of A (25, 50, 75, 100, 200) and B (1, 2, 3, 4, 5, 6), the best combination for SmartMesh was A=100 and B=2 (Figure 36). The predicted response was in good agreement with the experimental data (R^2=0.98 and RMSE=0.96).

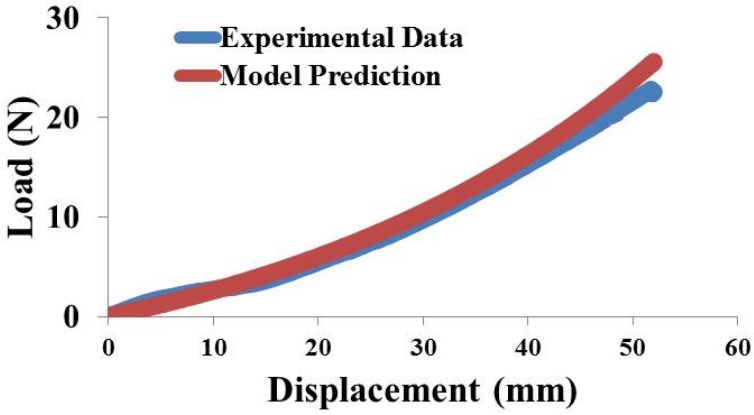

Figure 36 Spline fit experimental data plotted against the model simulated load-displacement response for SmartMesh along an arbitrary axis (A=100, B=2).

For the UltraPro mesh, two separates combinations of A and B were found to predict the behavior along the loading axes. Loading along O1, A and B were found to be 25 and 2, respectively (R^2=0.94 and RMSE=0.69). However, assuming a loading direction along O2, A was found to be 75 and B=5 (R^2=0.97 and RMSE=4.2; Figure 37).

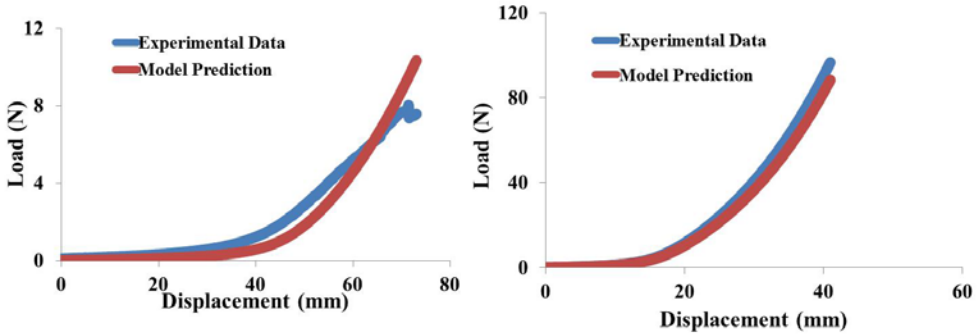

Figure 37 Fiber recruitment model of the stress strain relationship of the UltraPro mesh loaded along orientation 1 (left; A=25, B=2) and orientation 2 (right; A=75, B=5)

For each orientation (O1 and O2) of UltraPro a unique combination of A and B was found to best simulate the average experimental results. This provides us with further evidence

that the perpendicular orientations of UltraPro have specific properties, and it follows that it is indeed a more anisotropic material.

Sub-Window of A and B Parameters

This first attempt to find a suitable combination of A and B parameters to predict the load-displacement behavior of these synthetic prolapse meshes resulted in three sets of parameters, with a best set for each mesh. To improve the accuracy of A and B, a sub-range of A and B parameters was examined around the A and B values that best simulated the uniaxial behavior, which was identified in Section 5.2.2.3. This sub-range refined the A and B array to determine a more accurate combination of parameters that could better predict the averaged experimental data (Table 27).

Table 27 Sub-ranges of A and B parameters utilized to more preciselely simulate the load-displacement responses of SmartMesh, UltraPro O1, and UltraPro O2

	A	B
SmartMesh	**80, 90, 100, 110, 120**	**1.25, 1.5, 1.75, 2.0, 2.25**
UltraPro O1	**10, 20, 25, 30, 40**	**3.25, 3.5, 3.75, 4.0, 4.25**
UltraPro O2	**60, 70, 75, 80, 90**	**4.25, 4.5, 4.75, 5.0, 5.25**

Using the combinations of adjusted parameters, SmartMesh was found to have an A=90 and B=2 (Figure 38). These small changes in the A and B parameters improved the accuracy of the finite element simulation (R^2=0.996 and RMSE=0.428).

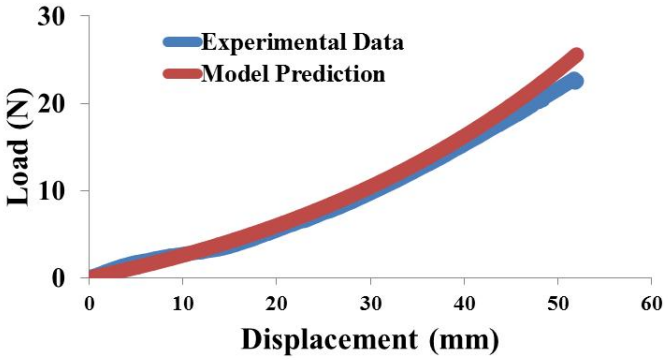

Figure 38 Simulated SmartMesh relative to the average experimental uniaxial data (A=90, B=2).

Identifying the best parameters to describe the UltraPro behavior along orientation 1 yielded an A of 30 and B of 3.5 (R^2=0.9469 and RMSE=0.652), while an A of 90 and B of 4.75 was found to best model UltraPro along the perpendicular orientation (R^2=0.993 and RMSE=2.36; Figure 39).

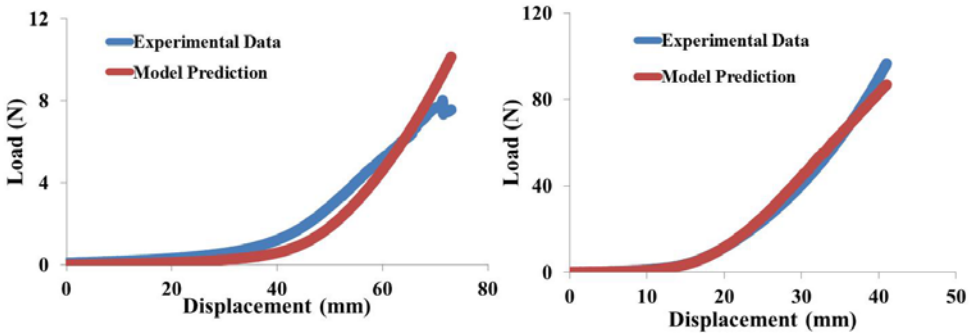

Figure 39 Predicted load-displacement behavior of UltraPro along orientation 1 (left; A=30, B=3.5) and orientation 2 (right; A=90, B=4.75)

A distinct advantage of utilizing the Timoshenko beam elements in conjunction with generating the mesh architecture is that together they allows us to predict the deformation of each mesh in addition to the load-displacement behavior. From these simulations, we can

develop a visually deformed mesh at increments of deformation. Below, we illustrate the propsed deformation of these synthetic graphs (SmartMesh, UltraPro O1, and UltraPro O2) at 0%, 50% and 100% deformation. For SmartMesh, we can see how the mesh elongates and no rotation of fibers is observed due to the square geometry of the mesh (Figure 40).

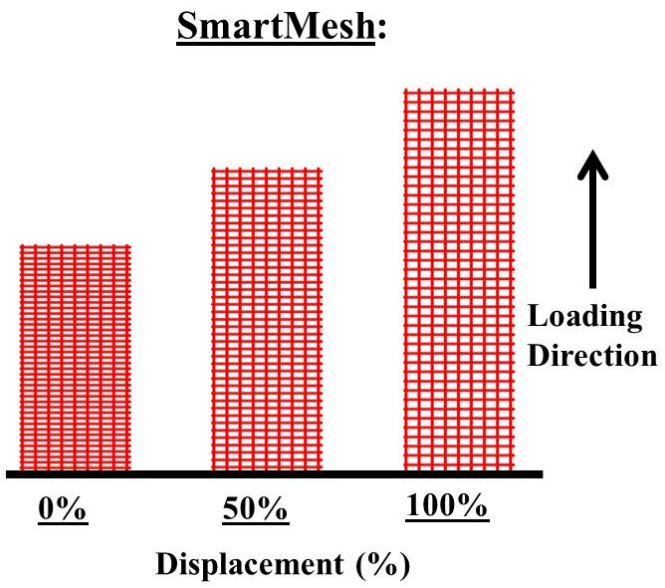

Figure 40 Graphical representation of mesh deformation simulated from the constitutive model

However, the individual elements of the mesh elongated with no rotation due to the geometry of SmartMesh. The lack of rotation in the finite element simulation under uniaxial tension translates to an elongation of the mesh network without a change in the predicted width (Figure 40).

Upon examination of the deformation of the UltraPro mesh, we found vastly different results compared to SmartMesh (Figure 41). Here, we can see that the mesh architecture greatly affects the deformation of the mesh while it is being loaded. Further, at 50% of its elongation the UltraPro samples being loaded along O2 are predicted to have a much more deformed and

aligned mesh as compared to both SmartMesh and UltraPro when loaded along O2. Therefore, the polypropylene fibers of UltraPro may be quicker to engage and resist deformation along orientation 2 which would partially explain why the load-elongation response is so different along each orientation.

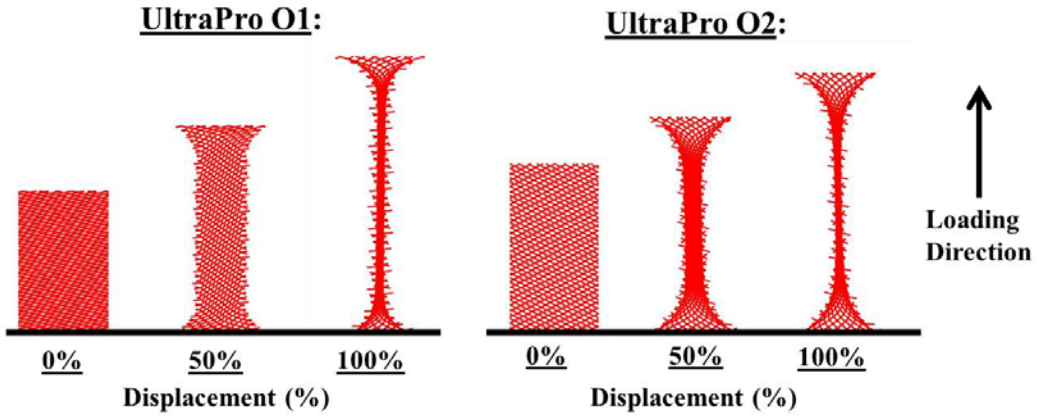

Figure 41 Representation of mesh deformation of UltraPro along orientation 1 (left) and orientation 2 (right). Each mesh undergoes a large degree of fiber rotation as depicted by the changes from 0% to 50% and 50% to 100%.

5.2.3 Discussion

In this study, we aimed to develop a model that could accurately predict the load-displacement response of SmartMesh and UltraPro. To further understand the behavior of these meshes, SmartMesh was assumed to be isotropic while UltraPro was simulated along two orientations (O1 and O2). For our model predictions, mesh framework was generated and divided into segments which were modeled as Timoshenko beam element to describe the local internal force of each mesh segment.

We first examined a simple linear relationship between stress and strain with the modulus of the mesh segments as our only input variable. From these results, we found that the non-

linearity of the mesh geometry could account for much of the load-displacement changes in the UltraPro mesh tested along O1; however, this model could not accurately describe the degrees of non-linearity in the SmartMesh or perpendicular direction of UltraPro. Further, inputted moduli values required to predict our experimental results were one or two orders of magnitude lower than published and calculated values of polypropylene. Therefore, alternative relationships for stress and strain were examined.

Due to the non-linearity present in a single knit strand, it was concluded that a fiber recruitment model would better predict the load-displacement behavior of these polypropylene meshes., commonly utilized for studying the elastic behavior of biological tissues. This two parameter (A, B) model implemented the stress-strain relationship along each Timoshenko beam element and was found to better predict the non-linear behavior of UltraPro in the perpendicular direction (O2) while accounting for the slight degree of non-linearity in the load-displacement properties of SmartMesh. In the present study, we found a unique set of A and B values that would best predict that behavior of SmartMesh (A=90, B=2), UltraPro loaded along O1 (A=30, B=3.5) and UltraPro loaded along O2 (A=90, B=4.75). The distinct A and B parameters required to describe UltraPro along each orthogonal direction further confirms the anisotropic behavior of this mesh. Our previous study (Section 3.2) predicted that UltraPro violated the assumption of an isotropic material, and in the future, this modeling approach will be a better means to quantify the anisotropic properties of additional meshes.

One of the limitations of the present study is the interpretation of A and B. A is commonly referred to as a scaling factor, and B helps govern the non-linearity; however, these parameters lack the physical significance that a single modulus value would have. It is important to note that the uniaxial tensile behavior of these meshes could be predicted utilizing a simple

two parameter fiber recruitment model to describe the relationship of local internal force and co-rotational theorem in place of a complex polynomial constitutive model commonly used to describe synthetic materials [92, 203].

This study represents the preliminary strides toward developing a constitutive model of these synthetic prolapse meshes by modeling their structural properties derived from a uniaxial test. Future studies will aim to expand the number of meshes simulated and validate their respective predicted deformation plots. In the future, we would like to develop 3D models to simulate our ball-burst protocols in order to assess the ability of this model to predict the biomechanical behavior of these meshes under multiple loading conditions.

5.3 MESH CHARACTERIZATION

5.3.1 Introduction

One of the limitations of the above finite element modeling approach is the inability to accurately represent the fiber diameters within many of these meshes, which is illustrated in Figure 25. To improve our modeling of these prolapse meshes, characterization of the synthetic mesh architecture is required to better understand the structural and mechanical properties of the meshes. Further, this knowledge may be useful in guiding the next generation of meshes through describing alteration in the fabrication process to achieve better suited structural and mechanical behavior.

Recently, an automated method has been developed by D'Amore *et al.* that makes it possible to extract the architecture from complex ECMs [204-206]. This methodology makes it possible to detect the fiber diameter distribution, network connectivity, orientation, and aspect ratio distribution. The fiber distribution can help identify the different fiber bundle populations. The network connectivity describes the number of nodes or intersecting mesh bundles, while the orientation designates the angle the fibers bundles within the synthetic mesh. Lastly, the aspect ratio is defined as the length divided by the width of each individual pore of the mesh, and the distribution of these calculated aspect ratios is used to better define the shape of these pores. All of these parameters affect the structural and mechanical properties of these synthetic grafts, and are important to characterize because r prolapse meshes have unique knit patterns that may affect their biomechanical properties [80]. However, little has been done to characterize the patterns of these synthetic meshes. Analysis of the architecture of each mesh will provide a better method for comparing the textile properties of current and future synthetic grafts to each other, utilizing a standard technique.

Synthetic prolapse meshes are often made of multiple, overlapping fiber populations. Several meshes (e.g. Gynemesh, UltraPro, and SmartMesh) may have multiple interlaced fibers which form larger bundles. Gynemesh also contains a second population of PP fibers that transect the larger pores. Still, other meshes (e.g. Novasilk and Polyform) are fabricated with mostly single fibers that are interlocked with each other via the knit pattern. The pore size of each mesh is often reported a single value; however, the shape and aspect ratios of each mesh, in conjunction with pore size and porosity, will help us better understand the textile profile of the meshes.

These parameters are important because synthetic meshes are often made of fiber and aspect ratio distributions. This is because meshes contain multiple fibers, via bundling of smaller fibers, and aspect ratios, due to the knit pattern. In the present study, an automated technique previously developed by D'Amore *et al.* was utilized to determine the diameter and aspect ratio distributions of the five prolapse meshes examined *ex vivo* in Section 3.0 .

5.3.2 Methods

Four digital macroscopic images of each mesh (Gynemesh, UltraPro, SmartMesh, Novasilk, and Polyform) were taken utilizing a CCD camera (COHU, San Diego, CA). Meshes were pictured with a standard ruler. Since the original program was aimed at analyzing SEM images, several additional steps were added to the original program to assist in analyzing the architecture of these macroporous synthetic meshes.

Each image was imported, and a scale was set using the impixel(*image_name*) command. The standard ruler was then removed via the built-in imcrop(*image_name*) function. Images were then filtered through a custom add-on program to adjust red:green:blue or grey thresholds (Appendix E). The goal of this program was to manually pre-process each image prior to using the following the methodology outlined by D'Amore *et al.* [204]. Briefly, an estimated fiber diameter of the mesh was entered into the program by impixel(*image_name*). A skeletonization, or skeleton extraction from a binary picture, of each image was then made and a representative matrix was created. From this representative image, the fiber diameter distribution and aspect ratio distribution were determined.

The raw fiber diameter and aspect ratio information from each image was then imported into an additional Matlab script (Appendix F). The following procedure was applied simultaneously for both the estimated fiber diameters (μm) and pore aspect ratios. Fiber diameter values were organized into a histogram. The fiber distribution data was then fit with a continuous multivariate Gaussian distribution. Clustering of multiple fibers can form different size fiber bundles within the mesh resulting in different functional fiber diameters of the mesh. For this initial phase, it was assumed that meshes consisted of two distant populations and were fit with a bimodal distribution resulting in two representative mean fibers and the respective deviation from these mean values. Due to the, distributions were assumed to be bivariate by default. In short, two mean fiber diameters were considered to be representative of the mesh and were denoted as d_1 and d_2. The mixed proportion (%), or fraction, that each distribution contributed to the overall mesh was also determined. Utilizing this percentage, it was possible to see what type of fiber distribution predominated within the mesh A large and small mean representative fiber diameters (d_1 and d_2) and pore aspect ratios (AR_1 and AR_2) were determined from for each mesh, and the respective mixed proportion (%) were grouped and compared utilizing a one-way ANOVA, with a Bonferroni post hoc (SPSS Version 18.0, Chicago, Il, $p<0.05$).

5.3.3 Results

Analysis of these images enabled the creation of an accurate skeletonized representation of each mesh (Gynemesh, UltraPro, SmartMesh, Novasilk, and Polyform). Figure 42 below depicts the raw image, the generated skeleton, and the aspect ratios for each mesh. The bivariate

distribution estimation found a lower and higher mean aspect ratio (AR) for each mesh, a deviation from this mean (σ), and a percentage within the population (Table 28).

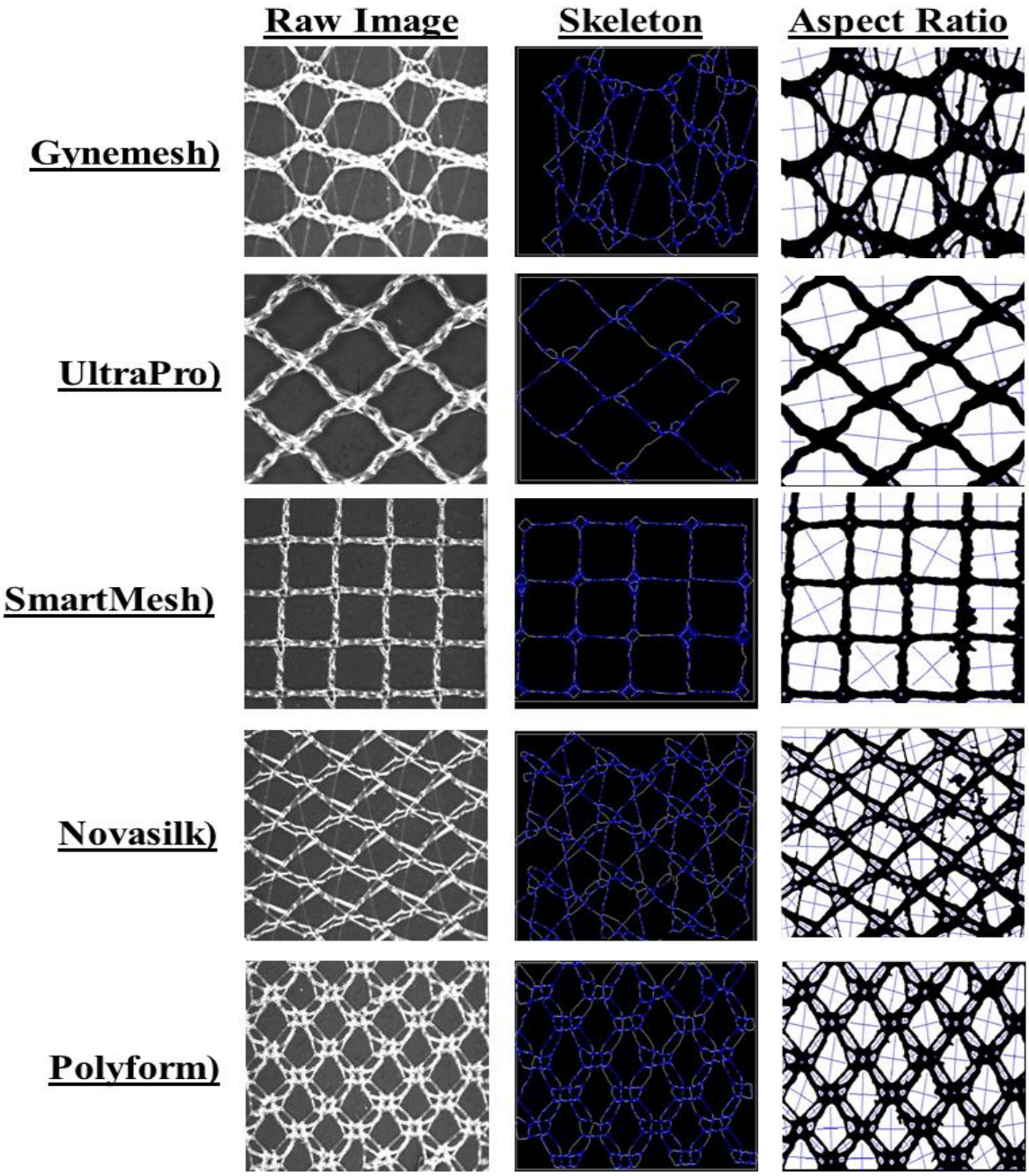

Figure 42 A digital image (first column), binary skeleton (second image), and aspect ratio (third column) is displayed for each individual mesh [Gynemesh, UltraPro, SmartMesh, Novasilk, and Polyform].

The lower aspect ratio (AR_1) of SmartMesh was significantly different than the small aspect ratio of Novasilk (p=0.013) and Polyform (p=0.021). The remaining comparisons between the lower aspect ratios were found to not be significantly different between the synthetic meshes. The upper aspect ratio of UltraPro (AR_2) was significantly smaller than that of Novasilk (p=0.009) and Polyform (p=0.027). No other differences in the mean ARs were found.

Table 28 Simulated aspect ratio (AR) data for each mesh. Data was fit with a bivariate normal distribution. The mean values (μ_1 and μ_2) represent the average aspect ratio for each distribution and the deviation from the mean (σ_1 and σ_2), along with the mixed percentage each mean is represented in the mesh framework.

	AR_1	σ_1	Mixed Proportion	AR_2	σ_2	Mixed Proportion
Gynemesh (n=4)	1.7 ± 0.33	0.46 ± 0.25	0.72 ± 0.38	4.03 ± 1.3	1.4 ± 1.2	0.28 ± 0.38
UltraPro (n=3)	1.3 ± 0.09	0.25 ± 0.03	0.50 ± 0.03	2.0 ± 0.16	0.39 ± 0.08	0.50 ± 0.03
SmartMesh (n=4)	1.1 ± 0.05	0.14 ± 0.05	0.76 ± 0.16	6.1 ± 2.4	3.1 ± 1.3	0.22 ± 0.16
Novasilk (n=4)	1.3 ± 0.04	0.22 ± 0.03	0.53 ± 0.03	2.8 ± 0.13	0.87 ± 0.19	0.47 ± 0.03
Polyform (n=4)	1.3 ± 0.06	0.19 ± 0.05	0.54 ± 0.04	2.7 ± 0.24	0.82 ± 0.27	0.46 ± 0.04
p-value	0.005	0.012	0.22	0.006	0.004	0.22

It is important to examine factors that could have influenced the aspect ratio measurements. Regarding the high aspect ratio of SmartMesh, this aspect ratio could have been skewed due to the cropping of the image creating the higher aspect ratio. Examining the percentage that each of these aspect ratios contribute to the mesh characteristics, we find that the lower aspect ratio constitute ~76% of the mesh while the higher aspect ratio makes up only about 22% of the textile characteristics. Several other meshes had a more equal distribution of aspect ratios within the mesh framework (Novasilk and Polyform). Upon examining the mesh architecture, we can see that these meshes had a distribution of aspect ratios that was better described by this bivariate model (Figure 42).

Many prolapse meshes consist of multiple fiber populations. To begin quantification of the different fibers populations present, the estimated fiber diameter histograms were fit with a

bivariate distribution fit utilizing a custom designed software. The mean values of each fiber distribution and their representation in the mesh (%) are presented in Table 29.

Table 29 Estimated diameter fibers for each mesh. Mean diameter values (μ_1 and $\mu 2$), deviation from the mean (σ_1 and σ_2), and representation of each mean fiber diameter in the mesh framework (%).

	d_1 (μm)	σ_1	Mixed Proportion	d_2 (μm)	σ_2	Mixed Proportion
Gynemesh (n=4)	177 ± 38.5	39.0 ± 27.4	0.51 ± 0.24	336.1 ± 59.9	48.0 ± 32.2	0.49 ± 0.24
UltraPro (n=3)	302.7 ± 11.9	59.3 ± 2.2	0.83 ± 0.07	579.3 ± 47.2	78.8 ± 44.7	0.17 ± 0.07
SmartMesh (n=4)	176.0 ± 37.7	44.5 ± 12.4	0.46 ± 0.07	260.3 ± 18.6	10.3 ± 1.1	0.54 ± 0.07
Novasilk (n=4)	134.6 ± 20.0	35.1 ± 9.5	0.60 ± 0.14	255.9 ± 26.0	23.5 ± 11.0	0.4 ± 0.14
Polyform (n=4)	169.3 ± 22.1	43.8 ± 5.8	0.76 ± 0.1	312.3 ± 50.3	39.1 ± 20.7	0.24 ± 0.1
p-value	<0..001	0.331	0.016	<0.001	0.029	0.016

The lower estimated mean diameter of UltraPro was found to consist of the thickest fiber bundles relative to Gynemesh ($p=0.025$), SmartMesh ($p=0.023$), Novasilk ($p<0.001$), and Polyform ($p=0.001$). Interestingly, the other meshes seemed to consist of a population of small fibers. The smaller diameters of these fiber distributions were not significantly different between any of the remaining meshes. A similar trend was observed in the upper estimated fiber diameter. UltraPro had the largest fiber diameter compared to Gynemesh, SmartMesh, Novasilk, and Polyform ($p=0.013$, $p=0.016$, $p=0.01$, and $p=0.007$, respectively).

After examining the representation of each fiber population in the mesh framework, it is clear that the small fiber diameter (d_1) of UltraPro, Novasilk, and Polyform comprised the majority of fibers within the mesh (83%, 60%, and 76%, respectively). However, Gynemesh and SmartMesh were found to have an equal distribution of fiber diameters throughout the framework (Table 29).

5.3.4 Discussion

This methodology presented two new approaches for characterizing the mesh architecture of synthetic prolapse meshes. First, it utilized a custom approach developed by D'Amore *et al*.to generate a mesh skeleton [204]. Second, it utilized the estimated aspect ratios and fiber diameters to determine a distribution of values centered around two average representative populations (AR_1, AR_2, d_1, and d_2). Further, this approach allowed us to examine how prevalent each mean AR and fiber diameter was portrayed in each prolapse mesh.

The AR of each mesh will provide us with a better understanding of how the mesh fiber framework is fabricated. The two aspect ratio parameters in conjunction with pore size and porosity may provide a better estimate of mesh burden on grafted tissues. Examining the mean fiber diameters it was clear that each mesh had multiple fiber distributions within their architecture. Since each mesh has a unique fabrication process, better characterization of these synthetic fibers will help researchers better compare multiple meshes and create more accurate constitutive models through the use of representative fiber diameters.

One limitation of this study is that it could not distinguish between individual fibers and a bundle of fibers. Even though the UltraPro mesh was found to have a significantly larger diameter (d_1 and d_2) examining the raw image of the mesh it is clear that these large fiber diameters can be attributed to a bundle of fibers. Therefore, these fiber diameter estimates should be considered an estimated size of fiber bundles and not of individual fibers. The last limitation of the present study was the assumption of a bivariate normal distribution. Although this was a first attempt to better understand the aspect ratio and fiber diameter of these meshes, a

method to determine the number of different aspect ratio and fiber distributions may lead to improved characterization and more accurate mesh comparisons.

These studies provide a critical step for the future development of mesh classification. The ability to detect and quantify the differences in the textile properties between these meshes is important for valid comparisons between each synthetic mesh. In the future, this approach may be utilized to characterize the connectivity of the mesh fiber, the orientation of the mesh fibers, and the tortuosity of the mesh.

5.4 CONCLUSION

These studies helped to better characterize the architecture of each synthetic prolapse mesh by examining their fiber and aspect ratio distributions. Additional studies aimed at depicting the connectivity and orientation of these grafts will provide us with better insight into the fabrication of these meshes. In conjunction with our modeling development, we may be able to better understand how changes in fiber diameter, connectivity, and fiber organization (e.g. aspect ratio and orientation) affect the load-displacement relationship.

Relating the textile properties to the structural properties of these meshes under different loading conditions will be a substantial step in the field. Farther down the line, this combination may allow us to direct the manufacturing design of the next generation of meshes by describing, in full, which textile properties are essential to obtain the ideal mesh structural properties.

6.0 OVERALL CONCLUSION

6.1 CLINICAL IMPLCATIONS

This dissertation illustrated several crucial findings within the field of urogynecology. To improve our current understanding on the effect of parity, three different animal models were examined: the rodent, sheep and NHP. This was the first study to illustrate the effect that parity had on the vaginal tissue and may provide us with better insight into the role that the vagina plays in pelvic organ support. Although parity did not significantly affect the mechanical properties in the rodent or sheep models, two additional findings from these studies are important to highlight. Due to its relatively small fetus size, the rodent may not suffer from a substantial maternal birth injury at the time of delivery. Subsequent studies found that simulating a maternal birth injury in the rodent led to a compromise of its vaginal mechanical properties, similarly to what was observed in the NHP. Parity negatively impacted the mechanical properties of the vaginal wall in the non-human primate (NHP) animal model. After vaginal delivery, the mechanical properties of parous NHP were consistent with data published on human vaginal tissue [106, 156]. Translation of this data into the clinical arena leads us to believe that if a woman has given birth, her pelvic floor and vaginal tissue support may be considerably inferior compared to a nulliparous women. This should encourage engineers and clinicians to re-examine what constitutes healthy tissue if parous, but supported, women already have inferior

vaginal mechanical properties. Further, it helped provide evidence that the NHP is the most viable animal model for studying implantation of prolapse meshes.

The second aim discussed that the current synthetic polypropylene (PP) grafts utilized to repair prolapse are largely implanted in parous women with a high number of post-surgical complications. This is, in part, due to the limited understanding of the textile and structural properties of these meshes. This dissertation examined porosity and the degree of anisotropy (DA) of each mesh through stereology. Porosity, an estimate of mesh burden on the tissue, was found to be significantly different between the meshes. This information should be considered by clinicians prior to implanting a synthetic graft into a patient. While the ideal burden a mesh should have on vaginal tissue is still unknown, most newer generation meshes were more porous and followed the current trend of decreasing mesh burden on the vagina. Secondly, the DA should make clinicians aware that orientation of mesh implantation is important. Gynemesh, UltraPro, and Novasilk meshes were found to be geometrically anisotropic while SmartMesh and Polyform may behave more like an isotropic material, and therefore, the method of fixation during surgery and implanted orientation could greatly affect the mesh-tissue interaction.

The structural properties of these synthetic prolapse meshes were characterized via uniaxial and ball-burst (BB) protocols. Each synthetic mesh was found to have a unique structural profile which further illustrates the need to identify the range of properties that would be ideal for successful implantation and host incorporation, while minimizing the clinical complications.

It is essential to gain a better understand the effect of mesh implantation to enable the development of better surgical techniques and mesh materials. In this dissertation, one implantation technique utilized was vaginal placement of prolapse meshes via an abdominal

sacrocolpopexy. From this study, we found initial evidence of a stress shielding mechanism following implantation into the NHP vaginal wall. After implantation with Gynemesh, recalling that it is the stiffest *ex vivo* mesh, there was a negative impact on the vaginal active and possible properties. This stress-shielding response and degradation of the native vaginal properties led to the conclusion that a more porous and less stiff prolapse mesh would help maintain better native tissue properties after implantation while positively augmenting the biomechanical properties of the weakened vaginal tissue. The evidence presented throughout this thesis makes it clear that clinicians should become more aware of and participate in studying the textile properties and structural properties of grafts that may led to improved patient outcome and therefore lower the current complication rate.

6.2 ENGINEERING SIGNIFICANCE

The research presented in this dissertation begins to bridge the fields of engineering and urogynecology. The field of urogynecology is not as developed in terms of biomechanics as many other clinical fields including orthopedics and cardiovascular systems, and therefore, additional preliminary research is needed to better understand the risk factors associated with prolapse development and to improve our knowledge regarding what leads to such a high rate of complications following surgical treatment.

From an engineering perspective, we examined the native vaginal tissue to better understand the properties that these synthetic mesh materials are commonly implanted onto for prolapse repair. The synthetic polypropylene (PP) meshes commonly used to repair prolapse

often have a high complication rate, partially because little is understood about the textile and structural properties of these meshes. Therefore, the next logical step of this dissertation was to examine the structural properties utilizing two different loading conditions: uniaxial and ball-burst. In addition, the textile properties of porosity and DA of these synthetic meshes were examined. These thorough studies lay the foundation for better defining mesh structural properties and textile characteristics.

However, simply performing the *ex vivo* structural tests is not adequate if a researcher desires to fully understand the properties of these meshes. Methodologies in this dissertation began to examine the use of finite element models to describe the structural behavior of these prolapse meshes. These mathematical models would provide researchers with the ability to identify textile properties (porosity, pore size, or fiber diameter) that would impact the structural properties. The current approach is different than previous attempts to model synthetic grafts [84, 92, 203]. Here, we have taken an approach to incorporate the mesh architecture utilizing a combination of a simple geometric co-rotational model [136, 191-193, 199]. A large advantage of the current approach is the ability to implement the stress-strain relationship of the polypropylene fibers. In this dissertation, we utilized a linear relationship and fiber recruitment model to predict the behavior of SmartMesh and UltraPro from a uniaxial tensile test. As an early approach for mesh modeling, this model was shown to have genuine potential for modeling these meshes. This finite element approach may evolve to include the multi-strands of fibers, total strand length, and individual fiber diameter and fully describe the structural properties under different loading conditions.

To develop these models, better characterization of synthetic meshes with in-depth modeling of the fibers, orientation, and pores can help create the structural models to improve

predictions of the load-elongation behavior. In this dissertation, we utilized a custom designed method to calculate different fiber diameters and the aspect ratios of the pores within each mesh [204, 206]. From this program, we have been able to create a skeletonization of each mesh. This method determined the multiple fiber populations within each mesh and the pore aspect ratios which can be inputted into the next revision of the finite element model. Further, this modeling approach may be able to take advantage of the skeletonization methods from this approach to recreate accurate geometry and fiber directions.

Lastly, this dissertation examined the *in vivo* properties of the mesh-tissue complex (MTC) after implantation into different animal models and tissue locations. These studies are important to better understand how physiological loading may affect native tissue properties after implantation. NHP studies are often difficult to perform in large numbers and can become exceedingly expensive, while rigorous biochemical and biomechanical analysis of the MTC in the human population has ethical and moral difficulties. Therefore, it is common to perform biomechanical or functional analyses of the host response in other animal models. Even though our clinical objective was to examine the effect of mesh implantation on the NHP vaginal tissue properties, we further aimed to examine the effect that these implants had on the rodent and NHP abdominal wall. Interestingly, from a biomechanical perspective we found that the results from the NHP abdomen and vagina mirrored each other, while graft placement did not significantly alter the native abdominal wall properties in the rodent model. Therefore, it will be important to define the specific research questions and limitations of particular animal models when examining biomechanical effects of mesh placement on native tissue, in future studies.

6.3 LIMITATIONS

There are a number of limitations regarding the work done in the present dissertation. Many limitations of the individual studies are mentioned within their respective discussions, but there are several other laying shortcomings that should be discussed. This work aimed at examining the use of different animal models to assess the effect of parity and mesh implantation on the underlying tissue. While parity was shown to have a significant change in the vaginal mechanical properties and pelvic floor support of the NHP direct comparisons between animal models is impossible to make. Therefore, it is difficult to assess the properties of the NHP that lead to a detectable change in vaginal mechanical properties that was absent from the other animals. We are left with a certain lack after implantation of commonly used animal models it is hard to propose

Another limitation of this study involves the characterization of the *ex vivo* properties of commonly used synthetic grafts. While performing structural tests under multiple loading conditions can provide us with insight into how each mesh may be have when subjected to different physiological loads, it is not an ideal method for understanding the structural behavior of these synthetic grafts. The development and validation of constitutive models will help provide a better interpretation of how the mesh architecture and properties of polypropylene (e.g. modulus) affect the resulting structural properties of the mesh. However, currently we are limited to a two parameters phenomenological model (A and B) to describe the local stress-strain relationship. An approach that involves the development of a structural model which could include the degree of anisotropy, orientation, connectivity, and multiple fiber diameters may be advantageous for better describing the load-displacement behavior of other meshes.

Lastly, our implantation technique did not allow for direct comparisons between animal models. For example, while we can assume a change in loading condition affect the host response between the rodent and NHP abdominal models additional research is required to validate this conclusion.

6.4 FUTURE DIRECTIONS

This dissertation aimed to quantify the effect of parity on the vaginal tissue, characterize and develop a constitutive on of commonly used prolapse meshes, and evaluate the tissue properties after mesh implantation. The research performed in this study has provided the groundwork required to better understand the native properties of vaginal tissue. It also began to examine the effects of parity, the largest risk factor for developing prolapse, on these different animal models. While much research on the effects of parity needs to be assessed, these results provide us with some important preliminary information.

In future studies it will be important to evaluate the effect of parity on vaginal tissue under a more physiological loading condition. For example, although no significant differences were found in the uniaxial tension properties of the rodent model a persistent effect of parity was evident by an *in vivo* study of vaginal biomechanical properties [135, 164]. This is because most tissues experience physiologic loads that are multi-axial resulting in a degree of tissue anisotropy. Tissues have a three-dimensional structure, which is a result of the complex extracellular matrix components that are specifically arranged to meet physiologic demands.

The question of anisotropy in the vagina can be assessed to some degree by testing longitudinally and circumferentially cut specimens independently and using a standard uniaxial testing protocol. This was done recently for sheep vaginal tissue samples and it was found that the stress-strain curves of the samples differed beyond the initial toe region, with circumferential specimens having a lower tangent modulus [106]. Although this provided evidence that tissues are anisotropic, tissues often display the phenomenon of axial coupling. In basic terms, this means that the mechanical properties of the tissue along one axis are dependent on the amount of stress or stretch applied to another axis. Planar biaxial testing of vaginal tissue has the potential to fully characterize the remodeling and effects of pregnancy, vaginal delivery, and birth injury. Utilizing a biaxial approach can improve the characterizing the mechanical properties by accounting for the coupled interactions of the circumferential and longitudinal axes of the vagina. In a preliminary study, we examined the coupling of these axes by determining the anisotropic index of planar vaginal tissue [207]. Following a previously described protocol, virgin (n=8) and pregnant (n=8) Long-Evan rats were subjected to equilbiaxial stress (0.1 MPa) [197, 198, 208]. The findings of this study show that the vagina is anisotropic and that the tissue becomes more distensible during pregnancy. These principles can later be used to perform large scale studies on vaginal biomechanical properties after different degrees of injury, genetic defects, or multiparous animals that would be deemed impossible to perform in larger and more expensive animal models. Therefore, future studies should examine vaginal tissue utilizing a biaxial testing device which will enable researchers subject the tissue to a more complex loading environment by involving the longitudinal and circumference fiber populations. These studies will better characterize the vaginal tissue; moreover, it will allow researchers to develop constitutive models of vagina tissue. These constitutive models could later be implemented into

a finite element analysis (FEA) to assess the behavior of the vagina under different loading conditions.

Synthetic meshes often utilized in prolapse are grafted to vaginal tissue; however, little is understood about the textile and structural properties. These studies characterized the porosity, degree of anisotropy, and through custom software began to rigorously characterize the mesh architecture. In addition, the *ex vivo* structural properties of five commonly used meshes was assessed via uniaxial and ball-burst testing. Lastly, the development of a constitutive model was used to predict the uniaxial tensile behavior of two commonly used synthetic grafts. While this dissertation took several strides to advance the lack of knowledge surrounding these prolapse meshes a great deal of research is still required. Teams of textile and material scientists, bioengineers, and clinicians need to form to between relate the material characteristics of these meshes and how they translate to structural properties and host tolerability and later translate to the clinical complication. Better defining the clinical goals of these meshes will allow bioengineers and textile scientist to evaluate the future properties of the next generation of prolapse meshes.

In the last aim of this thesis, we utilized multiple animal models (rodent and NHP) and two different implantation locations (abdomen and vaginal wall) to assess the biomechanical host response to graft implantation. Although each animal model is valuable and important during assessing the host response, it became clear that mesh implantation had a different host response depending on animal model and location. However, the principal finding from implantation in the NHP abdominal and vaginal wall was the degradation of biomechanical properties of the native tissue after implantation with Gynemesh compared to SmartMesh and UltraPro grafts. The use of the clinically relevant prolapse repair surgery in this dissertation is advantageous

because it found preliminary evidence of a stress-shieling response after being implanted with the stiff Gynemesh graft.

Future research should examine additional prolapses meshes to confirm the effect of increased stiffness on deterioration of the biomechanical properties. In addition, these future studies should involve biochemists experts. Upcoming studies should evaluate the inflammatory response, the collagen content and ratios, and the degree of cell apoptosis. These studies will improve our current understanding of what most lead to the current biomechanical results after implantation of Gynemesh, SmartMesh and UltraPro. From the present study it can be hypothesized that more lightweight and less stiff meshes will lead to a better host response and more correspond with decreased inflammation, higher collagen content, and less apoptosis. After combining the biochemical and biomechanical properties, clinicians should assess the demographical and epidemiological data from patients implanted with these synthetic grafts to assess how they perform in the clinical field. Pooling all this information can help researchers determine what properties lead to biochemical and biomechanical properties *in vivo* and the success of these meshes.

APPENDIX A

COMPARISON OF NULLIPAROUS UROGYNECOLOGICAL ANIMAL MODELS

To compare the mechanical properties between nulliparous animal models, vaginal tissue from nulliparous rat (Long-Evans), rabbits (New Zealand white), NHP (rhesus macaques), and sheep (mixed doreset) were examined histologically and biomechanically. Histological analysis was performed using standard Masson's trichrome staining on the vaginas of nulliparous rats (n=8), rabbits (n=6), primates (n=5) and sheep (n=8).

To determine the mechanical properties of the vagina, vaginal tissue was dissected away from the cervix, uterus, and bladder, placed in saline soaked gauze in a plastic bag and stored at -20^{o}C after sacrifice. On the day of testing, tissue was thawed at room temperature and a longitudinal section of tissue was isolated for uniaxial testing such that testing could be performed along the longitudinal direction of the vagina. Areas near the urethra were avoided so as not to include any connective tissues between the vagina and urethra. Each sample was then gripped using custom designed clamps for soft tissues. Once mounted in the clamps, each specimen was further dissected to a dog-bone shape ensuring that there was an area of uniform width and thickness along the length of the tissue providing an aspect ratio of 5. Subsequently, cross-sectional shape and area was measured using a laser micrometer system. Measurements

were taken at three locations along the mid-portion of the specimen and averaged. Throughout this protocol the sample is kept moist with 0.9% saline. A camera system (Keyence CV-2600) and motion analysis software (Spicatek, Inc. Maui, HI) were utilized to track the motion of contrast markers placed on the luminal face of the vagina during testing for strain measurements. Biomechanical testing of the tissue sample was conducted in a 37^{o}C saline bath fixed to the base of an Instron^{TM} testing machine (Instron 5565) [160]. The tissue was than subjected to a preload (0.1N), preconditioning (7% clamp-to-clamp strain), and load to failure protocol. Stress in the tissue was calculated by dividing the recorded force by the average of the three cross-sectional area measurements, while strain was calculated by dividing the pixel displacement of the markers placed on the tissue by the initial pixel distance between them. The linear region of the stress-strain curve was defined as the tangent modulus, while the tensile strength and ultimate strain were recorded at failure. The strain energy density was calculated by taking the area underneath the stress-strain curve until failure. Statistical analysis was performed using the parametric one-way ANOVA with a Bonferroni post hoc with a significance of $p=0.05$ (SPSS Version 18).

Histologically, the rabbit vagina was distinct from that of the rat, NHP and sheep with the muscularis of the rabbit vagina comprising a significantly greater volume of the total vaginal thickness (approx. 75-80% vs 40-50%). For the nulliparous animals, the tensile strength (0.43 ± 0.16 MPa) and tangent modulus (5.55 ± 2.36 MPa) of the rabbit vagina were substantially lower ($p<0.001$) than that of the NHP (2.44 ± 0.53 and 27.08 ± 11.46 MPa, respectively). However, these same parameters in the nulliparous rat (2.09 ± 0.65 MPa and 25.05 ± 5.07 MPa, respectively) and sheep (2.9 ± 1.0 MPa and 22.3 ± 9.81 MPa, respectively) were similar to the NHP (Figure 43).

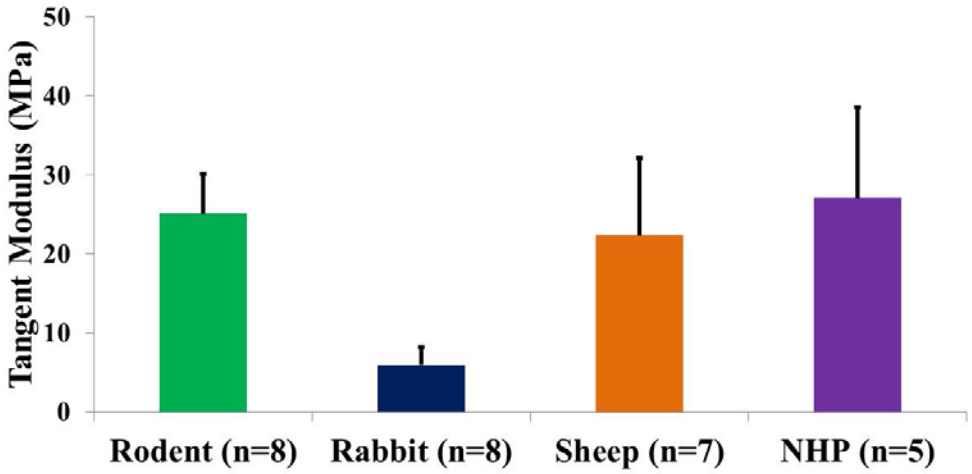

Figure 43 The tangent modulus derived from a uniaxial tension test of nulliparous rodents, rabbit, sheep, and non-human primates

The rabbit was found to have a tensile strength which was 78%, 82%, and 81% lower compared to the rodent ($p<0.001$), sheep ($p<0.001$), and NHP ($p<0.001$). Further, the strain-energy density was significantly lower in the rabbit ($p<0.001$) compared to all other urogynecological animal models. No significant differences in the tensile strength, ultimate strain, tangent modulus, and strain-energy density were found between the nulliparous rodent, sheep, and non-human primate.

Based on these data, although the NHP persists as the gold standard model for the testing of meshes prior to their use in humans, the nulliparous rodent and sheep animal models were found to have similar biomechanical properties as the nulliparous primate. The New Zealand White Rabbit had a unique histological composition, with an increase in muscle thickness compared to the rat, NHP, and sheep animal models. The biomechanical properties, specifically the tangent modulus, was markedly different from the rodent, NHP and sheep models deeming this species an inappropriate model for mesh analysis in spite of its wide-spread use.

APPENDIX B

MEAN INTERCEPT LENGTH CALCULATIONS

The following program was developed to determine the components of the mean intercept length (MIL) matrix (M) and fabric tensor (H). It was also used to export the eigenvalues and vectors, along with plotting the fabric ellipsoid detailed by Cowin and Doty [178]

```
% Andrew Feola
% 2011
clc
clear
% input measured length values (in mm)
L0 = 6.568;
L30 = 6.78;
L45 = 7.474;
L60 = 6.061;
L90 = 5.282;
% input number of intersections
Num_Int0 = [ 21, 16, 16];
Num_Int30 = 15;
Num_Int45 = 18;
Num_Int60 = 12;
Num_Int90 = [ 12, 16, 10];

MIL0 = (3*L0)/sum(Num_Int0);
MIL90 = (3*L90)/sum(Num_Int90);
MIL45 = L45/Num_Int45;
MIL30 = L30/Num_Int30;
MIL60 = L60/Num_Int60;

%empty vector that is defined below
MIL = [ 0, 0, 0, 0 , 0];
for  i=1:5
    if i== 1
        MIL(i) = 1/MIL0^2;
```

```
    elseif i == 2
        MIL(i) = 1/MIL30^2;
    elseif i == 3
        MIL(i) = 1/MIL45^2;
    elseif i == 4
        MIL(i) = 1/MIL60^2;
    else
        MIL(i) = 1/MIL90^2;
    end
end

x = [ degtorad(0), degtorad(30), degtorad(45), degtorad(60), degtorad(90)];
y = MIL;

fun = @(a,x) a(1)*cos(x).^2 + a(2)*sin(x).^2 + 2*a(3)*cos(x).*sin(x);

beta0 = [1 0.2 1];
[beta,r, J] = nlinfit(x,y,fun,beta0);
 if (beta(1)/beta(2)) ~= 1
     y2 = [ beta(2)/beta(1), beta(2)/beta(1)^(1/6)];
     x2 = [1, 1];
     fun2 = @(d,x) d(1)^2/d(2)^2 + d(1)/d(2)*x2;
     delta0 = [0.1 0.1 ];
     [delta,r, J] = nlinfit(x2,y2,fun2,delta0);
 end

M = [delta(1)^2*beta(1) delta(1)*delta(2)*beta(3); delta(1)*delta(2)*beta(3)
delta(2)^2*beta(2)];

H = inv(sqrtm(M));
detM = det(M);
detH = det(H);
[EgVecM,EgValM] = eig(M);
[EgVecH,EgValH] = eig(H);

 t = [degtorad(0), degtorad(30), degtorad(45),degtorad(60), degtorad(90)];
 MILs = [MIL0,MIL30, MIL45, MIL60, MIL90];
 polar(t,MILs, 'b*')
hold on
 t3 = 0:(45*pi)/180:2*pi;
MILs3 = [MIL0, MIL45, MIL90, MIL45, MIL0, MIL45, MIL90, MIL45, MIL0];

polar(t3,MILs3, 'c-')
hold off
pause

t2 = 0:(10*pi)/180:2*pi;
 for i2=1:length(t2)
 MILs2(i2) = beta(1)*cos(t2(i2))^2 + beta(2)*sin(t2(i2))^2 +
2*beta(3)*cos(t2(i2))*sin(t2(i2));
 end
 polar(t2,MILs2, 'k-')
```

APPENDIX C

EFFECTS OF ABSORPTION ON THE STRUCTURAL PROPERTIES OF ULTRAPRO

The recently developed vaginal mesh UltraPro is used in the Prolift +M™ kit for pelvic organ prolapse (Gynecare, Somerville, NJ). This mesh has been engineered to reduce host mesh burden by replacing a portion of the mesh with delayed absorbable fibers. As meshes with increased stiffness have been associated with increased rates of erosions and complications, we hypothesized that the resorption process would reduce mesh stiffness. However, little has been done to characterize the changes of the structural properties of this mesh with and without the absorbable fibers. Thus, we aimed to determine the uniaxial tensile properties of the mesh pre- and post- absorption.

Five separate sterile mesh samples of UltraPro were divided in half, and one half underwent a resorption process as described by the manufacturer. The *ex vivo* resorbed and unresorbed of each mesh specimen was determined by applying a 0.1 N preload, measuring the clamp-to-clamp length, and then a load to failure test at a rate of 50 mm/min was performed. From this tensile test the structural properties of the mesh could be determined: low stiffness, high stiffness, failure load, and relative elongation at failure. Additional samples underwent 3 separate protocols for cyclic loading to determine permanent deformation with submaximal

cyclic loading. Gynemesh, which does not contain an absorbable component underwent the same resorption and testing protocol as UltraPro as a control. Its permanent polypropylene fibers should not be affected by the resorption process. All comparisons for this portion were limited to within the respective mesh types pre- and post-absorption. Statistical analysis was done utilizing a paired t-test ($p<0.05$).

The load-elongation curves demonstrated a bilinear response with a period of lower stiffness (N/mm), followed by a period of higher stiffness (Figure 44).

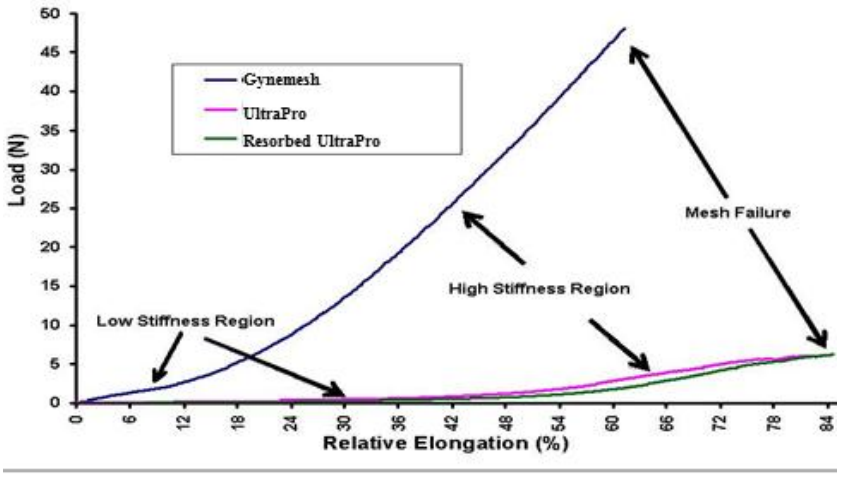

Figure 44 Load-relative elongation graph of Gynemesh and UltraPro pre- (pink) and post-(green) absorption

The maximal load at failure was lower in UltraPro after resorption (5.3 vs. 7.8 N, $p=0.02$, Table 30). There were no other differences in the biomechanical properties between pre- and post-resorption specimens for UltraPro including low stiffness, high stiffness, relative elongation at inflection point between low and high stiffness, and relative elongation at mesh failure (Table 30).

Table 30 Table displaying the structural properties derived from a uniaxial tensile test pre- and post-monofilament absorption.

	Low Stiffness (N/mm)	High Stiffness (N/mm)	Inflection Point (%)	Failure Load (N)	C1
UltraPro (n=5)	0.009 ± 0.002	0.24 ± 0.019	46.5 ± 5.2	7.8 ± 0.69	44.3 ± 3.6
Resorbed UltraPro (n=5)	0.007 ± 0.001	0.2 ± 0.029	48.2 ± 0.74	5.3 ± 0.72	45.2 ± N/A
p-value	0.21	0.12	0.69	0.02	N/A

Gynemesh demonstrated no differences for any parameters before and after resorption (Table 31).

Table 31 Gynemesh structural proeprties before and after undergoing the resorption process. No significant differences were found.

	Low Stiffness (N/mm)	High Stiffness (N/mm)	Inflection Point (%)	Failure Load (N)	C1
Gynemesh (n=5)	0.29 ± 0.015	1.4 ± 0.093	25.0 ± 0.89	46.3 ± 2.6	5.7 ± 1.1
Resorbed Gynemesh (n=5)	0.32 ± 0.042	1.4 ± 0.21	24.3 ± 1.4	46.4 ± 4.7	6.2 ± 1.3
p-value	0.22	0.78	0.15	0.94	0.48

. Gynemesh demonstrated no differences for any parameters before and after resorption. Resorption of the delayed absorbable portion of the Prolift +M™ mesh had little impact on the ex vivo tensile properties of the material. However, it is significantly less stiff than Gynemesh PS™ regardless of resorption status, which may be predictive of lower patient morbidity. It is not clear whether the decrease in failure load will impact clinical outcomes such as surgical failure and recurrence of prolapse. Further experiments are underway to define in vivo behaviour.

Although designed to reduce the resultant mesh burden experienced by the patient, there is little evidence that resorption of the delayed absorbable filaments of the UltraPro mesh have any effect on the tensile properties of the mesh. The only difference after resorption is a

reduction in the maximal load at mesh failure, a property with no clinical benefit. UltraPro is significantly less stiff than Gynemesh, the gold-standard pelvic mesh, which should help reduce mesh erosions when compared to this product.

APPENDIX D

VALIDATING CHANGES ASSOCIATED WITH SCALING THE ASTM BALL-BURST TESTING APPARATUS

Structural properties of meshes are often examined using uniaxial or ball-burst (BB) testing protocols. Current ASTM ball-burst standard testing devices require large square samples (75×75mm). Although this is typically not an issue in the textile industry, obtaining biological samples of this size or mesh samples post-implantation is difficult because studies of this nature utilize small animal models. Therefore, a scaled version of the ball-burst device must be used to test excised biological samples. Although failure loads and elongations will change with an altered sample size (differ by the scaling factor), stiffness measurements of a sample should theoretically remain constant between the ASTM and scaled ball-burst tests. The failure load and maximum extension should decrease by a change in diameter of the sample (~2.67), since the ratio of the ball to specimen diameter was kept constant. In addition, the energy absorbed should diminish by the change in surface area of the sample which was about 7.1. A direct comparison of the ASTM and scaled ball-burst can be seen in Figure 45.

ASTM BB	Scaled BB
Ball Diameter	**Ball Diameter**
25.4 mm	9.52 mm
Sample Diameter	**Sample Diameter**
44.5 mm	16.6 mm
Surface Area	**Surface Area**
1152 mm^2	216 mm^2

Figure 45 Comparison of the properties of the ASTM and scaled ball-burst testing apparatuses

In short, 75x75 mm and 25x25 mm square samples of Gynemesh, SmartMesh, Novasilk, and Polyform were tested on the ASTM or scaled ball-burst apparatus respectively. Prior to testing, samples were soaked in physiological saline (0.9% NaCl, 20^{o}C) for 15 minutes. Both the ASTM standard and scaled ball-burst samples were preloaded to 0.5 N and then loaded to failure at a rate of 10 mm/min (Figure 46).

Figure 46 ASTM standard ball-burst device (left) and scaled ball-burst device (right)

We have shown previously that mesh properties are not sensitive to small changes in strain rate, i.e. less than 1 order of magnitude. Parameters describing the structural properties of each mesh were obtained from the resulting load-elongation curves. To calculate stiffness (N/mm) the maximum slope over a range equal to 20% of the failure elongation was used. The failure load (N), corresponding to the ball breaking through the specimen, is also reported.

Comparisons between the ASTM and scaled ball-burst protocols were made using a paired t-test using the SPSS statistical software (18.0 SPSS Inc. Chicago, Il). Comparisons were made using a significance level of $p<0.05$.

There was no significant difference in the stiffness between the ASTM standard and scaled ball-burst protocols ($p=0.86$). Gynemesh and Novasilk had the largest variability with an 11% and 9.8% difference between ball-burst setups, respectively. Polyform was found to have a 5% difference while SmartMesh had only a 0.6% difference between the ASTM standard and scaled ball-burst. Relative changes are observed in Figure 47.

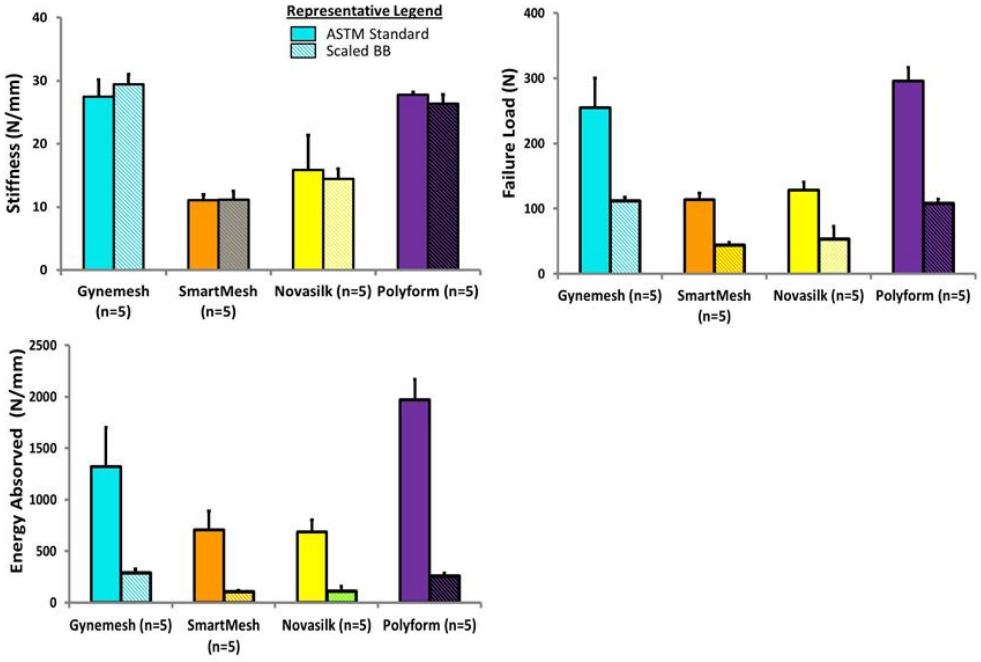

Figure 47 Comparison of ASTM standard structural properties (solid bars) to the scaled ball-burst apparatus structural properties (dashed bars). All failure load and energy absorbed parameters were significantly different between testing apparatuses, while no differences were observed in the stiffness.

The ASTM standard failure load was significantly higher ($p<0.001$) when compared to the scaled ball-burst loads. The difference in the reported failure load was roughly 2.5 and can

be attributed to the scaling factor of the ball-burst setup. A significant difference was also observed in the extension ($p<0.001$; data not shown) and energy absorbed ($p<0.001$). These differences were also accounted for the scaling factor of the sample diameter or surface area.

In this study, a scaled down ball-burst testing device was developed and validated. Roughly a 2% differences in stiffness was found between ASTM and scaled ball-burst protocols. While there was a 60% decrease in failure load and maximum extension compared to the 64% difference predicted by the decrease in sample size. Regarding the energy absorbed there was an 83% difference in the energy absorbed between utilizing the ASTM and scaled ball-burst apparatus where an 86% difference was expected based on the change in surface area. Based on these results the use of a scaled ball-burst apparatus is valid for future studies comparing the *ex vivo* properties of synthetic meshes and *in vivo* properties of mesh-tissue complexes after implantation.

APPENDIX E

MANUAL THRESOLD SCRIPT FOR SYNTHETIC MESH IMAGE ANALYSIS

E.1 RED GREEN BLUE THRESOLD PROGRAM

```
% Andrew Feola
% 2011
% This function is where you can input the image and load the image to matlab
% This portion can be easily combined with the before function and work
properly
% but was divided to allow different programs to load their images a
different way
function [C]=manualthreshold2(I)
global I
global level
global Rval
global Gval
global Bval
global imagetype
global hax
global invert
global C

%set original function and duplicate function
%Set Default values for red, green, and blue thresholds
Rval = 0.2989;
Gval= 0.5870;
Bval=0.1140;

%Allows the user to determine if they want to use the BW imge or a gray
%scale image
%Default is the gray scale image (1 =gray image, 2=BW image)
imagetype=1;

%Here we define as 0 as not invert BW image and 1 as an invert BW image
```

```
invert=0;

% Example code for uicontrol reference page
% Create a figure and an axes to contain a 3-D surface plot.
% rect = [left, bottom, width, height]
%scrsz = get(0,'ScreenSize');
%h=figure('Position',[100 100 800 450])
%figure (h)
f = figure('Name', datestr(now));
hax = axes('Units','pixels');
%I = surf(peaks)
%I = imread('Image4.jpg');
%original image file for reference;
%J=imread('testimage.jpg');
level = graythresh(I);
imshow(I)
ex_threshold
        h = uicontrol('String', 'Continue', 'Position', [200 360 100 30], ...
            'Callback', 'set(gcbf, ''Name'', datestr(now))');

waitfor(f, 'Name');
end


%This sets up the thresholding of the image
function ex_threshold

%defining global variables
global I
global level
global newthreshold
global Rval
global Gval
global Bval
global J
global imagetype
global hax
global invert
global boxhandle
global C

% Create a uicontrol object to let users change the colormap
% with a pop-up menu. Supply a function handle as the object's
% Callback:
uicontrol('Style', 'popup',...
    'String', 'Gray|Black and White',...
    'Position', [20 360 100 20],...
    'Callback', @setimage);       % Popup function handle callback
% Implemented as a subfunction

% Add a text uicontrol to label the push.
uicontrol('Style','text',...
    'Position',[20 380 100 15],...
    'String','Image Type')
```

```
% Add a slider uicontrol to control the black and white thresholding of the
image.
BWcontrol=uicontrol('Style', 'slider',...
    'Min',0,'Max',1,'Value',level,...
    'Position', [520 160 120 20],...
          'Callback', {@BWControl,hax});

newthreshold=get(BWcontrol,'Value');
%Add display of the value
uicontrol('Style','text','Position',[640 160 40
20],'String',num2str(newthreshold));

% Add a text uicontrol to label the slider.
uicontrol('Style','text',...
    'Position',[520 180 120 15],...
    'String','Black and White Threshold')


% Add a slider uicontrol to control the red scaling of the image.
redcontrol=uicontrol('Style', 'slider',...
    'Min',0,'Max',3,'Value',Rval,...
    'Position', [520 120 120 20],...
    'Callback', {@RedControl,hax});
%Export the current value for the red as a handle
%these exports are a redunant system (not required, place for future
%editing hat may involve handles)
Rval=get(redcontrol,'Value');
%Add display of the value
uicontrol('Style','text','Position',[640 120 40 20],'String',num2str(Rval));

% Add a text uicontrol to label the red scaling slider.
uicontrol('Style','text',...
    'Position',[520 140 120 15],...
    'String','Red Threshold')


%Slider to control the green scaling of the image.
greencontrol=uicontrol('Style', 'slider',...
    'Min',0,'Max',3,'Value',Gval,...
    'Position', [520 80 120 20],...
    'Callback', {@GreenControl,hax});
%Export the current value for the green as a handle
%these exports are a redunant system (not required, place for future
%editing hat may involve handles)
Gval=get(greencontrol,'Value');
%Add display of the value
uicontrol('Style','text','Position',[640 80 40 20],'String',num2str(Gval));

% Add a text uicontrol to label the green scaling slider.
uicontrol('Style','text',...
    'Position',[520 100 120 15],...
    'String','Green Threshold')
```

```
%Slider to control the blue scaling of the image.
bluecontrol = uicontrol('Style', 'slider',...
    'Min',0,'Max',3,'Value',Bval,...
    'Position', [520 40 120 20],...
    'Callback', {@BlueControl,hax});
%Export the current value for the blue as a handle
%these exports are a redunant system (not required, place for future
%editing hat may involve handles)
Bval=get(bluecontrol,'Value');
%Add display of the value
uicontrol('Style','text','Position',[640 40 40 20],'String',num2str(Bval));

% Add a text uicontrol to label the blue scaling slider.
uicontrol('Style','text',...
    'Position',[520 60 120 15],...
    'String','Blue Threshold')


% Add a different uicontrol. Create a push button that clears
% the current axes when pressed. Position the button inside
% the axes at the lower left. All uicontrols have default units
% of pixels. In this example, the axes does as well.
uicontrol('Style', 'pushbutton', 'String', 'Clear',...
    'Position', [20 20 50 20],...
    'Callback', 'cla');        % Pushbutton string callback


% Add a different uicontrol. Create a push button that clears
% the current axes when pressed. Position the button inside
% the axes at the lower left. All uicontrols have default units
% of pixels. In this example, the axes does as well.
stopthres=uicontrol('Style', 'pushbutton', 'String', 'Use Settings',...
    'Position', [20 0 100 20],...
    'Callback', @SaveSettings);        % Pushbutton string callback

% disp('breakloop value')
% breakloop=get(stopthres,'Value')

% Add a uicontrol push button that resets parameters
uicontrol('Style', 'pushbutton', 'String', 'Reset Default Values',...
    'Position', [140 0 100 20],...
    'Callback', @ResetSettings);        % Pushbutton string callback


%A pushbutton that allows the user to invert the image
boxhandle= uicontrol('Style', 'checkbox', 'String', 'Invert Image',...
    'Position', [520 220 120 20],...
    'Callback', @InvertImage);        % Pushbutton string callback
%Determines if the box is checked or not
end

%Distinguish between gray or black and white image
```

```
function setimage(hObj,event) %#ok<INUSD>
%Define global variables in sub routine
global imagetype
global I
global newthreshold
global Rval
global Gval
global Bval
% Called when user activates popup menu
val = get(hObj,'Value');
if val ==1
    %Gray Image
    imagetype=1;
    J = Rval*I(:,:,1)+Gval*I(:,:,2)+Bval*I(:,:,3);
    figure (1), imshow(J)
else
    %Black and white image
    J = im2bw(I,newthreshold);
    figure (1), imshow(J)
    imagetype=2;

end
end

%reset threshold of the black and white level
function BWControl(hObj,event, ~) %#ok<INUSL>
%Define global variables in sub routine
global I
global newthreshold
global Rval
global Gval
global Bval
global imagetype
global invert
val = get(hObj,'Value');

if imagetype==1 && invert==0
    %Gray thresholding
    J = Rval*I(:,:,1)+Gval*I(:,:,2)+Bval*I(:,:,3);
    figure (1), imshow(J)
    elseif imagetype ==2 && invert==0
    %Gray thresholding
    %J = Rval*I(:,:,1)+Gval*I(:,:,2)+val*I(:,:,3);
    J = im2bw(I,val);
    figure (1), imshow(J)
elseif imagetype == 2 && invert ==1
   %Gray thresholding
    %J = Rval*I(:,:,1)+Gval*I(:,:,2)+val*I(:,:,3);
    J = im2bw(I,val);
    J=~J;
    figure (1), imshow(J)
else
    %Gray thresholding
    J = Rval*I(:,:,1)+Gval*I(:,:,2)+Bval*I(:,:,3);
```

```
    J = im2bw(J,val);
    J=~J;
    figure (1), imshow(J)
end

uicontrol('Style','text','Position',[640 160 40 20],'String',num2str(val));
newthreshold=val;
end

%function alters the red threshold value
function RedControl(hObj,event,~) %#ok<INUSL>
%Define global variables in sub routine
global I
global level
global BW
global newthreshold
global Rval
global Gval
global Bval
global J
global imagetype
global invert

% Called to set Red threshold level in figure
% when user moves the slider control
val = get(hObj,'Value');
if imagetype==1 && invert==0
    %Gray thresholding
    J = val*I(:,:,1)+Gval*I(:,:,2)+Bval*I(:,:,3);
    figure (1), imshow(J)
elseif imagetype == 2 && invert==0
    %Gray thresholding
    J = val*I(:,:,1)+Gval*I(:,:,2)+Bval*I(:,:,3);
    J = im2bw(J,newthreshold);
    figure (1), imshow(J)
elseif imagetype == 2 && invert ==1
   %Gray thresholding
    J = val*I(:,:,1)+Gval*I(:,:,2)+Bval*I(:,:,3);
    J = im2bw(J,newthreshold);
    J=~J;
    figure (1), imshow(J)
else
    %Gray thresholding
    J = val*I(:,:,1)+Gval*I(:,:,2)+Bval*I(:,:,3);
    J = im2bw(J,newthreshold);
    J=~J;
    figure (1), imshow(J)
end
uicontrol('Style','text','Position',[640 120 40 20],'String',num2str(val));
Rval=val;
end

%function alters the green threshold level
function GreenControl(hObj,event,~) %#ok<INUSL>
```

```
%Define global variables in sub routine
global I
global level
global BW
global newthreshold
global Rval
global Gval
global Bval
global J
global imagetype
global invert

% Called to set Green threshold level in figure
% when user moves the slider control
val = get(hObj,'Value');
if imagetype==1 && invert==0
    J = Rval*I(:,:,1)+val*I(:,:,2)+Bval*I(:,:,3);
    figure (1), imshow(J)
elseif imagetype == 2 && invert==0
    %Gray thresholding
    J = Rval*I(:,:,1)+val*I(:,:,2)+Bval*I(:,:,3);
    J = im2bw(J,newthreshold);
    figure (1), imshow(J)
elseif imagetype == 2 && invert ==1
   %Gray thresholding
    J = Rval*I(:,:,1)+val*I(:,:,2)+Bval*I(:,:,3);
    J = im2bw(J,newthreshold);
    J=~J;
    figure (1), imshow(J)
else
    %Gray thresholding
    J = Rval*I(:,:,1)+val*I(:,:,2)+Bval*I(:,:,3);
    J = im2bw(J,newthreshold);
    J=~J;
    figure (1), imshow(J)
end
uicontrol('Style','text','Position',[640 80 40 20],'String',num2str(val));
Gval=val;
end

%function alters the blue threshold level
function BlueControl(hObj,event,~) %#ok<INUSL>
%Define global variables in sub routine
global I
global level
global BW
global newthreshold
global Rval
global Gval
global Bval
global J
global imagetype
global invert
```

```
% Called to set Blue threshold level in figure
% when user moves the slider control
val = get(hObj,'Value');
if imagetype==1 && invert==0
    %Gray thresholding
    J = Rval*I(:,:,1)+Gval*I(:,:,2)+val*I(:,:,3);
    figure (1), imshow(J)
elseif imagetype == 2 && invert==0
    %Gray thresholding
    J = Rval*I(:,:,1)+Gval*I(:,:,2)+val*I(:,:,3);
    J = im2bw(J,newthreshold);
    figure (1), imshow(J)
elseif imagetype == 2 && invert ==1
   %Gray thresholding
    J = Rval*I(:,:,1)+Gval*I(:,:,2)+val*I(:,:,3);
    J = im2bw(J,newthreshold);
    J=~J;
    figure (1), imshow(J)
else
    %Gray thresholding
    J = Rval*I(:,:,1)+Gval*I(:,:,2)+val*I(:,:,3);
    J = im2bw(J,newthreshold);
    J=~J;
    figure (1), imshow(J)
end
uicontrol('Style','text','Position',[640 40 40 20],'String',num2str(val));
Bval=val;
end

%function can enter a subroutine and exit the thresholding program
function SaveSettings(hObj,event,~) %#ok<INUSL>
%Define global variables in sub routine
global newthreshold
global Rval
global Gval
global Bval
global invert
global imagetype
global J
global C
global I
global RGB

disp('End of Manual Editing')
R=Rval;
G=Gval;
B=Bval;
%A=J;
if imagetype==1 && invert==0
    %Image is gray but not inverted
    J = R*I(:,:,1)+G*I(:,:,2)+B*I(:,:,3);
    RGB=J;
    C=J;
    %close all
elseif imagetype == 2 && invert==0
```

```
    %BW image with RGB thresholding, but not inverted
    J = R*I(:,:,1)+G*I(:,:,2)+B*I(:,:,3);
    J = im2bw(J,newthreshold);
    %if mesh is labeled as white it must be inverted prior to be converted
    %back to a real image (not logical (binary) data)
    J=~J
    %finds the binary points of connectivity
    CC = bwconncomp(J);
    %Labels the matrix with values (the non zeros are converted to a scale
    L = labelmatrix(CC);
    %sets the image as RBG a gray scale picture
    RGB = label2rgb(L,'gray');
    C=RGB;
    %close all
elseif imagetype == 2 && invert ==1
   %BW Image with RGB thresholding, but the image is inverted (mesh is
   %black in image)
    J = R*I(:,:,1)+G*I(:,:,2)+B*I(:,:,3);
    J = im2bw(J,newthreshold);
    %finds the binary points of connectivity
    CC = bwconncomp(J);
    %Labels the matrix with values (the non zeros are converted to a scale
    L = labelmatrix(CC);
    %sets the image as RBG a gray scale picture
    RGB = label2rgb(L,'gray');
    %imshow(RGB)
    C=RGB;
    %close all
else
    %Gray thresholding of RGB imaging (same as above)
    J = R*I(:,:,1)+G*I(:,:,2)+B*I(:,:,3);
    J = im2bw(J,newthreshold);
    %finds the binary points of connectivity
    CC = bwconncomp(J);
    %Labels the matrix with values (the non zeros are converted to a scale
    L = labelmatrix(CC);
    %sets the image as RBG a gray scale picture
    RGB = label2rgb(L,'gray');
    C=RGB;
    %close all
end
%add next function to continue onward
end

%function allows you to invert black and white images
function InvertImage(hObj,event,~) %#ok<INUSL>
%Define global variables in sub routine
global newthreshold
global Rval
global Gval
global Bval
global invert
global boxhandle
global I
% %redefines the variable for inverting the image
```

```
invert=get(boxhandle,'Value');
if invert ==1
% %Can only invert black and white images, this does not affect gray scale
% %images
     J = Rval*I(:,:,1)+Gval*I(:,:,2)+Bval*I(:,:,3);
     J = im2bw(J,newthreshold);
     J=~J;
     figure (1), imshow(J)
else
     J = Rval*I(:,:,1)+Gval*I(:,:,2)+Bval*I(:,:,3);
     J = im2bw(J,newthreshold);
     figure (1), imshow(J)
end
end

%function resets all threshold values to the default values
function ResetSettings(hObj,event,~) %#ok<INUSL>
%Define global variables in sub routine
global I
global level
global BW
global newthreshold
global Rval
global Gval
global Bval
global J
global imagetype
global hax
global invert
global boxhandle

%Default values
Rval = 0.2989;
Gval= 0.5870;
Bval=0.1140;
newthreshold = graythresh(I);

if imagetype==1 && invert==0
    %Gray thresholding
    J = Rval*I(:,:,1)+Gval*I(:,:,2)+Bval*I(:,:,3);
    figure (1), imshow(J)
elseif imagetype == 2 && invert==0
    %Gray thresholding
    %J = Rval*I(:,:,1)+Gval*I(:,:,2)+Bval*I(:,:,3);
    J = im2bw(I,newthreshold);
    figure (1), imshow(J)
elseif imagetype == 2 && invert ==1
   %Gray thresholding
   %J = Rval*I(:,:,1)+Gval*I(:,:,2)+Bval*I(:,:,3);
    J = im2bw(I,newthreshold);
    J=~J;
    figure (1), imshow(J)
else
    %Gray thresholding
```

```
    J = Rval*I(:,:,1)+Gval*I(:,:,2)+val*I(:,:,3);
    J = im2bw(J,newthreshold);
    J=~J;
    figure (1), imshow(J)
end

uicontrol('Style','text','Position',[640 160 40
20],'String',num2str(newthreshold));
uicontrol('Style','text','Position',[640 120 40 20],'String',num2str(Rval));
uicontrol('Style','text','Position',[640 80 40 20],'String',num2str(Gval));
uicontrol('Style','text','Position',[640 40 40 20],'String',num2str(Bval));

end
```

E.2 GREY IMAGE THRESHOLD

Sd

```
% Andrew Feola
% 2011
% This function is where you can input the image and load the image to matlab
% This portion can be easily combined with the before function and work
properly
% but was divided to allow different programs to load their images a
different way
function [C]=BWmanualthreshold2(I)
global I
global level
global imagetype
global hax
global invert
global C

%Allows the user to determine if they want to use the BW imge or a gray
%scale image
%Default is the gray scale image (1 =gray image, 2=BW image)
imagetype=1;

%Here we define as 0 as not invert BW image and 1 as an invert BW image
invert=0;

% Example code for uicontrol reference page
```

```
% Create a figure and an axes to contain a 3-D surface plot.
% rect = [left, bottom, width, height]
%scrsz = get(0,'ScreenSize');
%h=figure('Position',[100 100 800 450])
%figure (h)
f = figure('Name', datestr(now));
hax = axes('Units','pixels');
%I = surf(peaks)
%I = imread('Image4.jpg');
%original image file for reference;
%J=imread('testimage.jpg');
level = graythresh(I);
imshow(I)
ex_threshold
        h = uicontrol('String', 'Continue', 'Position', [200 360 100 30], ...
            'Callback', 'set(gcbf, ''Name'', datestr(now))');

waitfor(f, 'Name');
end


%This sets up the thresholding of the image
function ex_threshold

%defining global variables
global I
global level
global newthreshold
global J
global hax
global invert
global boxhandle
global C

% Add a slider uicontrol to control the black and white thresholding of the
image.
BWcontrol=uicontrol('Style', 'slider',...
    'Min',0,'Max',1,'Value',level,...
    'Position', [520 160 120 20],...
    'Callback', {@BWControl,hax});
newthreshold=get(BWcontrol,'Value');
%Add display of the value
uicontrol('Style','text','Position',[640 160 40
20],'String',num2str(newthreshold));

% Add a text uicontrol to label the slider.
uicontrol('Style','text',...
    'Position',[520 180 120 15],...
    'String','Black and White Threshold')

% Add a different uicontrol. Create a push button that clears
% the current axes when pressed. Position the button inside
% the axes at the lower left. All uicontrols have default units
% of pixels. In this example, the axes does as well.
```

```
uicontrol('Style', 'pushbutton', 'String', 'Clear',...
    'Position', [20 20 50 20],...
    'Callback', 'cla');        % Pushbutton string callback

% Add a different uicontrol. Create a push button that clears
% the current axes when pressed. Position the button inside
% the axes at the lower left. All uicontrols have default units
% of pixels. In this example, the axes does as well.
stopthres=uicontrol('Style', 'pushbutton', 'String', 'Use Settings',...
    'Position', [20 0 100 20],...
    'Callback', @SaveSettings);        % Pushbutton string callback

% disp('breakloop value')
% breakloop=get(stopthres,'Value')

% Add a uicontrol push button that resets parameters
uicontrol('Style', 'pushbutton', 'String', 'Reset Default Values',...
    'Position', [140 0 100 20],...
    'Callback', @ResetSettings);        % Pushbutton string callback


%A pushbutton that allows the user to invert the image
boxhandle= uicontrol('Style', 'checkbox', 'String', 'Invert Image',...
    'Position', [520 220 120 20],...
    'Callback', @InvertImage);        % Pushbutton string callback
%Determines if the box is checked or not
end



%reset threshold of the black and white level
function BWControl(hObj,event, ~) %#ok<INUSL>
%Define global variables in sub routine
global I
global newthreshold
global invert
val = get(hObj,'Value');

if  invert==0
    %Gray thresholding
    J = im2bw(I,val);
    figure (1), imshow(J)
else
    %Gray thresholding
    J = im2bw(I,val);
    J=~J;
    figure (1), imshow(J)
end
uicontrol('Style','text','Position',[640 160 40 20],'String',num2str(val));
newthreshold=val;
end

%function can enter a subroutine and exit the thresholding program
function SaveSettings(hObj,event,~) %#ok<INUSL>
```

```
%Define global variables in sub routine
global newthreshold
global invert
global J
global C
global I

if invert==0
    J = im2bw(I,newthreshold);
    [l, w, d]=size(J);
for i=1:(l)
    for i2=1:(w)
       if J(i,i2)==0
           C(i,i2) = random('Normal',0,0.1);
       else
           C(i,i2) = random('Normal',255,5);
       end
    end
end

else
    %Gray thresholding of RGB imaging (same as above)
    J = im2bw(I,newthreshold);
    [l, w, d]=size(J);
    J=~J;
for i=1:(l)
    for i2=1:(w)
       if J(i,i2)==0
           C(i,i2) = random('Normal',0,0.1);
       else
           C(i,i2) = random('Normal',255,5);
       end
    end
end
end
disp('End of Manual Editing')
C = uint8(round(C - 1));
imshow(C)
%add next function to continue onward
end

%function allows you to invert black and white images
function InvertImage(hObj,event,~) %#ok<INUSL>
%Define global variables in sub routine
global newthreshold
global invert
global boxhandle
global I
global J
% %redefines the variable for inverting the image
invert=get(boxhandle,'Value');
if invert ==1
% %Can only invert black and white images, this does not affect gray scale
% %images
```

```
     J = im2bw(I,newthreshold);
     J=~J;
     figure (1), imshow(J)
else
     J = im2bw(I,newthreshold);
     figure (1), imshow(J)
end
end

%function resets all threshold values to the default values
function ResetSettings(hObj,event,~) %#ok<INUSL>
%Define global variables in sub routine
global I
global level
global BW
global newthreshold
global J
global hax
global invert
global boxhandle

%Default values
newthreshold = graythresh(I);

if  invert==0
    %Gray thresholding
    %J = Rval*I(:,:,1)+Gval*I(:,:,2)+Bval*I(:,:,3);
    J = im2bw(I,newthreshold);
    figure (1), imshow(J)
else
    %Gray thresholding
    J = im2bw(I,newthreshold);
    J=~J;
    figure (1), imshow(J)
end

uicontrol('Style','text','Position',[640 160 40
20],'String',num2str(newthreshold));
end
```

APPENDIX F

FIBER DIAMETER AND ASPECT RATIO DISTRIBUTION ESTIMATION

```
%Andrew Feola
%2011
close all;
clear all;
clc;

path='Data\';
file=input('What is the prefix of the data: ','s');
ext='.csv';
filename=[path,file,ext];
FullData = importdata(filename);
[leng, wid]=size(FullData);

AR=FullData(:,1);
AR(:,2)=FullData(:,4);
Size=FullData(:,2);
Size(:,2)=FullData(:,5);
Diam=FullData(:,3);
Diam(:,2)=FullData(:,6);

A1=AR(:,1);
A2=AR(:,2);
S1=Size(:,1);
S2=Size(:,2);
D1= Diam(:,1);
D2= Diam(:,2);

for i=1:wid
    A=FullData(:,i);
    [n,xout] = hist(A);
    [f,xi,u] = ksdensity(A);
    data=xi';
    data2=xout';
    data2(:,2)=n';
    %-----------------------------------------
```

```
    %sets the tolerances and iteration limits
    options = statset('MaxIter',500,'TolTypeX', 'abs','TolX', 1e-
25,'Display','final');
    %fits the distribution with a 2 mu or binomial distribution
    obj = gmdistribution.fit(A,2,'Options',options);
    ComponentMeans = obj.mu;
    ComponentCovariances = obj.Sigma;
    MixtureProportions = obj.PComponents;
    mumax=max(ComponentMeans);
    mumin=min(ComponentMeans);

    %determines if mu1 and mu2 are within 80% of each other, if this holds
    %true then the data is fit with a single mu normal distribution
    mucomp=mumax*0.8;
    if mucomp<mumin
        disp('Second Method Compare')
        obj = gmdistribution.fit(A,1,'Options',options);
        ComponentMeans = obj.mu;
        ComponentCovariances = obj.Sigma;
        MixtureProportions = obj.PComponents;
    end

    if i==1 || i==4
        prefix='AspectRatio';
    elseif i==2 || i==5
        prefix='PoreSize';
    else
        prefix='FiberDiameter';
    end
    p=num2str(i);
    %writes the AR and fiber diameter data to a specific file
    %exporing mu1 mu2, covariances, and mixed proportions
    savename=[file,prefix,p];
    fid2=fopen(savename,'w');
    fprintf(fid2,'ComponentMeans\n');
    fprintf(fid2,'%5.3f\n',ComponentMeans);
    fprintf(fid2,'\nComponentCovariances\n');
    fprintf(fid2,'%5.3f\n',ComponentCovariances);
    fprintf(fid2,'\nMixtureProportions\n');
    fprintf(fid2,'%5.3f\n',MixtureProportions);
    status=fclose('all');
end

%creates multiple subplots of the smoothed data, the fit data based on the
%objective function and raw data
    figure
    subplot(2,2,1:2); plot(xi,f,'*k'); hold on; ezplot(@(x)pdf(obj,[x]), [0
max(xi)]);
    title('Overlap')
    subplot(2,2,3); bar(xout,n);
    title('Histogram')
    subplot(2,2,4); plot(xi,f,'*k')
    title('Kernel Smooth')
```

APPENDIX G

EFFECT OF INPUT PARAMETERS ON LOAD-DISPLACEMENT SIMULATIONS

Utilizing the co-rotational theorem and Timoshenko beam element to represent each segment, we first assumed a linear relationship between load stress and strain (Equation 4-7). From this approach, after each mesh was generated only three user inputs are required: material modulus, material diameter, and 'hinge factor'.

This simplistic approach allowed us to examine the effects each individual parameter in a controlled and linear manner. All below simulations had a step size of 5000 and were simulated to a displacement of 65 mm.

G.1 EFFECT OF FIBER DIAMETER

A fiber diameter range was created based on several estimated. The first three values of diameter examined were created based on the fiber representation presented in Figure 32. First, an average diameter of a single polypropylene strand was created. This diameter was determined to be 0.087 mm. Next the number of fibers to create a single bundle was determined. For

UltraPro this was found to be n=5. The second area estimate multiplied the average diameter of a single fiber by the number required to make then entire bundle (0.087 mm x 5). This gave a diameter measurement of 0.43. Next we calculated the area to determine the representative fiber diameter as outlined in Section 5.2.2.2. Lastly five measurements of the mesh thickness were made utilizing a digital caliper. This gave an average diameter of 0.4 mm for the mesh. For these simulations the modulus was kept constant at 90 MPa and the hinge factor was kept at 0.5.

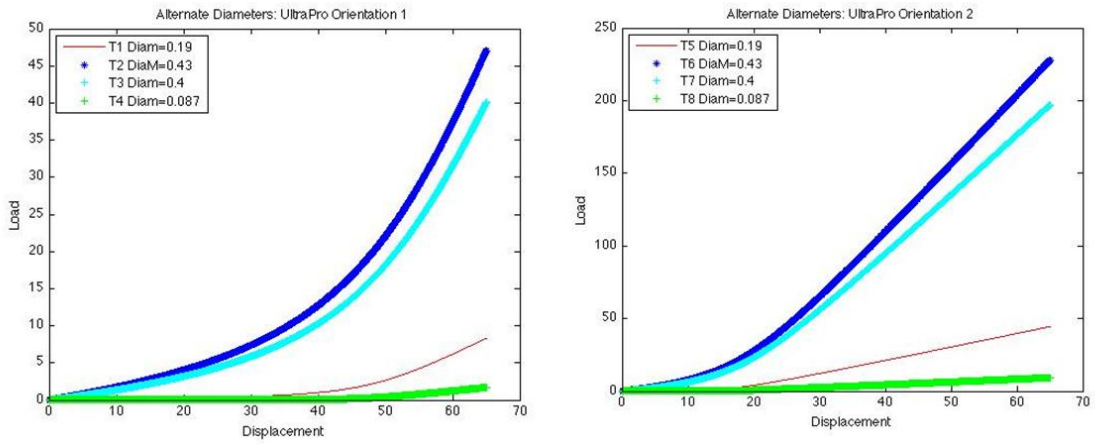

Figure 48 Simulation of UltraPro mesh along orientation 1 (left) and orientation 2 (right). This simulation aimed to examine the different effect fiber diameter [0.087, 0.4, 0.43, 0.19] mm. As diameter increased the load response also increased.

The diameter was found to have a considerable effect on the load-displacement predictions (Figure 48). It is apparent that as diameter increase to those measured by digital calipers (0.4 mm) or estimated by a five combined bundles (0.43 mm) greatly increased the load response. It was concluded that the most accurate measurement of diameter was the representative diameter estimate. This measurement of diameter accounted for the space between the fibers which is not accounted for in the two larger diameter measurements, while the single fiber does not represent the true amount of polypropylene present to resist deformation.

G.2 EFFECT OF THE HINGE FACTOR

To gain insight on the degree to which altering the moment transfer between two overlapping nodes, the hinge parameter was set to a range of values [0.3, 0.5, 0.75, and 1.0].

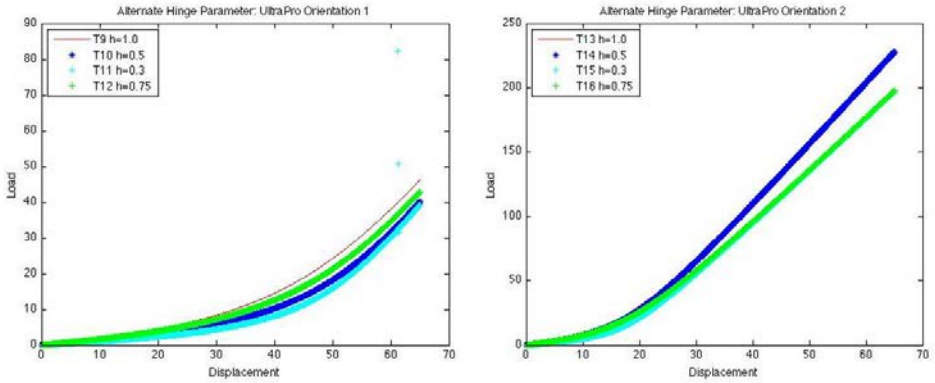

Figure 49 Figure illustrating the effect of the hinge parameter on the load-displacement prediction. The hinge parameter was set to 0.3, 0.5, 0.75, and 1.0 during simulations of the UltraPro mesh (O1, left and O2, right)

In this analysis the modulus of the material remained at 200 MPa and the diameter at 0.19 mm. Examining the effect of the hinge factor it is clear at all percentages of moment transfer at the mesh joints there is little change in the overall load-displacement relationship (Figure 49). The main effect of this parameter is how it alters the inflection point. The inflection point is described as the point at which the mesh alters exits the low stiffness and enters the high stiffness region. However, it should be noted that this parameter had little effect on the inflection point as well as the overall behavior of the mesh. It was concluded that future simulations would utilized a hinge parameter 0.5. This was assumed because the mesh does not behavior as a rigid beam (h=1.0) but there is an interlocking between the knit pattern at these joints therefore some

moment is transferred between these two nodes. Therefore, 50% of the moment was assumed to be transferred between these nodal elements.

G.3 EFFECT OF MODULUS

For the following simulations diameter (d_{rep}=0.19) and the hinge factor (h=0.5) were kept constant while the modulus parameter was changed from 90 to 200 and lastly 1100 MPa.

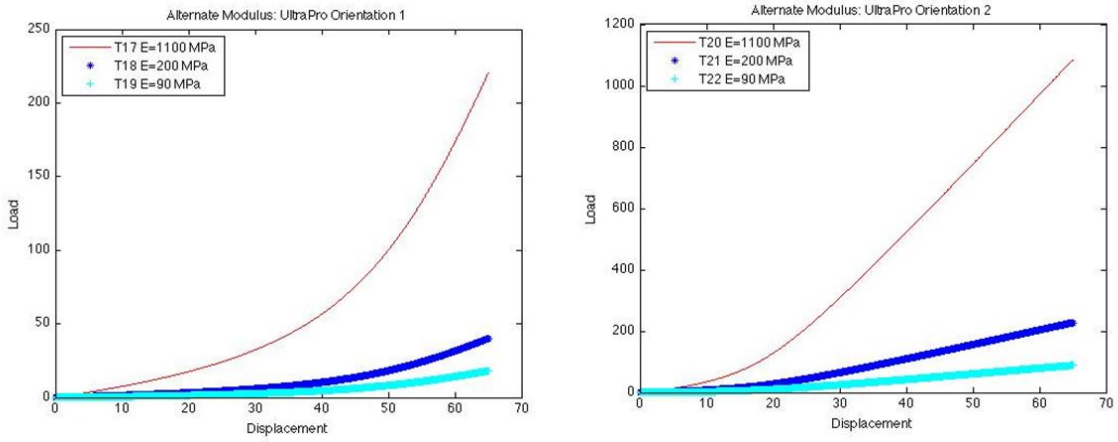

Figure 50 Illustration of how modulus would affect the load-displacement response. E=1100 MPa (red) was found to greatly increase the load response compared to E=200 MPa (dark blue) or E= 90 MPa (light blue) in simulations of the UltraPro mesh along O1 (left) and O2 (right)

From these simulations it was found that the modulus greatly affected the load-displacement response (Figure 50). An inputted value of the modulus (1.1 GPa) on the same order of magnitude as those from previously published literature of polypropylene greatly over estimates the load response by 1 to 2-fold. In addition, the inability of this linear stress-strain response to adequately predict the mesh uniaxial behavior of UltraPro under two different loading conditions has led to the development and use of a fiber recruitment model described in Section 5.2.2.4.

APPENDIX H

BIAXIAL MECHANICAL PROPERTIESAS

Previous research has focused on developing biaxial protocols for characterizing anisotropic behavior [197]. There are several biaxial techniques that have been adopted for testing biological tissues. These techniques include tubular and planar biaxial. Much of the research in this area has evolved from studies in the cardiovascular system. A series of studies have used biochambers to simulate the complicated loading conditions experienced by blood vessel via mimicking the *in vivo* pressure, axial force, and flow *in vivo* [1,2]. Varying the mentioned parameters (pressure, axial force, and flow) tubular biaxial protocols can describe how cross-sectional area changes as a function of intraluminal pressure (or flow) and length of the vessel. These data provide the pressure-diameter properties of the vessel which describe the distensibility of the sample. Further, the axial load and elongation of the sample provide the classic structural properties of the vessel. This information is valuable for characterizing and modeling the native properties of arteries and veins but also the growth and remodeling of vessels due to changes in loading conditions [24, 209-211].

Currently, the most commonly used biaxial approach is a planar biaxial protocol. Typically strain is measured optically in both directions. Commonly four to five tissue markers

are placed about the center of the tissue and the locate displacement is utilized to form the deformation gradient tensor (F). Strain can then be is calculated from F as:

$$E = \frac{1}{2}(F * F^T - I) \quad \textbf{6-1}$$

Where E is coined the Green-Lagrange strain tensor and I is the identity matrix. Stress of mechanically tested soft tissues is often calculated referring to the reference state. Forces along two orthogonal axes are normalized by the cross-sectional area (obtained from thickness, length, and width measurements) to determine the Lagrangian stress tensor (P):

$$P = \frac{Force}{A_o} \quad \textbf{6-2}$$

This measure of stress is similar to that assumed for uniaxial tensile protocol, where stress is a measure of force divided by the initial, or non-deformed, area. The ratio of stretch or stress can then be varied between the two axes to assess the degree of axial coupling. Although these tests are generally more challenging to perform, they are preferred for tissues like the vagina because these experimental data can then be incorporated into rigorous computational models that may be used for simulations [197].

H.1 BIAXIAL TESTING OF SOFT TISSUES

As the above study has shown (2.2.7), biaxial testing may be required to detect the effects of parity on the vaginal biomechanical properties in the rodent animal model. Further research has shown that simulated maternal birth injury leads to an change in the collagen I/(III+V) ratio and

inferior biomechanical properties. Here, biaxial testing protocols could fully describe the coupled interaction of the longitudinal and circumferential axes and better characterize the effect of a maternal birth injury. While the ability to perform mesh implantation studies onto the rodent vaginal tissue, the rodent model may provide us with a means to study the native properties of vaginal tissue after injury and improve our understanding of what changes during injury and then set the stage for prolapse to develop later in life.

Planar biaxial testing of vaginal tissue has the potential to fully characterize the remodeling and effects of pregnancy, vaginal delivery, and birth injury. Utilizing a biaxial approach can improve the characterizing the mechanical properties by accounting for the coupled interactions of the circumferential and longitudinal axes of the vagina. It has also been shown that multidirectional testing can be used for the development of constitutive models that may describe and, through rigorous work, later be used to predict tissue behavior [197, 208, 212].

In our first preliminary study we were interested assesses the coupled effects of these perpendicular axes within the vagina. It has been assumed that these maternal adaptations must greatly increase the distensibility of the vagina for the fetal head to pass during the second stage of labor and to minimize injury to the mother. This has been studied by examining the vaginal distensibilty of the rodent vagina in virgin, mid-pregnant, and postpartum rodents.

Using the rodent model, the aim of this study was to characterize the maternal adaptations and quantify the planar biaxial mechanical properties for both virgin and mid-pregnant vaginas in response to an equibiaxial stress protocol. Parameters used to describe these properties include the areal strain and the anisotropic index (AI). To reduce the risk for a maternal birth injury at the time of delivery, we hypothesize that the areal strains will increase during pregnancy and that the change will be predominantly observed in the circumferential

direction of the vagina, thereby increasing the anisotropic index. This is a pilot will provide us with a core protocol for determining the coupled biomechanical properties of the vaginal wall.

Methods:

For this study, 8 virgin and 8 mid-pregnant (Day 15-16) Long Evans rats were used. The protocol was performed in accordance with Institutional Animal Care and Use Committee guidelines (IACUC #0702224). The rats were dissected; reproductive tissues were isolated and stored in saline soaked gauze at -20°C.

On the day of testing each specimen was thawed and the vagina was isolated and cut across the proximal end just below the cervix and along the distal end just above the vaginal opening. The vagina was then cut open along the urethra to produce a planar-rectangular specimen. Width and length were measured using digital calipers while tissue thickness was measured across three areas of the vagina using a non-contact laser reflectance system [119]. A total of 16 hooks were placed around the tissue (four on each side) as seen in Figure 16. The tissue was then mounted onto the Bose Electroforce LM1 Testbench testing system using custom-made fixtures that distribute load evenly across each side of the specimen and allow for freely moving edges (Figure 51). Five graphite strain tracking markers were placed centrally on the specimen and a contrast based camera system (Bose 2-D DVE software) was used to record marker displacement. The specimen was completely immersed in a room-temperature 0.9% saline solution for the duration of testing.

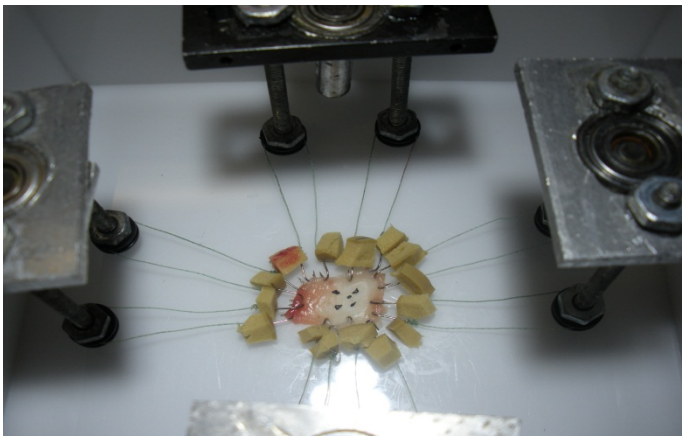

Figure 51 Setup showing placement of 16 hooks, five centrally placed strain markers, and free-moving fixtures in testing apparatus

Before each test, the specimens were preloaded to 0.1 N on each independent axis. The specimens were then preconditioned for 10 cycles to a maximum equibiaxial Lagrangian stress of 50 kPa over an interval of 15 seconds. A 15, 30, and 50 kPa equibiaxial Lagrangian stress was then applied to each specimen and the Green-Lagrange strain along the longitudinal (ε_{Long}) and circumferential (ε_{Circ}) axes was calculated based on marker displacements [213].

$$ArealStrain = \varepsilon_{circ} * \varepsilon_{long} + (\varepsilon_{circ} + \varepsilon_{long}) \quad \textbf{6-3}$$

The anisotropic index (AI) is a measure of the degree of anisotropy between the mechanical responses of the different tissue axes [213]. It was calculated using the following equation:

$$AI = \frac{\varepsilon_{circ} - \varepsilon_{long}}{0.5 * (\varepsilon_{circ} + \varepsilon_{long})} \quad \textbf{6-4}$$

Maximum strains, areal strain, and AI are expressed as mean ± standard deviation. Statistical analysis between virgin and pregnant animals was made using an independent t-test

and a one-sample t-test was performed to determine if the AI was significantly different from zero (zero = isotropic). All statistical tests had a significance level set to $p<0.05$.

Results:

All tests resulted in a non-linear stress versus strain relationship with some degree of grossly observable mechanical anisotropy between the tissue axes. Correspondingly, the maximum strain in the circumferential direction was approximately 8% more than the longitudinal axis for both groups. For the pregnant group, the maximum strain along the circumferential axis was significantly larger (0.21 ± 0.08) compared to virgin animals (0.12 ± 0.03, $p=0.01$).

The large variability in maximum strain along the longitudinal direction for the pregnant (0.05 ± 0.08) and virgin (0.039 ± 0.05) groups precluded a significant difference from being detected with this sample size ($p=0.76$). In terms of the areal strain, the significant increase in the maximum circumferential strain was reflected with a 61% increase in the areal strain for the pregnant group ($p=0.011$, Figure 52).

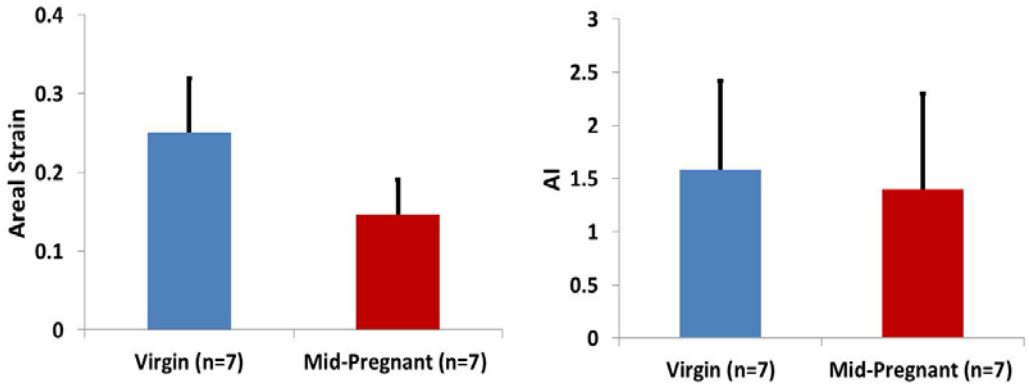

Figure 52 Areal Strain (left) and Anisotropic Index (right) for vaginas from virgin and mid-pregnant animals.

Again, due to the high variability in the longitudinal strains, the degree of anisotropy was not significantly different between groups ($p=0.82$, Figure 17). However, vaginal tissue from both groups was found to have an anisotropic index that was significantly greater than zero ($p=0.011$ and $p=0.009$ respectively).

Discussion:

In this study, we characterized vaginal adaptations during pregnancy in terms of changes in the mechanical behavior of virgin and mid-pregnant vaginas using a planar biaxial mechanical testing protocol. The findings of this study show that the vagina is anisotropic and that the tissue becomes more distensible during pregnancy.

The maximum strain in the circumferential direction was significantly increased during pregnancy, which is consistent with the changes that would be expected for vaginal delivery to occur with minimal maternal injury. The large variability in the longitudinal direction may be a consequence of choosing to evaluate the mechanics of the vagina at mid-pregnancy, as remodeling may not progress at the same rate for all animals. Based on these results, we will attempt to identify factors that govern these maternal adaptations in the rat in an effort to maximize tissue distensibility at the time of delivery. This strategy may eventually help to identify women at risk for birth injury based on incomplete adaptations and potential therapies to promote a less injurious vaginal delivery. These principles can later be used to perform large scale studies on vaginal biomechanical properties after different degrees of injury, genetic defects, or multiparous animals that would be deemed impossible to perform in larger and more expensive animal models. Additionally, we will begin to characterize collagen fiber orientation, changes in biochemical composition. Lastly, are final goal is to model the biaxial mechanical response of rodent vaginal tissue through the use of constitutive models as described below.

BIBLIOGRAPHY

1. Bump, R.C., et al., *The standardization of terminology of female pelvic organ prolapse and pelvic floor dysfunction.* Am J Obstet Gynecol, 1996. **175**(1): p. 10-7.

2. Heit, M., et al., *Predicting treatment choice for patients with pelvic organ prolapse.* Obstet Gynecol, 2003. **101**(6): p. 1279-84.

3. Barber, M.D., et al., *Sexual function in women with urinary incontinence and pelvic organ prolapse.* Obstet Gynecol, 2002. **99**(2): p. 281-9.

4. Weber, A.M., et al., *Sexual function in women with uterovaginal prolapse and urinary incontinence.* Obstet Gynecol, 1995. **85**(4): p. 483-7.

5. Olsen, A.L., et al., *Epidemiology of surgically managed pelvic organ prolapse and urinary incontinence.* Obstet Gynecol, 1997. **89**(4): p. 501-6.

6. Rogers, G.R., et al., *Sexual function in women with and without urinary incontinence and/or pelvic organ prolapse.* Int Urogynecol J Pelvic Floor Dysfunct, 2001. **12**(6): p. 361-5.

7. Drutz HP, A.M., *Pelvic organ prolapse: demographics and future growth prospects.* Int Urogynecol J Pelvic Floor Dysfunct, 2006. **17(Suppl 7)**: p. S6-S9.

8. Boyles, S.H., A.M. Weber, and L. Meyn, *Procedures for pelvic organ prolapse in the United States, 1979-1997.* Am J Obstet Gynecol, 2003. **188**(1): p. 108-15.

9. Brown, J.S., et al., *Pelvic organ prolapse surgery in the United States, 1997.* Am J Obstet Gynecol, 2002. **186**(4): p. 712-6.

10. DeLancey, J.O., *The anatomy of the pelvic floor.* Curr Opin Obstet Gynecol, 1994. **6**(4): p. 313-6.

11. DeLancey, J.O., *Anatomic aspects of vaginal eversion after hysterectomy.* Am J Obstet Gynecol, 1992. **166**(6 Pt 1): p. 1717-24; discussion 1724-8.

12. DeLancey, J.O., *Anatomy and biomechanics of genital prolapse.* Clin Obstet Gynecol, 1993. **36**(4): p. 897-909.

13. Norton, P.A., *Pelvic floor disorders: the role of fascia and ligaments.* Clin Obstet Gynecol, 1993. **36**(4): p. 926-38.

14. Carley, M.E., et al., *Obstetric history in women with surgically corrected adult urinary incontinence or pelvic organ prolapse.* J Am Assoc Gynecol Laparosc, 1999. **6**(1): p. 85-9.

15. Gurel, H. and S.A. Gurel, *Pelvic relaxation and associated risk factors: the results of logistic regression analysis.* Acta Obstet Gynecol Scand, 1999. **78**(4): p. 290-3.

16. Hendrix, S.L., et al., *Pelvic organ prolapse in the Women's Health Initiative: gravity and gravidity.* Am J Obstet Gynecol, 2002. **186**(6): p. 1160-6.

17. Lukacz, E.S., et al., *Parity, mode of delivery, and pelvic floor disorders.* Obstet Gynecol, 2006. **107**(6): p. 1253-60.

18. Moalli, P.A., et al., *Risk factors associated with pelvic floor disorders in women undergoing surgical repair.* Obstet Gynecol, 2003. **101**(5 Pt 1): p. 869-74.

19. O'Boyle, A.L., et al., *Pelvic organ support in pregnancy and postpartum.* Int Urogynecol J Pelvic Floor Dysfunct, 2005. **16**(1): p. 69-72; discussion 72.

20. DeLancey, J.O., et al., *The appearance of levator ani muscle abnormalities in magnetic resonance images after vaginal delivery.* Obstet Gynecol, 2003. **101**(1): p. 46-53.

21. DeLancey, J.O., et al., *Comparison of levator ani muscle defects and function in women with and without pelvic organ prolapse.* Obstet Gynecol, 2007. **109**(2 Pt 1): p. 295-302.

22. Stoffel, J.T., et al., *Urinary Incontinence After Stress Incontinence Surgery: A Risk Factor for Depression.* Urology, 2008.

23. Fung, Y.C., *Biomechanics: Mechanical Properties of Living Tissues*. 2nd ed. 1993, New York, NY: Springer.

24. Humphrey, J.D., *Mechanics of the arterial wall: review and directions.* Crit Rev Biomed Eng, 1995. **23**(1-2): p. 1-162.

25. Woo, S.L., M. Thomas, and S.S. Chan Saw, *Contribution of biomechanics, orthopaedics and rehabilitation: the past present and future.* Surgeon, 2004. **2**(3): p. 125-36.

26. Hall, R.J., et al., *Translabial ultrasound assessment of the anal sphincter complex: normal measurements of the internal and external anal sphincters at the*

proximal, mid-, and distal levels. Int Urogynecol J Pelvic Floor Dysfunct, 2007. **18**(8): p. 881-8.

27. Barber, M.D., *Contemporary views on female pelvic anatomy.* Cleve Clin J Med, 2005. **72 Suppl 4**: p. S3-11.

28. Wittman, A.B. and L.L. Wall, *The evolutionary origins of obstructed labor: bipedalism, encephalization, and the human obstetric dilemma.* Obstet Gynecol Surv, 2007. **62**(11): p. 739-48.

29. Schimpf, M. and P. Tulikangas, *Evolution of the female pelvis and relationships to pelvic organ prolapse.* Int Urogynecol J Pelvic Floor Dysfunct, 2005. **16**(4): p. 315-20.

30. Moalli, P.A., et al., *A rat model to study the structural properties of the vagina and its supportive tissues.* Am J Obstet Gynecol, 2005. **192**(1): p. 80-8.

31. Wen, Y., et al., *Differences in mRNA and protein expression of small proteoglycans in vaginal wall tissue from women with and without stress urinary incontinence.* Hum Reprod, 2007. **22**(6): p. 1718-24.

32. Goh, J.T., *Biomechanical and biochemical assessments for pelvic organ prolapse.* Curr Opin Obstet Gynecol, 2003. **15**(5): p. 391-4.

33. Jackson, S.R., et al., *Changes in metabolism of collagen in genitourinary prolapse.* Lancet, 1996. **347**(9016): p. 1658-61.

34. Abramowitch, S.D., et al., *Tissue mechanics, animal models, and pelvic organ prolapse: a review.* Eur J Obstet Gynecol Reprod Biol, 2009. **144 Suppl 1**: p. S146-58.

35. Chow, B.F. and C.E. Agustin, *Induction of premature birth in rats by a methionine antagonist.* J Nutr, 1965. **87**(3): p. 293-6.

36. Champlin, A.K., D.L. Dorr, and A.H. Gates, *Determining the stage of the estrous cycle in the mouse by the appearance of the vagina.* Biol Reprod, 1973. **8**(4): p. 491-4.

37. Moalli, P.A., et al., *Hormones restore biomechanical properties of the vagina and supportive tissues after surgical menopause in young rats.* Am J Obstet Gynecol, 2008. **199**(2): p. 161 e1-8.

38. Alperin, M., et al., *LOXL1 deficiency negatively impacts the biomechanical properties of the mouse vagina and supportive tissues.* Int Urogynecol J Pelvic Floor Dysfunct, 2008. **19**(7): p. 977-86.

39. Drewes, P.G., et al., *Pelvic organ prolapse in fibulin-5 knockout mice: pregnancy-induced changes in elastic fiber homeostasis in mouse vagina.* Am J Pathol, 2007. **170**(2): p. 578-89.

40. Huffaker, R.K., et al., *Histologic response of porcine collagen-coated and uncoated polypropylene grafts in a rabbit vagina model.* Am J Obstet Gynecol, 2008. **198**(5): p. 582 e1-7.

41. Ayen, E. and D.E. Noakes, *Displacement of the tubular genital tract of the ewe during pregnancy.* Vet Rec, 1997. **141**(20): p. 509-12.

42. Davies, F.G., *The occurrence of vaginal eversion and allied disorders in fat ewes.* Res Vet Sci, 1970. **11**(1): p. 86-90.

43. Hilson, R., R. Jackson, and N.R. Perkins. *An epidemiological study of vaginal prolapse in ewes*. in *society of sheep and beef cattle veterinarians NZVA*. 2003. Massey University.

44. Hosie, B.D., *Vaginal Prolapse and rupture in sheep.* In practice 1989. **11**: p. 215-218.

45. Low, J.C. and H.K. Sutherland, *A census of the prevalence of vaginal prolapse in sheep flocks in the Borders region of Scotland.* Vet Rec, 1987. **120**(24): p. 571-5.

46. Shepherd, P.R., *Vaginal prolapse in ewes.* Vet Rec, 1992. **130**(25): p. 564.

47. Winter, A.C., *Prolapse of the vagina and cervix in ewes.*, in *The Veterinary Annual, 36th issue*, M.E. Raw and P. T.J., Editors. 1996, Blackwell Science: Oxford. p. 385-90.

48. Otto, L.N., et al., *The rhesus macaque as an animal model for pelvic organ prolapse.* Am J Obstet Gynecol, 2002. **186**(3): p. 416-21.

49. Coates, K.W., et al., *The squirrel monkey: an animal model of pelvic relaxation.* Am J Obstet Gynecol, 1995. **172**(2 Pt 1): p. 588-93.

50. Lien, K.C., et al., *Levator ani muscle stretch induced by simulated vaginal birth.* Obstet Gynecol, 2004. **103**(1): p. 31-40.

51. Moalli, P.A., et al., *Remodeling of vaginal connective tissue in patients with prolapse.* Obstet Gynecol, 2005. **106**(5 Pt 1): p. 953-63.

52. Moalli, P.A., et al., *Impact of menopause on collagen subtypes in the arcus tendineous fasciae pelvis.* Am J Obstet Gynecol, 2004. **190**(3): p. 620-7.

53. Pierce, L.M., et al., *Effects of bilateral levator ani nerve injury on pelvic support in the female squirrel monkey.* Am J Obstet Gynecol, 2008. **198**(5): p. 585 e1-8.

54. Mant, J., R. Painter, and M. Vessey, *Epidemiology of genital prolapse: observations from the Oxford Family Planning Association Study.* Br J Obstet Gynaecol, 1997. **104**(5): p. 579-85.

55. Niyibizi, C., et al., *Type V collagen is increased during rabbit medial collateral ligament healing.* Knee Surg Sports Traumatol Arthrosc, 2000. **8**(5): p. 281-5.

56. Liang, R., et al., *Long-term effects of porcine small intestine submucosa on the healing of medial collateral ligament: a functional tissue engineering study.* J Orthop Res, 2006. **24**(4): p. 811-9.

57. Klinge, U., et al., *Abnormal collagen I to III distribution in the skin of patients with incisional hernia.* Eur Surg Res, 2000. **32**(1): p. 43-8.

58. Zong, W., L.A. Meyn, and P.A. Moalli, *The amount and activity of active matrix metalloproteinase 13 is suppressed by estradiol and progesterone in human pelvic floor fibroblasts.* Biol Reprod, 2009. **80**(2): p. 367-74.

59. Zong, W., et al., *Regulation of MMP-1 by sex steroid hormones in fibroblasts derived from the female pelvic floor.* Am J Obstet Gynecol, 2007. **196**(4): p. 349 e1-11.

60. Cosson, M., et al., *Mechanical properties of synthetic implants used in the repair of prolapse and urinary incontinence in women: which is the ideal material?* Int Urogynecol J Pelvic Floor Dysfunct, 2003. **14**(3): p. 169-78; discussion 178.

61. Cosson, M., et al., *A biomechanical study of the strength of vaginal tissues. Results on 16 post-menopausal patients presenting with genital prolapse.* Eur J Obstet Gynecol Reprod Biol, 2004. **112**(2): p. 201-5.

62. Mouritsen, L., *Classification and evaluation of prolapse.* Best Pract Res Clin Obstet Gynaecol, 2005. **19**(6): p. 895-911.

63. Pulliam, S.J., et al., *Use of synthetic mesh in pelvic reconstructive surgery: a survey of attitudes and practice patterns of urogynecologists.* Int Urogynecol J Pelvic Floor Dysfunct, 2007. **18**(12): p. 1405-8.

64. Nygaard, I., et al., *Prevalence of symptomatic pelvic floor disorders in US women.* JAMA, 2008. **300**(11): p. 1311-6.

65. Nicita, G., *A new operation for genitourinary prolapse.* J Urol, 1998. **160**(3 Pt 1): p. 741-5.

66. Flood, C.G., H.P. Drutz, and L. Waja, *Anterior colporrhaphy reinforced with Marlex mesh for the treatment of cystoceles.* Int Urogynecol J Pelvic Floor Dysfunct, 1998. **9**(4): p. 200-4.

67. Jameson, J.S., et al., *Effect of age, sex and parity on anorectal function.* Br J Surg, 1994. **81**(11): p. 1689-92.

68. Reay Jones, N.H., et al., *Pelvic connective tissue resilience decreases with vaginal delivery, menopause and uterine prolapse.* Br J Surg, 2003. **90**(4): p. 466-72.

69. Chen, C.C., B. Ridgeway, and M.F. Paraiso, *Biologic grafts and synthetic meshes in pelvic reconstructive surgery.* Clin Obstet Gynecol, 2007. **50**(2): p. 383-411.

70. Dora, C.D., et al., *Time dependent variations in biomechanical properties of cadaveric fascia, porcine dermis, porcine small intestine submucosa, polypropylene mesh and autologous fascia in the rabbit model: implications for sling surgery*. J Urol, 2004. **171**(5): p. 1970-3.

71. Fenner, D.E., *New surgical mesh.* Clin Obstet Gynecol, 2000. **43**(3): p. 650-8.

72. Ratner, B.D.H., A.S., Schoen F.J., Lemons, J.E., *Biomaterials Science*. 2nd Edition ed. 2004, San Diego: Elsevier Inc. 864.

73. Konstantinovic, M.L., et al., *Tensile strength and host response towards different polypropylene implant materials used for augmentation of fascial repair in a rat model.* Int Urogynecol J Pelvic Floor Dysfunct, 2007. **18**(6): p. 619-26.

74. Klinge, U., et al., *Functional and morphological evaluation of a low-weight, monofilament polypropylene mesh for hernia repair*. J Biomed Mater Res, 2002. **63**(2): p. 129-36.

75. Pascual, G., et al., *Early tissue incorporation and collagen deposition in lightweight polypropylene meshes: bioassay in an experimental model of ventral hernia.* Surgery, 2008. **144**(3): p. 427-35.

76. Klinge, U., et al., *Impact of polymer pore size on the interface scar formation in a rat model.* J Surg Res, 2002. **103**(2): p. 208-14.

77. Cobb, W.S., et al., *Textile analysis of heavy weight, mid-weight, and light weight polypropylene mesh in a porcine ventral hernia model.* J Surg Res, 2006. **136**(1): p. 1-7.

78. Bellon, J.M., et al., *Comparing the behavior of different polypropylene meshes (heavy and lightweight) in an experimental model of ventral hernia repair.* J Biomed Mater Res B Appl Biomater, 2009. **89B**(2): p. 448-55.

79. Dietz, H.P., et al., *Mechanical properties of urogynecologic implant materials.* Int Urogynecol J Pelvic Floor Dysfunct, 2003. **14**(4): p. 239-43; discussion 243.

80. Jones, K.A., et al., *Tensile properties of commonly used prolapse meshes.* Int Urogynecol J Pelvic Floor Dysfunct, 2009. **20**(7): p. 847-53.

81. Huebner, M., Y. Hsu, and D.E. Fenner, *The use of graft materials in vaginal pelvic floor surgery.* Int J Gynaecol Obstet, 2006. **92**(3): p. 279-88.

82. Amrute, K.V. and G.H. Badlani, *Female incontinence: a review of biomaterials and minimally invasive techniques.* Curr Opin Urol, 2006. **16**(2): p. 54-9.

83. Moalli, P.A., et al., *Tensile properties of five commonly used mid-urethral slings relative to the TVT.* Int Urogynecol J Pelvic Floor Dysfunct, 2008. **19**(5): p. 655-63.

84. Saberski, E.R., S.B. Orenstein, and Y.W. Novitsky, *Anisotropic evaluation of synthetic surgical meshes.* Hernia, 2011. **15**(1): p. 47-52.

85. Afonso, J.S., et al., *Mechanical properties of polypropylene mesh used in pelvic floor repair.* Int Urogynecol J Pelvic Floor Dysfunct, 2008. **19**(3): p. 375-80.

86. Ashton-Miller, J.A. and J.O. Delancey, *On the biomechanics of vaginal birth and common sequelae.* Annu Rev Biomed Eng, 2009. **11**: p. 163-76.

87. Chen, L., J.A. Ashton-Miller, and J.O. DeLancey, *A 3D finite element model of anterior vaginal wall support to evaluate mechanisms underlying cystocele formation.* J Biomech, 2009. **42**(10): p. 1371-7.

88. Rainis, E.J., et al., *Material properties of the axillary pouch of the glenohumeral capsule: is isotropic material symmetry appropriate?* J Biomech Eng, 2009. **131**(3): p. 031007.

89. Sweeney J, C.T., Coates PD, Ward IM, *Application of an elastic model to the large deformation, high temperature stretching of polypropylene.* Polymer, 1997. **38**(24): p. 5991-5999.

90. Sweeney J, S.R., Woodhead M. , *A Constitutive Model for Large Multiaxial Deformations of Solid Polypropylene at High Temperature.* Polymer Eng Science, 2009. **10**: p. 1902-1908.

91. Drozdov AD, K.A., *A Constitutive Model for Nonlinear Viscoelastic Behavior of Polymers.* Polymer Eng Science 1996. **36**(14): p. 1907-1919.

92. Kaiser, A., *mechanical characterization and modeling of textile meshes, used in soft tissue reconstruction*, in *Mechanics*. 2008, Swiss Federal Institute of Technology Zurich: Zurich.

93. Iglesia, C.B., D.E. Fenner, and L. Brubaker, *The use of mesh in gynecologic surgery.* Int Urogynecol J Pelvic Floor Dysfunct, 1997. **8**(2): p. 105-15.

94. Isom-Batz, G. and P.E. Zimmern, *Vaginal mesh for incontinence and/or prolapse: caution required!* Expert Rev Med Devices, 2007. **4**(5): p. 675-9.

95. Velayudhan, S., D. Martin, and J. Cooper-White, *Evaluation of dynamic creep properties of surgical mesh prostheses--uniaxial fatigue.* J Biomed Mater Res B Appl Biomater, 2009. **91**(1): p. 287-96.

96. Smith, D.B., et al., *Surface geometric analysis of anatomic structures using biquintic finite element interpolation.* Ann Biomed Eng, 2000. **28**(6): p. 598-611.

97. Song, Y., et al., *A three-dimensional finite element model of the human anterior cruciate ligament: a computational analysis with experimental validation.* J Biomech, 2004. **37**(3): p. 383-90.

98. Weiss, J.A., J.C. Gardiner, and C. Bonifasi-Lista, *Ligament material behavior is nonlinear, viscoelastic and rate-independent under shear loading.* J Biomech, 2002. **35**(7): p. 943-50.

99. Anderson, A.E., et al., *Subject-specific finite element model of the pelvis: development, validation and sensitivity studies.* J Biomech Eng, 2005. **127**(3): p. 364-73.

100. d'Aulignac, D., et al., *A shell finite element model of the pelvic floor muscles.* Comput Methods Biomech Biomed Engin, 2005. **8**(5): p. 339-47.

101. Gardiner, J.C. and J.A. Weiss, *Subject-specific finite element analysis of the human medial collateral ligament during valgus knee loading.* J Orthop Res, 2003. **21**(6): p. 1098-106.

102. Edelman, D.S., *Laparoscopic herniorrhaphy with porcine small intestinal submucosa: a preliminary study.* JSLS, 2002. **6**(3): p. 203-5.

103. Higgins, E.W., et al., *Effect of estrogen replacement on the histologic response to polypropylene mesh implanted in the rabbit vagina model.* Am J Obstet Gynecol, 2009. **201**(5): p. 505 e1-9.

104. Hilger, W.S., et al., *Histological and biomechanical evaluation of implanted graft materials in a rabbit vaginal and abdominal model.* Am J Obstet Gynecol, 2006. **195**(6): p. 1826-31.

105. Krause, H. and J. Goh, *Sheep and rabbit genital tracts and abdominal wall as an implantation model for the study of surgical mesh.* J Obstet Gynaecol Res, 2009. **35**(2): p. 219-24.

106. Rubod, C., et al., *Biomechanical properties of vaginal tissue. Part 1: new experimental protocol.* J Urol, 2007. **178**(1): p. 320-5; discussion 325.

107. Pierce, L.M., et al., *Biomechanical properties of synthetic and biologic graft materials following long-term implantation in the rabbit abdomen and vagina.* Am J Obstet Gynecol, 2009. **200**(5): p. 549 e1-8.

108. Pierce, L.M., et al., *Long-term histologic response to synthetic and biologic graft materials implanted in the vagina and abdomen of a rabbit model.* Am J Obstet Gynecol, 2009. **200**(5): p. 546 e1-8.

109. Boulanger, L., et al., *Development of an animal model to study meshes used in genital prolapse surgery.* Eur J Obstet Gynecol Reprod Biol, 2008. **136**(2): p. 254-9.

110. Boukerrou, M., et al., *Study of the biomechanical properties of synthetic mesh implanted in vivo.* Eur J Obstet Gynecol Reprod Biol, 2007. **134**(2): p. 262-7.

111. Horan, R.L., et al., *Biological and biomechanical assessment of a long-term bioresorbable silk-derived surgical mesh in an abdominal body wall defect model.* Hernia, 2009. **13**(2): p. 189-99.

112. Birk, D.E. and R. Mayne, *Localization of collagen types I, III and V during tendon development. Changes in collagen types I and III are correlated with changes in fibril diameter.* Eur J Cell Biol, 1997. **72**(4): p. 352-61.

113. Linsenmayer, T.F., et al., *Type V collagen: molecular structure and fibrillar organization of the chicken alpha 1(V) NH2-terminal domain, a putative regulator of corneal fibrillogenesis.* J Cell Biol, 1993. **121**(5): p. 1181-9.

114. Romanic, A.M., et al., *Copolymerization of pNcollagen III and collagen I. pNcollagen III decreases the rate of incorporation of collagen I into fibrils, the amount of collagen I incorporated, and the diameter of the fibrils formed.* J Biol Chem, 1991. **266**(19): p. 12703-9.

115. Birk, D.E., et al., *Collagen fibrillogenesis in vitro: interaction of types I and V collagen regulates fibril diameter.* J Cell Sci, 1990. **95 (Pt 4)**: p. 649-57.

116. Alperin, M., et al., *Collagen scaffold: a treatment for simulated maternal birth injury in the rat model.* Am J Obstet Gynecol, 2010. **202**(6): p. 589 e1-8.

117. Zong, W., et al., *Alteration of vaginal elastin metabolism in women with pelvic organ prolapse.* Obstet Gynecol, 2010. **115**(5): p. 953-61.

118. Lee, T.Q. and S.L. Woo, *A new method for determining cross-sectional shape and area of soft tissues.* J Biomech Eng, 1988. **110**(2): p. 110-4.

119. Moon, D.K., S.D. Abramowitch, and S.L. Woo, *The development and validation of a charge-coupled device laser reflectance system to measure the complex*

cross-sectional shape and area of soft tissues. J Biomech, 2006. **39**(16): p. 3071-5.

120. Abramowitch, S.D., et al., *A biomechanical and histological evaluation of the structure and function of the healing medial collateral ligament in a goat model.* Knee Surg Sports Traumatol Arthrosc, 2003. **11**(3): p. 155-62.

121. Woo, S.L., *Mechanical properties of tendons and ligaments. I. Quasi-static and nonlinear viscoelastic properties.* Biorheology, 1982. **19**(3): p. 385-96.

122. Woo, S.L., et al., *Biomechanics of knee ligaments.* Am J Sports Med, 1999. **27**(4): p. 533-43.

123. Scheffler, S.U., et al., *Structure and function of the healing medial collateral ligament in a goat model.* Ann Biomed Eng, 2001. **29**(2): p. 173-80.

124. Woo, S.L., et al., *Effects of postmortem storage by freezing on ligament tensile behavior.* J Biomech, 1986. **19**(5): p. 399-404.

125. Haut, R.C. and A.C. Powlison, *The effects of test environment and cyclic stretching on the failure properties of human patellar tendons.* J Orthop Res, 1990. **8**(4): p. 532-40.

126. Lanir, Y. and Y.C. Fung, *Two-dimensional mechanical properties of rabbit skin. II. Experimental results.* J Biomech, 1974. **7**(2): p. 171-82.

127. Pinto, J.G. and Y.C. Fung, *Mechanical properties of the heart muscle in the passive state.* J Biomech, 1973. **6**(6): p. 597-616.

128. Woo, S.L., M.B. Fisher, and A.J. Feola, *Contribution of biomechanics to management of ligament and tendon injuries.* Mol Cell Biomech, 2008. **5**(1): p. 49-68.

129. Woo, S.L., et al., *Tensile properties of the human femur-anterior cruciate ligament-tibia complex. The effects of specimen age and orientation.* Am J Sports Med, 1991. **19**(3): p. 217-25.

130. Woo, S.L., et al., *Temperature dependent behavior of the canine medial collateral ligament.* J Biomech Eng, 1987. **109**(1): p. 68-71.

131. Yin, F.C. and Y.C. Fung, *Mechanical properties of isolated mammalian ureteral segments.* Am J Physiol, 1971. **221**(5): p. 1484-93.

132. Moon, D.K., et al., *The effects of refreezing on the viscoelastic and tensile properties of ligaments.* J Biomech, 2006. **39**(6): p. 1153-7.

133. Goodman, G., Rall, T.W., Nies, A.S., Taylor P., ed. *The Pharmacological Basis of Therapeutics*. 8th Edition ed. 1990, Pergamon Press.

134. Lowder, J.L., et al., *Biomechanical adaptations of the rat vagina and supportive tissues in pregnancy to accommodate delivery.* Obstet Gynecol, 2007. **109**(1): p. 136-43.

135. Feola, A., et al., *Impact of Pregnancy and Vaginal Delivery on the Passive and Active Mechanics of the Rat Vagina.* Ann Biomed Eng, 2010.

136. Abramowitch, S.D., et al., *An evaluation of the quasi-linear viscoelastic properties of the healing medial collateral ligament in a goat model.* Ann Biomed Eng, 2004. **32**(3): p. 329-35.

137. Woo, S.L., et al., *The use of a laser micrometer system to determine the cross-sectional shape and area of ligaments: a comparative study with two existing methods.* J Biomech Eng, 1990. **112**(4): p. 426-31.

138. Davidge, S.T., R.E. Gandley, and M.K. McLaughlin, *Altered active but not passive properties of mesenteric resistance arteries from the vitamin E-deprived rat.* Br J Pharmacol, 1998. **123**(2): p. 275-80.

139. Daucher, J.A., et al., *Adaptations of the rat vagina in pregnancy to accommodate delivery.* Obstet Gynecol, 2007. **109**(1): p. 128-35.

140. Giraldi, A., et al., *Morphological and functional characterization of a rat vaginal smooth muscle sphincter.* Int J Impot Res, 2002. **14**(4): p. 271-82.

141. Kim, N.N., et al., *Effects of ovariectomy and steroid hormones on vaginal smooth muscle contractility.* Int J Impot Res, 2004. **16**(1): p. 43-50.

142. Allen, R.E., et al., *Pelvic floor damage and childbirth: a neurophysiological study.* Br J Obstet Gynaecol, 1990. **97**(9): p. 770-9.

143. Sheiner, E., et al., *Obstetric risk factors and outcome of pregnancies complicated with early postpartum hemorrhage: a population-based study.* J Matern Fetal Neonatal Med, 2005. **18**(3): p. 149-54.

144. Dietz, H.P. and M.J. Bennett, *The effect of childbirth on pelvic organ mobility.* Obstet Gynecol, 2003. **102**(2): p. 223-8.

145. Dietz, H.P., et al., *Does pregnancy affect pelvic organ mobility?* Aust N Z J Obstet Gynaecol, 2004. **44**(6): p. 517-20.

146. Aspden, R.M., *Collagen organisation in the cervix and its relation to mechanical function.* Coll Relat Res, 1988. **8**(2): p. 103-12.

147. Harkness, M.L. and R.D. Harkness, *Changes in the physical properties of the uterine cervix of the rat during pregnancy.* J Physiol, 1959. **148**: p. 524-47.

148. Hulmes, D.J., *The collagen superfamily--diverse structures and assemblies.* Essays Biochem, 1992. **27**: p. 49-67.

149. Kokenyesi, R. and J.F. Woessner, Jr., *Effects of hormonal perturbations on the small dermatan sulfate proteoglycan and mechanical properties of the uterine cervix of late pregnant rats.* Connect Tissue Res, 1991. **26**(3): p. 199-205.

150. Lin, A.S., et al., *Effect of simulated birth trauma on the urinary continence mechanism in the rat.* Urology, 1998. **52**(1): p. 143-51.

151. Resplande, J., et al., *Long-term effect of ovariectomy and simulated birth trauma on the lower urinary tract of female rats.* J Urol, 2002. **168**(1): p. 323-30.

152. Sievert, K.D., et al., *The effect of simulated birth trauma and/or ovariectomy on rodent continence mechanism. Part I: functional and structural change.* J Urol, 2001. **166**(1): p. 311-7.

153. Cannon, T.W., et al., *Effects of vaginal distension on urethral anatomy and function.* BJU Int, 2002. **90**(4): p. 403-7.

154. Woo, L.L., et al., *Simulated childbirth injuries in an inbred rat strain.* Neurourol Urodyn, 2009. **28**(4): p. 356-61.

155. Damaser, M.S., et al., *Effect of vaginal distension on blood flow and hypoxia of urogenital organs of the female rat.* J Appl Physiol, 2005. **98**(5): p. 1884-90.

156. Lei, L., Y. Song, and R. Chen, *Biomechanical properties of prolapsed vaginal tissue in pre- and postmenopausal women.* Int Urogynecol J Pelvic Floor Dysfunct, 2007. **18**(6): p. 603-7.

157. Swift, S.E., *The distribution of pelvic organ support in a population of female subjects seen for routine gynecologic health care.* Am J Obstet Gynecol, 2000. **183**(2): p. 277-85.

158. Junqueira, L.C., G. Bignolas, and R.R. Brentani, *Picrosirius staining plus polarization microscopy, a specific method for collagen detection in tissue sections.* Histochem J, 1979. **11**(4): p. 447-55.

159. Arruda, E.M., et al., *Denervation does not change the ratio of collagen I and collagen III mRNA in the extracellular matrix of muscle.* Am J Physiol Regul Integr Comp Physiol, 2007. **292**(2): p. R983-7.

160. Feola, A., et al., *Parity negatively impacts vaginal mechanical properties and collagen structure in rhesus macaques.* Am J Obstet Gynecol, 2010. **203**(6): p. 595 e1-8.

161. Musahl, V., et al., *The use of porcine small intestinal submucosa to enhance the healing of the medial collateral ligament--a functional tissue engineering study in rabbits.* J Orthop Res, 2004. **22**(1): p. 214-20.

162. Woo, S.L., et al., *Treatment with bioscaffold enhances the the fibril morphology and the collagen composition of healing medial collateral ligament in rabbits.* Tissue Eng, 2006. **12**(1): p. 159-66.

163. Gilbert, T.W., et al., *Collagen fiber alignment and biaxial mechanical behavior of porcine urinary bladder derived extracellular matrix.* Biomaterials, 2008. **29**(36): p. 4775-82.

164. Alperin, M., et al., *Pregnancy- and delivery-induced biomechanical changes in rat vagina persist postpartum.* Int Urogynecol J Pelvic Floor Dysfunct, 2010. **21**(9): p. 1169-74.

165. Davila, G.W., H. Drutz, and J. Deprest, *Clinical implications of the biology of grafts: conclusions of the 2005 IUGA Grafts Roundtable.* Int Urogynecol J Pelvic Floor Dysfunct, 2006. **17 Suppl 1**: p. S51-5.

166. Konstantinovic, M.L., et al., *Comparison of host response to polypropylene and non-cross-linked porcine small intestine serosal-derived collagen implants in a rat model.* BJOG, 2005. **112**(11): p. 1554-60.

167. Spelzini, F., et al., *Tensile strength and host response towards silk and type i polypropylene implants used for augmentation of fascial repair in a rat model.* Gynecol Obstet Invest, 2007. **63**(3): p. 155-62.

168. Carley, M.E. and J. Schaffer, *Urinary incontinence and pelvic organ prolapse in women with Marfan or Ehlers Danlos syndrome.* Am J Obstet Gynecol, 2000. **182**(5): p. 1021-3.

169. Falagas, M.E., et al., *Mesh-related infections after pelvic organ prolapse repair surgery.* Eur J Obstet Gynecol Reprod Biol, 2007. **134**(2): p. 147-56.

170. Margulies, R.U., et al., *Complications requiring reoperation following vaginal mesh kit procedures for prolapse.* Am J Obstet Gynecol, 2008. **199**(6): p. 678 e1-4.

171. Cardozo, L., and Staskin, D., ed. *Textbook of Female Urology and Urogynecology*. 2nd Edition ed. Vol. 1. 2006, Informa Healthcare.

172. Bent, A.E., Cundiff, G.W., Swift, S.E., ed. *Ostergard's urogynecology and pelvic floor dysfunction*. 6th Edition ed. 2008, Lippincott Williams & Wilkins.

173. Gomberg, B.R., P.K. Saha, and F.W. Wehrli, *Topology-based orientation analysis of trabecular bone networks.* Med Phys, 2003. **30**(2): p. 158-68.

174. Odgaard, A., et al., *Fabric and elastic principal directions of cancellous bone are closely related.* J Biomech, 1997. **30**(5): p. 487-95.

175. Smit, T.H., E. Schneider, and A. Odgaard, *Star length distribution: a volume-based concept for the characterization of structural anisotropy.* J Microsc, 1998. **191**(3): p. 249-257.

176. Kabel, J., et al., *Constitutive relationships of fabric, density, and elastic properties in cancellous bone architecture.* Bone, 1999. **25**(4): p. 481-6.

177. Dalstra, M., et al., *Mechanical and textural properties of pelvic trabecular bone.* J Biomech, 1993. **26**(4-5): p. 523-35.

178. Cowin, S.C., Doty, S.B., *Tissue Mechanics*. 2007, New York: Springer.

179. Deffieux, X., et al., *Vaginal mesh erosion after transvaginal repair of cystocele using Gynemesh or Gynemesh-Soft in 138 women: a comparative study.* Int Urogynecol J Pelvic Floor Dysfunct, 2007. **18**(1): p. 73-9.

180. Silva, W.A. and M.M. Karram, *Scientific basis for use of grafts during vaginal reconstructive procedures.* Curr Opin Obstet Gynecol, 2005. **17**(5): p. 519-29.

181. Schumpelick, V., et al., *[Meshes within the abdominal wall]*. Chirurg, 1999. **70**(8): p. 876-87.

182. Woo, S.L., et al., *The biomechanical and morphological changes in the medial collateral ligament of the rabbit after immobilization and remobilization.* J Bone Joint Surg Am, 1987. **69**(8): p. 1200-11.

183. Poitout, D.G., *Biomechanics and Biomaterials in Orthopedics*. 2004: Springer.

184. Majima, T., et al., *Stress shielding of patellar tendon: effect on small-diameter collagen fibrils in a rabbit model.* J Orthop Sci, 2003. **8**(6): p. 836-41.

185. Muellner, T., et al., *Light and electron microscopic study of stress-shielding effects on rat patellar tendon.* Arch Orthop Trauma Surg, 2001. **121**(10): p. 561-5.

186. Lind, M. and C. Bunger, *Factors stimulating bone formation.* Eur Spine J, 2001. **10 Suppl 2**: p. S102-9.

187. Nagels, J., M. Stokdijk, and P.M. Rozing, *Stress shielding and bone resorption in shoulder arthroplasty.* J Shoulder Elbow Surg, 2003. **12**(1): p. 35-9.

188. Moore, W.R., S.E. Graves, and G.I. Bain, *Synthetic bone graft substitutes.* ANZ J Surg, 2001. **71**(6): p. 354-61.

189. Brockman, J.B., N.W. Patterson, and W.S. Richardson, *Burst strength of laparoscopic and open hernia repair.* Surg Endosc, 2004. **18**(3): p. 536-9.

190. Papadimitriou, J. and P. Petros, *Histological studies of monofilament and multifilament polypropylene mesh implants demonstrate equivalent penetration of macrophages between fibrils.* Hernia, 2005. **9**(1): p. 75-8.

191. Battini, J., *Co-rotational beam elements in instability problems*, in *Mechanics*. 2002, Royal Institute of Technology: Stockholm.

192. Crisfield, M.A., *Non-linear Finite Element Analysis of Solids and Structures* Vol. Volume 2: Advanced Topics. 1997, New York: John Wiley & Sons Ltf.

193. Battini, J., Pacoste, C., *Co-rotational beam elements with warping effects in instability problems.* Computer Methods in Applied Mechanics and Engineering, 2002. **191**: p. 1755–1789.

194. Ferreira, A.J., *MATLAB Codes for Finite Element Analysis*, ed. G.M. Gladwell. 2009: Springer.

195. Battini, J., Pacoste, C., *Plastic instability of beam structures using co-rotational elements.* Computer Methods in Applied Mechanics and Engineering, 2002. **191**: p. 5811–5831.

196. Woo, S.L., G.A. Johnson, and B.A. Smith, *Mathematical modeling of ligaments and tendons.* J Biomech Eng, 1993. **115**(4B): p. 468-73.

197. Sacks, M.S., *Biaxial Mechanical Evaluation of Planar Biological Materials.* J Elasticity 2000. **61**: p. 199-246.

198. Sacks, M.S. and C.J. Chuong, *Orthotropic mechanical properties of chemically treated bovine pericardium.* Ann Biomed Eng, 1998. **26**(5): p. 892-902.

199. Woo, S.L., M.A. Gomez, and W.H. Akeson, *The time and history-dependent viscoelastic properties of the canine medical collateral ligament.* J Biomech Eng, 1981. **103**(4): p. 293-8.

200. Frisen, M., et al., *Rheological analysis of soft collagenous tissue. Part I: theoretical considerations.* J Biomech, 1969. **2**(1): p. 13-20.

201. Peirce, F.T., *The Geometry of Cloth Structure.* Journal of Textile Institute, 1937. **28**: p. 45-96.

202. Peirce, F.T., *Geometrical Principles Applicable to the Design of Functional Fabrics.* 1947, 1947. **17**(123-147).

203. Yeoman, M.S., et al., *A constitutive model for the warp-weft coupled non-linear behavior of knitted biomedical textiles.* Biomaterials, 2010. **31**(32): p. 8484-93.

204. D'Amore, A., et al., *Characterization of the complete fiber network topology of planar fibrous tissues and scaffolds.* Biomaterials, 2010. **31**(20): p. 5345-54.

205. Amoroso, N.J., et al., *Elastomeric electrospun polyurethane scaffolds: the interrelationship between fabrication conditions, fiber topology, and mechanical properties.* Adv Mater, 2011. **23**(1): p. 106-11.

206. Stella, J.A., et al., *On the biomechanical function of scaffolds for engineering load-bearing soft tissues.* Acta Biomater, 2010. **6**(7): p. 2365-81.

207. Tokar, S.F., A., Moalli, P., Abramowitch, S. *Characterizing the Biaxial Mechanical Properties of Vaginal Maternal Adaptiations During Pregnancy*. in *2010 American Society of Mechanical Engineers Summer Bioengineering Conference*. 2010. Naples, FL,.

208. Billiar, K.L. and M.S. Sacks, *Biaxial mechanical properties of the natural and glutaraldehyde treated aortic valve cusp--Part I: Experimental results.* J Biomech Eng, 2000. **122**(1): p. 23-30.

209. Gleason, R.L., et al., *A multiaxial computer-controlled organ culture and biomechanical device for mouse carotid arteries.* J Biomech Eng, 2004. **126**(6): p. 787-95.

210. Gleason, R.L. and J.D. Humphrey, *Effects of a sustained extension on arterial growth and remodeling: a theoretical study.* J Biomech, 2005. **38**(6): p. 1255-61.

211. Gleason, R.L., E. Wilson, and J.D. Humphrey, *Biaxial biomechanical adaptations of mouse carotid arteries cultured at altered axial extension.* J Biomech, 2007. **40**(4): p. 766-76.

212. Billiar, K.L. and M.S. Sacks, *Biaxial mechanical properties of the native and glutaraldehyde-treated aortic valve cusp: Part II--A structural constitutive model.* J Biomech Eng, 2000. **122**(4): p. 327-35.

213. Wang, C.C., et al., *Diabetes-induced alternations in biomechanical properties of urinary bladder wall in rats.* Urology, 2009. **73**(4): p. 911-5.